(NASA-TM-82235) NACA-UNIVERSITY CONFERENCE ON AERODYNAMICS, CONSTRUCTION AND PROPULSION. VOLUME 2: AERODYNAMICS (National Advisory Committee for Aeronautics.) 184 p
N81-74336
Unclas
00/02 42096

NATIONAL ADVISORY COMMITTEE FOR AERONAUTICS

NACA-UNIVERSITY CONFERENCE ON AERODYNAMICS, CONSTRUCTION, AND PROPULSION

VOLUME II
AERODYNAMICS

Lewis Flight Propulsion Laboratory
Cleveland, Ohio

October 20, 21, and 22, 1954

MAY 1981
RECEIVED
NASA STI FACILITY
ACCESS DEPT.

NACA

NASA FILE COPY

PLEASE RETURN TO CODE ETL
OFFICE OF TECHNICAL INFORMATION
AND EDUCATIONAL PROGRAMS
NATIONAL AERONAUTICS
AND SPACE ADMINISTRATION
Washington 25, D. C.

NACA-UNIVERSITY CONFERENCE ON AERODYNAMICS, CONSTRUCTION, AND PROPULSION

VOLUME II
AERODYNAMICS

Lewis Flight Propulsion Laboratory
Cleveland, Ohio

October 20, 21, and 22, 1954

INTRODUCTION

The NACA-University Conference was held to acquaint university personnel with recent developments in aeronautical research. Wherever possible, each paper reviews the status of the field under consideration, points out recent significant advances, and suggests promising avenues for future research.

The papers presented are considered to supplement, rather than substitute for, the reports in which the NACA customarily releases its work. Information regarding the NACA's regular reports may be obtained from the Division of Research Information, NACA, 1512 H Street N. W., Washington 25, D. C.

This volume (Volume II of three) contains the papers presented at the conference that deal with aerodynamics. Volume I of the series contains the papers on aircraft structures and materials, and Volume III contains the papers on aircraft propulsion.

CONFERENCE PROGRAM

VOLUME I

AIRCRAFT STRUCTURES

1. SOME APPLICATIONS OF GENERALIZED HARMONIC ANALYSIS TO PROBLEMS IN AIRPLANE DYNAMICS by Harry Press, John C. Houbolt and Franklin W. Diederich

2. SOME RECENT DEVELOPMENTS IN THE AERODYNAMIC THEORY OF OSCILLATING WINGS by I. E. Garrick and C. E. Watkins

3. STRENGTH ANALYSIS OF MULTI-WEB THIN WINGS by Norris F. Dow and Roger A. Anderson

4. SOME STRUCTURAL EFFECTS OF AERODYNAMIC HEATING by R. R. Heldenfels, E. E. Mathauser and W. A. Brooks

AERONAUTICAL MATERIALS

5. SOME CONSIDERATIONS ON STRUCTURAL MATERIALS FOR HIGH-SPEED FLIGHT by George J. Heimerl

6. REVIEW OF MATERIALS FOR JET ENGINES by G. Mervin Ault and G. C. Deutsch

7. APPLICATIONS OF PHYSICS OF SOLIDS TO THE STUDY OF PROBLEMS OF AERONAUTICAL MATERIALS by S. L. Simon

3556

VOLUME II

AERODYNAMICS

8. ON THE NATURE OF AIRCRAFT NOISE SOURCES by Harvey H. Hubbard and Arthur A. Regier

9. RECENT DEVELOPMENTS IN THE AERODYNAMICS OF HELICOPTERS by Alfred Gessow and Richard C. Dingeldein

10. FLIGHT EFFICIENCY OF HIGH-SPEED AIRPLANES by Mark R. Nichols

11. INLETS AND EXITS FOR HIGH-SPEED AIRPLANES by Fred D. Kochendorfer

12. BOUNDARY LAYER CONTROL FOR HIGH LIFT by Woodrow L. Cook

13. SOME APPLICATIONS OF DYNAMIC ANALYSIS TO AUTOMATIC CONTROL RESEARCH by Robert A. Gardiner and Leonard Sternfield

14. REVIEW OF RECENT ADVANCES IN KNOWLEDGE OF HEAT TRANSFER AND SKIN FRICTION IN HIGH-SPEED AERODYNAMICS by M. W. Rubesin

15. THEORETICAL AND EXPERIMENTAL ANALYSES OF SOME SUPERSONIC FLOW FIELDS by Max A. Heaslet

16. AERODYNAMICS OF AIRFOILS AND BODIES IN COMBINATION AT SUPERSONIC SPEEDS by Jack N. Nielson

17. TRANSONIC AERODYNAMICS OF WINGS by Edward C. Polhamus

18. THEORETICAL AND EXPERIMENTAL ANALYSIS OF TRANSONIC FLOW FIELDS by John R. Spreiter

19. THEORETICAL AND EXPERIMENTAL ANALYSIS OF HYPERSONIC FLOW FIELDS by A. J. Eggers Jr. and Clarence A. Syvertson

20. TRANSONIC TEST SECTIONS by William J. Nelson and Ray H. Wright

VOLUME III

PROPULSION

21. PROPULSION SYSTEMS AND THEIR APPLICATIONS by Richard J. Weber

22. TURBULENT FORCED CONVECTION HEAT TRANSFER IN PASSAGES by R. G. Deissler and L. V. Humble

23. SOME CHARACTERISTICS OF AIRCRAFT FUELS by Henry C. Barnett

24. BEARINGS AND LUBRICANTS FOR AIRCRAFT TURBINE ENGINES by Robert L. Johnson and Edmond E. Bisson

25. COMBUSTION PRINCIPLES IN JET ENGINES by Abraham Berlad

26. SOME CONSIDERATIONS IN TURBINE AERODYNAMIC DESIGN by Ambrose Ginsberg

27. SOME CONSIDERATIONS IN AXIAL FLOW COMPRESSOR DESIGN by Irving A. Johnsen

Page intentionally left blank

NACA-UNIVERSITY CONFERENCE

October 20-21-22, 1954

*Attendance List

Name	School
Abbott, I. H.	NACA-Washington
Abramson, H. N.	Texas Agricultural & Mining College
Albright, L. F.	University of Oklahoma
Ambrose, H.	University of Tennessee
Anderson, E. W.	Iowa State University
Andes, A. S.	University of Kansas
Archer, D. H.	Carnegie Institute of Technology
Ault, G. M.	NACA-Lewis
Bailey, N. P.	Renssalaer Polytechnic Institute
Baker, R. D.	University of Utah
Barzelay, M. E.	Syracuse University
Bates, G.	NACA-Washington
Beane, J.	University of Buffalo
Berlad, A.	NACA-Lewis
Bicknell, J.	Massachusetts Institute of Technology
Birkenhauer, Rev. H. F.	John Carroll University
Bisplinghoff, R. L.	Massachusetts Institute of Technology
Bisson, E. E.	NACA-Lewis
Bleich, H.	Columbia University
Bloom, M.	Polytechnic Institute of Brooklyn
Bogdanoff, J. L.	Purdue University
Bogdonoff, S. M.	Princeton University
Bolz, R. E.	Case Institute of Technology
Breuer, D. W.	U. S. Air Force Institute of Technology
Broadwell, J. E.	University of Michigan
Brull, M. A.	University of Michigan
Bryson, A. E.	Harvard University
Burggraf, Lt. O. R.	U. S. Air Force Institute of Technology
Burlage, H.	Case Institute of Technology
Calhoun, Maj. J. D.	U. S. Air Force Institute of Technology
Campbell, G.	Renssalaer Polytechnic Institute
Carter, W. M.	University of Kentucky
Choppesky, Rev. J. C.	St. Louis University
Chi Chou, P.	Drexel Institute of Technology
Chu, S. T.	Ohio State University

*Attended one or more days of the conference.

Name	School
Cocanougher, J. E.	Miami University (Ohio)
Cohen, H.	Carnegie Institute of Technology
Comp, L. A.	University of Oklahoma
Cook, W. L.	NACA-Ames
Corning, G.	University of Maryland
Cronk, A. E.	University of Minnesota
Crossley, F. R. E.	Yale University
Daley, Maj. D. H.	U. S. Air Force Institute of Technology
Dancy, Maj. A. G.	U. S. Military Academy
Dean, R. C.	Massachusetts Institute of Technology
Deissler, R. G.	NACA-Lewis
Dingeldein, R. C.	NACA-Langley
Dow, N. F.	NACA-Langley
Draper, C. S.	Massachusetts Institute of Technology
Dryden, H. L. .	NACA-Washington
Dubois, G.	Cornell University
Durham, F. P.	University of Colorado
Dutton, D. W.	Georgia Institute of Technology
Eckert, E. R. G.	University of Minnesota
Erdoss, B.	Stevens Institute of Technology
Eringen, J.	Purdue University
Farmer, A.	Renssalaer Polytechnic Institute
Farrar, D. F.	Vanderbilt University
Ferrell, W. L.	Ohio University
Fleming, W.	University of Buffalo
Fogel, C.	University of Buffalo
Folsom, R. G.	University of Michigan
Forstall, W.	Carnegie Institute of Technology
Frankel, S. J.	Illinois Institute of Technology
Galowin, L.	Polytechnic Institute of Brooklyn
Gardiner, R. A.	NACA-Langley
Garrick, I. E.	NACA-Langley
Gatewood, B. E.	U. S. Air Force Institute of Technology
Gawain, T H.	U. S. N. Postgraduate School-Calif.
Gessow, A.	NACA-Langley
Gilruth, R R.	NACA-Langley
Ginsburg, A.	NACA-Lewis

Name	School
Graham, P. F.	Ohio State University
Greiner, H.	Renssalaer Polytechnic Institute
Grove, C. S.	Syracuse University
Grummann, H.	St. Louis University
Hakkinen, R. J.	Massachusetts Institute of Technology
Halfman, R. L.	Massachusetts Institute of Technology
Harper, J. H.	Georgia Institute of Technology
Harrington, R. P.	Renssalaer Polytechnic Institute
Hawthorne, Q. J.	Tri-State College
Hazen, D. C.	Princeton University
Head, R. M.	U. S. N. Postgraduate School-Calif.
Heaslet, M.	NACA-Ames
Heimerl, G.	NACA-Langley
Heldenfels, R.	NACA-Langley
Hertler, E. G.	University of Maryland
Hooper, I. P.	Rose Polytechnic Institute
Houbolt, J. C.	NACA-Langley
Hubbard, H. H.	NACA-Langley
Humble, L. V.	NACA-Lewis
Ingard, K. U.	Massachusetts Institute of Technology
Jackson, T. W.	Georgia Institute of Technology
Jennings, B. H.	Northwestern University
Johnsen, I. A.	NACA-Lewis
Johnson, H. A.	University of California
Jones, B.	University of Cincinnati
Kahr, C. H.	U. S. N. Postgraduate School-Calif.
Kaplan, C.	NACA-Langley
Kawamura, R.	Cornell University
Keister, P. H.	U. S. Air Force Institute of Technology
Kestin, J.	Brown University
King, W. J.	University of California at Los Angeles
Kochendorfer, F.	NACA-Lewis
Korkegi, R.	University of Southern California
Korst, H. H.	University of Illinois
Kuerti, G.	Case Institute of Technology
Lairabee, E. E.	Massachusetts Institute of Technology
Landon, R. D.	University of Akron

Name	School
Lane, F.	New York University
Langhaar, H. L.	University of Illinois
Lee, E. H.	Brown University
Lee, J. D.	Ohio State University
Lesher, E. J.	University of Michigan
Lessen, M.	University of Pennsylvania
Lew, H. G.	Pennsylvania State College
Lo, H.	Purdue University
Lopez, H.	Renssalaer Polytechnic Institute
Love, E. S.	NACA-Langley
Ludewig, J. W.	Carnegie Institute of Technology
Martin, H. C.	University of Washington
Martinuzzi, F.	Stevens Institute of Technology
Mathauser, E. E.	NACA-Langley
Mattica, H. C.	Renssalaer Polytechnic Institute
McCloy, R. W.	University of Illinois
McKay, W.	Massachusetts Institute of Technology
Meyerhoff, L.	Brooklyn Polytechnic Institute
Miller, R. H.	Massachusetts Institute of Technology
Miller, W. H.	Catholic University
Morgan, G. W.	Brown University
Morkovin, M. V.	Johns Hopkins University
Murphy, G.	Iowa State University
Myers, P. S.	University of Wisconsin
Nelson, W. J.	NACA-Langley
Nichols, M. N.	NACA-Langley
Niedenfuhr, F. W.	Ohio State University
Nielsen, J. N.	NACA-Ames
O'Brien, M. P.	University of California
Osterle, J. F.	Carnegie Institute of Technology
Pai, S. I.	University of Maryland
Painter, N.	University of Chicago
Palmer, C.	NACA-Washington
Pangborn, D.	Renssalaer Polytechnic Institute
Pasqua, P. F.	University of Tennessee
Paxton, H. W.	Carnegie Institute of Technology
Peery, D. J.	University of Michigan

Name	School
Pell, W. H.	Brown University
Pinkerton, R. M.	North Carolina State University
Polhamus, E. C.	NACA-Langley
Poulson, Capt. J. A.	U. S. Air Force Institute of Technology
Press, H.	NACA-Langley
Prior, J. A.	University of Pennsylvania
Probstein, R. F.	Brown University
Purser, P. E.	NACA-Langley
Ranov, T.	University of Buffalo
Raspet, A.	Mississippi State College
Reid, E. G.	Stanford University
Regier, A. A.	NACA-Langley
Reinath, F.	Ohio University
Rex, Maj. E. M.	U. S. Air Force Institute of Technology
Rhines, F. N.	Carnegie Institute of Technology
Rhode, R.	NACA-Washington
Richardson, A. S.	Massachusetts Institute of Technology
Riparbelli, C.	Cornell University
Robinson, R. G.	NACA-Ames
Roshko, A.	California Institute of Technology
Rott, N.	Cornell University
Rouleau, W. T.	Carnegie Institute of Technology
Rubesin, M.	NACA-Ames
Ruptash, J.	University of Wichita
Rutkowski, J.	Wayne University
Saltzer, C.	Case Institute of Technology
Sandorff, D. E.	Massachusetts Institute of Technology
Saxon, D.	University of Chicago
Schmitt, A. F.	Purdue University
Schwartz, F. L.	University of Michigan
Seiff, A.	NACA-Ames
Sellars, J. R.	University of Michigan
Seltzer, L. Z.	West Virginia University
Sevin, E.	Illinois Institute of Technology
Shen, S. F.	University of Maryland
Sherling, W. G.	Alabama Polytechnic Institute
Sherwood, A. W.	University of Maryland
Smith, K. E.	University of Detroit
Smull, T. L. K.	NACA-Washington

Name	School
Spreiter, J. R.	NACA-Ames
Stanley, P.	Purdue University
Stenning, A. H.	Massachusetts Institute of Technology
Stewart, O. W.	University of Kentucky
Stillwell, H. S.	University of Illinois
Stolworthy, E. H.	University of New Hampshire
Sutton, J. F.	Clemson University
Sutton, M. A.	Ohio State University
Swanson, W. M.	Case Institute of Technology
Syvertson, C. A.	NACA-Ames
Taylor, E. J.	Ohio University
Teichman, F. K.	New York University
Thompson, F. L.	NACA-Langley
Tifford, A.	Ohio State University
Trangott, S. C.	Johns Hopkins University
Truitt, R. W.	Virginia Polytechnic Institute
Upson, R. H.	University of Minnesota
Uyehara, O. A.	University of Wisconsin
Veletsos, A. S.	University of Illinois
Vincent, E. T.	University of Michigan
Von Eschen, G. L.	Ohio State University
Vopat, W. A.	Cooper Union Institute of Technology
Vuilleumier, R.	Stevens Institute of Technology
Walsh, E. T.	Case Institute of Technology
Ward, V. G.	Ohio State University
Watkins, C.	NACA-Langley
Waxer, L. J.	Boston University
West, C. T.	Ohio State University
Winternitz, P. F.	New York University
Wright, R. H.	NACA-Langley
Wulff, J.	Massachusetts Institute of Technology
Yates, C. C.	University of Pittsburgh
Yeh, H.	Johns Hopkins University
Yen, K. T.	Renssalaer Polytechnic Institute
Yuan, S. W.	Polytechnic Institute of Brooklyn
Zimmerman, R. H.	Ohio State University

8. THE NATURE OF AIRCRAFT NOISE SOURCES

By H. H. Hubbard and A. A. Regier
Langley Aeronautical Laboratory

INTRODUCTION

Aircraft noise is now a major consideration in the design and operation of aircraft. Noise intensities are sufficiently great to cause fatigue failures of the airplane structure, malfunctioning of the electronic equipment, and interference with communications, as well as the better known physiological effects such as annoyance discomfort and hearing impairment. The trend toward ever more powerful propulsion systems has been the underlying cause of these serious noise problems.

When thrust is generated, a certain percentage of the energy will appear in noise as a by-product. Although the amount of noise energy rarely exceeds 1 percent of the total energy, the amount can in some cases be rather large. In order to give some insight into the energy involved, the data of figure 1 have been estimated. The estimated noise energy per airplane in horsepower is plotted as a function of time for the 50-year period since the first flight. The curves in each case are drawn generally through the maximum values. Where actual data are not available, as for the earlier years, the noise powers are estimated to be equal to 0.5 of 1 percent of the engine power. In interpreting the data it should be recognized that the earlier jet and propeller airplanes had mainly single engines, whereas the later ones are multiengine aircraft. It can be seen that the amounts of noise energy have increased at least a thousandfold since the first airplane and the trend seems to be in an upward direction. Although very few data are available with which to compare the values on the ordinate scale, it can be said that some of our current airplanes radiate several times as much noise as the large air raid sirens used in World War II.

Because of these high noise intensities, the operators of aircraft have been forced to adopt some emergency measures in order to make the noise less objectionable. These measures, some of which are very costly, have been needed for alleviating noise problems in both the near and far noise fields. With respect to the community, which is associated with the far noise field, acoustic screening and muffling have been useful in test operations and preferential runways and rapid climbouts have been useful in flight operations. Personal protective devices, extensive sound treatments, and strengthening of the airplane structure have been resorted to in many cases to alleviate undesirable conditions in the near noise field.

The practical objectives of research on noise are (1) to find ways of reducing the noise at the source, (2) to devise ways of reducing its detrimental effects at the receiver, and (3) to be able to predict, noise-wise, the results of changes in design and operational procedure. In order to achieve these objectives, researchers have been trying to get a better understanding of the nature of the sources and the basic mechanisms by which noise is generated.

TYPES OF AIRCRAFT NOISE

Some of the various noise sources currently encountered on aircraft are listed in figure 2. They have been grouped for convenience into three broad classifications, namely; periodic noises, random or nonperiodic noises, and transient noises. Also on the figure are shown schematically the type of pressure-time history that would be radiated to the observer in each case.

Periodic noises are those having wave forms which repeat periodically as illustrated by the sample in figure 2, and include noise from several sources on the aircraft. Some of these sources are: (1) steady forces on rotating blades as for a propeller (ref. 1); (2) the wakes of blunt bodies (ref. 2); (3) edge tones arising from unstable flows in the vicinity of sharp edges (ref. 3); (4) pulsing flows as from a pulse jet (refs. 4, 5, and 6), or reciprocating engine exhaust (ref. 7); (5) rough burning in jets (ref. 4); and (6) shock resonance in jets (refs. 8 and 9).

Random noises are characterized by a pressure-time history which varies in amplitude in a random manner as shown in the figure. This classification comprises noise from such sources as jet mixing (refs. 9 to 14), boundary layers (ref. 15), and vortex shedding from streamline bodies (ref. 16).

Transient noises are similar in character to those from explosions. Pressures are thus observed as pulses which last for only a fraction of a second at the observer. Two examples of this type of noise are sonic bangs (refs. 17 to 19) and the starting of afterburners.

As a further indication of the general quality of these noises, frequency spectrums of a periodic and a random noise are included in figure 3. These are two photographs of the viewing screen of a Panoramic type analyzer and show relative pressure amplitudes on the vertical scale as a function of frequency on the horizontal scale. As an example of a periodic noise, the propeller noise spectrum is seen to contain several discrete frequency components each of which is steady in amplitude. On the other hand, the spectrum of noise from a solid-fuel rocket engine is shown to be continuous. This type of spectrum

contains essentially all frequencies in the audible range and the individual frequency components vary in amplitude in a random manner with time. This latter spectrum is an example of a random noise.

Figure 2 serves as a rough outline of the remainder of this paper. The properties of some of the basic acoustic sources are first discussed with the aid of figure 4 and several equations. Then an attempt is made to describe briefly the state of knowledge concerning the generation of some of the periodic, random, and transient noises listed in figure 2.

BASIC ACOUSTIC ELEMENTS

One approach to the problem of formulating aircraft noise is to attempt to represent the sources on the aircraft with some basic acoustic sources whose radiation properties are known. Some of the characteristics of three basic sources with which this paper is concerned, namely; the monopole, dipole, and quadrupole, will be discussed with the aid of figure 4 from reference 20 and various equations. As shown in figure 4, the simple source, or monopole, may be represented by a pulsating sphere that is periodically changing its volume. It sends out sound energy equally in all directions. The monopole source can be related to any part of the aircraft that is emitting fluid in a periodic fashion, such as reciprocating engine exhausts, pulsejet engines, rough-burning jets, and rockets. Such aircraft noise sources are characterized by rather high acoustic efficiency and a rather low dependence on velocity as compared with other sources.

The dipole which is represented by an oscillating rigid sphere is derived from two monopoles of opposite phase (source and sink) in close proximity. The radiation pattern has two lobes with maximums in the direction of the force. The dipole has been extensively used in the theory of propeller noise.

Although the quadrupole has been used for many years in the theory of light and in wave mechanics, it has been largely ignored in acoustics. There are several kinds of quadrupoles, and the one illustrated schematically on the last line of figure 4 represents a type of lateral quadrupole. It is derived from the dipole by placing two equal and opposite dipoles side by side. There is no net force, but a shear or moment. The radiation pattern from such a quadrupole is a four-lobed clover-leaf pattern. It was Lighthill (ref. 21) who first pointed out the possibility of jet-noise generation in free jets due to quadrupole sources.

The last two columns of figure 4 give a rough indication of the relative efficiencies of these sources and the way the acoustic energy

may be related to some velocity of the aircraft noise generator. The next to last column in figure 4 gives a rough indication of the relative efficiences of these sources, and is based on the sound radiation from a sphere oscillating in various modes at a frequency having a wavelength twice the circumference of the sphere. For a given amplitude of the sphere, it may be noted that at the frequency considered the monopole-type source has 1000 times the efficiency of the quadrupole-type source.

The last column relates the sound energy to the kinetic energy and the Mach number of the aircraft noise source. When one derives the expression for the radiation power of the various acoustic sources, certain relations of frequency and speed of sound appear in the expressions. For example, as shown in the last column of figure 4, the speed of sound a appears as the first power in the monopole, as a^3 in the dipole, and as a^5 in the quadrupole. On the basis of dimensional analysis and on the assumption that frequency varies directly as velocity of the aircraft noise generator, one may arrive at expressions such as are given in the last column. The expressions relate the acoustic energy to physical quantities of the aircraft noise generator. In these relations, ρ is the density of the air, V is the velocity of a jet or moving body, A is area, and a is the speed of sound in the air.

Experience has shown that a single source or multiple sources in random phase seem to follow the trends with velocity shown in the last column. As is illustrated by propeller vortex noise, which is random, the dipole representation indicates that the noise should vary as the velocity to the sixth power. This is borne out by experience. When the source is moving at high velocity or is not of random phase, the sound energy follows entirely different laws. As an example of this, the rotational noise of a propeller, which can be represented by dipoles with definite phase relations, varies as a much higher power of the velocity.

If a jet can be represented by random-phase quadrupoles, one might expect that the sound energy should vary as the eighth power of the velocity. Experience has generally substantiated this for the far noise field of a jet and this expression is commonly referred to as Lighthill's 8^{th} power law (ref. 21).

Mathematical expressions for the pressures p, generated by these three sources are shown by the following equations. They have been arranged in such a manner to point up their similarities and differences. Each equation is composed of magnitude and phase terms and the two higher order sources have, in addition, trigonometric terms which define their characteristic radiation patterns.

$$p_{monopole} = i\rho A\left(\frac{\omega}{r}\right)e^{i\omega\left(t-\frac{r}{a}\right)} \tag{1}$$

$$p_{dipole} = i\rho B \cos\varphi\left(\frac{\omega^2}{ra} + \frac{i\omega}{r^2}\right)e^{i\omega\left(t-\frac{r}{a}\right)} \tag{2}$$

$$p_{quadrupole} = i\rho c \sin\varphi \cos\varphi\left(-\frac{\omega^3}{ra^2} + \frac{3i\omega^2}{r^2a} + \frac{3\omega}{r^3}\right)e^{i\omega\left(t-\frac{r}{a}\right)} \tag{3}$$

$$p_{force} = \frac{F \cos\varphi}{4\pi}\left(\frac{i\omega}{ra} + \frac{1}{r^2}\right)e^{i\omega\left(t-\frac{r}{a}\right)} \tag{4}$$

The quantities A, B, and C are the strengths of the respective sources which are related in each case to the rate of fluid emission; F is the magnitude of a concentrated oscillating force; φ is the azimuth angle with respect to the axis of the source; ω is the angular frequency; and r is the distance to the field point.

Equation (4) is the pressure field due to a concentrated force (ref. 22). It has radiation characteristics similar to the fluid dipole and is often referred to as the pressure dipole. This equation is the one generally used in the treatment of the propeller noise problem. The equations have been used to calculate the radiation pattern and sound energy relations in figure 4. In making such energy calculations, only the terms which vary inversely as the first power of the distance, or the far-field terms, are used. In the calculations of pressures near the source, the terms that vary inversely as the square and cube of the distance should also be considered. These higher order terms have a lower power dependence on frequency and, hence, also on the velocity. On the basis of these equations, one then would expect a difference in the frequency content, and variation of sound pressure with velocity between near-field and far-field measurements. Some of the subjects touched on in the discussions of figure 4 and equations (1) to (4), will be discussed further in subsequent sections of the paper.

SOURCES OF AIRCRAFT NOISE

It is of interest now to consider some of the actual sources of aircraft noise from figure 2, and how they are related to the basic acoustic elements of figure 4 and equations (1) to (4). Some discussion is first given on the periodic noise from propellers, pulsejets,

and flow over circular cylinders. Random noise from jets and boundary layers are then discussed and finally brief mention is made of the sonic bang phenomenon.

Propellers. - The main source of propeller noise eluded the investigators for many years; however, a theory that relates the noise to the steady aerodynamic loads on the blades has been developed by Gutin in reference 1. Some of the basic concepts of this theory are shown in figure 5 from reference 23.

Force is plotted against time for an area in the disk of the propeller. Each time a blade passes this area, the air will receive a bump as indicated schematically in the top of the figure. This bump may be resolved by Fourier analysis into a steady component which is the useful thrust of the propeller, and a series of oscillating components whose frequencies are integral multiples of the bump frequency. These oscillating components are associated with the propeller noise and consist not only of the fundamental frequency but a large number of integral harmonics.

Calculations of the far-field noise of the first four harmonics of a two-blade propeller are shown in figure 6 as a function of propeller tip Mach number at zero forward speed. In the notation of this paper, m is the order of the harmonic and B is the number of blades. The sound pressure of each harmonic is noted to increase at a rapid rate as a function of tip Mach number. The higher order harmonics increase in amplitude at a faster rate than the lower ones. For example, the sound energy radiated at $mB = 2$ varies as the 10^{th} power of the velocity, and at $mB = 8$ the sound energy varies at the 18^{th} power of the velocity. This results in a crossing over at high tip Mach numbers so that some of the higher order ones are then most intense. This difference in the velocity dependence for the various harmonics is due to the particular phasing of the dipoles around the propeller disk. The summation of the pressures at the observer from the sources on the disk is an important feature of the propeller noise theory. The theory of reference 1, which was used for the calculations of figure 6, has given good agreement with experiment as indicated in references 23 to 26.

Increases in power and speed of multiengine propeller aircraft have resulted in serious noise problems particularly in the near field or fuselage. As a consequence, the theory for predicting noise from a static propeller has recently been extended by Garrick and Watkins (ref. 27) to include the effects of forward speed. Some sample results of near-field calculations by this theory are shown in figure 7 along with some recent experimental flight data from reference 28. Pressure amplitudes are plotted as a function of propeller forward Mach number for the first two harmonics of a four-blade propeller. The data apply to a point in the plane of rotation and for the operating conditions of the figure.

The theory shows that the pressures first tend to decrease somewhat and then increase quite rapidly as forward Mach number increases. This effect is greater for the second harmonic than for the fundamental. The experimental free-space data of figure 7 show essentially the same trends as the theory. It should be pointed out that these comparisons are at a single field point and during these studies, some discrepancies were noted between the theoretical and experimental fore and aft pressure distributions.

Pulsejets. - Periodic noise from propellers has been seen to arise from the steady forces on the blades and to be represented by acoustic dipoles. Another periodic noise source which utilizes other noise-generating mechanisms is the pulsejet engine. Some sample results from references 4 to 6 for this pulsing flow source are shown in figure 8. The radiation pattern of the noise is shown on the left side of the figure, while the pressure wave form at the observer is given on the right. The peaks in the pressure wave form correspond to the firing frequency of the engine, which is the rate at which fluid is being emitted. These changes in volume can be represented by a monopole source and, in fact, the total acoustic energy of the pulsejet can be estimated satisfactorily, based on the assumption that it is a monopole or simple source, and that the energy is thus radiated equally in all directions. Since the radiation pattern is somewhat distorted in the downstream direction, there is thus some indication that higher order sources are present. These sources may include dipole sources associated with the thrust forces on the fluid as well as quadrupole sources associated with the high-speed gas flows in the mixing region.

In the case of periodic noise where its generation involves essentially potential flow, the noise magnitudes can be calculated from a knowledge of the geometry and the flow conditions. The sources of noise from flow separation, turbulent flow, and turbulent mixing comprises vortex noise, boundary layer or aerodynamic noise, and jet noise. Calculations involving such random phenomena are inherently semi-empirical in nature. Thus, analytical treatments of these problems can furnish the general laws of behavior of the noise and can indicate how the noise varies with changes in the various parameters even though the analyses are generally incapable of predicting absolute magnitudes.

Flow over circular cylinder. - The generation of noise due to flow separation on a rigid body such as a circular cylinder has been studied by a large number of investigators. Although much information is available in the literature as, for example, references 2, 29, and 30, understanding of the phenomenon is incomplete. Some of the ingredients of this problem are shown schematically in figure 9 from reference 30. Air is flowing from left to right over a circular rod for Reynolds numbers in a range where discrete vortices are formed in the wake. Noise arises from the forces on the rod which are perpendicular to the flow and which

result from changes in circulation around the rod. It is believed that the bulk of the radiated noise comes from the region near the rod as enclosed by the box of dotted lines. This radiated noise can be represented by acoustic dipoles. In the ideal case where the vortices are not increasing or decreasing in strength, it appears that very little if any radiation would come from the wake and even in practical cases it is believed to be relatively small.

Jet noise. - Up to this point the discussion has been concerned with noise generated by flow pulsations that can be represented by monopoles and noise generated by external forces acting on the fluid that can be represented by dipoles. Noise that is generated in free space as by the turbulent mixing of a free jet will now be discussed. The fundamental question is: What is the mechanism by which the kinetic energy of fluctuating shear motions is converted to acoustic energy involving longitudinal compression waves?

In the case where flow is supersonic, Ribner and Moore (refs. 31 and 32) have shown that when a shear wave passes through a shock wave shear, entropy, and sound waves result. Hence, in this case, there is a well-defined mechanism for conversion of shear flows into compressional sound waves. In the case where the flow is subsonic or shock-free, the mechanism of noise generation is somewhat open to controversy.

The fundamental theoretical work on the relation of noise to turbulence has been done by Lighthill in reference 21. It has received considerable attention and has influenced much of the thinking and experimental work on this subject. He considered the problem in which a region of turbulence is placed in an acoustic medium at rest. Lighthill found that this turbulent region could be represented by a volume distribution of acoustic quadrupoles whose strength is related to the turbulent stresses in the fluid.

Since both theoretical and experimental studies have shown the noise from jets to be related to their flow parameters, a brief discussion of some of the available flow data for jets is given with the aid of figure 10, which is taken from the work of references 33 and 34. If a circular jet issues from a settling chamber into air at rest, the mixing region is made up of those smaller regions shown schematically in figure 10. A potential core, within which velocity is constant and no mixing takes place, extends downstream approximately 4.5 diameters. Surrounding this core is a turbulent annulus within which mixing starts. At increased axial distances the jet broadens out as more air is entrained. Although the jet boundaries are difficult to measure, they have been shown theoretically by Goldstein (ref. 35) to have an included angle of approximately 30°. Beyond approximately 4.5 diameters the whole jet is a mixing region and the mean flow velocities decrease with increasing axial distance. This transition region extends downstream to-

approximately 10 diameters after which the flow is considered to be fully developed (having a constant nondimensional velocity profile). Noise sources are believed to be distributed throughout the jet, but there is evidence that a large amount of the noise comes from those regions nearer the jet in which the turbulent shear is greatest. Early aerodynamic investigations of jet flows were concerned mainly with the fully developed region and only recently have data become available in the part of the jet relatively close to the nozzle.

As a matter of interest, a shadowgraph of a two-dimensional jet is shown in figure 11. The jet exit in this case is a 1- by 6-inch rectangle and the shadowgraph is oriented so that the short dimension is in the plane of the paper. Although figure 11 is not directly comparable to figure 10 it gives a qualitative picture of the flow near the nozzle.

The noise field of a jet is very complex and the results obtained in experiments may vary widely in intensity and frequency for different field points. Some sample measurements in the near- and far-noise fields of a high-temperature model jet are given in figure 12. Sound pressures are plotted as a function of velocity of the jet, for a point 2 diameters from the jet and also for a point 150 diameters from the jet. It can be seen that velocity is an important parameter in noise generation. The data for the far-field point correspond approximately to the eighth-power law, whereas the near-field data correspond more nearly to a fourth-power law. The fact that velocity has a larger effect in the far field than in the near field, might be expected from inspection of equation (3).

Boundary layers. - Another random-type noise is that generated in the boundary layer. In some cases this noise may be the most important component of noise inside the airplane, particularly at high flight speeds. The results of some laboratory boundary-layer noise experiments on a 24-inch-diameter disk are shown in figure 13. Sound pressures are plotted as a function of the peripheral velocity of the disk for two field points. One of these points is near the disk at approximately 1/8 inch from the disk surface and the other is located also at the half-radius station but approximately 6 inches from the disk surface. The data measured nearer the disk correspond approximately to a fourth-power law of velocity. This result is in agreement with various aerodynamic noise measurements inside aircraft. A limited amount of data for a field point away from the disk indicates that the laws of variation with velocity may be different in the far field than in the near field. This difference is an indication that the noise-generating mechanisms in the boundary layer are closely related to those in jets.

The data of figure 13 are for the frequency range 200 to 20,000 cycles per second and apply to a disk roughened with 40-mesh sand. Pressures measured for a smooth disk were lower in value by approximately the ratios of the drag coefficients.

Sonic bang. - In contrast to the periodic and random noises which can conveniently be observed for a long period of time, the transient-type noise is observed for only a fraction of a second as in the case of an explosion. Since the advent of sonic and supersonic flight, a transient phenomenon known as the sonic bang has been widely observed. One way in which this type of noise may be generated is shown schematically in figure 14. An aircraft traveling uniformly at the speed of sound has created disturbances at several points along the line of flight. Waves travel in all directions from the disturbance points also at the speed of sound, and in the direction of motion these wave fronts tend to coalesce to form a shock wave. The pressure discontinuity represented by the shock wave will continue to travel in the same general direction indicated in figure 14 even though the aircraft then speeds up, slows down, or changes direction. An observer in the proper location will then experience this pressure discontinuity as the sonic bang phenomenon.

Figure 14 indicates the type of sonic bang one may expect from maneuvers near sonic speed. These bangs have generally been observed at large distances from an aircraft executing such maneuvers and in the region ahead of the aircraft as it passed through sonic speed. Since sonic bangs may be expected whenever the component of velocity of an aircraft in the direction of the observer equals the speed of sound, sonic bangs associated with level flight at supersonic speeds may also be expected.

CONCLUDING REMARKS

The nature of some of the present-day aircraft noise sources has been discussed in elementary terms. It is hoped that the references will fill in some of the details concerning the physical phenomena which are outside the scope of the present paper. It is recognized that human tolerance to noise is limited and cannot be indefinitely extended as more powerful noise machines are created. Hence, there is a necessity for seeking a solution to this problem. Professor Bolt in reference 36 has indicated that this solution is a systems problem covering many human, physical, and operational factors, thus requiring much additional research. In this research the colleges and universities are playing an important role in the matters that have been discussed in the present paper as well as in many other phases of the problem.

REFERENCES

1. Gutin, L.: On the Sound Field of a Rotating Propeller. NACA TM 1195, 1948.

2. Yudin, E. Y.: On the Vortex Sound from Rotating Rods. NACA TM 1136, 1947.

3. Curle, N.: The Mechanics of Edge-Tones. Proc. Roy. Soc. (London), ser. A, vol. 216, no. A1126, Feb. 10, 1953, pp. 412-424.

4. Lassiter, Leslie W.: Noise from Intermittent Jet Engines and Steady-Flow Jet Engines with Rough Burning. NACA TN 2756, 1952.

5. Powell, Alan: The Noise of a Pulse Jet. Jour. Helicopter Assoc. of Great Britain, vol. 7, no. 1, 1953.

6. Veneklasen, Paul S.: Noise Characteristics of Pulsejet Engines. Jour. Acous. Soc. Am., vol. 25, no. 3, May 1953, pp. 378-380.

7. Stokes, George M., and Davis, Don D., Jr.: The Attenuation Characteristics of Four Specially Designed Mufflers Tested on a Practical Engine Setup. NACA TN 2943, 1953.

8. Powell, Alan: On the Noise Emanating from a Two-Dimensional Jet Above the Critical Pressure Ratio. Aero. Quarterly, vol. 4, 1953, p. 103.

9. Lassiter, Leslie W., and Hubbard, Harvey H.: The Near Noise Field of Static Jets and Some Model Studies of Devices for Its Reduction. NACA TN 3187, 1954.

10. Westley, R., and Lilley, G. M.: An Investigation of the Noise Field from a Small Jet and Methods for Its Reduction. Rep. No. 53, The College of Aero. (Cranfield, England), Jan. 1952.

11. Lassiter, Leslie W., and Hubbard, Harvey H.: Experimental Studies of Noise from Subsonic Jets in Still Air. NACA TN 2757, 1952.

12. North, Warren J., Callaghan, Edmund E., and Lanzo, Chester D.: Investigation of Noise Field and Velocity Profiles of an Afterburning Engine. NACA RM E54G07, 1954.

13. Callaghan, Edmund E., Howes, Walter, and North, Warren: Tooth-Type Noise-Suppression Devices on a Full-Scale Axial-Flow Turbojet Engine. NACA RM E54B01, 1954.

14. Greatrex, F. B.: Engine Noise. Jour. Roy. Aero. Soc., vol. 58, no. 520, Apr. 1954, pp. 223-235.

15. Rogers, O. R.: Noise Level and Its Variation with Position and Air Speed in the XCG-4 Glider. No. 29618 MR No. EXP-MS1/VF2 (Addendum 13), Air Materiel Command, Army Air Forces, June 23, 1942.

16. Krzywoblocki, M. Zbigniew: Investigation of the Wing-Wake Frequency with Application of the Strouhal Number. Jour. Aero. Sci., Jan. 1945, pp. 51-62.

17. Lilley, G. M., et al: On Some Aspects of the Noise Propagation from Supersonic Aircraft. Rep. No. 71, The College of Aero. (Cranfield, England).

18. Walters, A. G.: The Noise from Aircraft. Jour. Roy. Aero. Soc., vol. 58, no. 517, Jan. 1954, pp. 65-71.

19. Coughlin, William J.: Sonic Boom: A Potential Weapon? Aviation Week, vol. 60, no. 10, Mar. 8, 1954, p. 13.

20. Regier, Arthur A.: Why do Airplanes Make Noise. Reprint of paper presented at the SAE Nat. Aero. meeting, Hotel Statler, New York (N. Y.), Apr. 12-15, 1954.

21. Lighthill, M. J.: On Sound Generated Aerodynamically. I. General Theory. Proc. Roy. Soc. (London), ser. A, vol. 211, no. 1107, Mar. 20, 1952, pp. 564-587.

22. Lamb, Horace: Hydrodynamics. Sixth ed., Dover Pub., 1932, pp. 501-503.

23. Regier, Arthur A., and Hubbard, Harvey H.: Status of Research on Propeller Noise and Its Reduction. Jour. Aero. Soc. Am., vol. 25, no. 3, May 1953, pp. 395-404.

24. Deming, Arthur F.: Propeller Rotation Noise Due to Torque and Thrust. NACA TN 747, 1940.

25. Hubbard, Harvey H., and Regier, Arthur A.: Free-Space Oscillating Pressures Near the Tips of Rotating Propellers. NACA Rep. 996, 1950. (Supersedes NACA TN 1870.)

26. Hubbard, Harvey H., and Lassiter, Leslie W.: Sound from a Two-Blade Propeller at Supersonic Tip Speeds. NACA Rep. 1079, 1952. (Supersedes NACA RM L51C27.)

27. Garrick, I. E., and Watkins, C. E.: A Theoretical Study of the Effect of Forward Speed on the Free-Space Sound-Pressure Field Around Propellers. NACA TN 3018, 1953.

28. Vogeley, Arthur W., and Kurbjun, Max C.: Measurements of Oscillating Pressures Near a Propeller Tip at Flight Mach Numbers to 0.72. (Proposed NACA TN.)

29. Stowell, E. Z., and Deming, A. F.: Vortex Noise from Rotating Cylindrical Rods. NACA TN 519, 1935.

30. Blokhintzev, D.: The Acoustics of an Inhomogeneous Moving Medium. Trans. from Russian by Res. Analysis Group, Brown Univ., Providence, (R. I.), Aug. 1952.

31. Ribner, H. S.: Shock-Turbulence Interaction and the Generation of Noise. NACA TN 3255, 1954.

32. Moore, Franklin K.: Unsteady Oblique Interaction of a Shock Wave with a Plane Disturbance. NACA Rep. 1165, 1954. (Supersedes NACA TN 1165.)

33. Kuethe, Arnold M.: Investigations of the Turbulent Mixing Regions Formed by Jets. Jour. Appl. Mech., vol. 2, no. 3, Sept. 1935, pp. A87-A95.

34. Alexander, Lloyd G., Baron, Thomas, and Comings, Edward W.: Transport of Momentum, Mass and Heat in Turbulent Jets. Bull. No. 413, Eng. Exp. Station, Univ. Illinois, 1953.

35. Goldstein, S., ed.: Modern Developments in Fluid Dynamics. Vol. II. Oxford Univ. Press, 1943.

36. Bolt, Richard H.: Aircraft Noise Problem. Jour. Acous. Soc. Am., vol. 25, no. 3, May 1953, pp. 363-442.

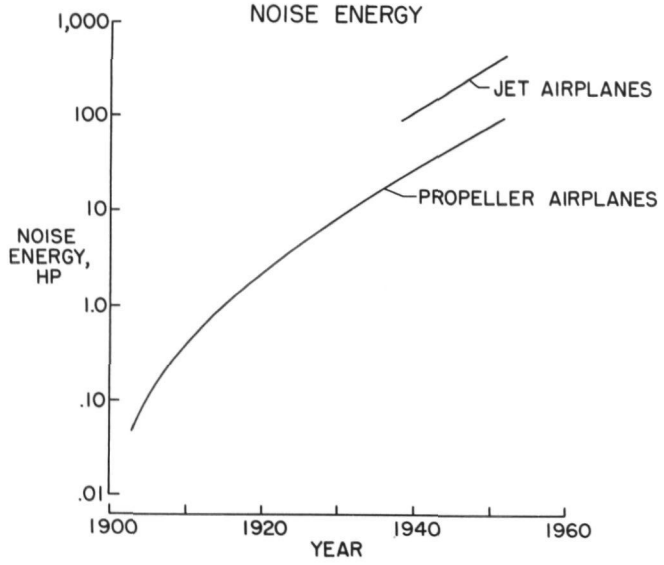

Figure 1

TYPES OF NOISE

PERIODIC

STEADY FORCES ON ROTATING BLADES
VORTEX SHEDDING FROM BLUNT BODIES
EDGE TONES
PULSING FLOWS
ROUGH BURNING IN JETS
SHOCK RESONANCES IN JETS

RANDOM

JET MIXING
BOUNDARY LAYERS
VORTEX SHEDDING FROM STREAMLINE BODIES

TRANSIENT

SONIC BANGS
STARTING OF AFTERBURNERS

Figure 2

NOISE SPECTRUMS

HIGH SPEED PROPELLER

SOLID FUEL ROCKET

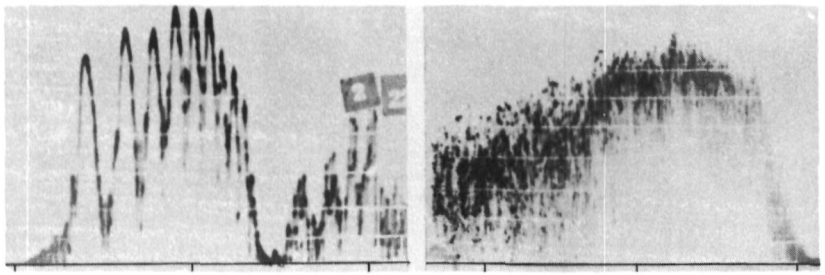

Figure 3

PROPERTIES OF ACOUSTIC SOURCES

SOURCE		REPRESENTS CHANGE	RADIATION PATTERN	RELATIVE ACOUSTIC EFFICIENCY	SOUND ENERGY FUNCTION OF -
TYPE	NAME				
	MONOPOLE	VOLUME		1	$\rho AV^3\left(\frac{V}{a}\right)$
	DIPOLE	FORCE	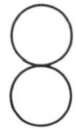	1/13	$\rho AV^3\left(\frac{V}{a}\right)^3$
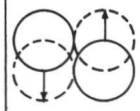	QUAD-RUPOLE	SHEAR		1/1,000	$\rho AV^3\left(\frac{V}{a}\right)^5$

Figure 4

IMPULSE TO THE AIR BY PROPELLER BLADE

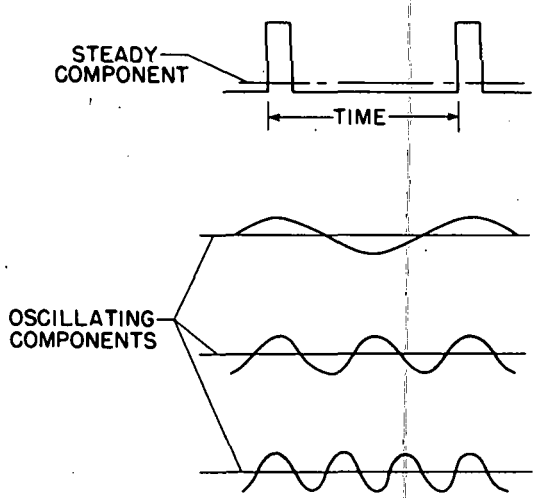

Figure 5

EFFECTS OF TIP MACH NUMBER

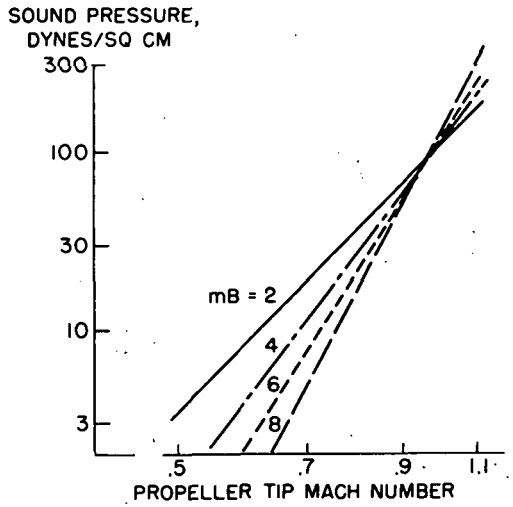

Figure 6

EFFECTS OF FORWARD MACH NUMBER

P = 1,050 HP; M_R = 0.72; DIAM. = 11.2 FT; TIP CLEARANCE = 1.5 FT

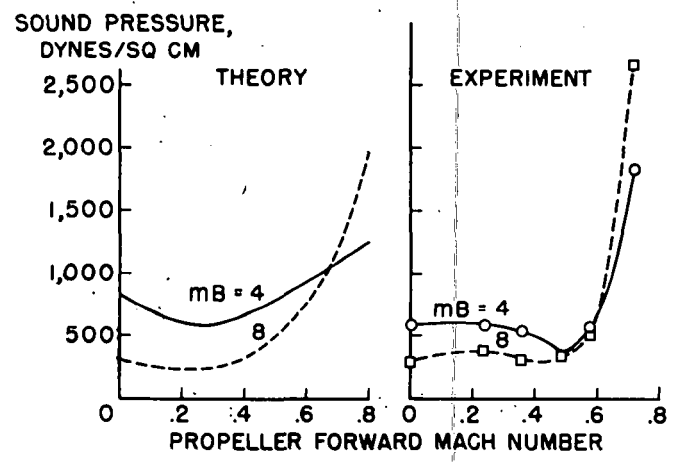

Figure 7

PULSE-JET NOISE

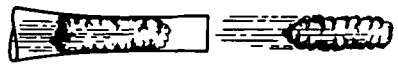

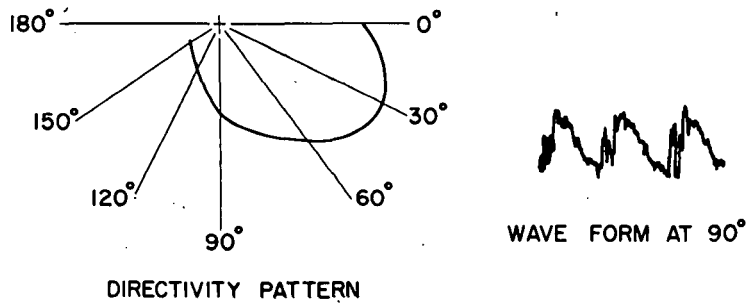

Figure 8

VORTEX NOISE FROM CIRCULAR ROD

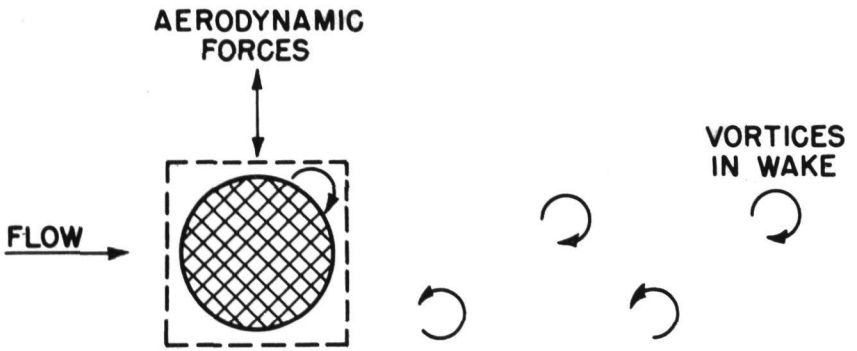

Figure 9

GENERAL FLOW REGIONS OF A JET

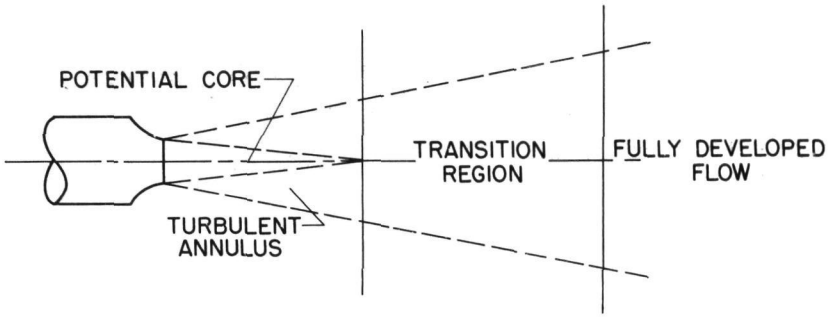

Figure 10

MIXING REGION OF TWO-DIMENSIONAL JET

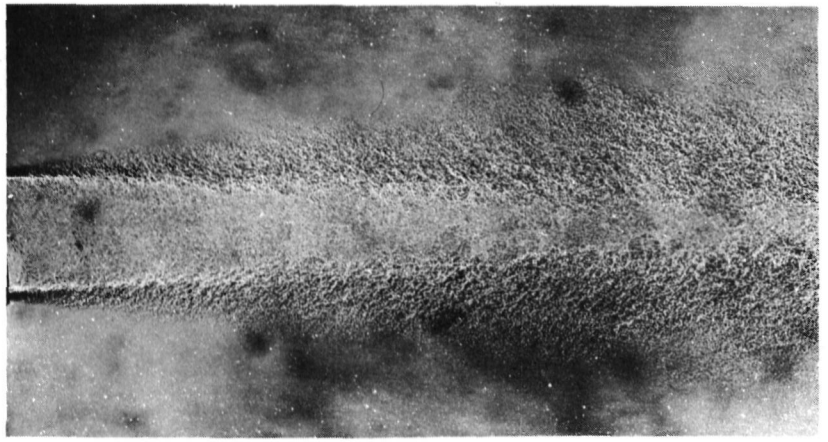

Figure 11

JET NOISE

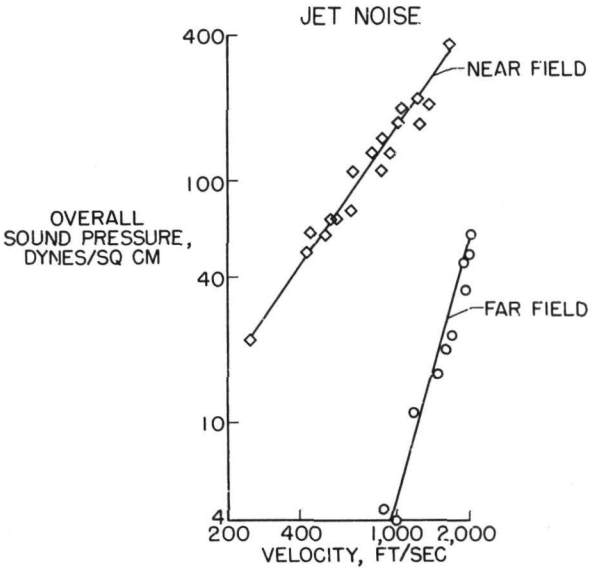

Figure 12

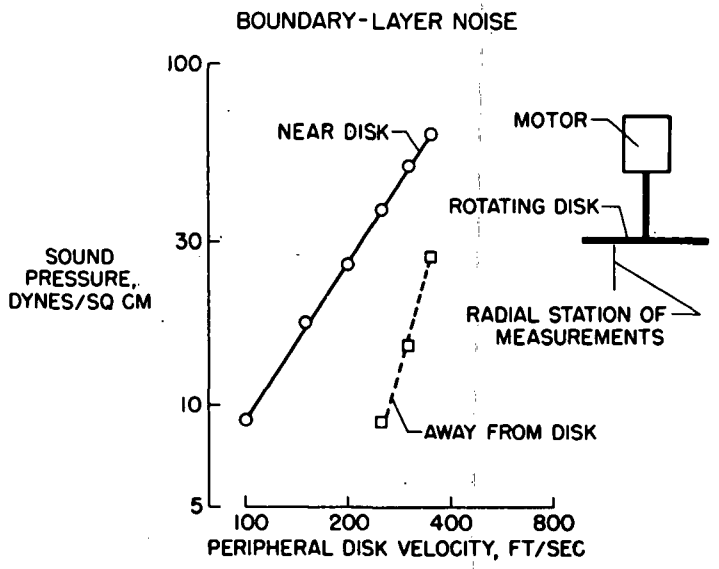

Figure 13

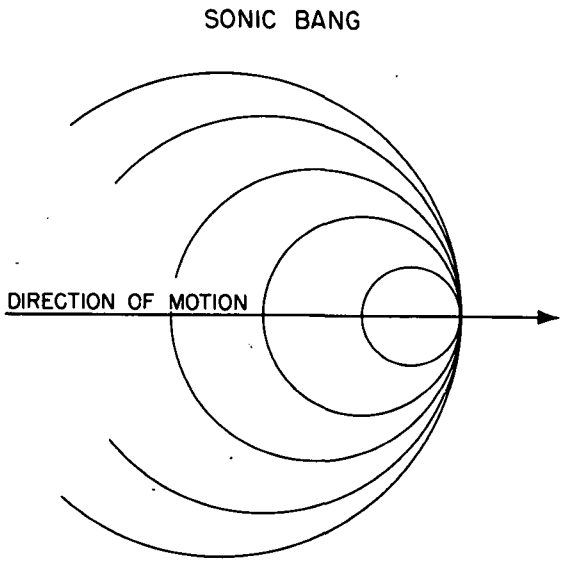

Figure 14

9. RECENT DEVELOPMENTS IN AERODYNAMICS OF HELICOPTERS

By Alfred Gessow and Richard C. Dingeldein
Langley Aeronautical Laboratory

INTRODUCTION

Although the helicopter has proved to be a very successful type of aircraft, it is still handicapped by a number of shortcomings that stand in the way of even more widespread use. Depending on the particular application, there are continuing needs for higher forward speed, greater load-carrying capacity, all-weather capabilities, decreased vibration and noise levels, improvements in power-plant design, and increased reliability and lower operating costs. As a result of an increased research and development effort, the understanding of helicopter aerodynamics has been expanded and this, in turn, has led to significant advances in the helicopter's capabilities in recent years. In this paper some of the recent progress made in predicting and understanding the aerodynamic behavior of the helicopter will be discussed. Instead of attempting a cursory review of all aspects of the subject, selected topics in rotor aerodynamics, helicopter stability and control, and helicopter load factors have been chosen.

ROTOR AERODYNAMICS

Extended rotor theory. - The computation of the characteristics of lifting rotors starts with the calculation of the resultant velocity and angle of attack at a blade element, typical pictures of which are shown in figure 1 for a low- and a high-speed helicopter. Once the resultant velocity and angle of attack are determined, the elemental forces can then be obtained with the use of appropriate airfoil data from which the forces produced by the rotor as a whole are obtained by integrating the elemental forces radially and azimuthwise over the disk. In order to simplify the integral equations, conventional rotor theory (ref. 1, for example) has assumed:

(1) Inflow angles small enough that the sine may be replaced by the angle and the cosine by unity

(2) Velocity at a blade element approximated by the tangential component

(3) Section lift and drag curves that do not account for stall, no matter how high the angle of attack

The theory based on these assumptions has proved perfectly satisfactory for predicting the aerodynamic behavior of today's operational

helicopters. However, for the higher-performance helicopters that are now being designed, and for helicopters having rotors that operate at very large attitudes (as in certain types of convertible aircraft), these assumptions break down in that, because of the greater forward tilt of the disk, the inflow angle φ is large and the resultant velocity can no longer be considered equal to the tangential component. Another aspect of high-speed flight is the existance of a large region of reversed velocity on the retreating side of the disk, which is normally highly stalled.

In order to make the theory applicable to high-performance helicopters, conventional theory was therefore extended to remove these assumptions (ref. 2). In extending the theory, use was made of the fact that, although φ and θ may be large, the section angle of attack α_r is ordinarily small. Any small-angle assumptions could therefore be more appropriately made to the angle of attack.

A comparison of the conventional and extended methods is illustrated in figure 2, which shows the computed ratios of profile power to thrust for two inflow conditions over a range of tip-speed ratios. At the low-inflow condition, corresponding to a low power, the two methods give essentially the same answers over the range of tip-speed ratios shown. At the high-inflow condition, corresponding to a high rate of climb or to a large forward tilt of the rotor at high speed, the two theories agree only at low tip-speed ratios and diverge very rapidly at the higher ones. At $\mu = 0.5$, the difference is about 2:1. Because some of the equations of the extended theory are lengthy, the thrust, power, and torque relations over a range of flight conditions were evaluated by the theory and are published in reference 3.

Although the extended theory takes into account stall in the reversed-velocity region, which occurs over the inboard portion of the retreating blades, it does not account for the more important stall that may also occur over the outboard portion of the retreating blades. Because the equations of the extended theory are already quite complex, it is not considered feasible to obtain closed-form equations that will take tip stall into account. Fortunately, it can be taken care of quite simply in specific cases by numerically integrating the elemental contributions to the rotor forces. Airfoil data that cover the extreme ranges of angles of attack encountered in such flight conditions are available for use in the calculations (refs. 4 and 5). Although the computing work is prohibitive by conventional calculating methods, the total time required is quite reasonable if high-speed automatic computers are used. By the same numerical procedures, other factors which are important in high-speed helicopter flight, such as hinge offset, blade mass factor, and root cut-out, can be taken care of in the same way.

Compressibility effects. - In addition to markedly increasing the profile power losses of the rotor, blade stall also imposes severe operational limitations on the top speed of the helicopter in the form of increased vibration and control difficulties. An effective way of achieving higher forward speeds with minimum-stall effects is to increase the rotor tip speed so that the blade-section angles of attack are reduced over the rotor as a whole or, in other words, to operate the rotor at lower mean lift coefficients. (See chart 10 of ref. 6 for a detailed discussion of rotor blade stall effects.)

The combination of high forward speeds and high tip speeds, if carried far enough, can lead to compressibility troubles on the advancing side of the disk, wherein the section velocities are highest, and to some extent on the rest of the disk wherein high angles of attack cause a reduction in the force-divergent Mach numbers. The limitations on helicopter forward speed brought about by the blade sections approaching and exceeding their force- and moment-divergent Mach numbers are not as well understood as stall limitations. Some limited experimental data are available, however (in ref. 7), that show the effects of compressibility on the performance of a helicopter rotor in the hovering condition. These data were obtained on the Langley helicopter tower for a rotor having relatively thick airfoil sections. The results are summarized in figure 3, which represents the nondimensional hovering performance of an untwisted rotor for several tip-speed values in terms of the variation of torque coefficient with thrust coefficient. The upper set of data points, representing operation at low tip speeds of 350 and 420 feet per second, wherein no compressibility losses are expected, compares favorably with a theoretical curve based on incompressible two-dimensional data. The data obtained at a tip speed of 770 feet per second are well represented by a calculated curve based on compressible section data. (The theory used for the calculations is presented in ref. 8.) The difference between the two sets of data represents the increase in power arising from the effects of compressibility.

Thus, the indications are that at least in hovering the primary effect of compressibility is a rapid increase in profile-drag power once the critical combination of tip angle of attack and tip speed is exceeded, and that the rate of growth of the rotor profile-drag losses, following drag divergence, can be predicted by calculations based on two-dimensional section data. Although similar theoretical predictions can be made for the forward-flight condition, the validity of using two-dimensional data to predict compressibility effects in forward flight has not yet been experimentally confirmed.

Aside from the effect on the power required, the hovering tests also indicated that the onset of compressibility appreciably increased

the rotor losses before any evidence of operating limitations due to vibration or loss of control was noted. The degree to which divergent Mach numbers can be exceeded over different parts of the disk before operating limitations set in still remains to be determined.

Some other methods, aside from increases in blade-section stall angle and rotor tip speed, which help delay both stall and compressibility limits are the use of more blades per rotor, higher blade twist, reduced parasite drag, and, for certain configurations, offset hinges. In order to achieve still higher forward speeds, it may be necessary to depart from the "pure" helicopter configuration. Two basic configuration changes that are being investigated in this regard are the addition of a propeller that can be used to change the forward tilt required or a fixed wing that can be used to unload the rotor and so delay both stall and Mach number limitations.

Rotor inflow. - Of fundamental importance in performance calculations, and indeed in calculations relating to stability, stress, and vibrations, is a knowledge of rotor inflow. The degree of exactness to which the rotor inflow must be known will vary with the type of calculation and the helicopter speed range under consideration. Although a precise determination of the inflow is very difficult to compute or to measure, enough information, both theoretical and experimental, has become available in recent years to be extremely useful in calculating and explaining various aspects of rotor behavior. A review of such information is published in a recent NACA paper (ref. 9). More detailed information on the distribution of rotor inflow has been obtained from recent Langley full-scale tunnel tests (ref. 10).

A sample of some of the data obtained in this study is shown in figure 4. The distribution of induced velocity along the longitudinal axis of the rotor plane, referred to the calculated value at the center of the rotor disk, is presented for a typical cruising flight condition. The measured points, shown by circles, are compared with the theoretical predictions based on uniform circulation along the rotor, indicated by the solid curve. The downwash is shown to increase in magnitude from a slight upwash at the leading edge of the disk to a maximum downwash at the trailing edge. In general, it is seen that the measured variation is predicted fairly well by the theory, both as to magnitude and shape. Although this agreement along the longitudinal axis looks fairly good, it is now known yet whether it is representative of the agreement along other axes.

In contrast to downwash distributions in the plane of the rotor, a quantitative evaluation of the vertical distribution of rotor downwash is important in designing and locating tail surfaces and in estimating interference effects of tandem-rotor configurations. A limited

number of such surveys was therefore made to determine the downwash distribution for a nonoverlapped tandem-rotor arrangement as compared with a single rotor. Figure 5 presents the vertical distribution of downwash in the longitudinal plane of symmetry at two locations: at the center of the front rotor, and just behind its trailing edge. The circles represent data obtained with an isolated rotor, and the solid line represents the theoretical prediction. The agreement between the two is fairly good. Adding the rear rotor to form a tandem configuration, as represented by the squares, did not change things very much except to cause a small upwash. In going from the centerline of the rotor to the trailing edge, we see that the local downwash angles have approximately doubled. Otherwise the agreement with single-rotor theory and the effect of adding the rear rotor are similar to what occurred at the centerline of the rotor.

The important point to be noted is that, for the rotor spacing tested, the rear rotor is enveloped in the fully developed wake of the front rotor. Therefore, the rear rotor effectively operates in a climb condition and thus absorbs more power than the front rotor in forward flight for the same thrust. In addition, the nonuniformity of the vertical distribution of downwash shown by the plots has a marked influence on certain stability and control characteristics of the tandem helicopter. The variation in downwash angle experienced by the rear rotor with attitude changes, for example, causes significant changes in angle-of-attack stability and speed stability. If, for example, the rear rotor were located in the upper region of reduced downwash, then an increase in fuselage attitude would cause the rotor to move into a region of increased downwash, thus adding to the instability with angle of attack.

Tandem helicopter power requirements. - The expanded use of multirotor configurations has brought about the need for evaluating different rotor arrangements from the standpoint of relative aerodynamic efficiency. As an example of some information that has been obtained on this subject (ref. 11), the power required over a range of level flight conditions for a tandem-rotor arrangement with no overlap will be reviewed. The power measurements are summarized in figure 6. The power absorbed by the front rotor, shown by the circles, is in good agreement with the results of calculations based on a single rotor. Considerably more power was measured for the rear rotor, although it produced about the same lift as the front rotor. When the rotor calculations were modified to include the increased induced-power losses of the rear rotor associated with its immersion in the fully developed downwash of the front rotor, the theoretical prediction is in reasonable agreement with the test results. Thus, the total power requirements for this particular tandem-rotor arrangement in level flight, obtained by adding the powers for the front and rear rotors, therefore can be predicted fairly well from the available single-rotor theory by considering the downwash effects on the rear rotor. A similar evaluation of the power requirements of a

coaxial-rotor arrangement has also been published in reference 11. This general configuration research is being continued for tandem- and side-by-side rotor arrangements to determine the effects of rotor overlap and gap.

STABILITY AND CONTROL

The subject of helicopter stability and control has received a great deal of attention from research workers during the past few years. The research effort has been directed along the lines of establishing minimum helicopter flying-quality requirements and towards establishing methods for predicting and satisfying these requirements. (See, e.g., ref. 12.) As a result, although not all of today's production helicopters have good flying qualities, enough information is available at present to design a general-purpose helicopter so that it has adequate stability and control in all flight conditions and can be flown by the pilot for relatively long periods without excessive fatigue. Although improvements have also been made in the handling characteristics of helicopters during instrument and precision maneuvers (ref. 13, e.g.), more information is needed to improve the flying-quality characteristics of special-purpose helicopters, particularly under instrument-flight conditions at the very low end of the helicopter speed range.

Helicopter stability theory has been developed to the point wherein it has proved extremely useful in finding means for satisfying the flying-quality criteria and for estimating whether a prospective helicopter will meet them. As for the fixed-wing airplane, helicopter stability theory involves both the determination of the applicable equations of motion and the necessary stability derivatives. The processes for handling equations of motion have been well established in conjunction with airplanes, and the modifications of these procedures for helicopter uses have been found a secondary problem in comparison with the provision of values of stability derivatives. In the past few years, considerable information has been published which permits the most pertinent rotor derivatives to be theoretically predicted with fairly good accuracy where no stall is present (ref. 14, for example). In the absence of analytical methods for determining derivatives under stalled conditions, the appropriate derivatives can be obtained from flight or wind-tunnel measurements.

An example of the usefulness of helicopter stability theory in flying-quality work is the theoretical estimation (published in ref. 15) of whether a prospective helicopter will meet the longitudinal divergence criterion. This criterion, which is illustrated in figure 7, states that, if the control stick were pulled back by a small amount and held, then in order for the maneuver stability to be satisfactory

to the pilot, the time history of the normal acceleration should become concave downward within 2 seconds. A bending over of the normal acceleration within 2 seconds has been found to insure the eventual leveling-off of the acceleration within a reasonable time.

If this time of 2 seconds is used in the theory to predict a boundary line separating combinations of significant stability derivatives which theoretically result in satisfactory characteristics or unsatisfactory characteristics, the result shown in figure 8 is obtained. The ordinate and abscissa represent stability derivatives that are important in determining the characteristics of the maneuver. Shown along with the theoretical curve are data points corresponding to several different helicopters. The derivatives for these configurations were measured in flight, and the adjacent number is the approximate time for the corresponding normal-acceleration time history to become concave downward. Although the location of the data points and the indicated times for the normal acceleration to become concave downward are subject to experimental error, it will be noted that the points for which the normal-acceleration time history becomes concave downward in less than 2 seconds fall in the satisfactory region; whereas, for times of more than 2 seconds and for the divergent case, the points fall in the unsatisfactory region. The theoretical curve is seen to be qualitatively correct in providing a boundary between satisfactory and unsatisfactory maneuver stability according to the 2-second criterion that is in reasonable agreement with the experimental results.

Helicopter stability theory has also proved useful in estimating the effects on helicopter characteristics of changes in the individual stability derivatives, and in indicating means for improvement. An example of this use of theory arose in connection with the flying-quality investigation of a tandem helicopter (ref. 16). As indicated by the experimental curve shown in the upper part of figure 9, a pulse disturbance of the helicopter control resulted in an unstable rolling velocity of short period. A theoretical calculation of the motion showed good agreement with the measured motion, both as to period and rate of growth. The theoretical studies showed that the primary source of the instability was a product-of-inertia effect due to the nose-down inclination of the principal longitudinal inertia axis with respect to the flight path. This effect is accentuated in the tandem type inasmuch as the moment of inertia in yaw is about 20 times greater than the moment of inertia in roll.

Because changes in inertia characteristics were not considered practical methods of improvement, calculations were made with an analogue computer in which only the stability derivatives were varied in order to find a basis for improvement; and it was predicted that a 50-percent reduction in rolling moment per degree sideslip angle would be

effective in preventing divergence of the oscillations. In order to check this prediction, the roll-due-to-sideslip derivative was changed experimentally by this amount by attaching plywood panels to the landing-gear struts of the helicopter, and the oscillation characteristics were again measured. As shown in the lower half of the figure, the predicted improvements were achieved, the oscillations now being about neutral. Thus, in this case, the theory was employed successfully to indicate the course to be followed in making an improvement.

As a result of theoretical studies and modifications made to the airframe design during the establishment of flying-quality criteria, a number of physical methods available to the designer for obtaining desired stability values by changing the airframe design have become apparent. These methods may be used either singly or in combination to affect one or more specific stability or control characteristics.

3556

MAXIMUM ROTOR LOAD FACTORS

In studying the pull-up characteristics of the helicopter, the designer is interested not only in stability characteristics but also in the loads imposed on the aircraft during the maneuver as well. A simple theoretical concept for estimating the maximum load factor that can be experienced by a helicopter in a given flight condition is to assume that, after the control displacement, the maximum thrust produced by the rotor occurs when each blade element in the rotor is operating at its maximum lift coefficient. The load factor thus produced would then be the ratio of the maximum lift coefficient of the blade sections to the mean lift coefficient of the rotor before the control displacement. A comparison of the maximum load factors as predicted by this method with those measured on two helicopters is shown in figure 10 (from ref. 17), which shows maximum load factors as a function of rotor mean lift coefficient. Considering the very simple concept on which the theory is based, the agreement of predicted and measured loads is quite good.

Aside from the agreement shown, the plot indicates that high-speed helicopters, which tend to operate at low mean lift coefficients, might be designed to withstand higher load factors than large, slow-flying, load-lifting helicopters that operate at high mean lift coefficients.

CONCLUDING REMARKS

From the results discussed it appears that recent research has provided methods by which the effects of various parameters on many helicopter characteristics can be analyzed theoretically. The analyses have contributed considerably to the understanding of the factors affecting some current helicopter problems.

Problems currently under study, for which a similar understanding is hoped, include improving the structural and mechanical reliability of the helicopter by a study of the vibratory loads experienced by the rotor and other helicopter components, by evaluating more thoroughly the effects of compressibility on design requirements and operating limitations, by obtaining satisfactory flying qualities in specialized applications involving low-speed instrument flight, and by improving the aerodynamic and propulsive characteristics of various helicopter propulsion systems.

REFERENCES

1. Bailey, F. B., Jr.: A Simplified Theoretical Method of Determining the Characteristics of a Lifting Rotor in Forward Flight. NACA Rep. 716, 1941.

2. Gessow, Alfred, and Crim, Almer D.: An Extension of Lifting Rotor Theory to Cover Operation at Large Angles of Attack and High Inflow Conditions. NACA TN 2665, 1952.

3. Gessow, Alfred, and Tapscott, Robert J.: Charts for Estimating Performance of High-Performance Helicopters. NACA TN 3323, 1954.

4. Wilson, Homer B., Jr., and Horton, Elmer A.: Aerodynamic Characteristics at High and Low Subsonic Mach Numbers of Four NACA 6-Series Airfoil Sections at Angles of Attack from -2° to 31°. NACA RM L53C20, 1953.

5. Critzos, Chris. C., Heyson, Harry H., and Boswinkle, Robert W., Jr.: Aerodynamic Characteristics of NACA 0012 Airfoil Section at Angles of Attack from 0° to 180°. NACA TN 3361, 1954.

6. Gessow, Alfred, and Myers, Garry C., Jr.: Aerodynamics of the Helicopter. The Macmillan Co., c. 1952.

7. Carpenter, Paul J.: Effects of Compressibility on the Performance of Two Full-Scale Helicopter Rotors. NACA Rep. 1078, 1952. (Supersedes NACA TN 2277.)

8. Gessow, Alfred: Effect of Rotor-Blade Twist and Plan-Form Taper on Helicopter Hovering Performance. NACA TN 1542, 1948.

9. Gessow, Alfred: Review of Information on Induced Flow of a Lifting Rotor. NACA TN 3238, 1954.

10. Heyson, Harry H.: Flow-Field Measurements Around Single and Tandem Rotors in the Langley Full-Scale Tunnel. NACA TN 3242, 1954.

11. Dingeldein, Richard C.: Wind-Tunnel Studies of the Performance of *Multirotor Configurations*. NACA TN 3236, 1954.

12. Gustafson, F. B.: Desirable Longitudinal Flying Qualities for Helicopters and Means to Achieve Them. Aero. Eng. Rev., vol. 10, no. 6, June 1951, pp. 27-33.

13. Crim, Almer D., Reeder, John P., and Whitten, James B.: Instrument-Flight Results Obtained with a Combined-Signal Flight Indicator or Modified for Helicoptor Use. NACA TN 2761, 1952.

14. Amer, Kenneth B., and Gustafson, F. B.: Charts for Estimation of Longitudinal-Stability Derivatives for a Helicoptor Rotor in Forward Flight. NACA TN 2309, 1951.

15. Amer, Kenneth B.: Method for Studying Helicopter Longitudinal Maneuver Stability. NACA TN 3022, 1953.

16. Amer, Kenneth B., and Tapscott, Robert J.: Studies of the Lateral-Directional Flying Qualities of a Tandem Helicopter in Forward Flight. NACA TN 2984, 1953.

17. Gustafson, F. B., and Crim, Almer D.: Flight Measurements and Analysis of Helicopter Normal Load Factors in Maneuvers. NACA TN 2990, 1953.

VELOCITIES, ANGLES, AND FORCES AT A BLADE ELEMENT

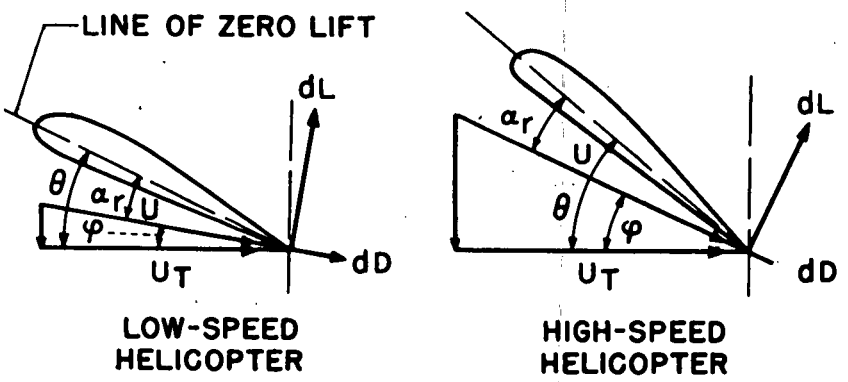

Figure 1

COMPARISON OF ROTOR PROFILE-DRAG POWER LOSS

$\frac{2C_T}{\sigma a} = 0.01$

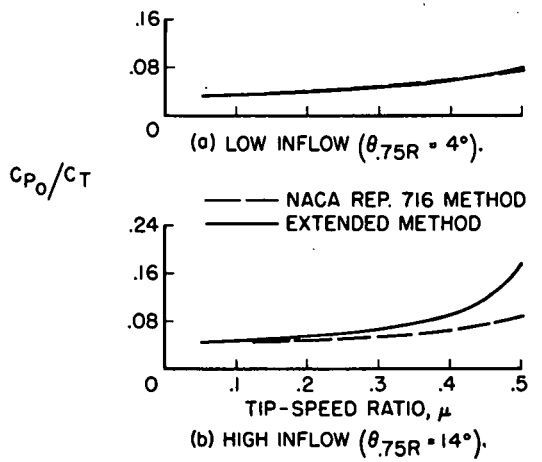

Figure 2

COMPRESSIBILITY EFFECTS IN HOVERING

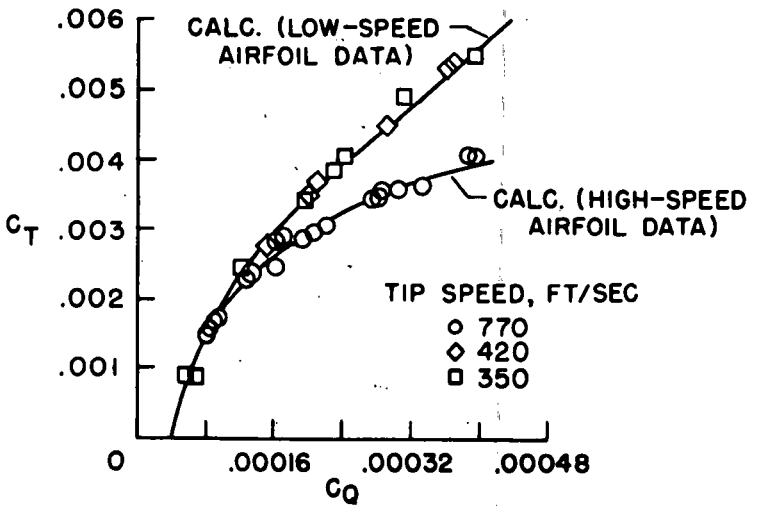

Figure 3

VARIATION OF INDUCED VELOCITY IN PLANE OF ROTOR

$\mu = 0.15$; $C_L = 0.32$

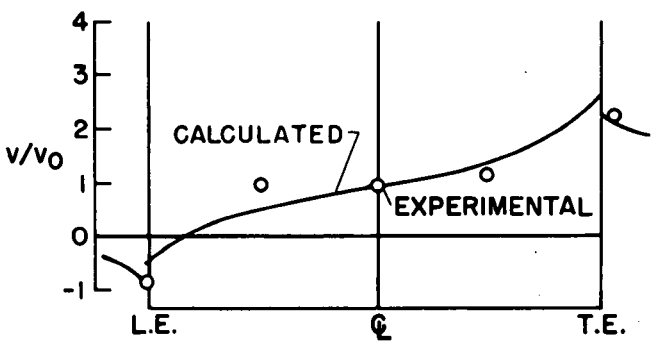

Figure 4

VARIATION OF DOWNWASH NEAR SINGLE AND TANDEM ROTORS

$\mu = 0.15$; $C_L = 0.30$

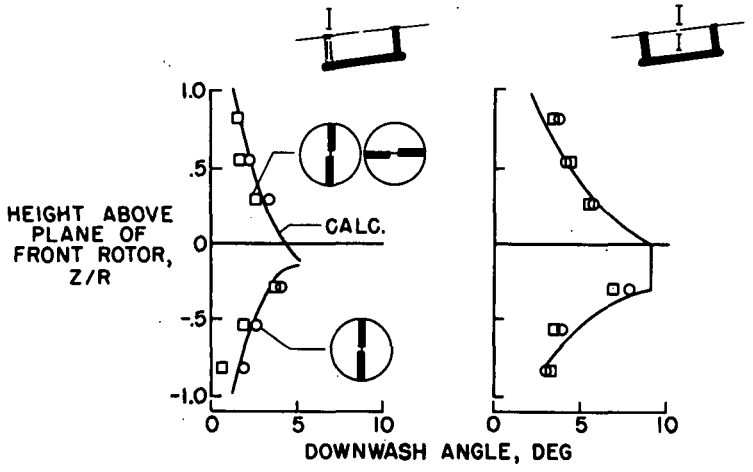

Figure 5

LEVEL-FLIGHT PERFORMANCE OF TANDEM ROTOR

$C_T = 0.0034$

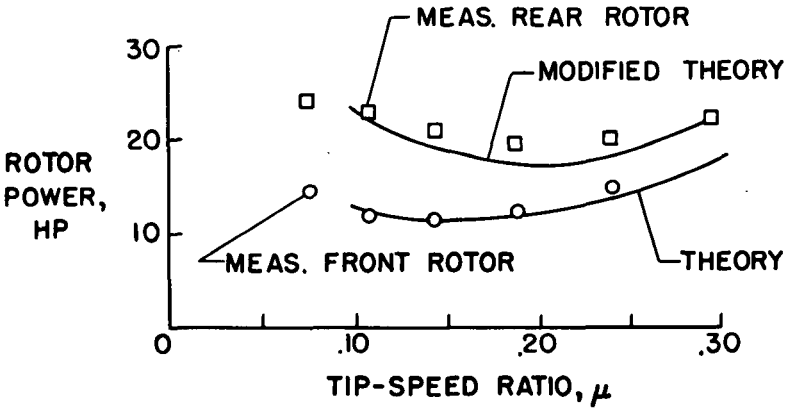

Figure 6

TYPICAL PULL-AND-HOLD MANEUVERS

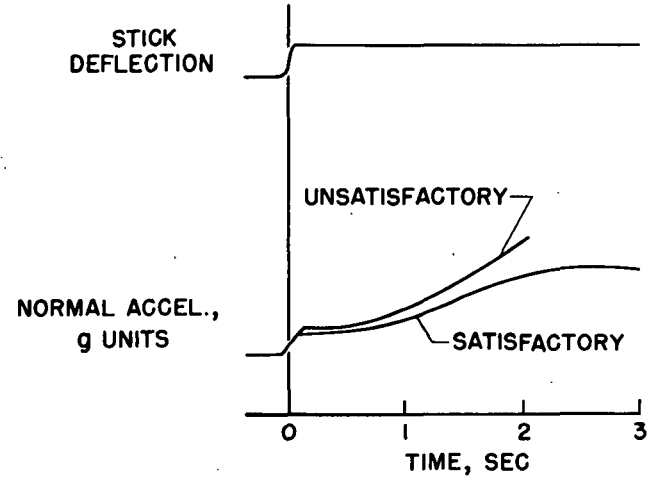

Figure 7

MANEUVER-STABILITY CHART FOR 2-SECOND CRITERION

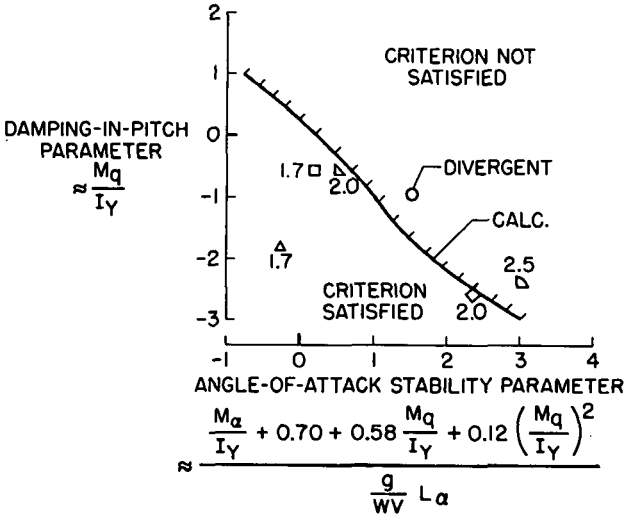

Figure 8

LATERAL OSCILLATIONS OF A TANDEM HELICOPTER

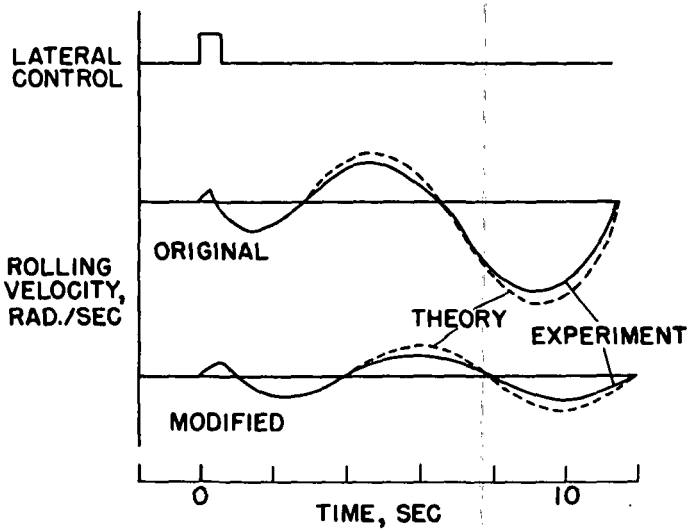

Figure 9

COMPARISON OF THEOR. AND FLIGHT-TEST VALUES OF MAX. LOAD FACTOR

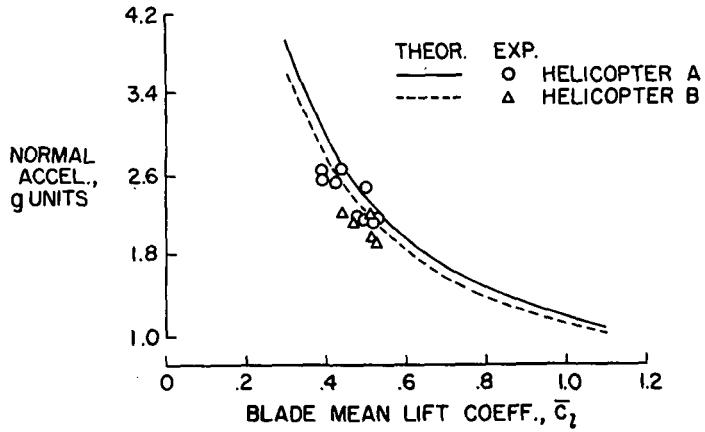

Figure 10

10. FLIGHT EFFICIENCY OF HIGH-SPEED AIRPLANES

By Mark R. Nichols
Langley Aeronautical Laboratory

INTRODUCTION

It is now quite apparent that most first-line combat airplanes of the immediate future must be able to fly at supersonic speeds in order to accomplish their missions. In order to achieve supersonic flight, the designer has been forced to utilize entirely new types of airframes in conjunction with jet or rocket engines. The characteristics of these airframes and engines differ greatly from their predecessors and, in addition, do not match each other as well throughout the flight range as was previously the case. The net result is that range and endurance problems have become far more critical and now play even greater roles in determining the airplane's configuration. The purpose of this paper is to review and explain this situation. The analysis presented is based on representative airframe and engine characteristics estimated, for the most part, from the information given in generally available papers, such as those listed in the references.

DISCUSSION

The way in which speed-altitude characteristics have changed is illustrated in figure 1. The data on the left are for a subsonic reciprocating-engine airplane similar to the B-29 flying at its combat weight. This airplane could cruise with 95 percent or greater of its maximum range efficiency, expressed in terms of miles per gallon, over the range of conditions defined by the shaded area. The choice of cruise altitude was fairly arbitrary because of the ability of the supercharged engine to maintain essentially constant power and efficiency over a broad range of altitude. The choice of cruise speed was rather limited, however, and there was only a small margin between these cruise conditions and the high-speed condition defined by the solid line.

The data in the right part of figure 1 pertain to a hypothetical supersonic jet airplane intended for the same general mission and also flying at its combat weight. This airplane can cruise efficiently only at high subsonic speeds and at altitudes near the tropopause. The maximum possible speed is very much higher than the cruise speed. The change from the one condition to the other, however, involves an increase in the kinetic energy of the airplane equivalent to a gain in altitude of nearly 25,000 feet and consequently requires an appreciable length of time and the expenditure of a large amount of fuel. Hence, it

may not be economical, or even possible, to accelerate all the way from the cruise speed to the maximum speed in the course of a normal mission.

The minimum level-flight drags for the two airplanes are presented in terms of their respective gross weights in figure 2. The parameter D/W is the inverse of the lift-drag ratio. The operating altitude varies continuously along each curve so that each airplane is always flying at its best attainable lift-drag ratio at each Mach number. (It will be explained later that this lift-drag ratio is not necessarily the same as the maximum lift-drag ratio of the airframe alone because of altitude limitations imposed by the engine.) The subsonic airplane had a very low cruise drag of about 6 percent of its gross weight, primarily because of its high aspect ratio. The maximum speed was limited by both compressibility effects and lack of power. Because of the lack of power, the airplane could fly only a little way up the compressibility drag rise. The drag-weight ratio remained fairly low, therefore, even in the high-speed operating condition.

The cruise drag of the hypothetical supersonic airplane is appreciably higher than that of the subsonic airplane, mainly because of its reduced aspect ratio. This and other features incorporated in the design (such as reduced wing thickness ratio, wing sweep, and increased body fineness ratio), however, greatly delay and reduce the magnitude of the transonic drag rise. The minimum drag of this particular supersonic airplane nearly doubles in the transonic range and then continues to increase with increasing Mach number. At the maximum Mach number of 1.56, as limited by engine thrust, it reaches the very high value of about 40 percent of the airplane weight or, in other words, the lift-drag ratio is about $2\frac{1}{2}$. These low lift-drag ratios are another reason for not flying at the maximum possible speed. In this case it would be desirable to limit the maximum Mach number for sustained flight to perhaps 1.4, where the lift-drag ratio is approximately 5.

The airframe designer, of course, has some control over the airframe drag and the lift-drag ratio. Estimated maximum lift-drag ratios for several airframes are plotted as a function of Mach number in figure 3. Progressing from left to right, the wings of these airframes have the following over-all geometric characteristics:

Aspect ratio	Average streamwise thickness ratio	Sweep, deg	Taper ratio
11	0.12	0 (c/4)	0.5
8	.12	35 (c/4)	.5
4	.06	45 (c/4)	.3
2.3	.03	60 (l.e.)	0

The first and third configurations from the left are the ones discussed in the preceding figures.

The first major aerodynamic advance in airframe design after World War II was the incorporation of sweep. The wing of the second airframe from the left is swept 35° and has an aspect ratio of 8 compared with 11 for the straight-wing airplane. This change in wing geometry delays adverse compressibility effects up to high subsonic speeds. In addition, because of the compactness of the jet engines and the elimination of a large amount of cooling drag, it also is possible to obtain a significant increase in lift-drag ratio compared with that for the reciprocating-engine airplane. This increase and the light weight of the jet engine are, of course, the basic factors that make the jet transport possible.

The lift-drag ratio for the second configuration of figure 3 becomes very low near $M = 1.0$. It is therefore necessary to further reduce the wing thickness ratio and to increase the body fineness ratios, as is done progressively in the two configurations on the right, in order to attain usable values of lift-drag ratio at supersonic speeds. An increase in wing sweep also would be of benefit in the low supersonic range. In all cases, a progressive decrease in aspect ratio is needed to compensate for the decrease in wing strength occasioned by the reduction in wing thickness ratio. The main points to note are that the lift-drag ratios always are much greater at subsonic speeds than at supersonic speeds and that the changes in design which provide increases in lift-drag ratios at supersonic speeds generally have important adverse effects on the lift-drag ratios at subsonic speeds. The designer must weigh this trade in lift-drag ratio carefully in choosing an airframe configuration to suit his particular purpose.

The engine efficiency picture also has changed. Over-all efficiencies of typical reciprocating and jet engines are plotted as a function of Mach number in figure 4. The over-all efficiency is the product of

two parts: (1) the cycle efficiency, which is concerned with the conversion of the available heat energy of the fuel into kinetic energy of the air on which the engine acts; and (2) the propulsive efficiency, which is the ratio of the thrust energy to this kinetic energy. The propulsive efficiency is the dominant variable at the low flight speeds for these two types of engine.

The reciprocating engine transmits its power to a propeller which then obtains thrust by increasing slightly the velocity of the large mass of air on which it acts. The kinetic energy lost in the slipstream is small relative to the thrust energy so that the propulsive efficiency and, consequently, the over-all efficiency are high even at very low speeds. The over-all efficiency remains high up to the point where the propeller itself encounters adverse compressibility effects. In contrast, the jet engine obtains its thrust by increasing the velocity of a small mass of air -- its internal flow -- a small amount. Thus, its efficiencies are very low at low speeds, but increase rapidly with flight Mach number. Its over-all efficiency at rated thrust becomes approximately equal to that for the reciprocating-engine - propeller combination at high subsonic speeds and finally approaches the maximum values for the reciprocating-engine - propeller combination at high supersonic Mach numbers. The efficiency of the afterburning jet engine falls well below that of the nonafterburning engine because of the much greater velocity of its exhaust. The maximum afterburning thrust case is illustrated.

Two points should be noted in figure 4. First, the over-all efficiency of the jet engine throughout the range of subsonic speeds of interest for take-off, climb, loiter, cruise, and so forth, is well below that for the reciprocating-engine - propeller combination. Second, in most present designs, the afterburner must be used everywhere above sonic speed in order to obtain the required thrust. Thus, if the airplane is flying in the Mach number range from 1 to 2, the over-all engine efficiency still is low compared with the maximum values for the reciprocating-engine - propeller combination at subsonic cruise speeds.

It is necessary to combine the engine and airframe variables in order to fully appreciate how the over-all flight efficiency has changed. Figure 5 presents typical results of range calculations made by use of the well known Breguet range equation. As shown in the upper right-hand part of the figure, this equation in general form states that range is equal to the available heat of combustion of the fuel × the over-all efficiency of the power plant × the airplane lift-drag ratio × the natural logarithm of the ratio of airplane gross weights before and after the cruise.

These calculations are highly idealized. Each curve applies to a family of airplanes of the configuration illustrated, all of which

have the same initial gross weight. The engine size or the engine operating conditions or both vary from point to point along each curve as required to optimize the range for the particular Mach number considered. (A reduction in the required engine size improves the lift-drag ratio and increases the amount of fuel that can be carried.) In addition, each airplane is assumed to begin its flight at its maximum gross weight and at the optimum flight altitude for the Mach number considered and to continue flying under optimum conditions at this Mach number until all its fuel is exhausted.

The two airplanes discussed previously fit into the families identified by the previously used illustrations and are the optimum configurations for reciprocating-engine and jet-engine airplanes at Mach numbers near 0.3 and 1.0, respectively. The reciprocating-engine airplane has an initial gross weight of 135,000 pounds of which about one-third is fuel. The supersonic airplane, which is equipped with turbojet engines having approximately the most favorable weight, frontal-area, and specific-fuel-consumption characteristics to be expected in the next several years, has an initial gross weight of 210,000 pounds of which nearly one-half is fuel. This difference in initial gross weight is necessary in order that the two airplanes be able to fly complete practical missions of the same radius, such as will be discussed later. All airplanes of the three swept-wing families use comparable turbojet engines and have the same initial gross weight of 210,000 pounds.

The maximum possible range of the family of reciprocating-engine airplanes drops off continuously with increasing Mach number. At first, in the region where the lift-drag ratio is nearly constant, this decrease is caused merely by the increase in engine power required to maintain constant thrust as the Mach number increases. (With constant power, the thrust would be inversely proportional to the flight speed.) Either the engine operating power is increased, thereby increasing the specific fuel consumption, or the engine size is increased, thereby adversely affecting the lift-drag ratio and reducing the amount of fuel that can be carried. At the higher Mach numbers, the range capability curve becomes even steeper because of compressibility effects on the airframe and propeller.

In the case of the turbojet airplanes, the optimum number and size of engines do not vary appreciably with speed in the subsonic region of essentially constant lift-drag ratio, because the jet-engine thrust tends to remain approximately constant in this range of Mach number rather than to decrease as does the thrust of the reciprocating engine. The maximum possible range therefore increases, as the engine efficiency increases, up to the point where the lift-drag ratio starts dropping off abruptly.

Except for the trend just discussed, the range variations for the three families of jet airplanes resemble the variations in the airframe

lift-drag ratio of figure 3 in many respects. The attainable range is a maximum at high subsonic speeds and decreases drastically when the design Mach number is shifted from subsonic to supersonic speeds. This result is caused partly by the abrupt decrease in airframe lift-drag ratio and partly by increases in the weight, specific fuel consumption, and nacelle drag of the engines. Also, the design changes made to permit supersonic flight (reduced wing aspect and thickness ratios, wing sweep, and a different type engine) reduce even its subsonic range capability far below that for an airplane designed solely for subsonic speeds. The more the supersonic efficiency is emphasized, the greater the loss at high subsonic speeds.

The curve of range capability against Mach number for the family of low-aspect-ratio swept-wing airplanes of figure 5 is compared in figure 6 with the range capability curve for the previously discussed airplane of the family that is optimum, as indicated by the x symbol, at $M = 1.0$. The effect of fixing the engine size rather than permitting it to vary continuously with Mach number, as can only be done analytically, is to cause important decreases in range capability at Mach numbers well above and well below the design point. In all cases, however, the attainable range continues to be much greater at subsonic than at supersonic speeds. For this reason, most supersonic turbojet airplanes of the near future may be expected to do most of their cruising at high subsonic speeds and to fly at supersonic speeds only in brief dashes. Thus, two widely separated regimes are of importance to the designer and he is faced with a critical choice concerning the degree to which the supersonic flight efficiency should be emphasized at the expense of flight efficiency in cruise. This choice can be made only on the basis of mission requirements.

In addition to the range capability losses caused by the engine sizing problem (fig. 6), additional important losses come about in the actual case because the airplane must take off, land, and fly over a broad range of off-design operating conditions. Engine and airframe characteristics will now be examined in somewhat greater detail in order to explain both types of losses.

Some effects of altitude on the performance of a typical turbojet engine are presented in figure 7. The ratio of the specific fuel consumption to that at 35,000 feet (approx. the tropopause) and the ratio of the thrust coefficient to the thrust coefficient also at 35,000 feet are plotted against altitude for flight Mach numbers of 0.9 and 1.8. Specific fuel consumption is defined as the weight of fuel consumed per hour per pound of thrust, and the thrust coefficient is the engine net thrust expressed in the same terms as the airplane drag coefficient. The variations shown are approximately applicable to either the rated thrust cases or the afterburning thrust cases. The main things to note

are that the engine specific fuel consumption becomes a minimum and the engine thrust coefficient becomes a maximum in the lower part of the stratosphere. With usual design practices, these characteristics require the airplane to cruise in or just below this region of the atmosphere in order to realize the maximum possible fuel economy and cause its maximum speed to occur at approximately the lower limit of this region.

Some effects of partial-power operation and Mach number on the performance of the turbojet engine in the lower part of the stratosphere, the region where its performance is most favorable, are illustrated in figure 8. Specific fuel consumption is plotted against thrust coefficient for the same two Mach numbers with all values shown normalized relative to the rated-thrust values for $M = 0.9$ as defined by the circular symbol. The engine thrust coefficient is reduced below the rated-thrust value by reducing the engine rpm and is increased above this value by use of the afterburner. Pressure losses and drags associated with the intake and jet exits have been taken into account along with corrections for accessory and auxiliary power. The most important new characteristic shown is that the maximum afterburning thrust coefficient at $M = 1.8$ is no larger than the rated thrust coefficient at $M = 0.9$. This zero variation is in marked contrast to the large increase in airplane drag coefficient between the same two Mach numbers due to the development of the pressure drag. Thus, as indicated by the square symbol, it is necessary to install an engine that is greatly oversize with regard to the cruise condition (and to operate it in cruise at the lowest percent thrust consistent with obtaining low specific fuel consumption) in order to allow some margin in thrust coefficient for overcoming the transonic drag rise. This situation brings about the important engine sizing or, more accurately, the airframe-engine matching problem that will be discussed in greater detail with the use of the next figure.

The lift-drag ratio of a bomber-type airframe is plotted against lift coefficient for a series of Mach numbers in the left half of figure 9. In order to obtain the maximum possible range, it would be desirable to fly in the lower part of the stratosphere and at approximately the maximum lift-drag ratio at each Mach number -- in other words, along the dashed line. The corresponding schedule of lift coefficient corresponds to a fixed variation of altitude with Mach number if the wing loading is fixed, as it always is in the case of a real airplane. The dashed curve in the right part of the figure defines the altitudes at which this particular airframe would have to fly in order to operate at maximum lift-drag ratio if the wing loading were a representative combat value of 70 pounds per square foot. These optimum altitudes vary from about 35,000 feet for the Mach 0.9 cruise condition to the extremely high altitude of 69,000 feet for a Mach 2.0 supersonic dash condition.

At this point one of the very serious consequences of nonmatching of the engine and airframe characteristics is encountered. The engines of the particular airplane considered were sized so that it could cruise at M = 0.9 at 35,000-foot altitude with about two-thirds of its rated engine thrust. Even so, when a thrust-available, thrust-required type of analysis is made using the assumed thrust characteristics of these engines and the airframe characteristics given on the left, it is found that this airplane can fly only up to the altitudes limited by the lower boundary of the right part of the figure with rated thrust and only up to the altitudes limited by the higher boundary with maximum afterburning thrust. Thus, the dotted curve can be followed only up to the upper boundary.

When the airplane is flown at the higher attainable Mach numbers, such as the values identified by the circular and square symbols in the right part of figure 9, it necessarily operates at altitudes and lift coefficients well below the optimum. In consequence, as shown by the corresponding symbols on the left, the flight lift-drag ratio is only three-fourths of the maximum value possible at a Mach number of 1.4 and one-half of the maximum value possible at the maximum Mach number of 1.56. Thus, the actual flight efficiency in the higher Mach number dashes is appreciably lower than was indicated by idealized range calculations of the type presented in figure 5. Losses of this type did not occur in the case of the reciprocating-engine airplane because engine supercharging permitted the attainment of near optimum altitudes in the high-speed flight condition.

To recapitulate briefly, the flight efficiency of the supersonic airplane suffers in two ways through basic nonmatching of the airframe and engine characteristics. It is penalized first at subsonic speeds by the engine being unnecessarily large and heavy, and then it is penalized again at supersonic speeds by the combination of high airframe drag and insufficient engine thrust preventing the attainment of the optimum flight altitudes. This situation is expected to persist for a long time. Significant improvement can be obtained only by finding ways to improve airframe lift-drag ratios at the lower lift coefficients at supersonic speeds without reducing the maximum lift-drag ratio at high subsonic speeds and by finding ways to obtain greatly increased engine thrust per unit frontal area and per unit weight in the high-altitude, high Mach number case without penalizing engine performance in take-off and cruise to an unacceptable extent.

As was mentioned previously, changes in airframe, engine, and mission characteristics also have caused important changes in operating efficiency in the off-design flight conditions. Typical flight plans for the long-range bomber-type airplane previously discussed are presented in figure 10. Flight altitude is plotted against range with

flight Mach numbers spotted on the curves. The reciprocating-engine airplane operated the equivalent of 5 minutes at normal power on the ground in warm-up and taxiing and then took off and climbed at rated power. Inasmuch as the cruise efficiency was high over a broad range of altitude, it was possible to fly the initial part of the mission at low altitudes in order to lighten the airplane before climbing along the dotted line to the target altitude. At the target altitude a high-speed run was made to the target with military power followed by a 180° turn, indicated by the loop in the curve, and then by an escape dash also at high speeds and altitudes. Following the escape dash, it was possible to make an efficient let-down followed by a cruise home at some arbitrary lower altitude. Loitering over base could be accomplished efficiently at a low percentage of power either at altitude or at sea level because of the efficiency characteristics of the propulsion system.

The flight plan and operating efficiency of the supersonic jet airplane differ from those of the reciprocating-engine airplane in several important respects. A much larger amount of fuel (expressed in terms of airplane initial gross weight) is used in warm-up, taxiing, and take-off because of the inherently lower efficiency of the jet engine at low altitudes and speeds and because the afterburner is used in take-off. Because of the very narrow range of efficient cruise operating conditions, an acceleration and climb with military power is made at once to the optimum cruise altitude, which is higher than the dash altitude for the reciprocating-engine case. This climb at heavy weight is, of course, costly with regard to fuel usage. Following the climb, the airplane cruises at the optimum combination of lift coefficient and high-subsonic Mach number with the altitude increasing as fuel is used. At the end of the initial cruise, it accelerates and climbs with full afterburning thrust along the dotted line. Then, with partial or full afterburning, it performs a high-speed dash over the target, turns 180°, and executes an escape dash. Fuel usage is particularly large relative to that of the reciprocating-engine airplane in the acceleration-to-dash speed because of the much larger amount of kinetic energy gained and in the turn because of the much greater turning time required in order to keep within the same allowable load factors.

The homeward cruise of the jet airplane is accomplished under the same conditions as the outward cruise, and it arrives over its base at extremely high altitudes. Loitering is preferably accomplished at high altitudes rather than at sea level to avoid engine efficiency losses associated with operation at low altitude, low flight speed, and low percentage of power. In order to conserve fuel in the descent, the generally proposed practice is to throttle the engines as much as is permissible and then, by utilizing jet reversers and extending speed brakes, landing gear, and other drag-producing devices, descend as rapidly as permitted by tank and cabin vents and human comfort. Even with these ideal procedures, however, the fuel usage in descent and loiter is still very large.

For this particular mission, the total off-design fuel requirements (fuel reserve plus fuel used in excess of the minimum amount required to go the same distance in the optimum cruise and dash conditions) of the jet airplane are greater than those for the reciprocating-engine airplane by an amount equivalent to about one-half the differences in the empty-to-take-off gross-weight ratios for the two airplanes. In other words, about half of the weight advantage of the jet engine is lost with regard to range performance. The penalty would be somewhat less severe, of course, in the case of a jet transport because of elimination of the high-speed dash but would be much more severe in the case of a fighter airplane that spends only a small period of time cruising. This situation stresses the need for operating the jet airplane in an optimum manner and for a minimum length of time on the off-design flight conditions and leads naturally to the ideas of air refueling, transport or towage by another airplane, and other related schemes in order to stretch the range. In many cases, such schemes may prove to be the only immediate solution for obtaining the high levels of range performance currently considered necessary.

CONCLUDING REMARKS

In summary, the necessity of flying at supersonic speeds has resulted in a great increase in the severity of range and endurance problems. The maximum attainable range decreases drastically when the flight speed is increased from subsonic to supersonic values. In addition, the design changes which make supersonic flight possible cause important reductions in range capability at the subsonic flight speeds of interest for long-range cruise. Other important range losses also come about as a result of basic nonmatching of airframe-drag and engine-thrust characteristics and because of decreased airframe and engine efficiencies in the off-design operating conditions. Consequently, in order to attain useful range, most of the piloted supersonic airplanes of the near future may be expected to do most of their cruising at high subsonic speeds, to engage in supersonic flight only in brief dashes, to operate in a closely specified manner in off-design phases of flight, and to rely on special schemes such as aerial refueling for long-range missions.

REFERENCES

1. Jones, Robert T.: Estimated Lift-Drag Ratios at Supersonic Speed. NACA TN 1350, 1947.

2. Puckett, A. E., and Stewart, H. J.: Aerodynamic Performance of Delta Wings at Supersonic Speeds. Jour. Aero. Sci., vol. 14, no. 10, Oct. 1947, pp. 567-578.

3. Lawrence, T.: Charts of the Wave Drag of Wings at Zero Lift. C. P. No. 116, British A.R.C., Nov. 1952.

4. Cooper, Morton, and Grant, Frederick C.: Minimum-Wave-Drag Airfoil Sections for Arrow Wings. NACA TN 3183, 1954.

5. Vincenti, Walter G.: Comparison Between Theory and Experiment for Wings at Supersonic Speeds. NACA Rep. 1033, 1951. (Supersedes NACA TN 2100.)

6. Love, Eugene S.: Investigation at Supersonic Speeds of 22 Triangular Wings Representing Two Airfoil Sections for Each of 11 Apex Angles. NACA RM L9D07, 1949.

7. Vincenti, Walter G., Nielsen, Jack N., and Matteson, Frederick H.: Investigation of Wing Characteristics at a Mach Number of 1.53. I - Triangular Wings of Aspect Ratio 2. NACA RM A7I10, 1947.

8. Vincenti, Walter G., Van Dyke, Milton D., and Matteson, Frederick H.: Investigation of Wing Characteristics at a Mach Number of 1.53. II - Swept Wings of Taper Ratio 0.5. NACA RM A8E05, 1948.

9. Nielsen, Jack N., Matteson, Frederick H., and Vincenti, Walter G.: Investigation of Wing Characteristics at a Mach Number of 1.53. III - Unswept Wings of Differing Aspect Ratio and Taper Ratio. NACA RM A8E06, 1948.

10. Berggren, Robert E., and Summers, James L.: Aerodynamic Characteristics at Subsonic and Supersonic Mach Numbers of a Thin Triangular Wing of Aspect Ratio 2. I - Maximum Thickness at 20 Percent of the Chord. NACA RM A8I16, 1948.

11. Walker, Harold J., and Berggren, Robert E.: Aerodynamic Characteristics at Subsonic and Supersonic Mach Numbers of a Thin Triangular Wing of Aspect Ratio 2. II - Maximum Thickness at Midchord. NACA RM A8I20, 1948.

12. Welsh, Clement J.: Results of Flight Tests to Determine the Zero-Lift Drag Characteristics of a 60° Delta Wing with NACA 65-006 Airfoil Section and Various Double-Wedge Sections at Mach Numbers from 0.7 to 1.6. NACA RM L50F01, 1950.

13. Bromm, August F., Jr.: Investigation of Lift, Drag, and Pitching Moment of a 60° Delta-Wing-Body Combination (AGARD Calibration Model B) in the Langley 9-Inch Supersonic Tunnel. NACA TN 3300, 1954.

14. Thompson, Jim Rogers, and Mathews, Charles W.: Effect of Wing Sweep, Taper, and Thickness Ratio on the Transonic Drag Characteristics of Wing-Body Combinations. NACA RM L8K01, 1948.

15. Kurbjun, Max C., and Faber, Stanley: Transonic Drag Characteristics of a Wing-Body Combination Using a Thin Tapered Wing of 45° Sweepback. NACA RM L50H22, 1950.

16. Alexander, Sidney R., and Katz, Ellis: Drag Characteristics of Rectangular and Swept-Back NACA 65-009 Airfoils Having Aspect Ratios of 1.5 and 2.7 as Determined by Flight Tests at Supersonic Speeds. NACA RM L6J16, 1947.

17. Tucker, Warren A., and Nelson, Robert L.: Drag Characteristics of Rectangular and Swept-Back NACA 65-009 Airfoils Having Various Aspect Ratios as Determined by Flight Tests at Supersonic Speeds. NACA RM L7C05, 1947.

18. Katz, Ellis: Flight Tests to Determine the Effect of Airfoil Section Profile and Thickness Ratio on the Zero-Lift Drag of Low-Aspect-Ratio Wings at Supersonic Speeds. NACA RM L7K14, 1948.

19. Pittel, Murray: Flight Tests at Supersonic Speeds to Determine the Effect of Taper on the Zero-Lift Drag of Sweptback Low-Aspect-Ratio Wings. NACA RM L50F30a, 1950.

20. Alexander, Sidney R., and Nelson, Robert L.: Flight Tests to Determine the Effect of Taper on the Zero-Lift Drag of Wings at Low Supersonic Speeds. NACA RM L7E26, 1947.

21. Morrow, John D.: Measurements of the Effect of Trailing-Edge Thickness on the Zero-Lift Drag of Thin Low-Aspect-Ratio Wings. NACA RM L50F26, 1950.

22. Nelson, Warren H., and McDevitt, John B.: The Transonic Characteristics of 17 Rectangular, Symmetrical Wing Models of Varying Aspect Ratio and Thickness. NACA RM A51A12, 1951.

23. Polhamus, Edward C.: Summary of Results Obtained by Transonic-Bump Method on Effects of Plan Form and Thickness on Lift and Drag Characteristics of Wings at Transonic Speeds. NACA RM L51H30, 1951.

24. Ellis, Macon C., Jr., and Grigsby, Carl E.: Aerodynamic Investigation at Mach Number 1.92 of a Rectangular Wing and Tail and Body Configuration and Its Components. NACA RM L9L28a, 1950.

25. Whitcomb, Richard T.: An Investigation of the Effects of Sweep on the Characteristics of a High-Aspect-Ratio Wing in the Langley 8-Foot High-Speed Tunnel. NACA RM L6J01a, 1947.

26. Edwards, George G., and Boltz, Frederick W.: An Analysis of the Forces and Pressure Distribution on a Wing with the Leading Edge Swept Back 37.25°. NACA RM A9K01, 1950.

27. Jackson, H. Herbert, Rumsey, Charles B., and Chauvin, Leo T.: Flight Measurements of Drag and Base Pressure of a Fin-Stabilized Parabolic Body of Revolution (NACA RM-10) at Different Reynolds Numbers and at Mach Numbers from 0.9 to 3.3. NACA RM L50G24, 1950.

28. Carros, Robert J., and James, Carlton S.: Some New Drag Data on the NACA RM-10 Missile and a Correlation of the Existing Drag Measurements at M = 1.6 and 3.0. NACA TN 3171, 1954.

29. Chapman, Dean R., and Perkins, Edward W.: Experimental Investigation of the Effect of Viscosity on the Drag and Base Pressure of Bodies of Revolution at a Mach Number of 1.5. NACA Rep. 1036, 1951. (Supersedes NACA RM A7A31a.)

30. Bromm, August F., Jr., and Goodwin, Julia M.: Investigation at Supersonic Speeds of the Wave Drag of Seven Boattail Bodies of Revolution Designed for Minimum Wave Drag. NACA TN 3054, 1953.

31. Boltz, Frederick W., and Buell, Donald A.: Wind-Tunnel Investigation of the Effects of a Jet-Engine Nacelle on the Aerodynamic Characteristics of a 37.25° Swept-Back Wing at High Subsonic Speeds. NACA RM A50H23, 1950.

32. Dannenberg, Robert E.: The Development of Jet Engine Nacelles for a High-Speed Bomber Design. NACA RM A7D10, 1947.

33. Friedman, Morris D.: Arrangement of Bodies of Revolution in Supersonic Flow to Reduce Wave Drag. NACA RM A51I20, 1951.

34. Hoerner, Sighard F.: Aerodynamic Drag. The Otterbein Press (Dayton, Ohio), 1951.

35. Pinkel, Benjamin, and Karp, Irving M.: A Thermodynamic Study of the Turbojet Engine. NACA Rep. 891, 1947. (Supersedes NACA WR E-241.)

36. Lundin, Bruce T.: Theoretical Analysis of Various Thrust-Augmentation Cycles for Turbojet Engines. NACA Rep. 981, 1950. (Supersedes NACA TN 2083.)

37. Hall, Eldon W., and Wilcox, E. Clinton: Theoretical Comparison of Several Methods of Thrust Augmentation for Turbojet Engines. NACA Rep. 992, 1950. (Supersedes NACA RM E8H11.)

38. Küchemann, Dietrich, and Weber, Johanna: Aerodynamics of Propulsion. McGraw-Hill Book Co., Inc., 1953.

39. Cleveland Laboratory Staff: Performance and Ranges of Application of Various Types of Aircraft-Propulsion System. NACA TN 1349, 1947.

40. Lubarsky, Bernard: Performance and Load-Range Characteristics of Turbojet Engine in Transonic Speed Range. NACA TN 2088, 1950.

41. Sears, R. I., and Merlet, C. F.: Flight Determination of the Drag and Pressure Recovery of an NACA 1-40-250 Nose Inlet at Mach Numbers from 0.9 to 1.8. NACA RM L50L18, 1951.

42. Ferri, Antonio, and Nucci, Louis M.: Preliminary Investigation of a New Type of Supersonic Inlet. NACA Rep. 1104, 1952. (Supersedes NACA TN 2286.)

43. Fradenburgh, Evan A., and Wyatt, DeMarquis D.: Theoretical Performance Characteristics of Sharp-Lip Inlets at Subsonic Speeds. NACA TN 3004, 1953.

44. Brajnikoff, George B.: Method and Graphs for the Evaluation of Air-Induction Systems. NACA Rep. 1141, 1953. (Supersedes NACA TN 2697.)

45. Rutowski, Edward S.: Energy Approach to the General Aircraft Performance Problem. Jour. Aero. Sci., vol. 21, no. 3, Mar. 1954, pp. 187-195.

46. Kelly, L.: Optimum Climb Technique for a Jet Propelled Aircraft. Rep. No. 57, The College of Aero. (Cranfield, England), Apr. 1952.

47. Luskin, Harold: Predictions of Supersonic Airplane Performance. Jour. Aero. Sci., vol. 17, no. 1, Jan. 1950, pp. 5-12.

48. Johnson, Clarence L.: Airplane Configurations for High Speed Flight. Preprint No. 164, SAE, 1953.

49. Flight Propulsion Panel: Optimization of Power-Plant and Airplane Performance - A Symposium. Aero. Eng. Rev., vol. 13, no. 6, June 1954, pp. 42-56; discussion, pp. 56-61.

SPEED-ALTITUDE CHARACTERISTICS

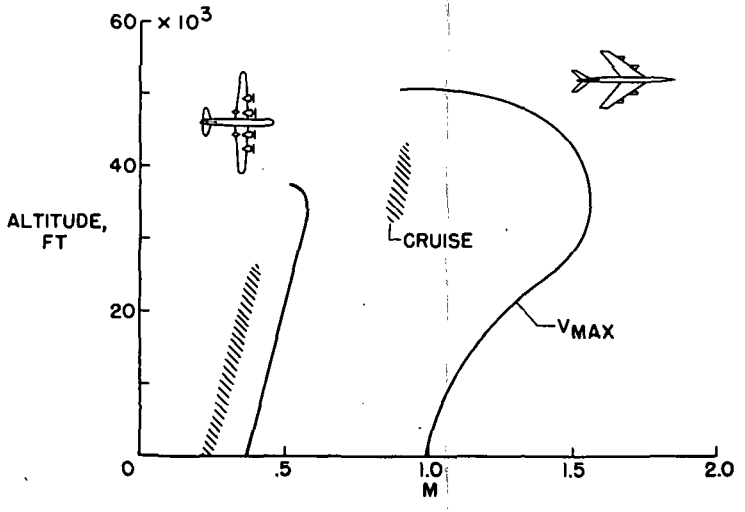

Figure 1

MINIMUM LEVEL-FLIGHT DRAG

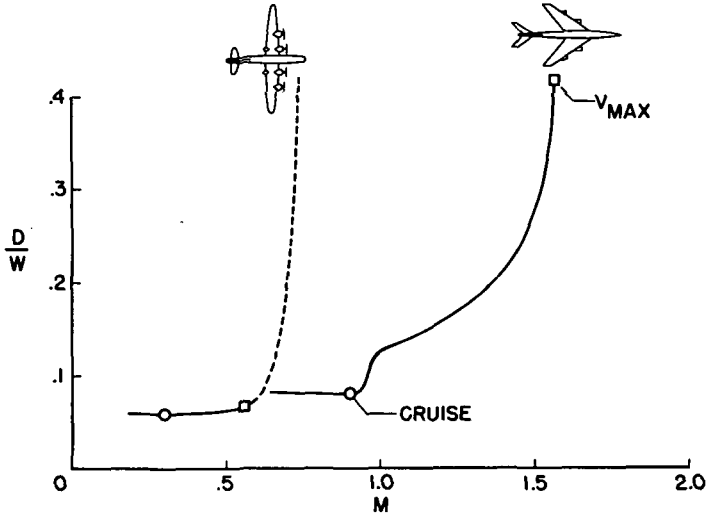

Figure 2

TYPICAL MAXIMUM LIFT-DRAG RATIOS

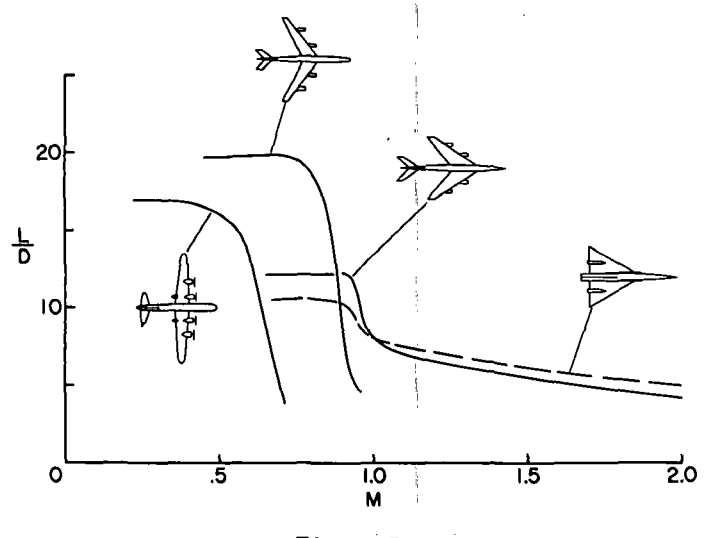

Figure 3

OVER-ALL ENGINE EFFICIENCY

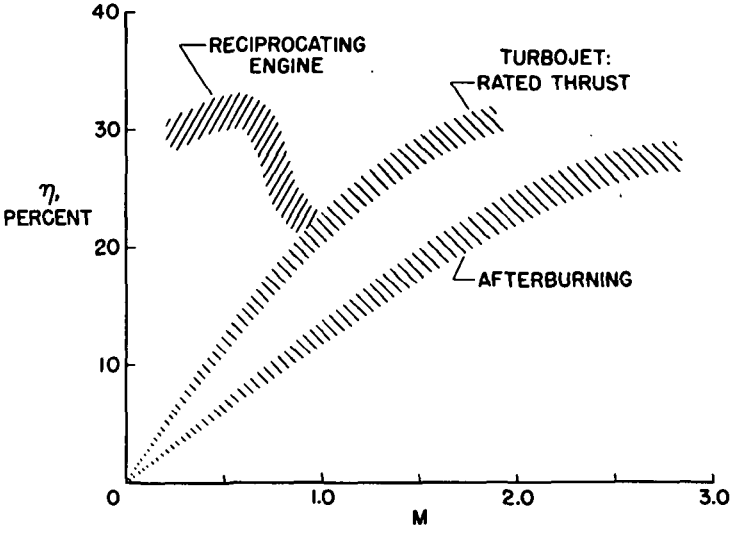

Figure 4

MAXIMUM POSSIBLE RANGE AT DESIGN SPEED

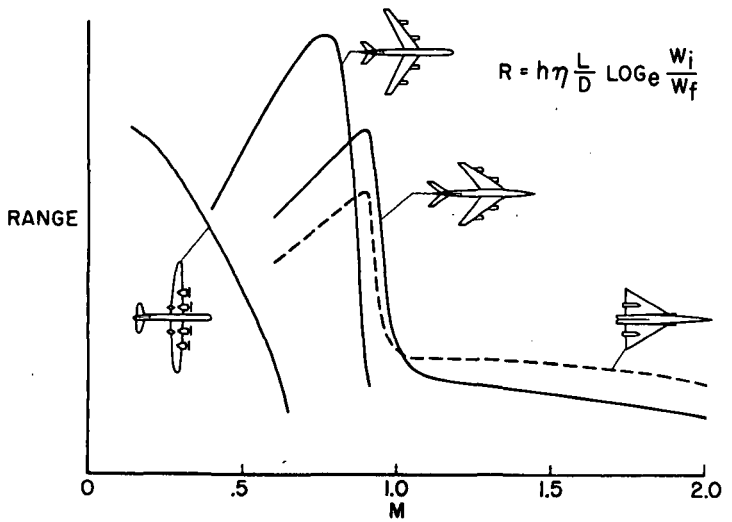

Figure 5

EFFECT OF ENGINE SIZING ON MAXIMUM POSSIBLE RANGE

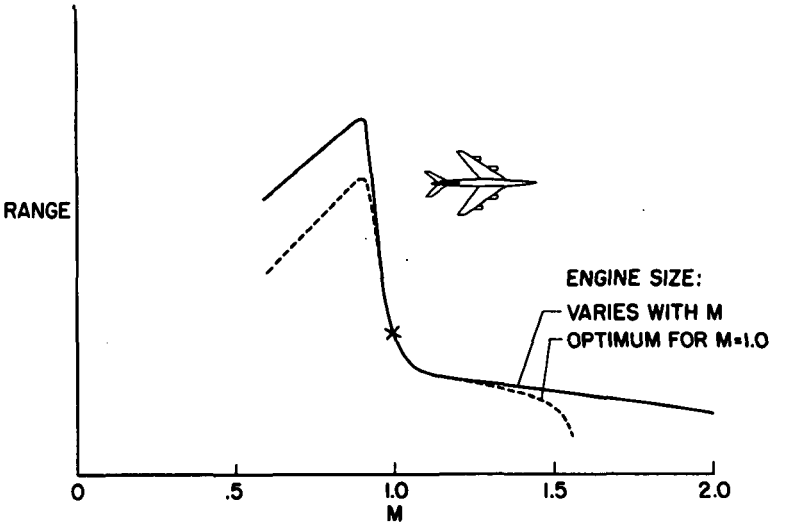

Figure 6

TURBOJET PERFORMANCE
EFFECTS OF ALTITUDE

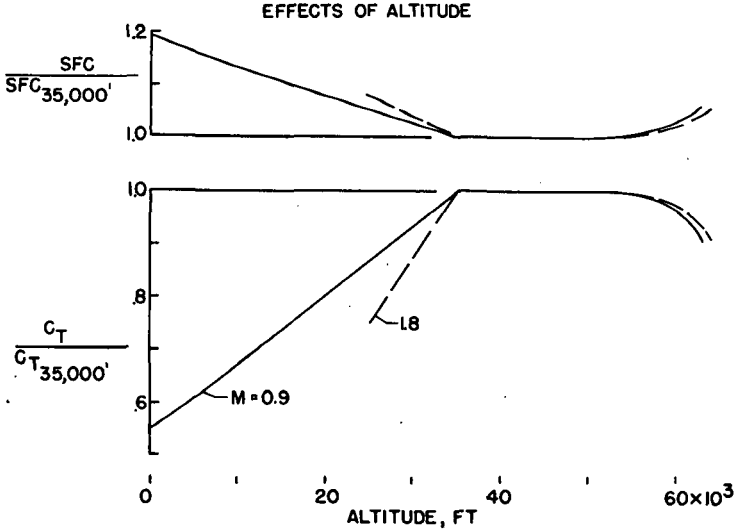

Figure 7

TURBOJET PERFORMANCE IN STRATOSPHERE
EFFECTS OF PARTIAL POWER & MACH NUMBER

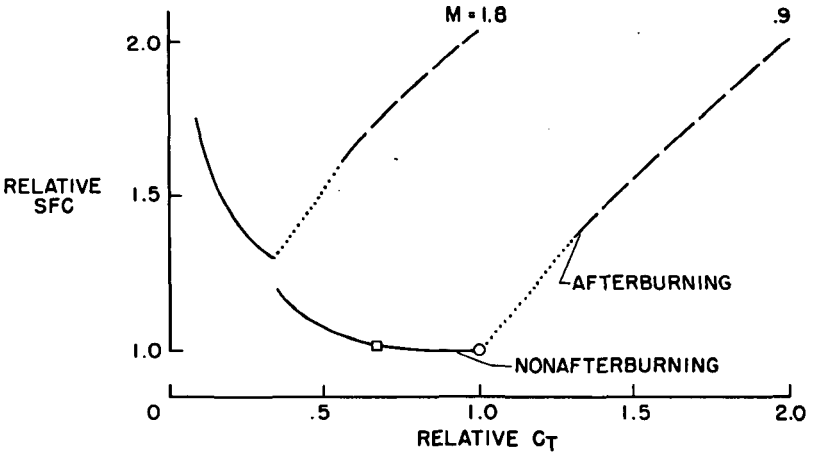

Figure 8

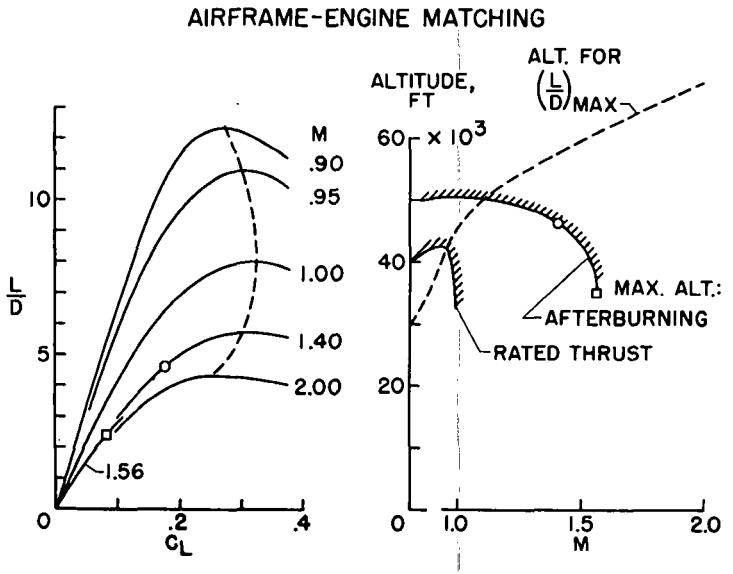

Figure 9

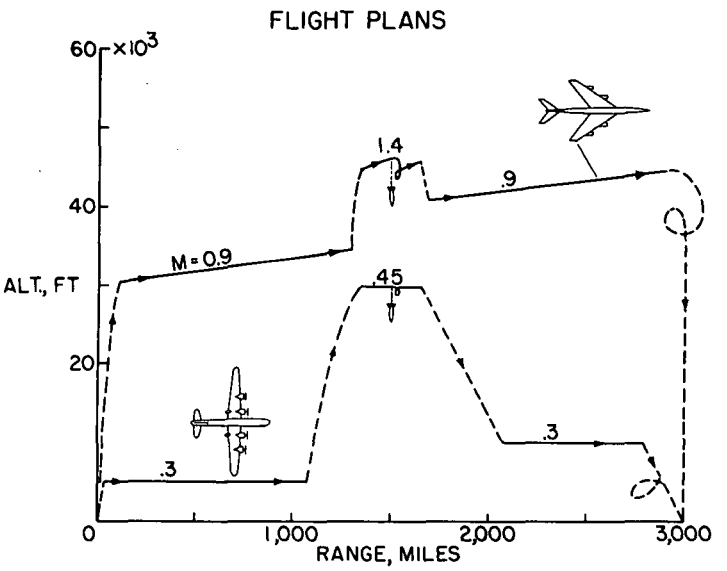

Figure 10

11. INLETS AND EXITS FOR HIGH-SPEED AIRCRAFT

By F. D. Kochendorfer
Lewis Flight Propulsion Laboratory

Solutions to the problems involved in designing inlets and exits for jet aircraft have become more and more important as flight speeds have increased. For subsonic aircraft, losses are generally small, since inlets and outlets can have good efficiencies over wide operating ranges. At supersonic speeds, however, efficient operation is difficult to obtain, especially over wide ranges. The importance of these problems arises from the fact that, for jet aircraft, inefficiencies of the inlet or exit are reflected as large performance losses. For example, a loss in inlet pressure recovery of 1 percent may represent an overall thrust loss of as much as 1.5 percent. The problems associated with high-speed inlets and exits and their solutions (where available) are discussed herein.

Consider first the performance of the inlets shown in figure 1. Theoretical pressure recovery is plotted as a function of flight Mach number for several inlet types. The theoretical recovery, which accounts only for shock losses, is defined as the ratio of the total pressure after diffusion to the free-stream total pressure. Since losses due to friction, mixing, and so forth, are not included, experimental results will, in general, fall about 5 percent, or at the higher speeds 10 percent or more, below these curves.

In the first inlet, compression is obtained by means of a single normal shock. The resulting losses increase rapidly with speed, and the inlet is not suitable for flight Mach numbers greater than about 1.7. If a cone or wedge is placed ahead of the inlet, part of the compression occurs externally through a single oblique shock, recovery is improved, and the performance in the Mach 2 region is acceptable. It is obvious, however, that, at flight Mach numbers of 2.5 or better, multioblique shock compression is desirable. The pressure recovery shown for the inlet having isentropic external compression represents what may be the best available with an external-compression inlet. Because a practical limit exists on the amount of external compression that can be obtained, a normal shock is necessary to complete the compression process. The recovery shown thus drops off somewhat with speed.

The use of theoretically high recovery inlets creates other problems, however. Each additional shock increases both the compression and the turning. Increasing compression increases the separation tendency of the boundary layer on the cone surface; increasing turning not only increases the cowl lip angle and thus increases drag, but also aggravates the design problem for the subsonic diffuser where the fluid must be returned to an axial direction. In general, inlet design involves a compromise between high pressure recovery on one hand and low drag and wide operating range on the other.

The necessity for compromise again arises when considering inlet locations. The inlets shown are nose inlets, and as such would be suitable for most nacelle and many fuselage installations. However, frequently with the engine buried in the fuselage an aft inlet location is preferred in order to minimize ducting. In addition, space in the nose is often required for other equipment. Several aft inlet types are illustrated in figure 2. These include the half cone, the two-dimensional ramp, the normal wedge, and the scoop-type inlets. In the scoop inlet the compression surface is located outboard and the entering flow is turned inward toward the fuselage.

In an aft position the inlet operates in a disturbed flow field. This may be partly to the good. In some cases shocks from the fore portions of the fuselage can be utilized to decrease the Mach number at the inlet face. One difficulty is that the disturbed field is usually nonuniform. However, the most important problem associated with aft locations is usually the fact that the inlet no longer operates in a field that is free from boundary layer.

The effect of boundary layer on the performance of aft inlets is illustrated in figure 3. Percentage of nose inlet recovery is plotted as a function of scoop-height parameter, which is defined as the ratio of the scoop height to the boundary-layer thickness. As the scoop height increases, an increasing percentage of the boundary layer is scooped off and less enters the inlet. The theoretical curve shown differs from nose inlet recovery by an amount equal to the boundary-layer defect (see ref. 1). The experimental curve represents the results of a test of a scoop-type boundary-layer removal system in which the scoop exit was vented to free-stream static pressure. It can be seen that the loss of pressure recovery is considerably higher than theoretical. The difference between the theoretical and experimental recoveries represents internal losses that occur because of the inability of the boundary layer to sustain pressure gradients. As a result, the operation of both the inlet shock system and the compression surface of the subsonic diffuser is affected adversely. As the height of the boundary-layer scoop is increased, recovery increases rapidly. For complete removal ($h/\delta = 1$), the performance can approach nose inlet recovery. For this reason, when aft inlets are employed, some type of boundary-layer control is included.

In figure 2 the half cone and the scoop inlets are shown with scoop-type removal systems, while the ramp and the normal wedge are shown with the diverter type, in which the boundary layer is trapped between a splitter plate and the fuselage and is then diverted around the inlet by a wedge. The arrows indicate the path of boundary-layer flow. If the wedge is placed so as to have a negligible effect on the boundary layer ahead of the splitter plate, this diverter system can perform as well as the scoop type, and good recovery can be obtained with moderate drag.

Until now the discussion has been concerned only with operation at the design point. Of equal importance is off-design performance, since aircraft generally must operate over a wide range of speeds and altitudes.

A typical inlet characteristic is shown in figure 4. Total-pressure recovery is plotted for a ramp-type inlet as a function of the corrected inlet air flow for a range of flight speeds. In the corrected air flow, T_2 and P_2 are the total temperature and pressure, respectively, after diffusion. The particular parameter $w\frac{\sqrt{T_2}}{P_2}$ is used for convenience in inlet-engine matching. In this form the inlet air flow must be proportional to the area of the throttling device to which the inlet is coupled. In the ram jet this throttling device is the exit nozzle; in the turbojet it is the engine.

Consider first the effect of throttle area on the performance at a fixed flight speed, at $M_0 = 2$, for example. If the exit area is chosen to permit operation at the critical point, thrust is maximum because the best recovery is obtained. Conditions in the inlet are as shown in the middle sketch. The terminal shock stands at the throat. Since a full stream tube of air is taken in, external drag is minimum. Critical operation thus corresponds to the maximum value of thrust minus drag. If the throttle area is increased, the corrected air flow will be greater than critical and the inlet is said to be operating supercritically. This condition is shown in the lower sketch. The terminal shock recedes into the inlet and pressure recovery decreases. The actual air flow is constant, but because the pressure P_2 decreases, corrected air flow increases. External drag is again minimum, but thrust is lower than critical because of the low recoveries.

In the second operating range the air flow is less than critical. Pressure recovery may decrease slightly. This subcritical region is characterized by a detached shock that stands ahead of the cowl lip. Air is spilled around the cowl with a drag rise that depends on flight Mach number and amount of spillage. Besides the high drags, inlet operation in the subcritical region may also be accompanied by a pulsating flow of potentially destructive magnitude. This so-called buzz problem will be discussed later.

As flight Mach number decreases, the inlet curves shift to higher recoveries. The important feature with respect to inlet-engine matching (ref. 2) is the dashed curve showing loci of the critical points. For the particular inlet illustrated, the critical flow increases slightly as flight Mach number decreases. In the upper portion of figure 5 this curve is replotted for two geometrically similar but different sized inlets. The dashed curves again represent critical inlet flow, but in this figure flow is plotted as a function of flight Mach number. Also

shown is the required air flow - Mach number characteristic for a typical turbojet engine. The engine flow decreases with increasing flight speed. The offset in the curve at cruise, $M_0 = 0.9$, results from an assumed altitude change from sea level to 35,000 feet. The form of the engine curve is obviously quite different from that of the inlet, so that, in general, it will be impossible to size a fixed inlet to operate critically over the speed range.

Consider first the larger inlet, labeled A. This inlet is sized to match the engine flow at cruise, $M_0 = 0.9$. The critical inlet flow is greater than the required engine flow at all other speeds. Above design the inlet operates subcritically, and flow is spilled through the mechanism of shock waves standing ahead of the lip. As indicated by the sketch at $M_0 = 2.5$, all the spillage occurs through a bow wave. The performance is indicated in the lower portion of the slide. Thrust minus drag is expressed as a percentage of ideal thrust (that is, thrust obtainable with 100-percent recovery). For inlet A, performance is good at design but then falls off rapidly with increasing speed because of the spillage drags (ref. 3). Before discussing the situation below design, it should be mentioned that, for subsonic operation, critical flow is defined as the flow necessary to choke the inlet. Therefore, critical operation is accompanied by high inlet velocities and, as a result, at the lower flight speeds no longer corresponds to the optimum design point. For the inlet being considered, the critical flow is greater than required by the engine, but, even so, the ratio of throat to stream velocity increases sufficiently to cause large recovery losses for this sharp-lipped inlet (see ref. 4). Thrust at take-off is poor.

If as an alternative the smaller inlet, labeled B, is employed - that is, if the match point is taken as the high-speed point, $M_0 = 2.5$ - the inlet is too small at all lower speeds. Thrust is again good at design. Below design the inlet operates supercritically and the thrust decreases because of the poor pressure recoveries. At take-off this inlet is useless.

Various methods can be used to achieve a better match. For example, the amount of flow spilled can be varied by varying the angle of the compression surface and/or its axial position. Inlet capacity can be increased by auxiliary inlets, or excess air may be spilled ahead of the engine through a bypass flap. Figure 6 illustrates the results of good matching. The inlet utilizes double oblique shock compression for higher recovery at high speeds. The inlet is variable in that the ramp is hinged and can be rotated downward as flight speed is reduced until the first surface is parallel to the air stream. Since the critical inlet flow is still greater than the engine flow, the excess is bypassed. At subsonic speeds, however, the bypass is closed to avoid unnecessarily high inlet velocity ratios and the resulting pressure losses. The lower

curve shows a much improved thrust ratio as compared with that of the fixed inlet. At take-off, however, performance is still poor. If the bypass flap is opened inward - that is, if the system is operated in reverse as an auxiliary inlet - performance at take-off can be improved further.

An additional factor that emphasizes the need for variable inlet systems is the oscillating, buzz-type flow that accompanies subcritical operation. The occurrence of buzz was first noted in the early experiments of Oswatitsch. Since then much work has been done on its explanation and control. If buzz is assumed to be a resonance phenomenon and if the inlet-engine-nozzle configuration is taken as an organ pipe or a Helmholz resonator, it can be shown that buzz can occur only if the slope of the inlet pressure-recovery - mass-flow characteristic is sufficiently positive. In figure 7 two typical inlet curves are illustrated. In one of the inlets the recovery is high at the critical point but drops off rapidly with decreasing flows. Because buzz accompanies the positive slope, this inlet cannot operate subcritically. With the second inlet, a range of subcritical flows is possible before the slope becomes positive. Because of this feature, the second inlet would be preferred in many cases, even though the first gives better peak recovery.

In the resonance theory the factors associated with the excitation of buzz are not, of course, considered. These factors and the role they play are not clearly understood at present. One buzz triggering mechanism, for example, is the separation of the boundary layer on the cone or cowl surface. A simplified explanation of this phenomenon is illustrated in the left-hand sketch of figure 8. It can be seen that boundary-layer separation reduces the effective area of the inlet passage. The flow in the subsonic diffuser accelerates and pressure recovery falls. Since the corrected air flow must be constant, the air flow itself must decrease and the shock is forced outward. As the shock nears the cone tip, the possibility for reattachment improves. If reattachment occurs as shown in the sketch on the right, the shock moves back and the process is repeated.

Still another buzz-producing condition is associated with the slip line emanating from the intersection of the normal and oblique shocks. If this slip line enters the inlet, it can cause buzz in a manner somewhat similar to that just described.

At present, then, two methods for limited control of buzz are available to the designer. The first consists in eliminating the possibility of the slip line's crossing the cowl lip. The second consists in increasing the cone angle above that required for optimum recovery. The latter procedure decreases the strength of the terminal shock and thereby reduces the separation tendency of the boundary layer.

In addition to the problems just discussed, the high-speed turbojet-powered aircraft has severe nozzle-exit problems. The operating conditions of a typical exhaust nozzle are illustrated in the upper portion of figure 9. The relative throat areas for maintaining the basic engine at rated-speed operation and the available nozzle pressure ratios are shown as functions of flight Mach number. The nozzle throat area is primarily governed by the amount of afterburning, which in turn depends on the particular flight plan. It is sufficient to note, however, that, for complete flexibility, throat-area variations of about 80 percent should be possible. On the other hand, the nozzle pressure ratio is, to a first order, independent of the degree of afterburning. Thus, the nozzle would have to operate over a range of pressure ratios from about 2 at take-off to as high as 15 at a Mach number of 2.4.

The extent to which the available engine thrust may be penalized by the use of fixed-geometry exhaust nozzles is shown in the lower portion of figure 9. The convergent nozzle has a high velocity coefficient at the low flight speeds, and hence a high fraction of the potential thrust is realized. As flight speed increases, however, this simple nozzle cannot effectively utilize the higher available pressure ratios. Hence, at a Mach number of 2.4, 20 percent of the potential engine thrust would be lost. If a divergent passage is added, optimum thrust can be obtained at high speeds. The significant point, however, is the thrust lost at low speeds. At low pressure ratios, the jet expands in the divergent portion to pressures much lower than the ambient static pressures. A drag force is produced on parts of the divergent passage; and, as a result, at subsonic cruise, 20 percent at the potential engine thrust is again lost.

To obtain optimum thrust over the flight range, both throat area and expansion ratio would have to be variable. As yet, for axially symmetric convergent-divergent nozzles of the type shown, no simple mechanical means has been devised to provide this variation. For two other types, however, area variations appear to be feasible. The first of these is the plug nozzle, which is illustrated in figure 10. The configuration differs from that of the simple nozzle by the addition of the central plug. The contour of the plug surface downstream of the throat forms the divergent portion and can be chosen to permit isentropic expansion at the high-pressure design point. The jet configuration at high speed is shown on the right. The jet expands around the edge of the shell, the light lines representing Prandtl-Meyer expansion waves that are cancelled at the plug. The thrust of this nozzle can thus equal that of the optimum convergent-divergent type. The important feature, however, is that the overexpansion loss at low pressure ratios can be greatly minimized. The sketch on the left shows the jet contracting around the plug. The losses at low speeds are limited to those associated with plug drag, and a satisfactory nozzle results. Throat area variations with this type of plug nozzle can be obtained by employing an iris-type shell as shown.

Another nozzle having good potential off-design performance is shown in figure 11. In this configuration the exit nozzle acts as the primary nozzle of an ejector and is enclosed within a second nozzle called the shroud. Low-energy air can be bled through the annulus between the two nozzles. For the high-pressure-ratio condition of the right-hand sketch, the secondary stream cushions the primary expansion, in effect forming a virtual divergent passage for the primary. If the value of the ratio of the shroud to nozzle diameter is equal to that required for complete expansion at the particular pressure ratio, thrust can be within a few percentage points of the optimum. At low pressure ratios, the secondary flow prevents any great amount of overexpansion, and thrusts can again be high. With this nozzle the overexpansion losses are traded for the smaller losses associated with the handling of the secondary air. To obtain near-optimum thrust over the speed range, the shroud diameter should, in general, be variable. An iris-type nozzle would then be required for the shroud as well as for the primary nozzle.

A bonus feature of this nozzle is that at take-off and at low flight speeds the ejector can be used to pump cooling air for both the afterburner and the nozzle itself. Thus, although the plug nozzle has a slight potential thrust advantage, this may be offset by the cooling feature of the ejector.

In summary, it has been shown that, in order to attain optimum performance over the entire flight range, high-speed jet aircraft will require complicated air-inlet and exit-nozzle systems as compared with subsonic aircraft. The alternative, however, appears to be an automatic reduction in available engine thrust of from 30 to 40 percent in certain portions of the flight plan.

REFERENCES

1. McLafferty, George: Theoretical Pressure Recovery Through a Normal Shock in a Duct with Initial Boundary Layer. Jour. Aero. Sci., vol. 20, no. 3, Mar. 1953, pp. 169-174.

2. Wyatt, DeMarquis D.: An Analysis of Turbojet-Engine-Inlet Matching. NACA TN 3012, 1953.

3. Sibulkin, Merwin: Theoretical and Experimental Investigation of Additive Drag. NACA RM E51B13, 1951.

4. Fradenburgh, Evan A., and Wyatt, DeMarquis D.: Theoretical Performance Characteristics of Sharp-Lip Inlets at Subsonic Speeds. NACA TN 3004, 1953.

PERFORMANCE OF INLET TYPES

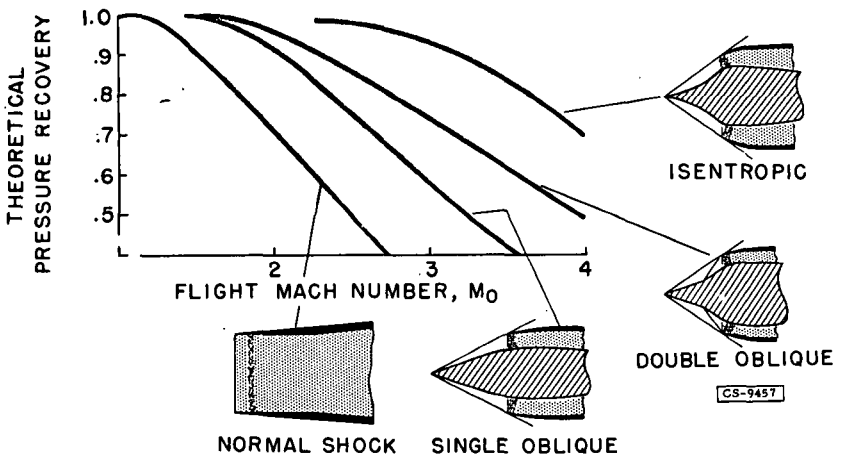

Figure 1

AFT INLETS

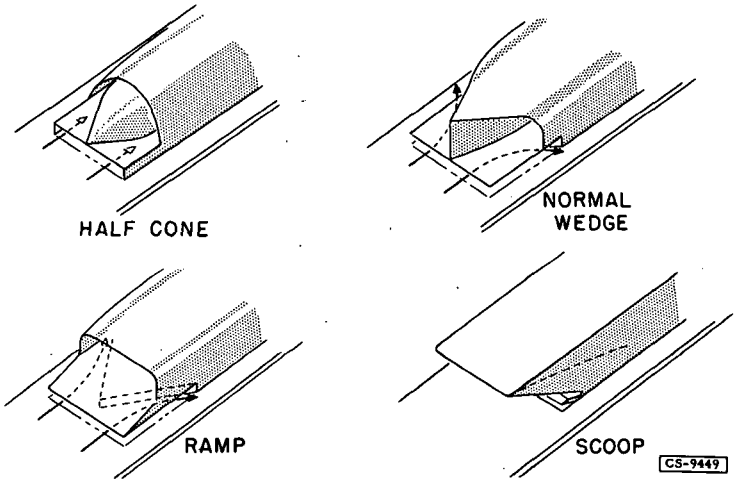

Figure 2

BOUNDARY-LAYER REMOVAL

RAM SCOOP

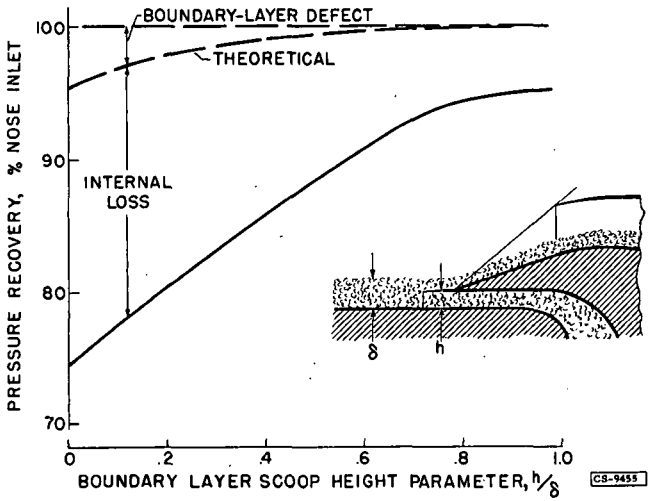

Figure 3

OFF DESIGN OPERATION

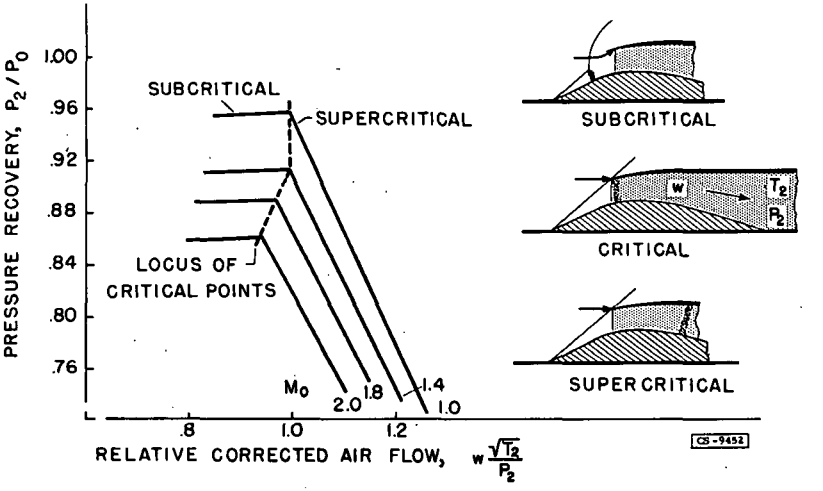

Figure 4

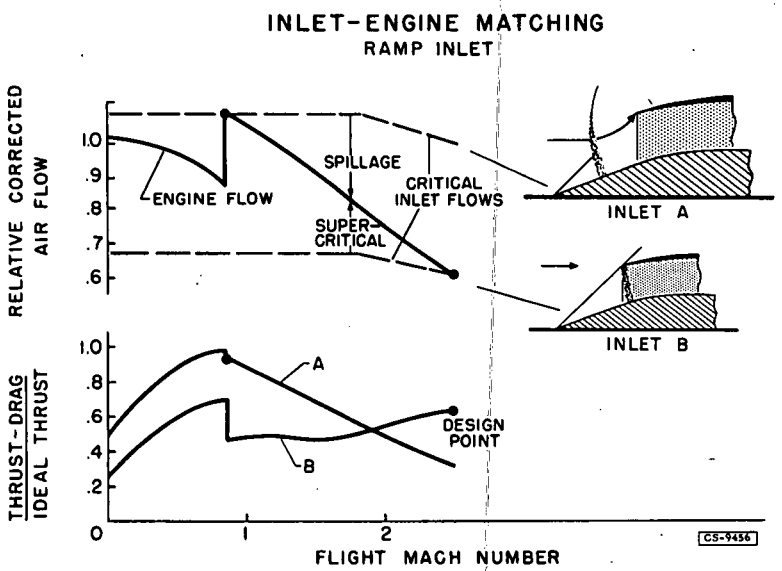

Figure 5

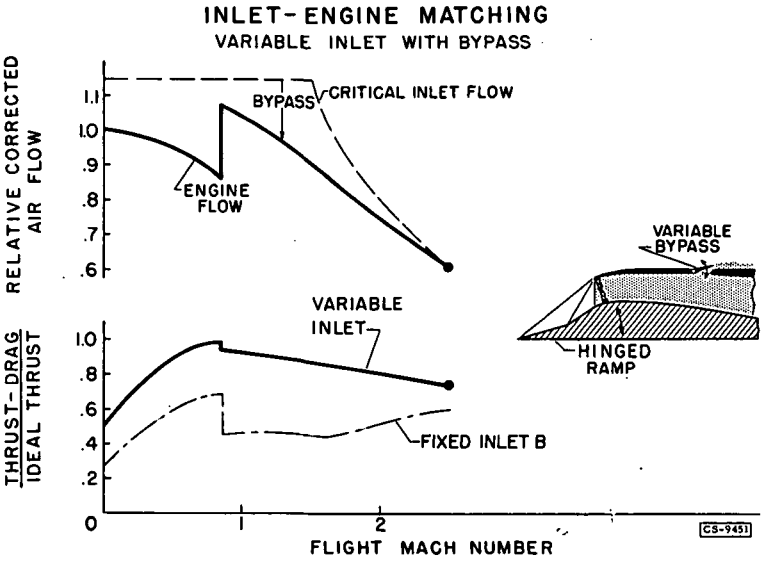

Figure 6

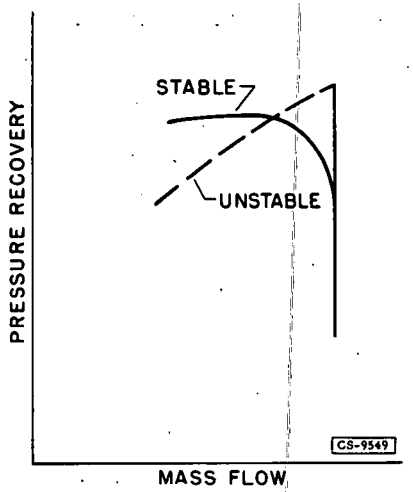

Figure 7

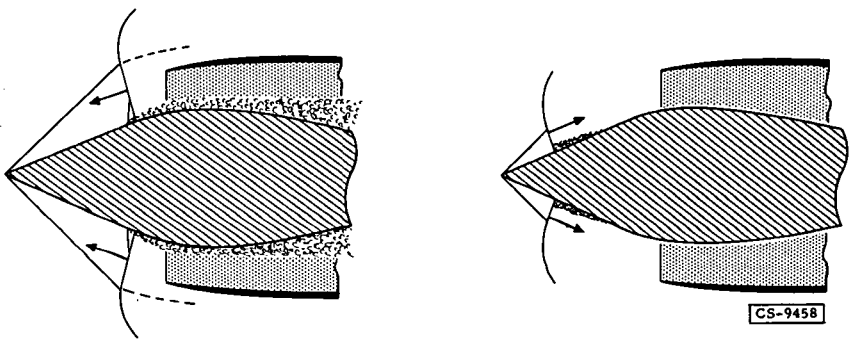

Figure 8

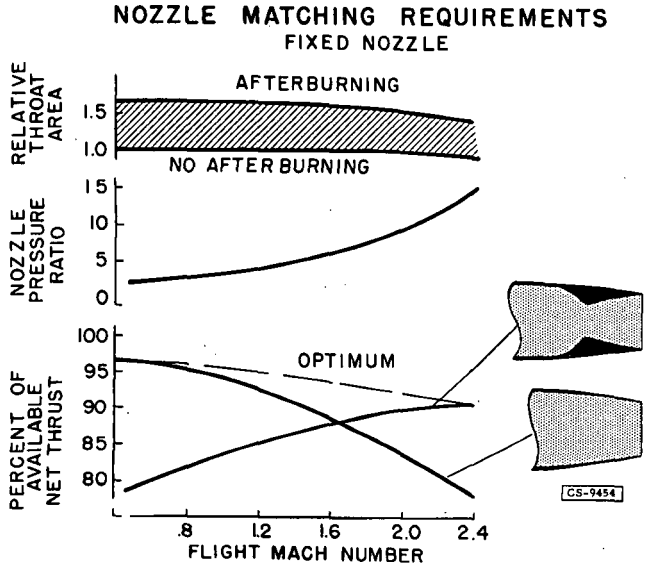

Figure 9

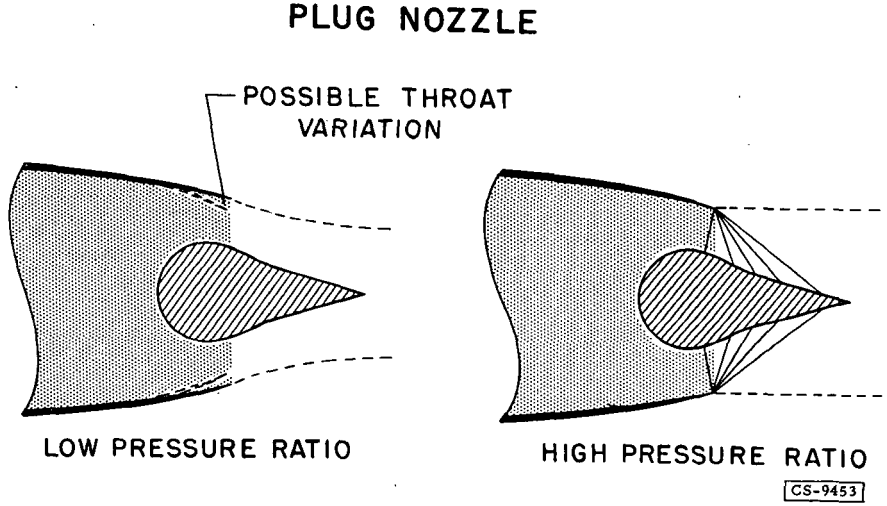

Figure 10

EJECTOR

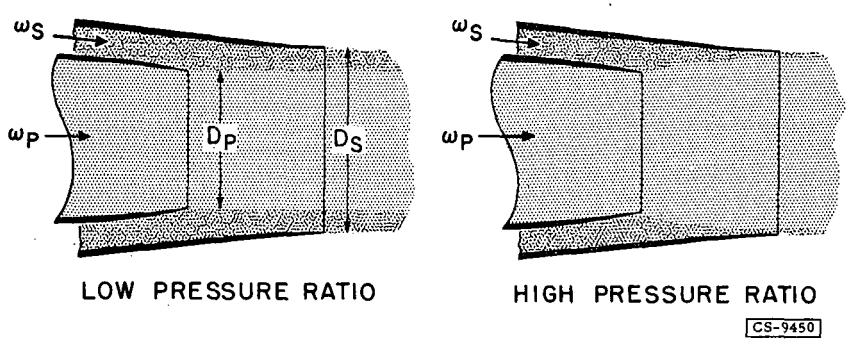

Figure 11

12. BOUNDARY-LAYER CONTROL FOR HIGH LIFT

By Woodrow L. Cook
Ames Aeronautical Laboratory

Boundary-layer control is discussed herein with regard to improving low-speed flight by blowing and sucking to produce high lift. Particular emphasis is placed on the boundary-layer control systems that are most promising practically. In addition, areas of research are indicated where a more fundamental study of the phenomena involved should result in significant gains in the application of boundary-layer control.

Before discussing in detail any one type of boundary-layer control, the function of boundary-layer control and the various positions on the airfoil sections where it has been effectively applied are briefly reviewed. The maximum lift coefficient of airfoil sections or the maximum lift increment of trailing-edge flaps is usually limited by separation of the air flow from the surface due to a pressure rise too great for the boundary-layer air to penetrate without aid. The upper part of figure 1 illustrates the usual locations on an airfoil where the pressure peaks and consequent adverse pressure rises occur. In all three cases, boundary-layer control applied in the region of most severe pressure rise shown by the dots at the leading edge, leading-edge flap, and trailing-edge flap permits greater peak pressures without air-flow separation, as indicated by the dashed curves. The curves in the lower part of the figure illustrate the type of lift gains attainable with boundary-layer control applied at the three positions. For the left and center case, an increase in angle of attack is required to realize the gains; whereas the third case requires only an increase in flap deflection. The NACA and others have found that the application of boundary-layer control at any of these three points will control separation and give the desired lift increases.

The effectiveness of boundary-layer control by removing the surface boundary layer through slots has been studied for many years. The primary factor in preventing general use of suction through slots has been the large quantities of air that have to be removed. More recently, analytical studies on the prevention of leading-edge air-flow separation by Thwaites and others have indicated that the air-flow quantities required for slot suction can be greatly reduced through the use of area suction; that is, suction through a porous surface rather than discrete slots. Experimental results have shown that, in practice, these large flow quantities required with a slot can be reduced by a factor of 3 to 5 with area suction.

The theories of Thwaites and Schlichting are compared in figure 2 with experiment for area suction applied to the airfoil leading edge. The variation of the ratio of normal inflow velocity to free-stream velocity with chordwise position is shown. The critical values of inflow velocity near the leading edge for both experimental distributions (uniform and nonuniform porosity) were approximately 10 times the value of Thwaites' theory and $2\frac{1}{2}$ times the maximum value of Schlichting's theory. It should be noted that use of these theories in the high adverse gradient is subject to question. It is also questionable whether a truly porous area or continuous suction as defined by theory was actually obtained experimentally. Both experimental distributions of suction, that with uniform porosity and that with nonuniform porosity, were the minimum values of air flow associated with the distributions that successfully prevented leading-edge air-flow separation at the particular lift coefficient. However, with uniform porosity, considerable excess air was removed unnecessarily from the rear portion of the porous area, and the flow requirements were much greater than desirable.

Another important factor in determining total air-flow quantities required is the length of chord over which area suction must be applied. A method based on Thwaites' analysis for determination of the required chordwise extent of area suction is illustrated in figure 3. Two pressure distributions are shown to an enlarged scale in the inset for the region near the leading edge. The solid curve is the pressure distribution at an angle of attack just before air-flow separation on the section with no boundary-layer control, while the dashed curve is the pressure distribution at the desired lift coefficient. The shaded area at the leading edge indicates the chordwise extent over which area suction must be applied. The lower pressure rise is the maximum the boundary layer can traverse without suction. The chordwise extent of area suction required is from the peak pressure point to the point where the remaining pressure rise is equal to that which was traversed without suction. This reasoning has been verified in several investigations; and, although three-dimensional effects modify the results to a degree, the method appears sound. For leading-edge flaps or trailing-edge flaps, the extent of area suction is determined in a similar manner. In each case, the position of application is in the region of pressure rise directly following the negative pressure peak.

The major portion of the recent work on area-suction boundary-layer control has been directed at preventing air-flow separation on trailing-edge flaps and thus improving their effectiveness. Figure 4 shows the over-all results of the lift increment obtainable with area suction applied to plain flaps. Here the ratio of flap lift increment to theoretical flap lift increment determined by first-order thin-airfoil theory is shown for a range of flap deflections with and without area suction. The increment of flap lift can be nearly doubled with boundary-layer control at flap deflections from 55° to 65°.

Although experiments have proved that area-suction boundary-layer control has reduced the necessary suction-air quantities to practical values, a great difference still exists between the values predicted by available theory for leading-edge suction and the values so far realized by experiment; and, furthermore, no known theory exists for suction on flaps. It is important, therefore, that analytical studies be made to provide adequate theories and that accompanying experimental studies of area suction be made, particularly in adverse pressure gradients. It is hoped that such work will resolve the existing discrepancies between experiment and theory and lead to further reduction in suction air-flow quantities.

Turning now to boundary-layer control by blowing, all the recent work on blowing has been directed toward improving trailing-edge flaps. Typical examples of the increases in flap effectiveness achieved by blowing a jet of air over a flap are given in figure 5, which presents the variation of the flap lift increment with the jet momentum coefficient C_μ. The jet momentum coefficient is chosen as a controlling parameter, since what is being measured is the effect of transferring momentum from the jet to the boundary layer. The jet momentum coefficient in this relation is the product of the mass-flow coefficient C_Q and the ratio of jet velocity to free-stream velocity, which in turn is a function of the pressure difference between the duct and free stream and can be expressed as either a pressure coefficient C_p or as pressure ratio for a particular flight condition. Thus, a given value of C_μ can be realized either by using high pressure ratio and low mass flow or low pressure ratio and high mass flow. For example, for the two cases shown, there is a 16-fold change in nozzle depth d/c and about a 2.5-fold change in pressure ratio; yet the lift for a given value of C_μ is changed only slightly. Also, as momentum coefficient is increased, a point is reached where the rate of increase in lift with momentum reduces sharply. Analyses indicate that at this point the jet has eliminated separation and achieved full boundary-layer control, and that the lift corresponding to this point is very close to the predicted value by first-order thin-airfoil theory. Since it has been determined that this lift due to boundary-layer control is the major portion of the lift realized from blowing, it then becomes of interest to examine means of reducing the mass-flow and pressure requirements for boundary-layer control.

All the discussion thus far on blowing has been for flaps with blowing from a nozzle placed on the wing forward of the slotted flap. Research with area suction has shown that optimum results are obtained by applying suction in the region of pressure rise directly following the point of minimum pressure. Based on this, it appears that reductions in the momentum coefficient would result if the jet momentum were put into the boundary layer at this point of minimum pressure. An estimation of the possible reductions in C_μ are shown in figure 6.

In making the calculation for the dashed curve, it was assumed that the significant momentum of the jet was that confined to a depth of the order of the boundary-layer thickness. Since a jet expands rapidly downstream of a nozzle, after traversing a distance of some 60 nozzle depths from the exit to the minimum-pressure point on this particular slotted flap, much of the jet momentum is in the free stream outside the boundary layer. Then the reduction in C_μ for a given lift coefficient is estimated by assuming that the nozzle is moved to the minimum pressure point and that the C_μ required is only that left in the boundary-layer depth in the case of the slotted flap. Such a reduction in C_μ would represent a large reduction in flow and pressure coefficients and hence power required for boundary-layer control.

The foregoing results on boundary-layer control by blowing demonstrate that experimental evidence exists to show that full boundary-layer control can be obtained through use of a jet. It should be emphasized, however, that neither theoretical nor experimental knowledge exists regarding the exact mechanism involved. In order to ensure most efficient use of the jet momentum, studies must be made of the transfer of energy from subsonic and supersonic jets to the boundary layer, and effects on boundary-layer stability in adverse pressure gradients.

At this point, it is interesting to compare in figure 7 the variation of the lift increments as a function of mass flow C_Q for the area-suction type boundary-layer control and the blowing type boundary-layer control on trailing-edge flaps. As nearly as could be determined by experiment, separation was eliminated in each case at the value of C_L indicated by the solid triangle. It is apparent that, with area-suction boundary-layer control, the lift increased only slightly as the flow coefficient was increased beyond that required to eliminate separation; whereas, with blowing boundary-layer control, significant increases in lift were obtained with further increases in mass flow.

This additional lift increment greater than the lift due to boundary-layer control is known to include contributions from at least three distinct sources. One of these, the momentum lift resulting from turning the jet, can be quantitatively evaluated. Only a qualitative understanding yet exists of the other two. Experiments have shown that a jet directed downstream from a trailing edge will move the stagnation point downstream and cause the lift of an airfoil at angle of attack to increase as though its chord were extended. Also, it has been found that a high-velocity jet directed over the upper surface of an airfoil will induce a sink effect and hence increase circulation about the airfoil. However, it should be noted that the flow quantities required to realize these lift increments greater than attributable to boundary-layer control, by any of these three methods, appear prohibitive at the present time on the basis of current experiments.

In summary, an attempt has been made in this paper to show that, with the aid of limited theories, boundary-layer control for high lift has been developed by experiment to a practical point. Much theoretical and experimental work remains to be done if the apparent potential of the several procedures is to be fully realized. It is hoped that other groups will devote their attention to some of these studies.

BIBLIOGRAPHY

1. Dannenberg, Robert E., and Weiberg, James A.: Section Characteristics of a 10.5-Percent-Thick Airfoil with Area Suction as Affected by Chordwise Distribution of Permeability. NACA TN 2847, 1952.

2. McCullough, George B., and Gault, Donald E.: An Experimental Investigation of an NACA 63_1-012 Airfoil Section with Leading-Edge Slots. NACA TN 1683, 1948.

3. Thwaites, B.: A Theoretical Discussion of High-Lift Aerofoils with Leading-Edge Porous Suction. R. & M. No. 2242, British A. R. C., July 1946.

4. Schlichting, H.: An Approximate Method for Calculation of the Laminar Boundary Layer with Suction for Bodies of Arbitrary Shape. NACA TM 1216, 1949.

5. Rebuffet, P., and Poisson-Quinton, Ph.: Investigations of the Boundary-Layer Control of a Full Scale Swept Wing with Air Bleed off from the Turbojet. NACA TM 1331, 1952.

6. Schwier, W.: Lift Increase Produced by Blowing a Wing of a Profile Thickness of 9%, Equipped with a Slat and a Slotted Flap. Rep. No. F-TS-645-RE, Hdq., Air Materiel Command, Wright Field, Dayton (Ohio), Sept. 1946.

7. Helmbold, H. B.: On the Lift of a Blowing Wing in a Parallel Stream. Eng. Study 110, Univ. of Wichita, Aug. 1953. (Contract N-onr-20101.)

LIFT INCREASES WITH BOUNDARY LAYER CONTROL

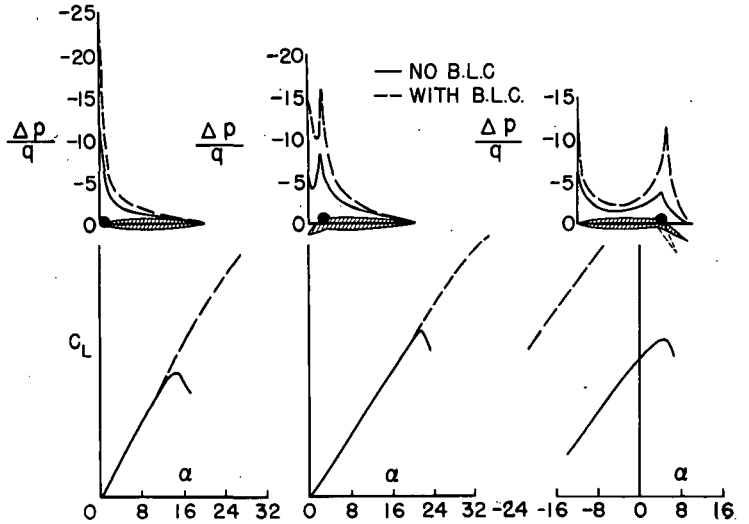

Figure 1

EXPERIMENTAL AND THEORETICAL DISTRIBUTION OF SURFACE INFLOW VELOCITY

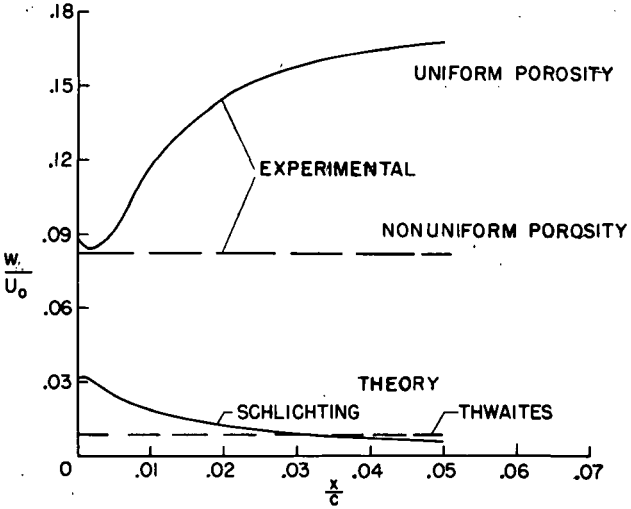

Figure 2

PRINCIPLE OF AREA SUCTION

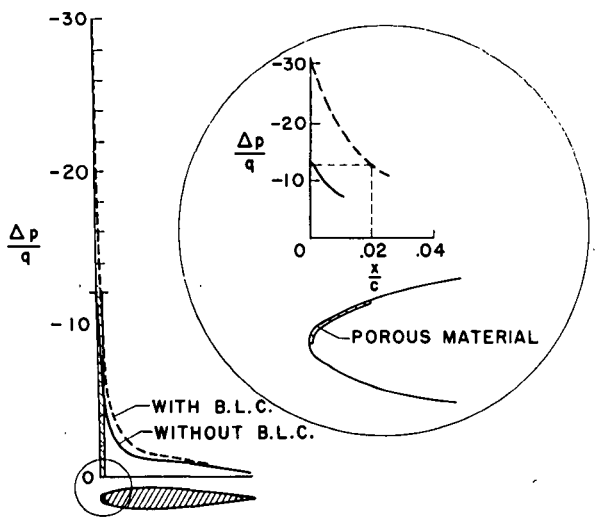

Figure 3

LIFT INCREMENTS FOR A RANGE OF TRAILING-EDGE FLAP DEFLECTIONS

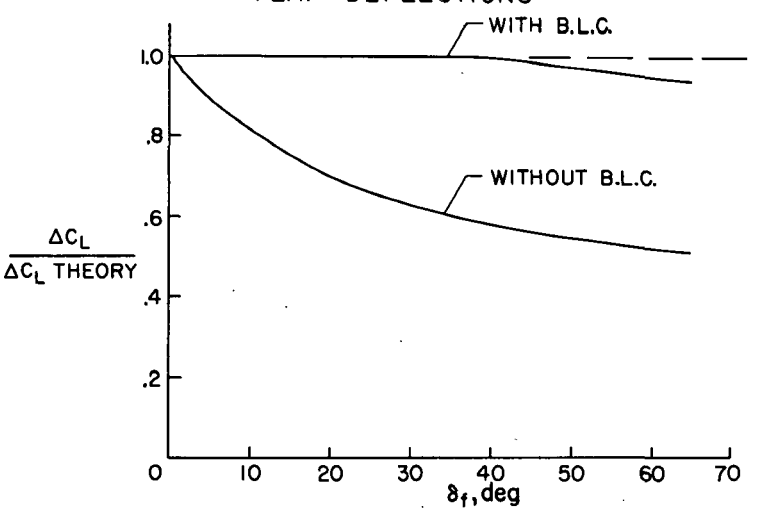

Figure 4

VARIATION OF LIFT INCREMENT WITH MOMENTUM COEFFICIENT

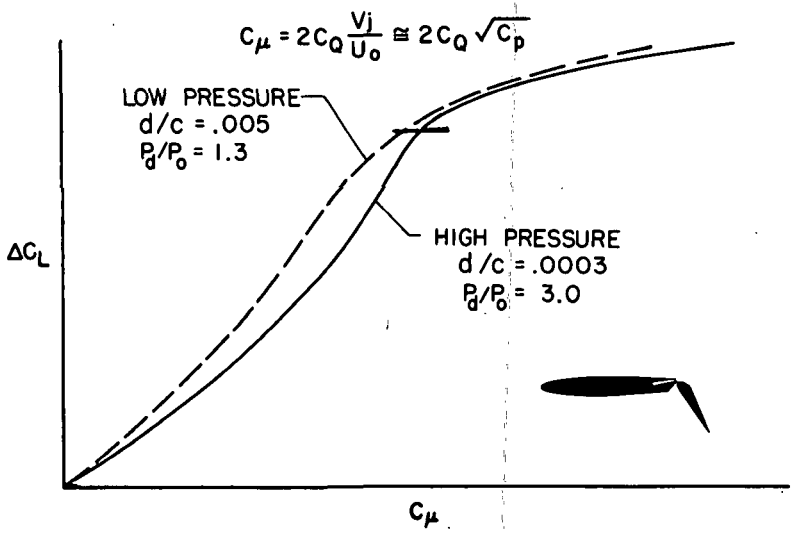

Figure 5

EFFECT OF JET LOCATION

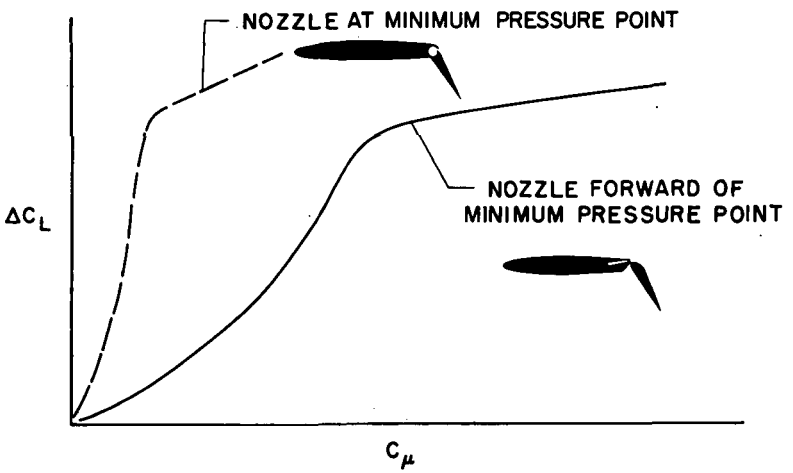

Figure 6

FLAP LIFT INCREMENTS OBTAINABLE WITH AREA SUCTION AND WITH BLOWING

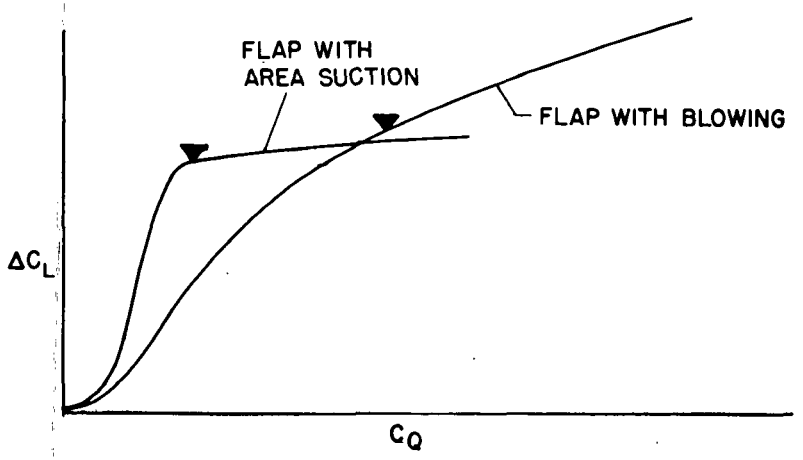

Figure 7

13. SOME APPLICATIONS OF DYNAMIC ANALYSIS TO AUTOMATIC CONTROL RESEARCH

Robert A. Gardiner and Leonard Sternfield
Langley Aeronautical Laboratory

INTRODUCTION

In recent years dynamic system analysis has progressed so that it can now be considered an engineering science. The universities have contributed heavily in this field, generally on the basis of sponsorship of armed forces contracts for systems for fire control, missile, and automatically controlled aircraft.

Methods which the NACA has applied to airframe analysis and to automatic control systems are described herein. These methods, which are only a few of those available, are presented to show their use in the design of automatic control systems. This use is really a new importance which dynamic analysis has taken on since the advent of missiles and new interceptor aircraft.

Figure 1, the block diagram of an automatically controlled missile or airplane, illustrates the manner in which aerodynamics and other control characteristics are integral parts of the same system. The stability and the quality of response of a feedback system similar to the one shown are dependent on the dynamic characteristics of all the elements, the airframe, and the general autopilot, which may have several components such as, servomotor, sensing elements, and shaping networks. The operation of new interceptor aircraft and missiles is dependent on the proper response of control systems such as this one.

Of prime importance in such a system are the dynamic characteristics of the airframe. These dynamic characteristics can be represented in the frequency domain. Figure 2 illustrates a simple mass-spring-damping system with the well-known differential equation $m\ddot{x} + c\dot{x} + kx = \delta \sin \omega t$. Frequency response defines the steady-state frequency dependent response of the output of a component to a sinusoidally varying input function, expressed quantitatively by a plot of amplitude ratio and phase angle against frequency. An analytical expression which defines the frequency response throughout the frequency range is, when defined in terms of the Laplace transform variable, the transfer function of the system.

The first part of this paper discusses briefly some of the methods used to determine the transfer function or the frequency response of the airframe from flight-test results. The second part of the paper consists of a discussion of a method of analysis used for automatic control and illustrates the use of airframe transfer functions. No attempt is made to examine all the known methods of analyzing dynamic responses and omission of any method is not intended to imply lack of merit.

TRANSFER FUNCTIONS FROM FLIGHT TEST

Longitudinal motion. - The first methods to be discussed will be applied to the short-period longitudinal motion of an aircraft. The short-period longitudinal characteristics of an aircraft can be determined from the following well-known linear differential equations, where the aircraft is assumed to have two degrees of freedom, translation normal to the flight path, and rotation in pitch about the center of gravity:

Normal force:

$$mV(\dot{\theta} - \dot{\alpha}) = L_{\alpha}\alpha$$

Pitching moment:

$$mk_y^2 \ddot{\theta} = M_{\alpha}\alpha + M_{\dot{\alpha}}\dot{\alpha} + M_{\dot{\theta}}\dot{\theta} + M_{\delta}\delta$$

Transfer function:

$$\frac{\alpha}{\delta}(D) = \frac{K_o}{D^2 + K_1 D + K_2}$$

The change in forward velocity which results in an additional long-period oscillation, the phugoid, is assumed small and is neglected in this analysis of the short-period oscillation. One of the transfer functions of this system is $\frac{\alpha}{\delta} = \frac{K_o}{D^2 + K_1 D + K_2}$ where K_o, K_1, and K_2 are functions of the mass and aerodynamic parameters, for example, L_{α}, M_{α}, $M_{\dot{\theta}}$, usually termed stability derivatives and appearing in the equations of motion. Other transfer functions such as $\dot{\theta}/\delta$ or the normal acceleration per δ may be required for control-system design.

From free-flight tests of small heavily loaded missiles, data similar to the curves shown as solid lines on figure 3 are obtained, where time histories of lift L, angle of attack α, and control deflection δ are plotted as a function of time. For underdamped responses such as these, which incidentally characterize most missile responses, reduction to aerodynamic derivatives is made on the basis of the well-known spring mass damping system from the period and damping of the oscillation and also from the steady-state value. When the aerodynamic derivatives are known, the transfer function of α/δ at any operating altitude or any of the other transfer functions of the system can be determined and the frequency response calculated.

As distinguished from missiles, current full-scale aircraft may have a highly damped response such as the dashed curves of figure 3 but still with the same characteristic equation. To determine the aerodynamic coefficients from such a response, a number of points along the time history are chosen. The use of a least-squares-curve fitting procedure and the application of matrix methods can be used to determine the required aerodynamic stability coefficients. These can be used as before to calculate transfer function or frequency response.

Lateral motion. - Recently, another method of determining the stability derivatives of an aircraft has been proposed which is based upon the properties of rotating time vectors. Figure 4 shows the path generated by the vector through 1 revolution where it represents the complimentary solution to the differential equation of the mass-spring-dashpot system $\ddot{x} + 2\zeta\omega_n\dot{x} + \omega_n^2 x = 0$ where ξ is the damping ratio and ω_n is the undamped frequency of the system. The projection of this rotating vector on the real axis forms the damped sinusoidal oscillation. The vector rotates at a constant angular velocity of $\omega_n\sqrt{1 - \xi^2}$, and the length of the vector decreases exponentially with time. The fundamental property of time vectors which is of interest here is the relation between a vector and its successive derivatives at a given instant. As shown in figure 5, the amplitude of the derivative of a time displacement vector is equal to the amplitude of the displacement vector at the same instant multiplied by the undamped rotational frequency of the vector ω_n and the derivative leads the displacement vector by a phase angle of $90^\circ + \varepsilon$ where $\varepsilon = \tan^{-1}\frac{\xi}{1 - \xi^2}$. This simple amplitude and phase relation between the time vector and its derivative are time invariant. Also, in a system with several degrees of freedom, the amplitude and phase relations between the degrees of freedom are time invariant.

The method has been applied successfully to the lateral motion of an aircraft described by the three degrees of freedom, roll, yaw, and sideslip. The first step is to determine from flight records of the time histories the phase and amplitude relations among the oscillatory components of the several degrees of freedom together with the period and damping of the oscillations. The resulting phase and amplitude ratios can be presented as a vector diagram (fig. 6). To determine the stability derivatives, each equation of motion is treated separately. For example, the rolling moment derivatives are obtained from the rolling moment equation

$$I_x\dot{p} - I_{xz}\dot{r} = L_p p + L_r r + L_\beta \beta$$

where

I_x moment of inertia in roll

p rolling velocity

I_{xz} product of inertia

r yawing velocity

L_p damping-in-roll velocity

L_r cross derivative of rolling moment due to yawing velocity

L_β effective-dihedral derivative

β sideslip angle

There are three unknown stability derivatives, L_p, L_r, L_β, but by this method the value of one of them must be estimated to find the values of the other two. For the case presented herein, the derivative L_p was well known from experimental wind-tunnel results. In any other case, the derivative that is best known should be used. From the rolling moment equation, it is seen that the sum of the three vectors on the right side of the equation is equal to the sum of the two vectors on the left side or, in other words, the sum of all the vectors in the equation results in a closed polygon as shown in figure 7. Assuming that the inertia characteristics of the aircraft are known, permits one to plot the vectors $I_x\dot{p}$ and $I_{xz}\dot{r}$. The direction of the $L_r r$ and L_β vectors is already indicated and, therefore, the magnitudes are uniquely determined so that a closed polygon results and the derivatives can be obtained. As in the longitudinal case, transfer functions can be determined.

Fourier method. - In the previous methods, a basic assumption made is that the form of the transfer function is known. For the examples cited, the transfer function assumes the form as determined from the equations of motion for a rigid aircraft. If the aircraft were flexible, its transfer function would undoubtedly be different from the transfer function for a rigid aircraft. A method will now be discussed, referred to as the Fourier transform, which does not make any assumption on the equations of motion and enables one to determine the frequency response of the system by analyzing the time-history responses of the aircraft to an arbitrary input. This method has been found useful for analysis of flight tests or of servomotor responses. The procedure is indicated by the expression

$$\frac{\alpha}{\delta}(\omega) = \frac{\int_0^\infty \alpha(t)e^{-i\omega t}\,dt}{\int_0^\infty \delta(t)e^{-i\omega t}\,dt} = Re^{i\Phi}$$

which represents the vector ratio of the Fourier integral of the output α to the Fourier integral of the input δ. At any particular frequency ω, the ratio of the Fourier integrals results in a vector $Re^{i\varphi}$ where R is the amplitude ratio of α to δ and φ is the phase relation between α and δ for a sinusoidal δ input to the system. This method gives data points in amplitude ratio and phase angle at a number of discrete frequencies through which a fairing can be made. The Fourier integral can be integrated by several methods; the NACA has used both manual methods and special machines, which have been reported upon in the literature.

Three methods dependent on the equations of motion have been discussed by means of which airframe stability derivatives can be obtained. These derivatives can be used to obtain any of the transfer functions at any operating altitude.

A method has been discussed which allows examination of airframe frequency response independently of the equations. This method is useful for nonrigid airframes or for inclusion of other unsuspected motions. However, it is limited since the transfer function is applicable only for the data recorded and to the operating condition where the data are obtained.

Error analysis of these methods is a field that may be worthy of exploration.

USE OF TRANSFER FUNCTIONS

The material presented has dealt with the application of dynamic analysis methods for determining airframe stability characteristics. The next part of the paper illustrates a method that has been used by the NACA to study airplane and missile automatic control systems. That is, the method demonstrates the use made of the stability derivatives or transfer functions of the airframe after they have been determined.

The system chosen for illustrative purposes is a system that controls the acceleration of the aircraft normal to the flight path. Figure 8 shows the system in block diagram form. Each of the blocks represents one of the components of the system which would have a transfer function to be used in the analysis; for example, the acceleration block represents the acceleration response of the airframe; a control surface deflection input is operated on by the airframe dynamics to produce an acceleration output.

The servomotor block represents the control surface servomotor; a signal to this motor is acted upon by the motor dynamics and produces a control surface deflection, and so on for the other blocks.

The adjustment of the gains and natural frequencies of a system of this type is very difficult and tedious if based on the solution of differential equations. As a matter of fact, ordinarily, some of the components cannot be represented by differential equations. In this case the use of the experimentally obtained transfer functions is mandatory. Fortunately, the time required to analyze the system performance is reduced if the work is done using frequency characteristics.

For the particular system under consideration, the over-all frequency response of the system without the feedback closure (called the open-loop response) is obtained by a process of multiplication and division of the various component transfer functions. Details of this process may be found in the literature.

It is sufficient to say here that the transfer functions are composed of two parts, amplitude and phase angle functions of frequency. The open-loop transfer function is also composed of two plots, an amplitude plot and a phase plot. These two plots define a frequency dependent vector. For the system being considered, the open-loop response is shown in figure 9.

Stability determination. - If the locus of the tip of this vector is plotted on polar coordinates, the well-known Nyquist diagram results. From this polar plot of the open-loop system shown in figure 10, valuable stability and response characteristics may be determined directly.

Of course, the most direct indication of stability is obtained by factoring the characteristic equation of the system. The presence of positive real roots indicates instability or divergence in the time response. The classical methods of Routh also indicate stability from an examination of the characteristic equation.

Another way of distinguishing stable and unstable roots is to plot them as points in a complex plane as shown in figure 11. A system which has roots only in the left plane is stable, since all real parts of the roots are negative, indicating a damped time response, while the presence of any roots in the right plane indicates instability.

However, since generally only the frequency response or transfer function is available, the need here is for a method of determining the presence or lack or real roots by an examination of the frequency characteristics of the system since equations representing the system are not available.

The imaginary axis in this complex plane corresponds to a frequency axis where the frequency varies from $+\infty$ to $-\infty$. If a method is available that scans the right half of this plane and indicates the lack of roots in the plane, then this method will show that the system is stable.

Function mathematics shows that the path traced by the frequency locus from $+\infty$ to $-\infty$ of the open-loop response (the Nyquist diagram) corresponds to scanning the complex plane. For practical purposes, a frequency locus for positive frequencies from $\omega = 0$ to $\omega = \infty$, which encloses the "critical point" at unit amplitude and 180° phase indicates that the system is unstable. Thus, the stability of a system may be determined directly from examination of the Nyquist diagram.

Performance. - In addition to determination of stability, the designer is also faced with the necessity for determination of quality of performance or degree of stability. Because of the relatively simple relation between the open-loop and closed-loop frequency response, the degree of stability or the quality of performance can be estimated by means of the Nyquist diagram.

Constant values of the closed-loop frequency response may be plotted on the Nyquist or open-loop plane. These are shown in figure 12. The closed-loop contours appear as a family of circles. Everywhere along a particular circle the closed-loop frequency response has a constant value. Intersection of the open-loop-system response plot with a closed-loop contour means that the amplitude of the closed-loop system response is equal to the value indicated by the particular contour. Tangency between the open-loop plot and a contour generally indicates a peak value for the closed-loop amplitude equal to the tangent contour. By the use of this family of circles, the open-loop response may be adjusted to produce a desired closed-loop characteristic.

Extrapolation of experience gained with second-order systems allows the design of higher order systems to be performed with some assurance that the desired performance will be attained. For example, the magnitude of the peak of the frequency response and the overshoot in a step-function response are related. Also, the range of frequencies between zero and the natural frequency controls the rise time in the transient response. A further refinement considers the effect of the open-loop low-frequency asymptote on the closed-loop steady-state behavior.

Thus through shaping and gain changing of the open-loop response the designer can, with experience, produce a specified quality of performance in the control system.

The preceding method is rather fundamental and has in practice been succeeded by a number of refinements such as root-locus methods, Bode diagrams, and logarithm amplitude-phase plots. However, an understanding of the simple graphical techniques described provides a clearer understanding and easier assimilation of the more advanced procedures.

Analog computers. - No discussion of dynamic analysis would be complete without mention of the powerful tool provided by analog computation.

It is probably sufficient to say that it has been our experience that physicists, mathematicians, and aeronautical, mechanical, and electrical engineers can grasp the principles involved and apply analog computers if a background such as implied by this paper is provided.

CONCLUDING REMARKS

Several methods applicable to airframe dynamic analysis have been described as well as one rather fundamental method used for study of automatic control systems. No attempt has been made to examine all the known methods of dynamic analysis, since the methods which prove most useful in one problem may not be the best for a different problem. Several methods which have been applied in practice and the growing part which dynamic analysis will play as a tool for the engineer in the design of future high-speed missiles and aircraft have been indicated.

REFERENCES

1. Bollay, William: Aerodynamic Stability and Automatic Control (The Fourteenth Wright Brothers Lecture). Jour. Aero. Sci., vol. 18, no. 9, Sept. 1951.

2. Breudaus, W. O.: Summary of Dynamic Stability and Control Flight Research Conducted Utilizing a B-25J Airplane. Rep. No. TB-405-F-10, Cornell Aero. Lab., Inc. May 1948.

3. Brown, G. S., and Campbell, D. P.: Principles of Servomechanism. John Wiley & Sons, New York, 1948.

4. Curfman, Howard J., Jr., and Gardiner, Robert A.: Method for Determining the Frequency-Response Characteristics of an Element or System from the System Transient Output Response to a Known Input Function. NACA Rep. 984, 1950. (Supersedes NACA TN 1964.)

5. Den Hartog, J. P.: Mechanical Vibrations. McGraw-Hill Book Co., Inc., 1934.

6. Doetach, K. H.: The Time Vector Method for Stability Investigations. Royal Aircraft Establishment. Rep. Aero. 2495, Aug. 1953.

7. Donegan, James J.: Matrix Methods for Determining the Longitudinal-Stability Derivatives of an Airplane from Transient Flight Data. NACA TN 2902, 1953.

8. Donegan, James J., and Pearson, Henry A.: Matrix Method of Determining the Longitudinal-Stability Coefficients and Frequency Response of an Aircraft from Transient Flight Data. NACA Rep. 1070, 1952. (Supersedes NACA TN 2370.)

9. Eggleston, John M., and Mathews, Charles W.: Application of Several Methods for Determining Transfer Functions and Frequency Response of Aircraft from Flight Data. NACA TN 2997, 1953.

10. Evans, W. R.: Servo Analysis by Locus of Roots Method. Rep. 787, Aerophysics Lab., North American Aviation, Inc., Nov. 1, 1948; Graphical Analysis of Control Systems. A.I.E.E. Trans., vol. 67, 1948.

11. Greenberg, Harry: A Survey of Methods for Determining Stability Parameters of an Airplane from Dynamic Flight Measurements. NACA TN 2340, 1951.

12. Jones, Arthur L., and Briggs, Benjamin R.: A Survey of Stability Analysis Techniques for Automatically Controlled Aircraft. NACA TN 2275, 1951.

13. Lappi, U. O.: A Transient Method for Determining Frequency Response in Lateral Stability. Rep. No. TE-543-F-1, Cornell Aero. Lab., Inc., May 1948.

14. LaVerne, Melvin E., and Boksenbom, Aaron S.: Frequency Response of Linear Systems from Transient Data. NACA Rep. 977, 1950. (Supersedes NACA TN 1935.)

15. Milliken, William F., Jr.: Dynamic Stability and Control Research. Report No. CAL-39, Cornell Aero. Lab., Inc. (Presented at Third International Joint Conference of the R.A.S.-I.A.S. (Brighton, England), Sept. 3-14, 1951.)

16. Nyquist, H.: Regeneration Theory. Bell System Jour., vol. XI, 1932.

17. Seamans, R. C., Blasingame, B. P., and Clementson, G. C.: The Pulse Method for the Determination of Aircraft Dynamic Performance. Jour. Aero. Sci., vol. 17, no. 1, Jan. 1950.

18. Schetzer, J. D.: Notes on Dynamics for Aerodynamicists. Rep. No. SM-14077, Douglas Aircraft Co., Inc., Nov. 1951.

19. Schumaker, Lloyd F.: A Method for Evaluating Aircraft Stability Parameters from Flight Test Data. USAF Tech. Report No. WADC-TR-52-71, Wright Air Development Center, U.S. Air Force, June 1952.

20. Shinbrot, Marvin: A Least Squares Curve Fitting Method with Applications to the Calculation of Stability Coefficients from Transient-Response Data. NACA TN 2341, 1951.

21. Sternfield, Leonard: A Vector Approach to the Analysis of the Dynamic Lateral Stability of Aircraft. Jour. Aero. Sci., vol. 21, no. 4, Apr. 1954.

22. Swanson, Robert S., and Mastrocola, N.: Survey of Methods for Determining Stability Derivatives in Free Flight. U. S. Naval Air Missile Test Center (Pt. Mugu, Calif.), Aug. 1948.

SIMPLIFIED BLOCK DIAGRAM OF AIRFRAME-AUTOPILOT SYSTEM

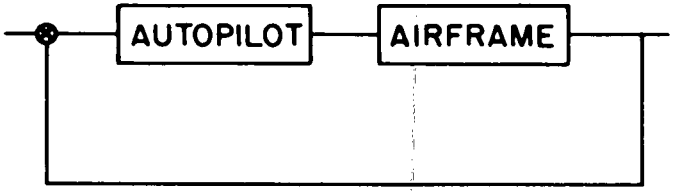

Figure 1

MASS-SPRING-DAMPING FREQUENCY RESPONSE

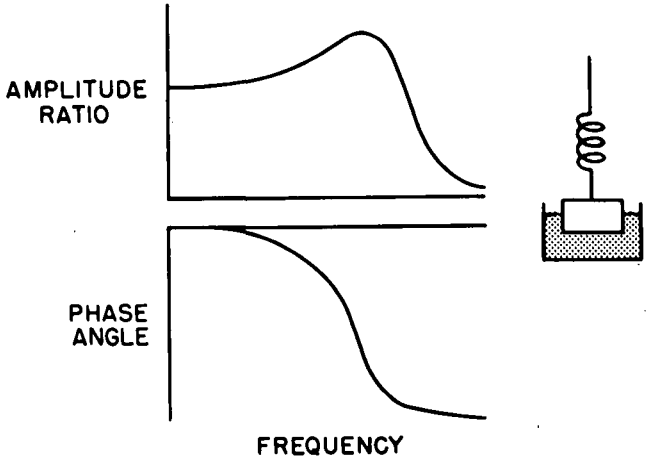

Figure 2

FREE-FLIGHT TIME HISTORIES

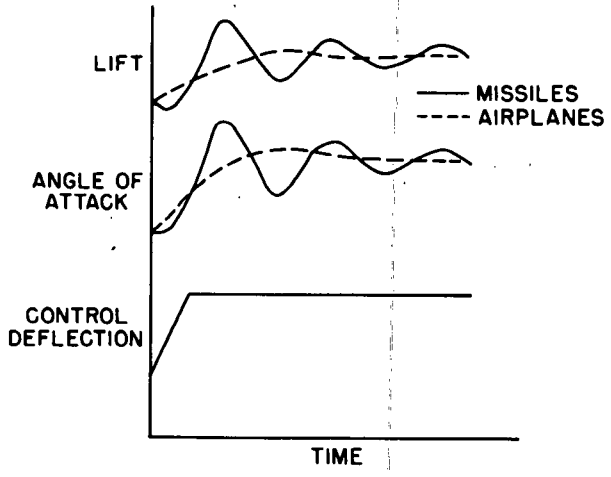

Figure 3

ROTATING-VECTOR PATH

$$\ddot{x} + 2\zeta\omega_n \dot{x} + \omega_n^2 x = 0$$

$$x = x_0 e^{-\zeta\omega_n t}\cos(\omega_n \sqrt{1-\zeta^2}\ t + \lambda)$$

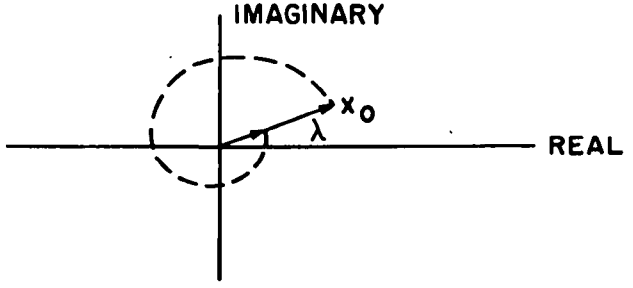

Figure 4

RELATION BETWEEN DISPLACEMENT VECTOR AND DERIVATIVE

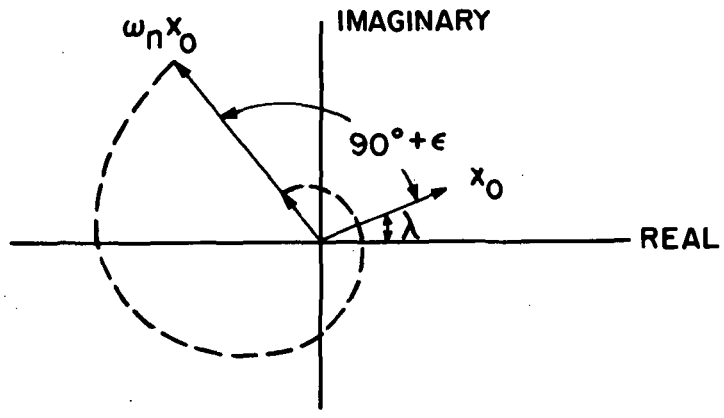

Figure 5

RELATION BETWEEN PHASE AND AMPLITUDE FOR THE LATERAL DEGREES OF FREEDOM

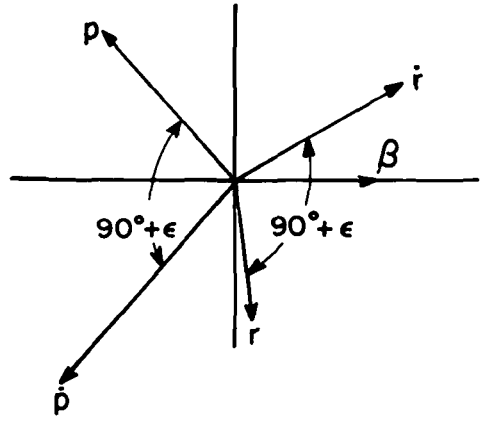

Figure 6

DETERMINATION OF L_r AND L_β DERIVATIVES

$$I_X\dot{\bar{p}} - I_{XZ}\dot{\bar{r}} = L_p\bar{p} + L_r\bar{r} + L_\beta\bar{\beta}$$

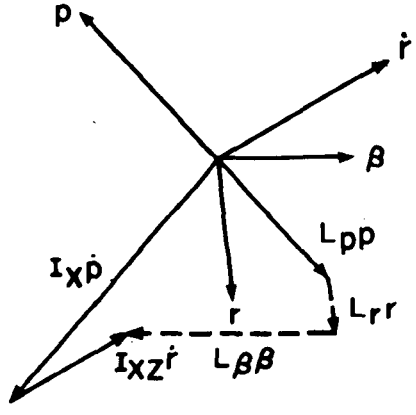

Figure 7

CONTROL-SYSTEM BLOCK DIAGRAM

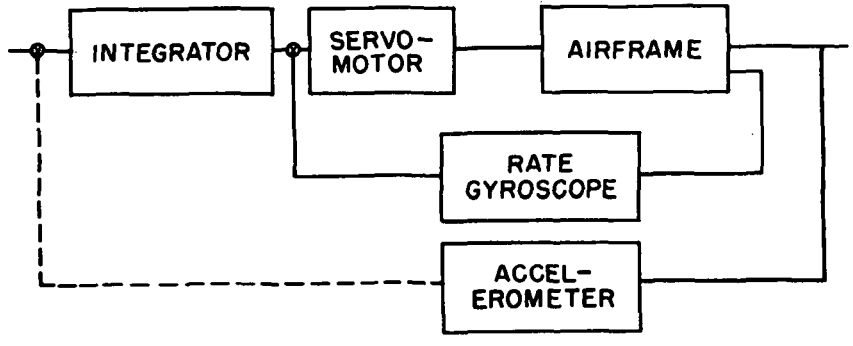

Figure 8

OPEN-LOOP FREQUENCY RESPONSE

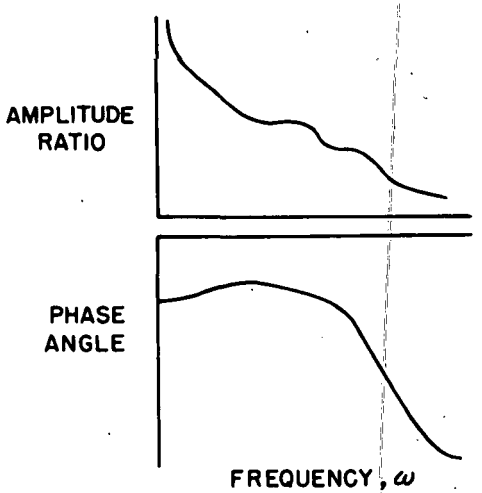

Figure 9

NYQUIST DIAGRAM

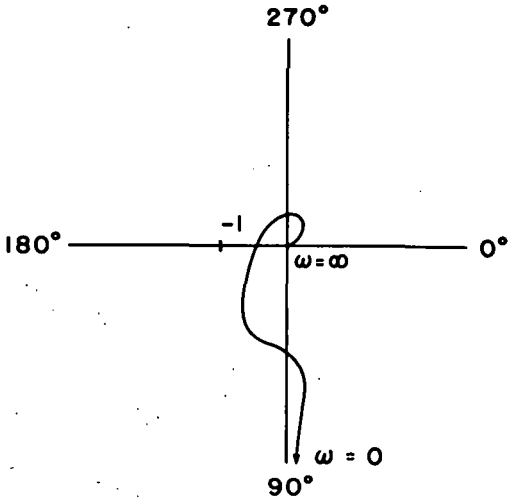

Figure 10

PLOT OF ROOTS IN COMPLEX PLANE

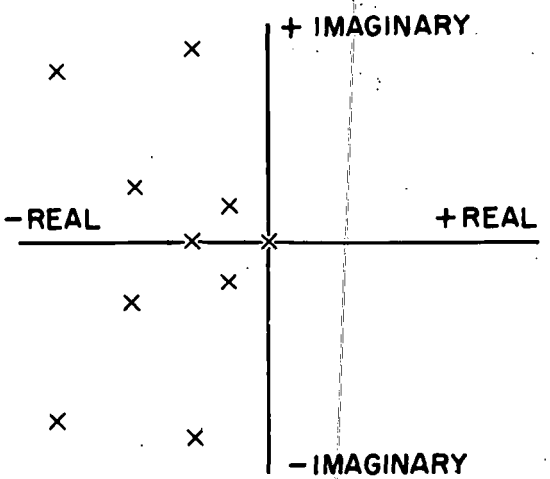

Figure 11

NYQUIST DIAGRAM WITH CLOSED-LOOP CONTOURS

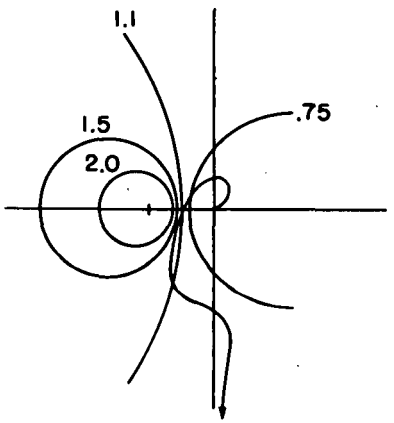

Figure 12

14. A REVIEW OF RECENT ADVANCES IN KNOWLEDGE OF HEAT TRANSFER AND SKIN FRICTION IN HIGH-SPEED AERODYNAMICS

By M. W. Rubesin
Ames Aeronautical Laboratory

This paper is a review of recent advances in the knowledge of heat transfer and skin friction occurring on the surfaces of high-speed aircraft. The subject matter is placed in the following four main categories: boundary-layer transition, heat transfer and skin friction in laminar boundary layers, heat transfer and skin friction in turbulent boundary layers, and transpiration cooling.

Transition must be considered first in boundary-layer problems. Before a solution to a particular boundary-layer problem can be obtained, the question of whether the boundary layer is laminar, turbulent, or transitional and the extent of each region must be determined. The discussion of laminar and turbulent boundary layers has been separated because (1) the theoretical approaches are inherently different and (2) most experiments concentrate on one type of boundary layer or the other. The discussion of transpiration cooling has been set apart from the rest primarily for emphasis on a method which may aid in the solution of the problem of intolerably high heat-transfer rates in high-speed aircraft.

Boundary-Layer Transition

Boundary-layer transition has recently become the object of several investigations at supersonic speeds. Increased interest in this subject has resulted from evidence indicating the possibility of maintaining extensive regions of laminar flow on the surfaces of high-speed aircraft, with the advantage of both lower skin friction and lower heat transfer. The evidence which has led to these investigations was originally provided by Lees-Lin extension of the Tollmien-Schlichting stability theory to include the effects of compressibility (refs. 1 to 4). Although there is no exact relation between stability and transition, the two are related at times when instability can be considered as the starting process of transition. Thus, conditions that are favorable in delaying instability should also be favorable in delaying transition. The factors considered by stability theory to influence boundary-layer transition are shown in table I. They are Mach number, ratio of wall to free-stream temperature, and surface pressure gradient. For certain conditions of Mach number and wall to free-stream temperature, the stability theory predicts the boundary layer to be stable at Reynolds numbers approaching infinity. Also the

theory has shown that negative pressure gradients tend to increase stability, while positive pressure gradients tend to decrease stability (ref. 4).

When experiments on transition are performed to establish the validity of the trends predicted by stability theory, it is found that additional factors not included in the ideal theory are introduced. These additional factors, also shown in table I, are the free-stream turbulence, the surface roughness, and the external disturbances such as are produced by shock waves, noise, or wakes. It has been found that any one of these additional factors, or the surface pressure gradient, can be the controlling factor in establishing the position of transition and that when this occurs systematic variations in the other quantities produce very small effects. Since the free-stream turbulence, surface roughness, and external disturbances are very difficult to control, or even measure, it is not surprising that existing data on transition cannot be universally correlated. All that can be deduced from existing experiments is the influence of the individual factors shown in table I under conditions when the influence of the other factors is believed to be relatively small. The effect of these individual factors, as far as they can be separated from the other factors, is shown in figures 1 to 4.

In figure 1 is shown the effect of surface temperature on the transition Reynolds number for several experiments. Only the beginning of transition is shown. The general trend shown is that heating decreases the transition Reynolds number; cooling increases it. This corresponds qualitatively with the predictions of stability theory. The data included were obtained in flight, in a free-flight wind tunnel, and in conventional wind tunnels. It should be noted that Reynolds numbers as high as 90×10^6 were obtained on a cone 8 feet long in flight (ref. 5). Data obtained in the free-flight wind tunnel (ref. 6), even though hampered by the small physical size of the body of revolution which causes the surface roughness to become relatively large, show Reynolds numbers as high as 12×10^6. The highest Reynolds number obtained in wind tunnels is 28×10^6, which was obtained on a parabolic body of revolution 50 inches long (ref. 7). Data more characteristic of the usual wind-tunnel results are represented by the flat-plate (ref. 8) and cone-cylinder (ref. 9) tests.

The inconsistencies shown in figure 1 can be attributed to effects other than those produced by heat transfer alone. For instance, for the unheated case where $T_w/T_r = 1$, data obtained in the same wind tunnel under identical conditions show a marked effect of the model shape (ref. 10) or, in effect, the pressure gradient. In comparing the data of the parabolic body of revolution, an ogive cylinder, and a cone cylinder, the parabolic body of revolution, which has a favorable pressure gradient for about three-fourths of its length, shows the highest

transition Reynolds number based on the total length of the body. The ogive cylinder, which has an extended favorable pressure gradient over about the first quarter of its length followed by a relative short length of severe unfavorable pressure gradient, shows the next highest transition point. The lowest transition Reynolds number is experienced by the cone cylinder, which has an extremely short favorable pressure gradient followed by a long adverse pressure gradient.

Pressure-gradient effects also become evident when cylindrical bodies fly at an angle of attack (ref. 6). This is shown in figure 2, where the transition Reynolds number on the sheltered side of the body at angles of attack is much smaller than on the windward side. The effect shown can actually be correlated with a pressure-rise coefficient along a streamline passing from the windward to the sheltered side of the body. The experimental effects shown in figures 1 and 2 again qualitatively agree with the results of stability theory.

Studies have also been conducted of the nonideal conditions produced by free-stream turbulence and surface roughness. The qualitative effects of the free-stream turbulence level (ref. 11) are shown in figure 3. The ordinate on this figure represents the fraction of the time a point on the abscissa is fully turbulent. Data of this nature were taken by high-speed photography and indicate that transition occurs at a point which moves about with time. The so-called "transition region" is shown to occur because the position of the transition points moves about with time yielding a continuous statistical distribution. This effect has also been observed in free-flight tests (ref. 6). The effect of increasing the free-stream turbulence from 0.75 percent to 9.4 percent in the stagnation chamber of a wind tunnel is to move the beginning of transition forward. The end of transition in these tests, however, did not vary largely with the change in the turbulence level.

The effect of distributed surface roughness (ref. 6) is shown in figure 4. In this figure the variation of the transition Reynolds number on a model fired in a free-flight tunnel is plotted against the ratio of roughness height to the laminar boundary thickness at transition. The roughness height in this figure is the depth of the screw thread used to create the roughness. It is apparent that increasing the roughness moves transition forward for each of the total-length Reynolds numbers tested.

Laminar Boundary Layer

When the position of boundary-layer transition has been located in a particular boundary-layer problem, the problem resolves itself to an application of existing knowledge concerning the individual types of

boundary layers: the laminar, the turbulent, and, from a statistical viewpoint, the transitional boundary layer. Recently, after years of development, a major advance was made in laminar-boundary-layer theory. The partial differential equations of the laminar boundary layer were solved independently by Cohen and Reshotko (ref. 12), Li and Nagamatsu (ref. 13), and Levy (ref. 14) under conditions which include the effects of variations in gas properties, frictional dissipation, and, primarily, the influence of streamwise pressure variations when heat transfer occurs at the surface. A family of particular solutions of the equations under these conditions was achieved through a transformation of coordinates and is only possible if the Mach number variation at the outer edge of the boundary layer is a certain unique function of the transformed streamwise coordinate. Of course, in the practical case the Mach number variation outside the boundary layer will seldom satisfy the conditions necessary in the analyses. The inability of rigorously applying these analyses directly to practical problems, however, does not depreciate their value. The value of the analyses is fourfold: first, they point out the effects of the major variables such as pressure gradient and heat transfer; second, they provide a standard with which to compare more general but approximate analytical methods; third, they provide information which can be used to formulate new approximate methods capable of being applied generally; and fourth, in some cases, as will be shown presently in an example, they may be applied in an approximate manner using the assumption that the local Mach number variation is controlling, neglecting the effect of the Mach number variation ahead of the point considered.

3556

The results of these analyses, restricted to a Prandtl number of unity and a linear viscosity-temperature relation, are shown in figures 5 to 7. In figure 5 curves are presented showing the effect of pressure gradient on the local skin-friction coefficient. The relation between skin friction and pressure gradient cannot be seen explicitly in this figure because, of necessity, both the ordinate and the abscissa are dependent on the pressure gradient. The term β in the abscissa is related to the local Mach number by the equation $M_1 = cX^{\beta/(2-\beta)}$. The term c is an arbitrary constant. From the equation defining β, it is observed that for an increasing Mach number the exponent of X must be greater than zero, thus requiring $\beta > 0$. Thus, $\beta > 0$ represents a decreasing pressure or favorable pressure gradient, while $\beta < 0$ represents an increasing pressure or an unfavorable pressure gradient. Of course, $\beta = 0$ represents the flat-plate case. In the ordinate, the local skin-friction coefficient and Reynolds number are based on the local velocity and pressure at the outer edge of the boundary layer and the surface temperature. The term F in the denominator of the ordinate depends on the pressure variation also. This dependence is complex, but all that need be indicated is that F is greater than its value on a flat plate when $\beta > 0$, or less when $\beta < 0$. Thus, when $\beta > 0$ the ordinate and

consequently $\frac{C_f}{2}\sqrt{R_x}$ becomes larger than its value for a flat plate. The converse is true for $\beta < 0$. In general, then, a favorable pressure gradient tends to increase the local skin-friction coefficient while an unfavorable pressure gradient decreases it. The effect of heat transfer is shown by the three curves, with the ratio of wall to stagnation temperature as a parameter. In a favorable pressure gradient, raising the surface temperature tends to increase the skin-friction coefficient, while cooling reduces it. Heating and cooling have the inverse effect in an unfavorable pressure gradient.

In figure 6 curves are shown of the ratio of half the skin friction coefficient to the Stanton number, a dimensionless heat-transfer coefficient. On a flat plate with zero pressure gradient, this ratio has the value of unity when the Prandtl number is unity. For each surface-temperature condition a favorable pressure gradient tends to increase this ratio. Physically this means that the skin friction increases more than the heat transfer. Again, the inverse occurs in an unfavorable pressure gradient, the skin friction being reduced much more than the heat transfer.

A comparison is made between these theories and experimental results in figure 7. The data represent local values of the heat-transfer parameter $Nu/\sqrt{Re}$ (ref. 15). The data were obtained on a body of revolution composed of a hemisphere with a cylindrical afterbody. The free-stream Mach number of the tests was 1.97. For these test conditions, the theories could only be applied rigorously at the stagnation point and, in the limit, far downstream on the afterbody. The continuous curve between these points was obtained through an approximation based on the assumption that the local Mach number variation is controlling. This neglects the effect of the Mach number variations ahead of the point considered. Where the theory is applicable rigorously, the comparison with experiment is quite good, considering the scatter in the data. In fact, even where the theory is applied approximately, there is quite good agreement between theory and experiment.

It is interesting to interject, at this point, some experimental results obtained on another hemisphere-cylinder body (ref. 16). Average heat-transfer measurements on the hemispherical nose were found to correlate with subsonic data when the conditions behind the normal shock of the nose were used in the Nusselt and Reynolds numbers. The tests covered Mach numbers between 0.2 and 5.04.

Turbulent Boundary Layer

The foregoing discussion of the laminar boundary layer placed emphasis on the theoretical advances in that subject. Similar emphasis

cannot be made for the compressible turbulent boundary layer. Existing knowledge of the mechanism of turbulence in shear flow, even for the incompressible case, is so meager that most of the theories on this subject are largely syntheses based on assumed turbulent mechanisms. It is known that these assumptions do not conform even with the rudimentary knowledge of the physical phenomenon. The value of these theories, however, should not be depreciated. The assumed turbulence mechanisms introduced constants which, when evaluated empirically, yielded general expressions which allowed existing data to be extrapolated to regions where no data existed at all (ref. 17). At present, as more experimental data are accumulated, the trend in theoretical work is to go from theories using synthesis, based on assumed models, to theories using analysis (refs. 18 and 19), based on close examination of existing data. In the present paper, a most simple theoretical analysis of skin friction (ref. 20) will be presented, although the bulk of the discussion will be confined to experimental results.

A summary of data obtained from experiments dealing with the compressible turbulent boundary layer is shown in figure 8 (refs. 17, 18, and 20 to 24). The ordinate of this figure represents the ratio of skin friction under conditions of compressibility to the corresponding incompressible value at the same length Reynolds number. The ordinate also represents the same ratio for heat transfer. Both local and average quantities are considered in these ratios. The abscissa is the Mach number. Another parameter corresponding to each of the points is the surface-temperature level. The solid symbols represent skin-friction data obtained by direct-force measurements or deceleration tests. The open symbols represent skin-friction data obtained by determining momentum decrements through boundary-layer surveys. The X's represent skin-friction data obtained through velocity-gradient measurements and the +'s represent heat-transfer measurements. The lines shown are analytical predictions (ref. 20) based on the Kármán-Schoenherr equation for incompressible flow except that the properties are evaluated at a reference temperature T' defined by the equation shown on figure 8. The constants of this equation were evaluated using the data at $M = 3$ and at the two temperature levels. The lowest line represents the analytical prediction for surfaces at the recovery temperature where most of the data were obtained. The highest line represents surfaces at the free-stream static temperature. Short segments of lines represent the analytical predictions for intermediate surface temperatures and correspond to the data points for the Mach number at the center of the lines. Shaded areas represent the range of analytical predictions of a group of points at different temperatures.

The most evident fact shown by this figure is that compressibility effects reduce the skin friction and heat transfer. Even extreme cooling, $T_w = T_\infty$, cannot eliminate the favorable effects of compressibility.

It is evident that skin-friction data obtained at recovery temperature by direct-force measurements differ from those obtained by momentum-decrement measurements. In general, it is believed that direct-force measurements are less subject to error than are the momentum measurements.

Another point of interest is that the reduction of heat transfer is essentially the same as the reduction of skin friction. The heat-transfer data were obtained with the surface temperature sufficiently close to the recovery temperature so as to be directly comparable with the skin-friction data. The similarity of the reduction of heat transfer and skin friction indicates that the modifications to Reynolds analogy applicable to the incompressible case are also applicable to the compressible case. This confirms theoretical predictions (ref. 25). An examination of existing high-speed heat-transfer results at other temperature levels has revealed results essentially identical to those shown here (ref. 26).

An additional effect shown by some of the data on this figure is that severe cooling tends to increase the skin friction above that of the insulated case (data points near the upper line). Although this increase does not occur consistently in the data represented by the X's, when the small variation of T_w/T_∞ occurring in these tests is considered (using the analytical results as a guide), it is apparent that the effect expected is small and may be lost in the scatter of the data. On examination of the figure as a whole, it is remarkable how well the simple analytical theory based on the data at $M = 3$ represents the data throughout the body of experimental knowledge.

Transpiration Cooling

Although the effect of compressibility is to reduce the heat-transfer coefficients, the reduction is not sufficient to avoid the aerodynamic heating problem which occurs at high-flight speeds. From considerations of effective cooling systems for aircraft, it has become apparent that one of the most promising is a transpiration cooling system. A transpiration cooling system is defined as one in which the coolant itself passes through the material to be cooled. The coolant may pass through as a gas or as a liquid that would evaporate on the surface. Thus, for an aircraft the coolant would pass through the skin and into the surrounding boundary layer. Naturally, the outer skin of the aircraft would have to be porous. The porosity, however, introduces engineering problems of strength and of manufacture. Because additional problems are introduced, consideration of transpiration cooling would only be made if it could be shown to be very effective. There are two reasons why a transpiration cooling system is thought to be effective. First, from the heat-exchanger viewpoint, a transpiration

cooling system is most efficient in that it raises the temperature of the coolant to the temperature of the outer surface, where the highest temperature in the system exists. Thus, the coolant absorbs the maximum possible amount of heat, thereby being utilized to the fullest. In addition, when the coolant leaves the surface as a gas, it affects the boundary layer so as to reduce the amount of heat entering the body. These two reasons, utilizing the coolant to its fullest and reducing the amount of heat entering the aircraft, make a transpiration cooling system exceptionally effective. A secondary feature is that the skin friction is reduced also.

Much of the existing research on transpiration cooling has been confined to laminar boundary layers (refs. 27 to 29), such as occur on turbine blades. Recently, theories have been formulated (refs. 30 and 31) dealing with the effects of transpiration on high-speed turbulent boundary layers with air as the transpired gas. These theories employ mixing-length concepts and, although guided by subsonic test results (ref. 32), to date they may be considered only as speculative. Representative results of these theories are shown in figure 9 along with results applying to laminar boundary layers. The ordinate represents the ratio of the heat-transfer coefficient under the conditions of transpiration to its value on an impermeable surface, or the similar ratio for the skin-friction coefficient. The abscissa represents the ratio of the mass flow per unit area through the surface to the mass flow per unit area of the free stream divided by the skin-friction coefficient for the no-blowing case. The skin-friction coefficient in the abscissa aids in correlation by removing most of the effect due to the length Reynolds number. Because the Prandtl numbers in these theories are not unity, there is a difference in the curves for skin friction and heat transfer. The most striking point revealed by this figure is the large reductions caused by the transpired gas. The effect on the laminar boundary layer is greater than that on the turbulent boundary layer. It appears that if sufficient coolant is available, the amount of heat entering the body could be reduced to any desired value. It should be pointed out, in conclusion, that although these theories were evaluated for air as the coolant, the results may approximate those produced by stream as the coolant, where the high latent heat of vaporization for water has been utilized.

Thus, in summary, it has been shown that considerable progress has been made recently in the knowledge of skin friction and heat transfer occurring on the surface of high-speed aircraft. In spite of this progress, however, significant gaps still remain and considerable additional research is necessary to establish an adequate foundation for attacking the problem of severe aerodynamic heating and frictional drag.

TABLE I. - FACTORS INFLUENCING BOUNDARY-LAYER TRANSITION

Stability theory	Experimental
Mach number	Mach number
Surface temperature / Free-stream temperature	Surface temperature / Free-stream temperature
Surface pressure gradient	Surface pressure gradient
	Free-stream turbulence
	Surface roughness
	External disturbances (shock waves, noise, wakes)

REFERENCES

1. Lees, Lester, and Lin, Chia Chiao: Investigation of the Stability of the Laminar Boundary Layer in a Compressible Fluid. NACA TN 1115, 1946.

2. Lees, Lester: The Stability of the Laminar Boundary Layer in a Compressible Fluid. NACA Rep. 876, 1947. (Supersedes NACA TN 1360.)

3. Van Driest, E. R.: Calculation of the Stability of the Laminar Boundary Layer in a Compressible Fluid on a Flat Plate with Heat Transfer. Aero. Lab., North American Aviation, Sept. 3, 1951.

4. Low, George M.: Cooling Requirements for Stability of Laminar Boundary Layer with Small Pressure Gradient at Supersonic Speeds. NACA TN 3103, 1954.

5. Sternberg, Joseph: A Free-Flight Investigation of the Possibility of High Reynolds Number Supersonic Laminar Boundary Layers. Jour. Aero. Sci., vol. 19, no. 11, Nov. 1952, pp. 721-733.

6. Jedlicka, J. R., Wilkins, M. E., and Seiff, A.: Experimental Determination of Boundary-Layer Transition on a Body of Revolution at M = 3.5. NACA TN 3342, 1954.

7. Czarnecki, K. R., and Sinclair, Archibald R.: An Extension of the Investigation of the Effects of Heat Transfer on Boundary-Layer Transition on a Parabolic Body of Revolution (NACA RM-10) at a Mach Number of 1.61. NACA TN 3166, 1954. (Supersedes NACA RM L53B25.)

8. Higgins, Robert W., and Pappas, Constantine C.: An Experimental Investigation of the Effect of Surface Heating on Boundary-Layer Transition on a Flat Plate in Supersonic Flow. NACA TN 2351, 1951.

9. Eber, G. E.: Recent Investigation of Temperature Recovery and Heat Transmission on Cones and Cylinders in Axial Flow in the N.O.L. Aeroballistics Wind Tunnel. Jour. Aero. Sci., vol. 19, no. 1, Jan. 1952, pp. 1-6.

10. Hilton, John H., Jr., and Czarnecki, K. R.: An Exploratory Investigation of Skin Friction and Transition on Three Bodies of Revolution at a Mach Number of 1.61. NACA TN 3193, 1954.

11. Evvard, J. C., Tucker, M., and Burgess, W. C., Jr.: Statistical Study of Transition-Point Fluctuations in Supersonic Flow. NACA TN 3100, 1954.

12. Cohen, Clarence B., and Reshotko, Eli: Similar Solutions for the Compressible Laminar Boundary Layer with Heat Transfer and Pressure Gradient. NACA TN 3325.

13. Li, T. Y., and Nagamatsu, H. T.: Similar Solution of Compressible Boundary Layer Equations. Presented at 1954 Heat Transfer and Fluid Mech. Inst., Univ. of Calif. (Berkeley), June 30-July 1, and 2, 1954.

14. Levy, S.: Effect of Large Temperature Changes (Including Viscous Heating) upon Laminar Boundary Layers with Variable Free-Stream Velocity. Jour. Aero. Sci., vol. 21, no. 7, July 1954, pp. 459-474.

15. Stine, H. A., and Wanlass, K.: Theoretical and Experimental Investigation of Aerodynamic Heating and Isothermal Heat Transfer Parameters on a Hemispherical Nose with Laminar Boundary Layer at Supersonic Mach numbers. NACA TN 3344, 1954.

16. Stalder, Jackson R., and Nielsen, Helmer V.: Heat Transfer from Hemisphere-Cylinder Equipped with Flow-Separation Spikes. NACA TN 3287, 1954.

17. Rubesin, Morris W., Maydew, Randall C., and Varga, Steven A.: An Analytical and Experimental Investigation of the Skin Friction of the Turbulent Boundary Layer on a Flat Plate at Supersonic Speeds. NACA TN 2305, 1951.

18. Coles, D.: Measurements in the Boundary Layer on a Smooth Flat Plate in Supersonic Flow. Ph.D. Thesis, C.I.T., 1953.

19. Clauser, Francis H.: Turbulent Boundary Layers in Adverse Pressure Gradients. Dept. Aero., Johns Hopkins Univ., June 1953. (Contract AF 33(038)9862.)

20. Sommer, S. C., and Short, B. J.: Some Measurements in Free Flight of the Skin Friction of Turbulent Boundary Layers at High Rates of Heat Transfer and High Supersonic Speeds. (Proposed NACA TN)

21. Chapman, Dean R., and Kester, Robert H.: Turbulent Boundary-Layer and Skin-Friction Measurements in Axial Flow Along Cylinders at Mach Numbers Between 0.5 and 3.6. NACA TN 3097, 1954.

22. Lobb, R. K., Winkler, E. M., and Persh, J.: Experimental Investigation of Turbulent Boundary Layers in Hypersonic Flow. Preprint No. 452, Inst. Aero. Sci., 1954.

23. Pappas, C. C.: Measurement of Heat Transfer in the Turbulent Boundary Layer on a Flat Plate in Supersonic Flow and Comparison with Skin-Friction Results. NACA TN 3222, 1954.

24. Brevoort, M. J., and Rashis, B.: Turbulent-Heat-Transfer Measurements at a Mach Number of 2.06. (Proposed NACA TN)

25. Rubesin, Morris W.: A Modified Reynolds Analogy for the Compressible Turbulent Boundary Layer on a Flat Plate. NACA TN 2917, 1953.

26. Seiff, Alvin: Examination of the Existing Data on the Heat Transfer of Turbulent Boundary Layers at Supersonic Speeds from the Point of View of Reynolds Analogy. NACA TN 3284, 1954.

27. Eckert, E. R. G.: Heat Transfer and Temperature Profiles in Laminar Boundary Layers on a Sweat Cooled Wall. Tech. Rep. no. 5646, Air Materiel Command, Nov. 3, 1947.

28. Brown, W. Byron, and Donough, Patrick L.: Tables of Exact Laminar-Boundary-Layer Solutions When the Wall is Porous and Fluid Properties are Variable. NACA TN 2479, 1951.

29. Emmons, H. W., and Leigh, D.: Tabulation of the Blasius Function with Blowing and Suction. Combustion Aero. Lab., Harvard Univ., Nov. 1953.

30. Dorrance, W. H., and Dore, F. J.: The Effect of Mass Transfer on the Compressible Turbulent Boundary Layer Skin Friction. Jour. Aero. Sci., vol. 21, no. 6, June 1954.

31. Rubesin, M. W.: An Analytical Approximation of the Effect of Transpiration Cooling on the Heat Transfer and Skin Friction Characteristics of a Compressible, Turbulent Boundary Layer. NACA TN 3341, 1954.

32. Mickley, H. S., Ross, R. C., Squyers, A. L., and Steward, W. E.: Heat, Mass, and Momentum Transfer for Flow over a Flat Plate with Blowing or Suction. NACA TN 3208, 1954.

EFFECT OF SURFACE TEMPERATURE ON TRANSITION

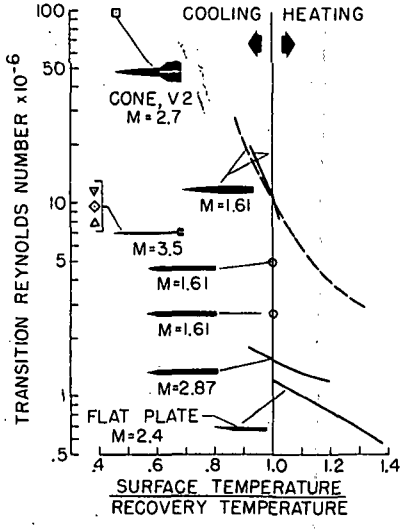

Figure 1

EFFECT OF ANGLE OF ATTACK ON TRANSITION

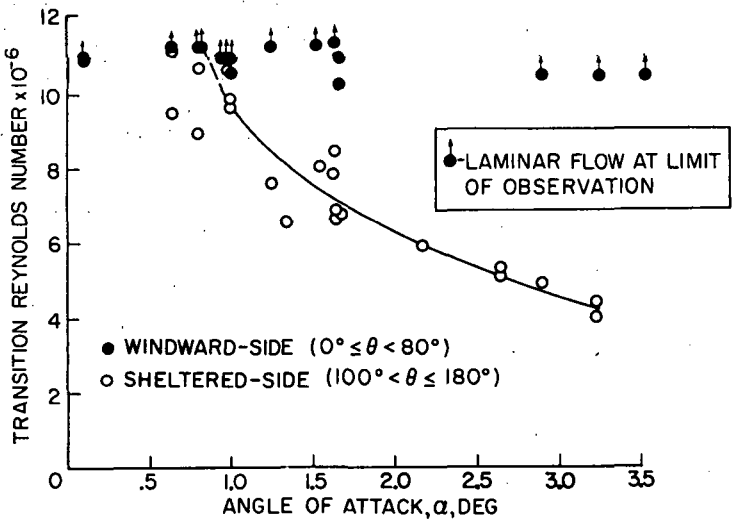

Figure 2

STATISTICAL DISTRIBUTION OF TRANSITION-POINT LOCATION ON A CONE

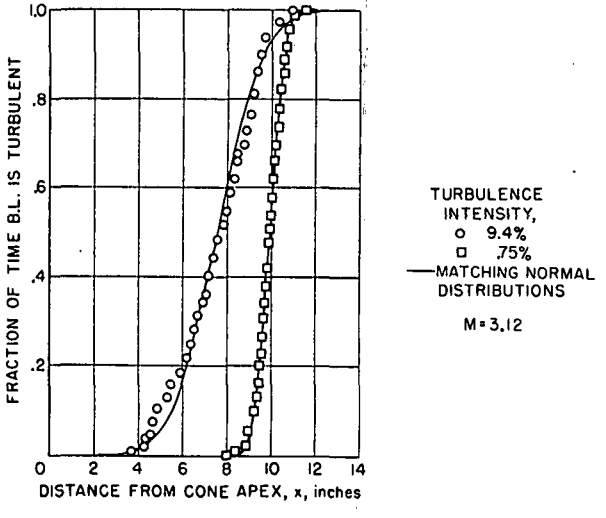

Figure 3

EFFECT OF ROUGHNESS ON TRANSITION
OGIVE-CYLINDER

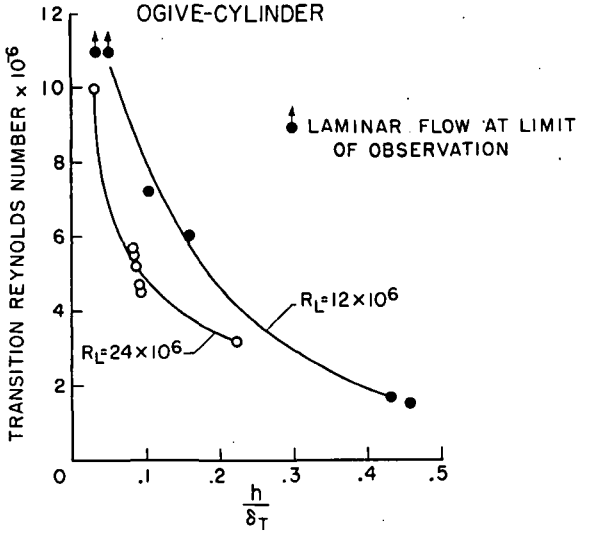

Figure 4

EFFECT OF PRESSURE GRADIENT ON LOCAL SKIN FRICTION

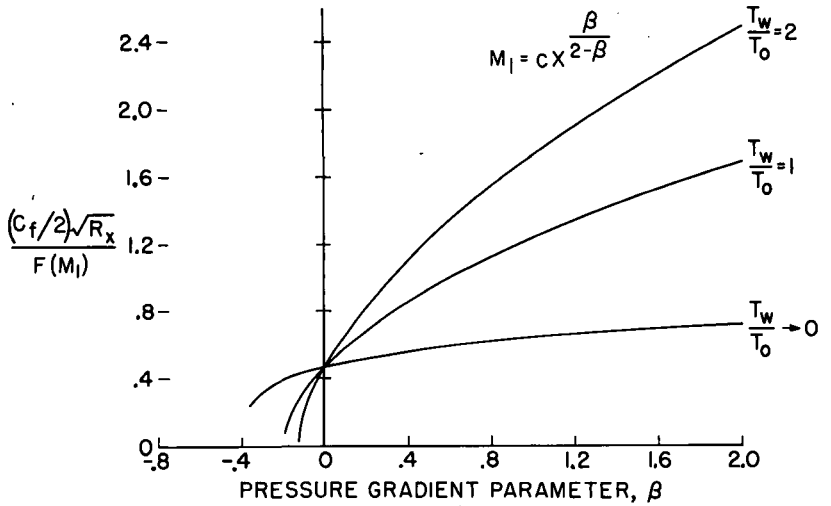

Figure 5

EFFECT OF PRESSURE GRADIENT ON RATIO OF SKIN FRICTION TO HEAT TRANSFER

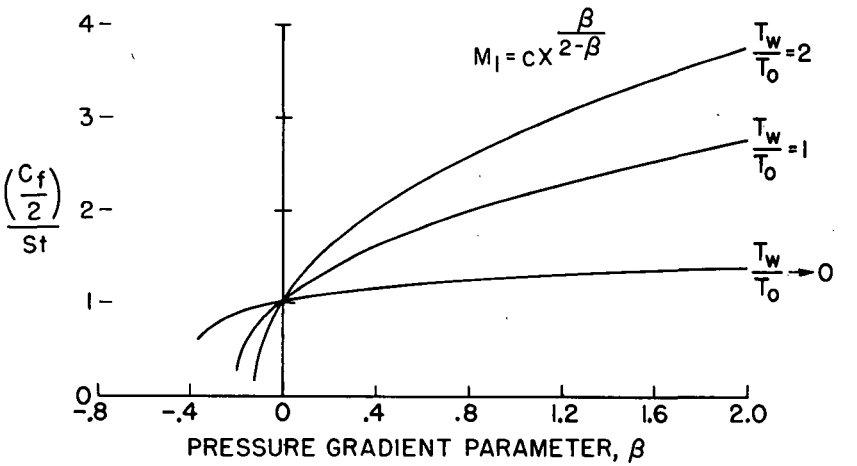

Figure 6

COMPARISON OF LAMINAR BOUNDARY LAYER DATA WITH THEORY

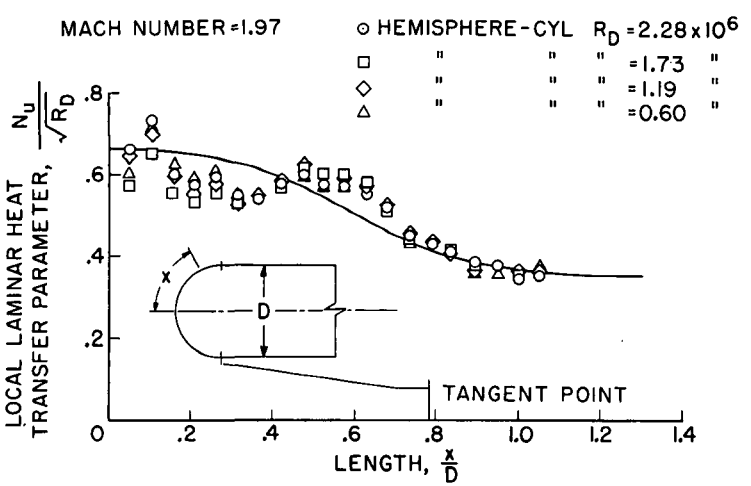

Figure 7

COMPRESSIBILITY EFFECT ON TURBULENT BOUNDARY LAYER

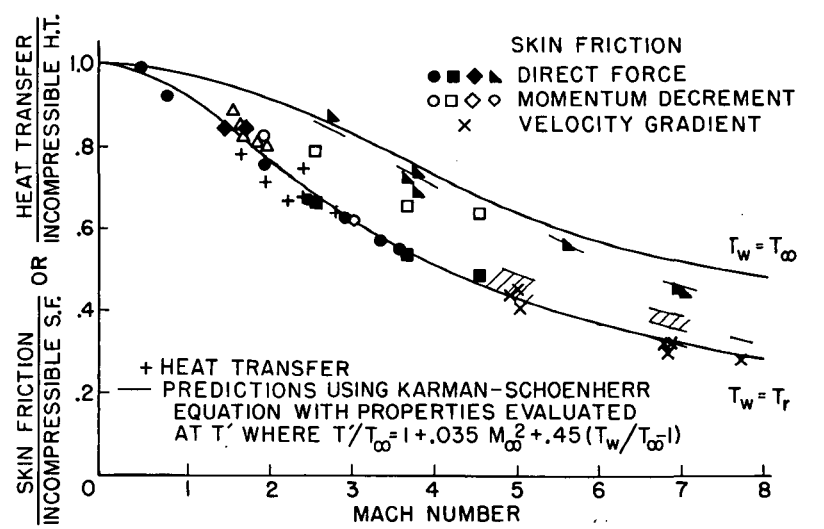

Figure 8

EFFECT OF TRANSPIRATION ON HEAT TRANSFER AND SKIN FRICTION

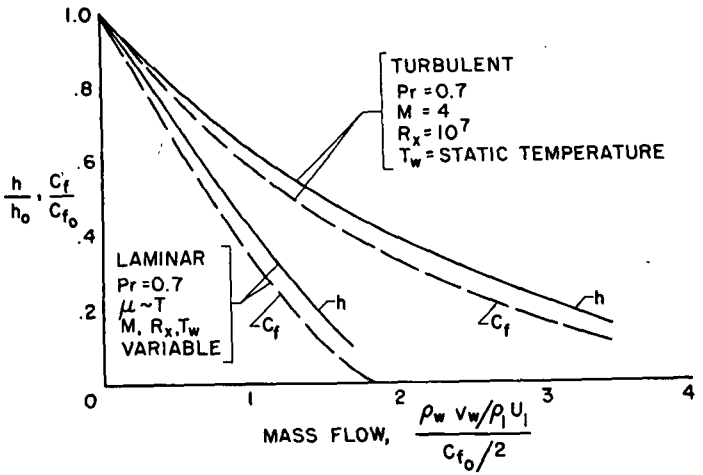

Figure 9

15. THEORETICAL AND EXPERIMENTAL ANALYSES OF SOME SUPERSONIC FLOW FIELDS

By Max A. Heaslet
Ames Aeronautical Laboratory

INTRODUCTION

In studying the phenomena of high-speed flow, both experimentalists and theorists are forced to idealizations that, a priori, may seem drastic; but economic as well as technical limitations continually force the scientist into a position of attempting to attain a proper compromise between the true physical occurrence and the formulation of a model for work and study. Considerable simplification is, however, achieved at the outset if study can be limited to airplanes or missiles designed to be kept aloft by forces associated with the compression and rarefaction of a continuous atmospheric medium. Many difficulties yet remain to be considered; for example, insistence upon excessive flight speed can result in high stagnation temperatures which must be considered in defining the properties of the air; but in theoretical aerodynamic studies of currently feasible aircraft, it is customary to relate the basic variables (that is, the three air-velocity components, pressure, density, and temperature) by means of

(a) The three Eulerian momentum equations

(b) The continuity condition

(c) The equation of state with constant specific-heat coefficients

(d) The energy relation

Furthermore, heat conduction is neglected and the effect of viscosity is treated separately.

In practice, this approach leads to differential relations applying to the continuous part of the field and the Rankine-Hugoniot shock-wave relations that hold at discontinuity surfaces. These shock waves appear throughout the transonic, supersonic, and hypersonic flight regions and will play an important role in the subsequent papers on transonic and hypersonic flow. For present purposes, further restrictions are made that enable study of the purely supersonic region by relatively simple means. To this end, aircraft are assumed to be designed to keep disturbance velocity components and their gradients small relative to flight and sound speed, with some characteristic body length used for reference. The small-disturbance theory has proved to be the most successful way of studying both transonic and supersonic flow, particularly for three-dimensional shapes. In the supersonic theory the basic equations are linearized and, in effect, deal with first-order acoustic theory; mathematically, the dependent variable is a scalar, perturbation-velocity potential satisfying the wave equation.

SMALL-PERTURBATION THEORY AND EXPERIMENT

Figure 1 is a schematic representation showing some of the important features of the physical and theoretical problems under steady-state conditions. For purposes of clarity, the tip effects on the wing are not included. Point P is the position of an observer who wishes to record the induced effects of the wing at that point. In the idealization reached, the equation at the top of the figure is the one satisfied by the steady-state perturbation potential, the coordinate system being fixed on the wing. A free stream of velocity U_o and Mach number M_o is directed at the wing and the observer at P hears signals only from disturbances lying within the Mach fore-cone from P, the entire disturbance field lying downstream of the Mach waves extending back from the wing leading edge. The cross-hatched area of the wing plan form thus defines the disturbance region affecting P with an added portion that is due to the wake behind the wing. Two properties of the theoretical model should be mentioned explicitly:

(a) The Mach waves (or characteristic lines) of the flow field are straight lines inclined at the free-stream Mach angle $\mu \equiv \arcsin(1/M_o)$ to the stream direction.

(b) Under the assumptions made, pressures on the wing are additive functions of thickness and angle of attack or camber, thickness pressure being the same on the upper and lower surface and lifting pressure being equal in magnitude but opposite in sign when measured relative to free-stream or ambient pressure.

Far away from a wing or body, the Mach waves are displaced so that the straight-line approximation does not agree with observations; this effect is more pronounced for bluff shapes. Near the surface of thin and properly streamlined shapes, the results are satisfactory. Furthermore, the equal division of load as well as the assumption of small perturbations from values of ambient pressure and density can also become invalid for various reasons. Suppose, for example, that an airplane is to fly at 60,000 feet altitude where the ambient pressure is approximately 150 pounds per square foot. For a wing loading of 50 pounds per square foot, the differential supporting pressure is one-third the ambient pressure and the neglected quadratic terms in the analysis are appreciable in size. Increases in altitude or wing loading thus can not be tolerated indefinitely without modifications in the methods of prediction.

Figures 2(a) and 2(b) show, for two pressure orifices, a comparison between theory and tests of pressure coefficient on the tip of a wing of trapezoidal plan form (ref. 1). The wing section is a symmetrical wedge of $5^\circ 43'$ total included angle in the streamwise direction. Free-stream Mach number is 1.9; the wing-tip leading edge is swept back 70° and the Mach lines (shown dashed in the insert) are swept back 58°.

This means that the component of the stream normal to the edge tip is less than 1 (a subsonic-type edge). Pressure coefficient is plotted against wing angle of attack, the points representing experimental values and the dashed lines giving values predicted by small-disturbance theory. In figure 2(a), the solid curve shows predicted values based on exact potential theory which can be applied without difficulty in this case, since the pressure orifice lies outside the region of influence of the wing tip and the flow has a two-dimensional character. As can be seen on either graph, the small-perturbation theory yields acceptable results over a sizable angle-of-attack range, but it obviously fails completely for more extreme values of α.

Although the wave equation is a classical form arising in mathematical physics, the aerodynamic boundary conditions are such as to require elaboration of conventional methods of solution. In general, three standard methods of approach are used:

(a) Source and lifting-element theory analogous to conventional incompressible-flow methods (see, e.g., refs. 2 to 5).

(b) Re-expression of the problem in terms of transform theory. In supersonic flow, Laplace or Heaviside transforms are most advantageous (see, e.g., refs. 6 to 9).

(c) Treatment of problems involving conical and quasi-conical flow (see, e.g., refs. 10 to 13).

These methods are not mutually exclusive: conical-field theory can be developed from source and vortex theory; transform theory, which appears to fit well into the study of bodies of revolution, can also be replaced in this case by source and vortex rings. It is well to recognize, however, that each method has an affinity to certain types of problems and that, furthermore, other techniques, such as the method of separation of variables, are also available and may be useful in particular instances.

Figure 3 shows a comparison between theory and experiment for a lifting wing of triangular plan form at a free-stream Mach number equal to 1.49 (ref. 14). The wing section is a 6 percent thick, circular-arc profile modified to have a rounded nose and a leading-edge sweep angle of 70°. Chordwise-loading coefficient is plotted against percentage of local chord at two spanwise stations for angles of attack equal to 2°, 4°, and 6°. The dashed lines represent theoretical predictions and the solid lines are faired through the experimental points. Results that were measured farther outboard showed greater deviations.[1] Figure 4

[1]This effect is due to leading edge separation and is thus associated with viscous properties of the air. On highly swept wings, however, it is possible to remain within the framework of potential analysis and at the same time achieve improvements in the theoretically predicted loadings for such conditions. In this connection, see refs. 15 and 16.

shows the span loading of the wing for the same angles of attack and, in the inset, the integrated lift as a function of angle of attack. These figures indicate the interesting fact that the integrated lift of linearized theory can maintain its validity for thin wings even beyond angles of attack for which the details of the flow field deviate from those predicted.

RECIPROCAL RELATIONS AND THEIR APPLICATION

If the attempt to calculate the local details of the flow about wings is abandoned and the prediction of total aerodynamic forces and moments is made a prime consideration, a powerful tool becomes available to us. Suppose, for example, that it is desired to calculate the integrated lift on a wing induced by a change in camber. The problem becomes one of integrating over the plan form a lift influence function associated with the camber change, and this calls to mind the interdependence of influence functions in elasticity theory based on small deflections and quadratic strain-energy relations. Figure 5 shows how these latter concepts are applied to a cantilevered beam. Under one condition the beam is subjected to a force F at point A and the resultant deflection D is measured at point B. If, on the other hand, a force $\overline{F}$ had been applied at B and the deflection $\overline{D}$ measured at A, the relation on the figure holds true; that is, force at A times deflection at A due to the force at B is equal to the force at B times the deflection at B due to the force at A. This law stems from energy considerations and holds for generalized forces and deflections; for example, the forces may be torques if the deflections are measured in angular units (ref. 17). General dynamical systems starting from rest obey similar laws where the generalized forces is replaced by impulse and deflection, by velocity. The problem now is to seek a corresponding result in wing theory. The left side of figure 6 shows a wing of given plan form flying into still air at a Mach number M_0. On the element of area at A a pressure is applied and the stream deflection is measured at B; similarly, a pressure can be applied at B and the deflection measured at A. The analogue to the structural problem follows without difficulty if the proper symmetrization is provided by assuming that the wing in its second mode is subjected to the same static atmospheric conditions but is flying at the same speed in the reverse direction. The first equation on the figure then establishes a reciprocal relation between pressure and upwash in the two fields, the bar notation denoting conditions in reverse flight (see refs. 18 and 19).

As derived, the reciprocal relation applies to unsteady motion and thus includes transient effects; for steady-state flight and certain unsteady motions, the much simpler form in the second equation applies

where the timewise integration is deleted. The results hold in subsonic as well as supersonic flight subject only to the assumptions of small disturbances; restrictions to planar conditions can also be relaxed. As a first example, consider a flat plate wing placed at the same angle of attack in forward and reverse flow. Upwash velocities w and $\bar{w}$ are equal in magnitude and constant; it is concluded, after integration, that lift curve slope in either direction is the same (ref. 20). Figure 7 shows experimental evidence of this for a number of wing plan forms at $M_o = 1.53$ (ref. 21). (It should be remarked that some of the difference between theory and experiment observed may be attributable to the structural flexibility of the models.) The dashed curve was originally calculated by analyzing each plan form separately, and the difficulty of the labor forced a curtailment of the predictions at the sweep angle -40^o. By abandoning the frontal attack and resorting to reverse-flow theorems, unnecessary labor is avoided, and, at the same time, the range of predicted values is extended.

Reciprocal theorems can also be used to relate drag and aerodynamic moments in fore and aft flow, but these characteristics are more sensitive to scale effects and thus difficult to check experimentally. The insert shows the experimental value of total drag as well as the theoretical wave drag. The discrepancy at zero sweep is attributable to viscous drag. For sweep angles yielding sonic edges, the predicted wave drag is less reliable and tends to overestimate the true value. In the determination of transient characteristics where both theoretical and experimental methods are usually difficult as well as tedious, reciprocal theorems offer a valuable research tool. (Theoretical application of these techniques can be found, for example, in refs. 22 and 23.)

Two large areas of application of reciprocal theorems remain to be discussed. The first of these appears in the determination of influence functions; the second appears in the minimization of the wave drag of shapes under geometric constraints. As an example of the first type of problem, consider, as shown in figure 8, a lattice of two-dimensional lifting planes in a subsonic free stream. The angle-of-attack loading can be calculated by potential theory and is indicated in figure 8(a). In figure 8(b), the plates are held at zero angle of attack and flaps on the rear portion are deflected. The resultant loading is shown, and the problem is to integrate under this curve and find the lift on one of the airfoils due to collective flap deflections. Application of the reciprocal relation reveals that this loading is equal to the integral over the flap itself of the original flat plate loading in reverse; the cross-hatched areas in figures 8(b) and 8(c) are therefore equal, and load due to flap deflection can be determined, at least by potential theory, by a single quadrature.[2]

[2]The expression for the angle-of-attack load distribution was derived by Mr. Paul F. Byrd of the Ames Aeronautical Laboratory. His

SUPERSONIC WAVE DRAG AND ITS MINIMIZATION

In supersonic flight, the induced vortex drag due to lift is augmented by wave drag due to both thickness and lift. As in the Trefftz-plane analysis of vortex drag, the wave drag in linear theory can be evaluated by momentum control-surface methods, and Hayes (ref. 11) has developed from such concepts the idea of "equivalent positions" of thickness and lifting elements. In this way, counterparts to Munk's stagger theorem for vortex drag now appear in supersonic wave drag. It is natural that one should apply all available avenues of attack to minimize wave drag under given constraints, just as it was natural that Prandtl and his students sought to minimize vortex drag under the condition of given lift. Such problems will no doubt occupy the attention of aerodynamicists for some time. If, at the outset, one limits oneself, for simplicity, to nonlifting configurations and treats wave drag due to thickness alone, a large array of aerodynamic configurations yet remains to be considered.

It is important to realize that the thickness wave drag is not necessarily present (ref. 24). By proper shrouding of an object, for example, the waves can be held captive and a form of D'Alembert's paradox survives in supersonic flow. Figure 9 shows schematic arrangements of configurations that, in the absence of lift, experience no drag in small-disturbance theory. The first case (example (a)) is two-dimensional, the airfoil having above and below it shrouding plates that produce favorable interference pressures on the rear portion of the airfoil. Example (b) shows the extension of this idea to an axially symmetric body encased within a cylindrical tube. Example (c) shows a proper fairing on the inside of a cylindrical tube with a geometry and a pressure field that are symmetric fore and aft so that drag is again zero. There also remains the fourth possibility of an infinite-aspect-ratio wing with angle of sweep greater than that of the free-stream Mach lines, drag being zero by virtue of the fact that the disturbance field is expressible in terms of a harmonic potential function. Further cases could be exhibited, but these examples are representative. In the class of problems usually considered, the more involved problems of shrouded figures and arbitrary spatial distributions are neglected and one deals with configurations that more nearly resemble conventional wings and body

---

integration of the final expression in the figure yielded the following for lift due to flap deflection:

$$\frac{L}{q_o} = \frac{8\epsilon}{\beta\lambda} \frac{1 + \tanh c\lambda}{1 + \tanh c\lambda + \operatorname{sech} c\lambda} \left\{ \tan^{-1} \left[\frac{\tanh c\lambda - \tanh \lambda(c - d)}{(1 - \tanh c\lambda) \tanh \lambda(c - d)} \right]^{1/2} \right.$$

$$\left. - \frac{\operatorname{sech} \lambda c}{1 + \tanh \lambda c} \tan^{-1} \left[\frac{\tanh c\lambda - \tanh \lambda(c - d)}{(1 + \tanh c\lambda) \tanh \lambda(c - d)} \right]^{1/2} \right\}$$

where $\lambda = \pi/\beta h$

shapes. It is apparent that a high degree of arbitrariness is involved in setting up such problems and that by shifting attention to other shapes, for example, to highly swept wings of relatively large aspect ratio, the minimum wave drag of one class of wings may be well below that of another class.

For purposes of illustration, one problem can be discussed that embodies several ideas in drag minimization. On figure 10 is shown a cylindrical surface of radius R and length l. Immediately external to this surface is draped an axially symmetric shape of given volume and minimum wave drag. In the figure, a source-strength distribution function $A(x)$ is also drawn along the body axis, the function being determined in such a way that it induces streamlines that conform with the external body shape. The external wave drag of the body can then be evaluated in two ways: in terms of the distribution of its cross-sectional area $S(x)$ (ref. 8), and in terms of the source function $A(x)$ (ref. 25). The equations on the figure give the explicit form of the two drag relations; they are quadratic functions in the streamwise gradients of $A(x)$ and $S(x)$, and $W(x)$ is a known transcendental function. It remains to determine an expression for volume and then to minimize the wave drag. Here again the two formulas lead to different algebraic techniques. The minimization of the first formula establishes a criterion that could have been derived easily from the reciprocal theorem extended to bodies of revolution; namely, that the condition of minimum drag under the restriction of constant volume is that the so-called "pressure in the combined flow field" is a linear function of the streamwise dimension. R. T. Jones has applied these concepts to the study of supersonic wings (refs. 26 and 27). In the present case, however, the second drag formula is used (ref. 28), since it led to more familiar methods. In figure 11, body geometry is indicated for three values of reduced fineness ratio; the curves are drawn with equal maximum ordinates so that comparison of them is easier. For vanishing R, the well-known Sears-Haack slender body appears (refs. 29 and 30); for infinitely large R the result reduces by necessity to the two-dimensional form of the answer, that is, to the biconvex arc. It is possible to give an explicit expression for the body shape, and the intermediate case shown is calculated from this result. Considered as a function of $\beta R/l$, the area distribution quickly approaches the two-dimensional answer. In the insert the minimum drag is plotted with appropriate nondimensionalization factors involving body length l, added external volume V_e, and stream dynamic pressure q_o. The dashed curve shows drag calculated according to quasi-cylindrical theory but under the assumption that the pressure distribution as well as the geometry remains two-dimensional throughout the entire range. Here again, the prediction based on the assumption of two-dimensionality quickly becomes a good approximation as $\beta R/l$ increases.

CONCLUDING REMARKS

Essentially, the discussion has been confined to comparisons of experiments and results obtainable from first-order steady-state analysis. In closing, two further avenues of investigation should also be mentioned, since it appears that they may play increasingly important roles in the theoretical development of supersonic research. The first of these is concerned with the investigation of transient effects and unsteady flow fields in general. It has recently been found possible, for example, to predict nonlinear thickness effects on the aerodynamic damping of harmonically oscillating airfoils (ref. 31), and also to extend to the time-dependent analysis of wings (ref. 22) the important concept of "reflected area" discovered by Evvard for steady-state flow (ref. 5). The extent to which the study of unsteady motion is developed will possibly be affected by the demands of aircraft design, since the labor involved in actual predictions is great and the analysis is closely related to the nature of the wing structure. The techniques of prediction are, however, available for exploitation.

A final field of investigation appears in the extension of the linearized steady-state theory to attain more accurate predictions and, in particular, to achieve improvements in the details of the flow field. Linear analysis usually yields singularities in pressure at the subsonic edges of wings, but these inconsistencies can be removed by proper treatment and pressure distributions correct to higher order can then be calculated (refs. 32 and 33). The hope of extending three-dimensional supersonic theory into the fully nonlinear range of potential theory is a somewhat optimistic one at the present time, and the orderly refinement of existing results will probably be a more rewarding endeavor from the practical point of view.

REFERENCES

1. Jagger, James M., and Mirels, Harold: Experimental Pressure Distributions over Wing Tips at Mach Number 1.9. I - Wing Tip with Subsonic Leading Edge. NACA RM E8K26, 1949.

2. Prandtl, L.: Theorie des Flugzeugtragflügels im zusammendrückbaren Medium. Luftfahrtforschung, Bd. 13, Nr. 10, Oct. 1936, pp. 313-319.

3. Puckett, Allen E : Supersonic Wave Drag of Thin Airfoils. Jour. Aero. Sci., vol. 13, no. 9, Sept. 1946, pp. 475-484.

4. Heaslet, Max A., and Lomax, Harvard: The Application of Green's Theorem to the Solution of Boundary-Value Problems in Supersonic Wing Theory. NACA Rep. 961, 1950. (Supersedes NACA TN 1767.)

5. Evvard, John C.: Use of Source Distributions for Evaluating Theoretical Aerodynamics of Thin Finite Wings at Supersonic Speeds. NACA Rep. 951, 1950.

6. Gunn, J. C.: Linearized Supersonic Airfoil Theory, Pt. I, II. Phil. Trans. Roy. Soc. (London), ser. A, vol. 240, no. 820, 1947, pp. 327-373.

7. Lighthill, M. J.: Supersonic Flow Past Slender Bodies of Revolution the Slope of Whose Meridian Section is Discontinuous. Quart. Jour. Mech. and Appl. Math., vol. 1, pt. 1, Mar. 1948, pp. 90-102.

8. Ward, G. N.: The Approximate External and Internal Flow Past A Quasi-Cylindrical Tube Moving at Supersonic Speeds. Quart. Jour. Mech. and Appl. Math., vol. 1, pt. 2, June 1948, pp. 225-245.

9. Ward, G. N.: Supersonic Flow Past Slender Pointed Bodies. Quart. Jour. Mech. and Appl. Math., vol. II, pt. 1, Mar. 1949, pp. 75-97.

10. Busemann, Adolf: Infinitesimal Conical Supersonic Flow. NACA TM 1100, 1947.

11. Hayes, W. D.: Linearized Supersonic Flow. Rep. AL-222, North American Aviation, 1947.

12. Lagerstrom, P. A.: Linearized Supersonic Theory of Conical Wings. NACA TN 1685, 1950.

13. Heaslet, Max A., and Lomax, Harvard: General Theory of High Speed Aerodynamics, sec. D. Princeton Univ. Press, 1954, pp. 186-206.

14. Drougge, G., and Larsson, P. O.: Rep. 57, Aero. Res. Inst. (Sweden). (To be published.)

15. Legendre, Robert: Ecoulement au voisinage de la pointe avant d'une aile a forte fleche aux incidences moyennes. La Recherche Aeronautique, Bulletin Bimestriel, ONERA, Nov.-Dec. 1952-Jan.-Feb. 1953.

16. Brown, C. E., and Michael, W. H., Jr.: On Slender Delta Wings with Leading-Edge Separation. (Proposed NACA TN.)

17. Rayleigh: The Theory of Sound. Dover Pub., N. Y., 1944.

18. Heaslet, Max A., and Spreiter, John R.: Reciprocity Relations in Aerodynamics. NACA Rep. 1119, 1953. (Supersedes NACA TN 2700.)

19. Flax, A. H.: Reverse Flow and Variational Theorems for Lifting Surfaces in Non-Stationary Compressible Flow. Jour. Aero. Sci., vol. 19, 1952, pp. 361-374.

20. Brown, Clinton E.: The Reversibility Theorem for Thin Airfoils in Subsonic and Supersonic Flow. NACA Rep. 986, 1950. (Supersedes NACA TN 1944.)

21. Vincenti, Walter G.: Comparison Between Theory and Experiment for Wings at Supersonic Speeds. NACA Rep. 1033, 1951. (Supersedes NACA TN 2100.)

22. Lomax, Harvard, Fuller, Franklyn B., and Sluder, Loma: Generalized Indicial Forces on Deforming Rectangular Wings in Supersonic Flight. NACA TN 3286.

23. Tobak, Murray: On the Use of the Indicial Function Concept in the Analysis of Unsteady Motions of Wings and Wing-Tail Combinations. NACA Rep. 1188, 1954.

24. Busemann, A.: Aerodynamischer Auftreib bei Überschallgeschwindigkeit. (5th Volta Congress Lecture.) Luftfahrtforschung, Bd. 12, Nr. 6, Oct. 3, 1935, pp. 210-220.

25. Parker, Hermon M.: Minimum-Drag Ducted and Pointed Bodies of Revolution Based on Linearized Supersonic Theory. NACA TN 3189, 1954.

26. Jones, R. T.: The Minimum Drag of Thin Wings in Frictionless Flow. Jour. Aero. Sci., vol. 18, no. 2. Feb. 1951, pp. 75-81.

27. Jones, R. T.: Theoretical Determination of the Minimum Drag of Airfoils at Supersonic Speeds. Jour. Aero. Sci., vol. 19, no. 12, Dec. 1952, pp. 813-822.

28. Heaslet, Max A., and Fuller, Franklyn B.: Axially Symmetric Shapes with Minimum Wave Drag. (Proposed NACA TN.)

29. Sears, William R.: On Projectiles of Minimum Wave Drag. Quart. Appl. Math., vol. 14, no. 4, Jan. 1947.

30. Haack, W.: Geschossformen kleinsten Wellenwiderstandes. Lilienthal-Gesellschaft fur Luftfahrtforschung, Ber. 139, Oct. 9-10, 1941, pp. 14-28.

31. Van Dyke, Milton D.: Supersonic Flow Past Oscillating Airfoils Including Nonlinear Thickness Effects. NACA TN 2982, 1953.

32. Van Dyke, Milton D.: The Second-Order Compressibility Rule for Airfoils. Jour. Aero. Sci., vol. 21, no. 9, 1954.

33. Van Dyke, Milton D.: Subsonic Edges in Thin-Wing and Slender-Body Theory. NACA TN 3343, 1954.

IDEALIZED SUPERSONIC FLOW ABOUT WING

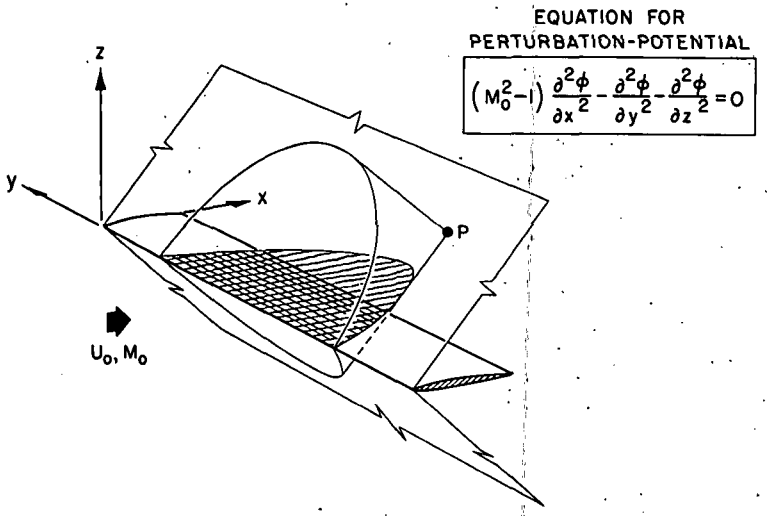

Figure 1

EXPERIMENTAL AND THEORETICAL PRESSURE COEFFICIENT ON TIP OF TRAPEZOIDAL PLAN-FORM WING

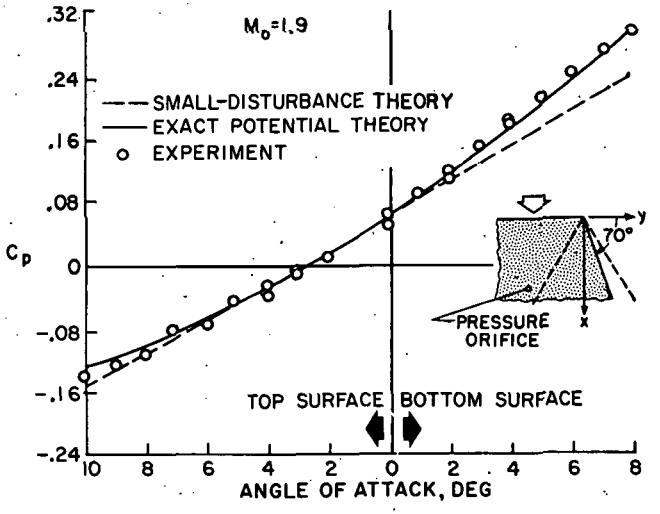

Figure 2a

EXPERIMENTAL AND THEORETICAL PRESSURE COEFFICIENT ON TIP OF TRAPEZOIDAL PLAN-FORM WING

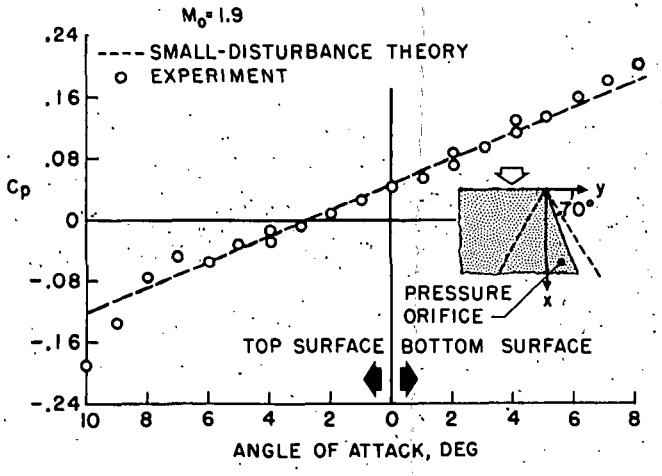

Figure 2b

TYPICAL CHORDWISE LOAD DISTRIBUTIONS ON TRIANGULAR WINGS
M_0=1.49

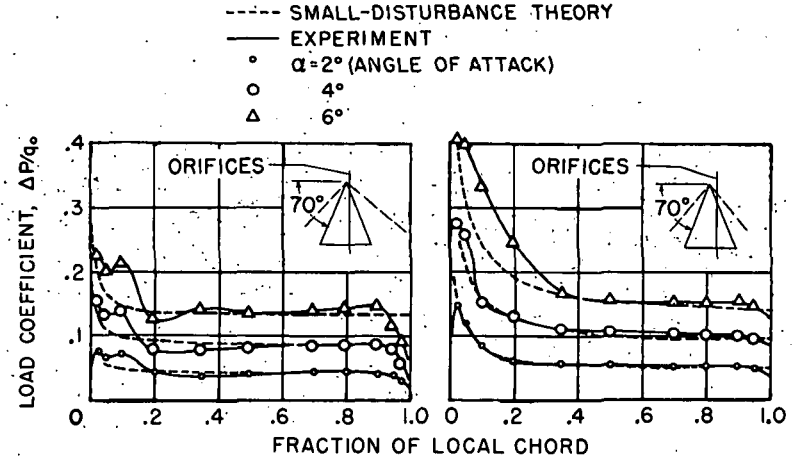

Figure 3

INTEGRATED LOADING ON TRIANGULAR WING M=1.49

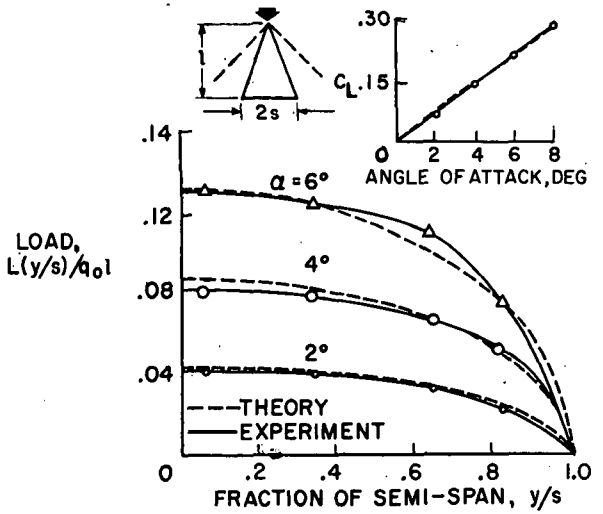

Figure 4

RECIPROCAL RELATIONS IN AERODYNAMICS

RELATION FOR UNSTEADY MOTION, WINGS IN FORWARD AND REVERSE FLIGHT

$$\iiint \delta p(A)\,\bar{w}(A)\,dS\,dt = -\iiint \delta \bar{p}(B)\,w(B)\,dS\,dt$$

RELATION FOR WINGS IN STEADY, OSCILLATING, OR INDICIAL MOTION

$$\iint \delta p(A)\,\bar{w}(A)\,dS = -\iint \delta \bar{p}(B)\,w(B)\,dS$$

Figure 6

RECIPROCAL RELATION FOR STATIC DEFLECTIONS (ELASTICITY THEORY)

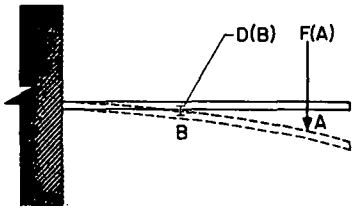

$$F(A)\bar{D}(A) = \bar{F}(B)D(B)$$

F, $\bar{F}$ = GENERALIZED FORCE
D, $\bar{D}$ = GENERALIZED DISPLACEMENT

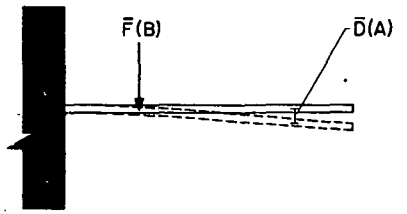

Figure 5

AERODYNAMIC CHARACTERISTICS OF WINGS IN FORWARD AND REVERSE FLOW M_0=1.53

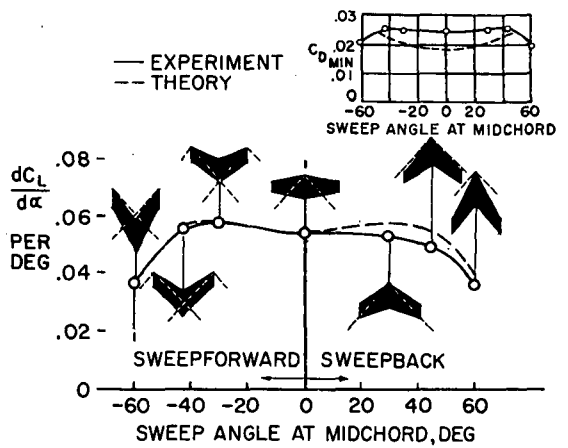

Figure 7

LATTICES IN SUBSONIC POTENTIAL FLOW

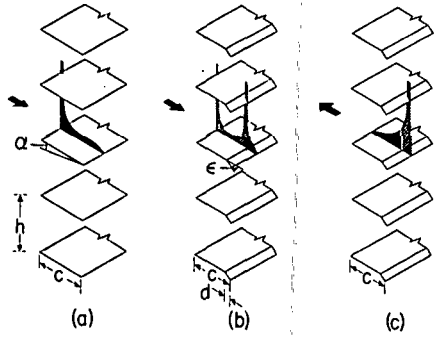

ANGLE-OF-ATTACK LOAD DISTRIBUTION ON ONE PLATE

$$\frac{\Delta p}{q_0} = \frac{4\alpha}{\beta} \operatorname{sech} \frac{\pi c}{2\beta h} \sqrt{\frac{\sinh[\pi(c-x)/\beta h]}{\sinh[\pi x/\beta h]}}$$

LIFT ON ONE PLATE DUE TO FLAP DEFLECTIONS

$$\frac{L}{q_0} = \frac{4\epsilon}{\beta} \operatorname{sech}\left(\frac{\pi c}{2\beta h}\right) \int_{c-d}^{c} \sqrt{\frac{\sinh[\pi x_1/\beta h]}{\sinh[\pi(c-x_1)/\beta h]}}\, dx_1$$

Figure 8

EXAMPLES OF AERODYNAMIC CONFIGURATIONS WITH ZERO WAVE DRAG

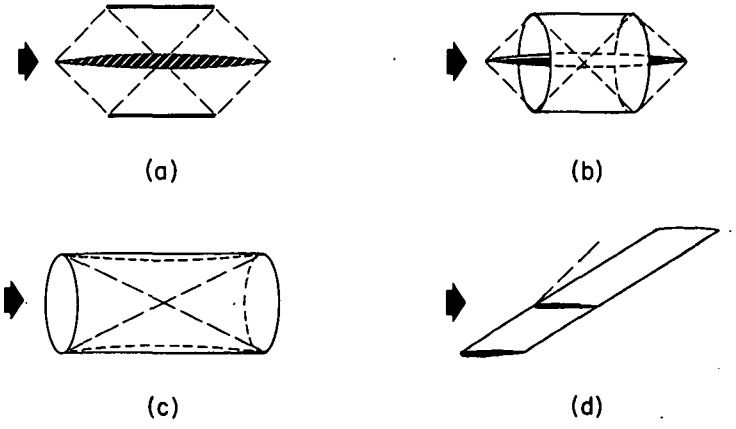

Figure 9

QUASI-CYLINDRICAL BODY AND RELATIONS FOR CALCULATING EXTERNAL WAVE DRAG

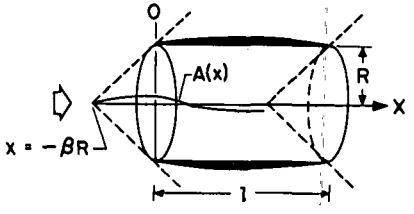

WAVE DRAG IN TERMS OF CROSS-SECTIONAL AREA S(x)

$$D/q_0 = \frac{1}{\pi\beta R}\int_0^1 [S'(x_1)]^2 dx_1 - \frac{1}{2\pi(\beta R)^2}\int_0^1\int_0^1 S'(x_1)S'(x_2)\, W\left(\left|\frac{x_2-x_1}{\beta R}\right|\right) dx_1\, dx_2$$

WAVE DRAG IN TERMS OF SOURCE-DISTRIBUTION FUNCTION A(x)

$$D/\rho_0 = \frac{1}{4\pi}\int_{-\beta R}^{1-\beta R}\int_{-\beta R}^{1-\beta R} A'(x_1)A'(x_2)\,\text{COSH}^{-1}\left|\frac{(1-x_1)(1-x_2)-\beta^2R^2}{\beta R\,(x_1-x_2)}\right| dx_1\, dx_2$$

Figure 10

VOLUME DISTRIBUTION AND WAVE DRAG FOR OPTIMUM BODIES

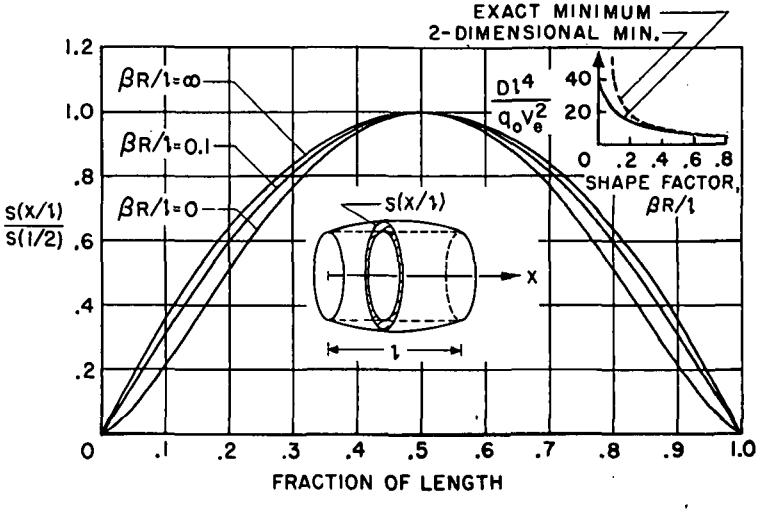

Figure 11

16. AERODYNAMICS OF AIRFOILS AND BODIES IN COMBINATION AT SUPERSONIC SPEEDS

By Jack N. Nielsen
Ames Aeronautical Laboratory

INTRODUCTION

The aerodynamics of bodies and wings in combination at supersonic speeds is discussed herein with respect to slender-body theory and interference. The first part of the paper is concerned with linear effects, and the second part with nonlinear viscous effects and higher-order compression-expansion effects. In recent years the trend toward supersonic configurations has been characterized by low-aspect-ratio wings and by smaller wing sizes relative to the body size; that is, by slender configurations. For this reason references 1 to 3 have developed a special theory for slender combinations based on the airship theory of Munk (ref. 4). For supersonic configurations the aerodynamic characteristics of the airframe are no longer dominated by the characteristics of the wing alone, but are rather the result of the relatively equal effects of the wing, body, and interference between wing and body. Thus, problems of interference have assumed greater importance for supersonic flight than for subsonic flight. New problems have also been created by the appearance on the aerodynamic scene of supersonic missiles and very high altitude interceptors. At extreme altitudes both missile and aircraft must maneuver at high angles of attack to intercept evasive targets and thereby must operate in a regime of nonlinear aerodynamics. Nonlinear effects can, in fact, also be important at low angles of attack. In this discussion of recent developments in slender-body theory, interference, and nonlinear aerodynamics, future trends are also considered when possible.

SLENDER-BODY THEORY

Consider an aerodynamic shape flying through still air at a speed V and a Mach number M at an angle of attack α as shown in figure 1(a). Let the x, y, and z coordinate system be a set of axes fixed in the body and coinciding with the axes of symmetry of the shape, and consider the problem of determining the combination loading. If it is assumed that the flow about the shape at any Mach number is linearized, compressible, potential flow, then the partial differential equation governing the velocity potential for the flow is

$$(1 - M^2)\varphi_{xx} + \varphi_{yy} + \varphi_{zz} = 0 \qquad (1)$$

where subscripts denote partial differentiation. The essential boundary condition is that the flow be tangential to the body surface at every point. Consider conditions under which the term $(1 - M^2)\varphi_{xx}$ is negligible. These conditions obviously occur when M is near unity or when φ_{xx} is small. Now the term φ_{xx} will be small if the configuration has no rapid change in cross-sectional shape over the body length; that is, if the body is "slender." The geometric conditions implied by slenderness are given in reference 2. For a slender body the differential equation for the velocity potential is thus Laplace's equation for flow in planes normal to the body axis:

$$\varphi_{yy} + \varphi_{zz} = 0 \tag{2}$$

Within the range of slender-body theory the flow in any crossflow plane fixed to the body is a steady incompressible flow such as that shown for the plane $x = x_0$ in figure 1(b). Thus, the tools of potential theory, including theory of complex variables and conformal transformations, can be used to calculate solutions to flow in the crossflow planes. Consider now a crossflow plane fixed in the fluid as the body flies through it. At any particular instant of time the flow in the plane is the steady incompressible flow corresponding to the body cross section in the plane. However, as the body passes through the plane and the cross-sectional shape changes with time, the resultant flow is a succession of steady incompressible flows. It is clear that the way in which the body cross section in the fixed plane varies with time will determine the pressure field, which is calculated by Bernoulli's equation for unsteady flow (ref. 5). By applying Newton's second law of motion to the crossflow, it is possible to obtain simple expressions for the lift of complicated slender configurations with horizontal planes of symmetry. In this technique the mass of air that can be thought of as rigidly attached to the cross section for the purpose of evaluating the momentum is known as the apparent mass (refs. 4 and 6) and depends only on the cross-sectional shape of the body in the plane under consideration. The lift between two sections can then be very simply calculated from the apparent masses of the two cross sections. It should be noted that the foregoing application of slender-body theory does not permit the calculation of the effects of thickness on the flow field.

Slender-body theory is also useful for determining pressure distributions on slender wings, bodies, wing-body combinations, and wing-body-tail combinations (refs. 1 to 4, 7, and 8). It has been formulated to include the effects of thickness at subsonic speeds in reference 8 and extended to not-so-slender bodies in reference 9. Another field in which the theory has been useful is the computation of stability derivatives as demonstrated in references 6 and 10. An analysis of slender-body theory for unsteady flow paralleling that of Ward (ref. 2) for steady

flow has been made in reference 11. One point of interest with regard to slender-body lifting problems for combinations with horizontal planes of symmetry is that they are mathematically identical to problems in subsonic flow of determining span loadings for minimum induced drag using Trefftz plane methods (ref. 12).

Wing-Body Interference

An interference flow field results when two or more aerodynamic objects having their own flow fields are brought together so that any object lies wholly or in part in the region of influence of another. Consider figure 2, which shows a body alone of potential φ_B and a wing alone of potential φ_W. Let the wing alone and the body alone be brought together to form the wing-body combination with potential φ_C. Then the difference between the combination potential and the sum of the wing-alone and the body-alone potentials is defined to be the interference potential:

$$\varphi_i = \varphi_C - (\varphi_B + \varphi_W) \tag{3}$$

What is taken to be the body alone or the wing alone is arbitrary. For instance, the wing alone could be taken as the wing panels joined together or as a larger wing including the area blanketed by the body as shown in the figure. If the definition of the wing alone is changed, the combination or body-alone potentials will remain constant, but in accordance with equation (3) the interference potential must change. Thus, the interference depends on what is taken to be the wing alone or the body alone. All potentials are to satisfy the equation of linearized flow for the Mach number range under consideration. The combination potential is to satisfy the boundary conditions that the flow be tangential to the combination and that there be no upstream waves. In the general case the wing-alone and body-alone potentials are known, and the problem is to find the interference potential. The foregoing example of wing-body interference between two objects illustrates the general problem of interference among many objects. Other problems include tail-body, wing-tail, and body-body interference.

In the application of slender-body theory to the interference problem, it is unnecessary to determine the interference potential, since the combination potential can be calculated directly. If only the lift-curve slope is required, it can easily be calculated from the apparent mass of the combination cross section. The apparent mass of many cross sections can be found in reference 13. This procedure has been used to determine the lift-curve slopes of the family of triangular wing and body combinations shown in figure 3. The theoretical lift-curve slopes so obtained are shown as a function of the aspect ratio A. They are to be compared

with the experimental data obtained in the 1- by 3-foot supersonic wind tunnel of the NACA Ames laboratory. It is seen that only for low values of the aspect ratio are theory and experiment in good accord. This is due to the fact that only for low aspect ratios are the combinations slender. However, it is interesting that the usefulness of slender-body theory is not limited to slender configurations. For instance, it is known that slender-body theory predicts accurately the ratio of the lift of the combination to that of the wing alone for nonslender combinations. Thus, an accurate estimate of the lift of a combination can be made from the value of this ratio and an accurate estimate of the lift of the wing alone.

In cases where the detailed pressure distribution is desired for a combination that is not slender, a boundary-value problem for the interference potential must be solved. The several methods for doing this all involve considerable work. The Ferrari iteration method (refs. 14 and 15), which is similar to the Schwarz alternating procedure, assumes the wing to be acting in the body-alone field and, without regard for the body shape, determines a potential additive to the wing-alone potential. The process is then repeated for the body, and again for the wing. In principle the process converges, but it becomes mathematically complicated after the first iteration. A second method based on Laplace transform theory which makes use of approximate Green's functions is due to Morikawa (ref. 16). A third approach (refs. 17 and 18) takes the interference potential to be the sum of a series of Fourier harmonics corresponding to cosines of even multiples of the polar angle around the body. The Fourier harmonics are then computed precisely for as many terms as necessary. One or two terms are sufficient to determine span loading, but about four terms are necessary to establish the pressure distribution. A comparison is made in figure 4 between the pressure distributions for a rectangular wing and body combination as measured (ref. 19) and as calculated by the last method. The measured and predicted pressure distributions are in good accord for both the wing-body juncture and the top of the body. In the juncture the pressure coefficient as expressed in the figure would have the uniform value 2 for the wing alone, but the actual value of 4 at the leading edge shows the importance of interference at this point.

Other Interference Problems

Other interference problems include those of the effect of the wing vortices on afterbody and tail, and the shaping and arrangement of configurations to produce minimum drag. With regard to the first subject, it has been known for some time how to compute the effect of a wing on a tail in subsonic airplane design (ref. 20) using the Silverstein-Katzoff method. The first part of the problem pictured in figure 5 is to determine the flow field induced in the region of the tail by the

wing. This subject has been considered for wings alone (ref. 21) and for wing-body combinations (ref. 22) at supersonic speeds. Because of the wing-induced flow, the tail is essentially twisted and to a lesser degree cambered. The second part of the problem is then to determine the reaction of the tail to this distortion. A technique for determining gross tail loads, developed by Alden and Schindel (ref. 23), consists of a strip integration across the tail using the span-loading of the reversed untwisted tail as a weighting factor; but this method does not take account of tail-body interference. The technique has been generalized using reversibility theorems (refs. 24 and 25) to include tail-body interference; but to obtain the weighting factors it is necessary to determine the span loading of the reversed untwisted tail-body combination.

The question of properly shaping and arranging configurations to take maximum benefit of interference to reduce the wave drag is a problem still in its early stages. An interesting result in this field is found in references 26 and 27, where the resultant wave drag of a body of revolution with two similar satellite bodies is considered (fig. 6). In their analysis the authors consider essentially the effects of longitudinal buoyancy and assume that the satellite bodies are limp so that they conform to the flow field of the larger body and do not set up secondary interference effects. By placing the satellite bodies close to the parent body with their maximum cross sections near the trailing wave, it is possible to eliminate an amount of wave drag equal to the drag of the satellite bodies. A variety of unsolved problems of this type are to be found in the field of external stores. Another way in which wave drag can be reduced is by the use of camber and twist of the wing, as discussed in references 28 to 30. It is anticipated that efforts to find configurations favorable for the reduction of wave drag will be expanded in the future and that some attempts to account for the interaction between wave drag and friction drag will be made.

NONLINEAR EFFECTS

Nonlinear effects in supersonic aerodynamics arise from a number of causes, and two of these causes are known as viscous effects and higher-order effects of compression and expansion. By viscous effects is meant the departure of the actual flow from the inviscid flow because of the action of viscosity. One of the manifestations of important viscous effects is the appearance of vortices in the flow. An approach used successfully by the aerodynamicist in the study of viscous effects is to devise a vortex model of the flow in better agreement with the observed flow than the ordinary potential model. In this approach the vorticity is all concentrated at isolated points, lines, or sheets, and the intervening flow is inviscid so that a velocity potential still exists.

Figure 7 shows an example of the vortex-type flow associated with viscous crossflow about a body of revolution at high angles of attack. The roll-up sheets are fed by vortex lines that originate near the flow-separation points on the leeward side of the body, but exactly where and how the vortex sheets start has not yet been determined. This vortex model has been used (ref. 31) for predicting the increase in lift of a a body of revolution at high angles of attack due to viscous crossflow. In this theory attention is focused on independent crossflow planes, and the flow in successive planes is assumed to correspond to viscous flow at successive instants of time about a circular cylinder impulsively moved normal to itself. The cross force due to viscosity is specified by a crossflow drag coefficient C_{d_c} which depends on crossflow Reynolds number and crossflow Mach number. In figure 8 the effects of crossflow on the lift of a body of revolution are shown. The variation of the lift coefficient with angle of attack is linear on the basis of inviscid theory; but it is quadratic on the basis of viscous crossflow theory, since the crossflow dynamic pressure varies as the angle of attack squared. The large predicted nonlinear effect of viscosity is substantiated by the good agreement between crossflow theory and experiment. Other problems amenable to the vortex type of analysis include the flow over a triangular wing with leading-edge separation (ref. 32) and flow past a streamwise tip.

Nonlinearities due to higher-order effects of compression and expansion are associated with many sources, such as large perturbation velocities, nonlinear potential equations, thick wings, large angles of attack, and so forth. The study of these problems is complicated by the fact that superposition of pressures due to thickness and angle of attack is no longer premissible. An example of the inability of linear theory to cope with these effects is shown in figure 9. According to linear theory, the loading on a triangular wing is constant along any ray from the wing apex, and in particular the loading is uniform in front of the Mach wave from the apex. The loading is said to be conical with respect to the apex. The figure shows the interesting result that for an angle of attack as low as 3° the theory and experiment are not in good accord. The failure of linear theory in this case is due to a coupling between the lifting pressures and the thickness pressures which are not conical with respect to the wing apex because of the wing geometry. Span loading and lift are still given closely by linear theory. This example illustrates the need at the present time for a simple theory to account for higher-order effects of compression and expansion for three-dimensional wings. For the present wing, the surface is conical with respect to the wing tip insofar as a point in front of the Mach line from the apex is concerned. Thus, the loading in this region would be expected to be conical with respect to the tip to the order of nonlinear theory. The data of the figure, when correlated on this basis, confirm the expectation. The solution for the pressure field of the wing in front of the

Mach wave from the apex is amenable to calculation by a conical shock-expansion theory. However, the solution is still unknown behind the wave. A start toward a second-order theory for three-dimensional wings has been made in reference 33.

REFERENCES

1. Jones, Robert T.: Properties of Low-Aspect-Ratio Pointed Wings at Speeds Below and Above the Speed of Sound. NACA Rep. 835, 1946. (Supersedes NACA TN 1032.)

2. Ward, G. N.: Supersonic Flow Past Slender Pointed Bodies. Quart. Jour. Mech. and Appl. Math., vol. 2, pt. 1, Mar. 1949, pp. 75-97.

3. Spreiter, John R.: The Aerodynamic Forces on Slender Plane- and Cruciform-Wing and Body Combinations. NACA Rep. 962, 1950. (Supersedes NACA TN's 1662 and 1897.)

4. Munk, Max M.: The Aerodynamic Forces on Airship Hulls. NACA Rep. 184, 1924.

5. Lamb, Horace: Hydrodynamics. First Am. ed., Dover Pub., 1945, p. 21.

6. Sacks, Alvin H.: Aerodynamic Forces, Moments, and Stability Derivatives for Slender Bodies of General Cross Section. NACA TN 3283, 1954.

7. Lomax, Harvard, and Byrd, Paul F.: Theoretical Aerodynamics Characteristics of a Family of Slender Wing-Tail-Body Combinations. NACA TN 2554, 1951.

8. Heaslet, Max A., and Lomax, Harvard: The Calculation of Pressure on Slender Airplanes in Subsonic and Supersonic Flow. NACA TN 2900, 1953.

9. Adams, Mac C., and Sears, W. R.: Slender-Body Theory - Review and Extension. Jour. Aero. Sci., vol. 20, no. 2, Feb. 1953, pp. 85-98.

10. Bryson, A. E.: Stability Derivatives for a Slender Missile with Application to a Wing-Body-Vertical Tail Configuration. Jour. Aero. Sci., vol. 20, no. 5, May 1953.

11. Miles, John W.: Unsteady Supersonic Flow Past Slender Pointed Bodies. Navord Rep. 2031, May 1953.

12. Durand, William Frederick, ed.: Aerodynamic Theory. Vol. II, Div. E. III. Mathematical Foundations of the Theory of Wings of Finite Span, pp. 135-139.

13. Kuerti, G., McFadden, J. A., and Shanks, D.: Virtual Mass of Cylinders with Radial Fins and of Polygonal Prisms. Navord Rep. 2295, 1952.

14. Ferrari, Carlo: Interference Between Wing and Body at Supersonic Speeds - Theory and Numerical Application. Jour. Aero. Sci., vol. 15, no. 6, June 1948, pp. 317-336.

15. Ferrari, Carlo: Interference Between Wing and Body at Supersonic Speeds - Note on Wind Tunnel Results and Addendum to Calculations. Jour. Aero. Sci., vol. 16, no. 9, Sept. 1949.

16. Morikawa, G. K.: The Wing-Body Problem for Linearized Supersonic Flow. Doctoral Thesis, C.I.T., 1949.

17. Nielsen, J. N.: Supersonic Wing-Body Interference. Doctoral Thesis, C.I.T., 1951.

18. Nielsen, Jack N., and Pitts, William C.: Wing-Body Interference at Supersonic Speeds with an Application to Combinations with Rectangular Wings. NACA TN 2677, 1952.

19. Pitts, William C., Nielsen, Jack N., and Gionfriddo, Maurice P.: Comparison Between Theory and Experiment for Interference Pressure Field Between Wing and Body at Supersonic Speeds. NACA TN 3128, 1954.

20. Silverstein, Abe: Toward a Rational Method of Tail-Plane Design. Jour. Aero. Sci., July 1939.

21. Spreiter, J. R., and Sacks, A. H.: The Rolling Up of the Trailing Vortex Sheet and Its Effect on the Downwash Behind Wings. Jour. Aero. Sci., vol. 18, no. 1, Jan. 1951, pp. 21-32; 72.

22. Rogers, Arthur Wm.: Application of Two-Dimensional Vortex Theory to the Prediction of Flow Fields Behind Wings of Wing-Body Combination at Subsonic and Supersonic Speeds. NACA TN 3227, 1954.

23. Alden, H. L., and Schindel, L. H.: The Lift, Rolling Moment, and Pitching-Moment in Wings in Nonuniform Supersonic Flow. Jour. Aero. Sci., vol. 19, no. 1, Jan. 1952.

24. Flax, A. H.: Integral Relations in the Linearized Theory of Wing-Body Interference. Jour. Aero. Sci., vol. 20, no. 7, July 1953.

25. Heaslet, Max A., and Spreiter, John R.: Reciprocity Relations in Aerodynamics. NACA Rep. 1119, 1953. (Supersedes NACA TN 2700.)

26. Friedman, Morris D.: Arrangement of Bodies of Revolution in Supersonic Flow to Reduce Wave Drag. NACA RM A51I20, 1951.

27. Friedman, Morris, and Cohen, Doris: Arrangement of Fusiform Bodies to Reduce the Wave Drag at Supersonic Speeds. NACA TN 3345, 1954.

28. Beane, Beverly: Examples of Drag Reduction for Delta Wings. Rep. No. SM-14447, Douglas Aircraft Co., Jan. 1953.

29. Beane, Beverly: Drag Reduction Due to Wing Incidence and Twist for Wing-Body Combinations. Rep. SM-14740, Douglas Aircraft Co., Mar. 1953.

30. Jones, R. T.: Theoretical Determination of Minimum Drag of Airfoils at Supersonic Speeds. Jour. Aero. Sci., vol. 19, no. 12, Dec. 1952.

31. Allen, H. Julian: Estimation of the Forces and Moments Acting on Inclined Bodies of Revolution. NACA RM A9I26, 1949.

32. Brown, C. E., and Michael, W. N., Jr.: On Slender Delta Wings with Leading-Edge Separation. (Proposed NACA TN.)

33. Clarkson, M. H.: A Second-Order Theory for Three-Dimensional Wings in Supersonic Flow. Quart. Jour. Mech. and Appl. Math., vol. VII, pt. 2, June 1954.

AXES AND CROSSFLOW FOR SLENDER AERODYNAMIC BODY

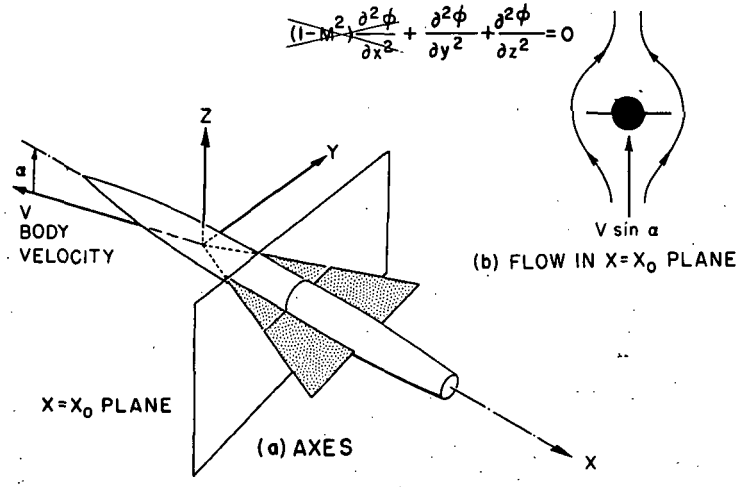

Figure 1

BODY ALONE, WING ALONE, AND WING-BODY COMBINATION

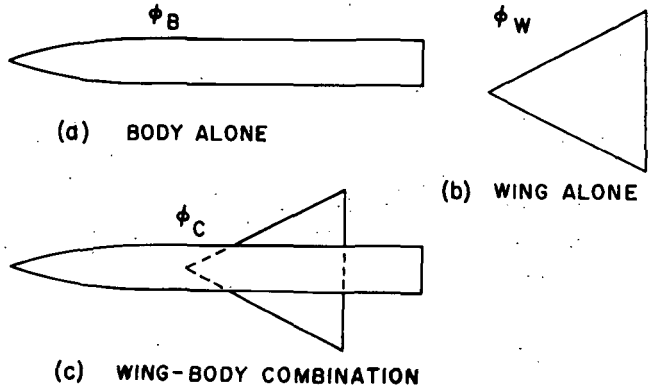

$$\phi_I = \phi_C - (\phi_W + \phi_B)$$

Figure 2

COMPARISON OF SLENDER-BODY THEORY AND EXPERIMENT FOR LIFT OF WING-BODY COMBINATIONS

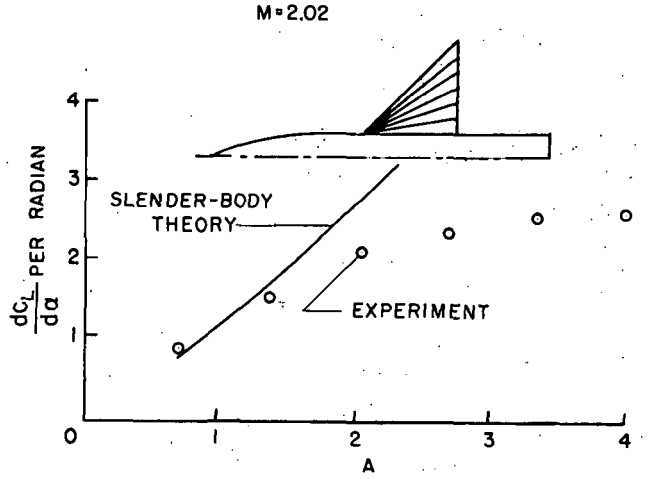

Figure 3

COMPARISON OF LINEAR THEORY AND EXPERIMENT FOR WING-BODY PRESSURE DISTRIBUTION

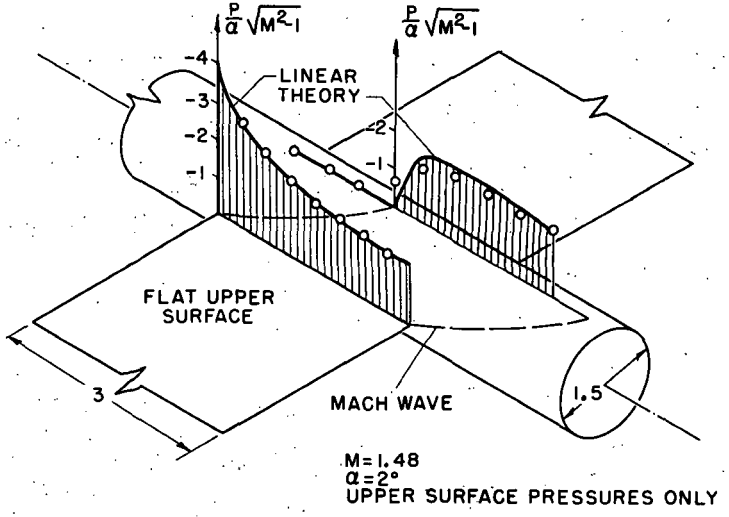

Figure 4

DOWNWASH FIELD DUE TO WING

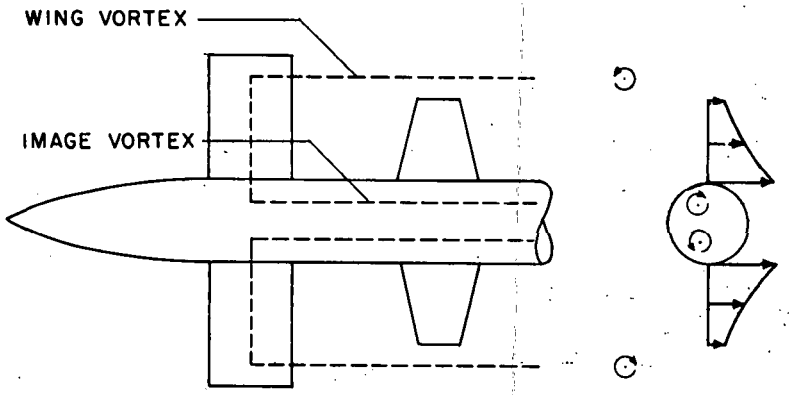

(a) WING-BODY VORTEX SYSTEM (b) DOWNWASH FIELD

Figure 5

PARENT BODY WITH SATELLITE BODIES

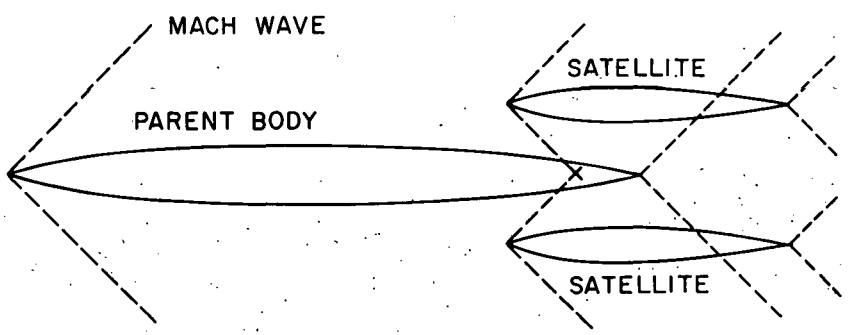

Figure 6

VORTEX SYSTEM IN CROSSFLOW PLANE

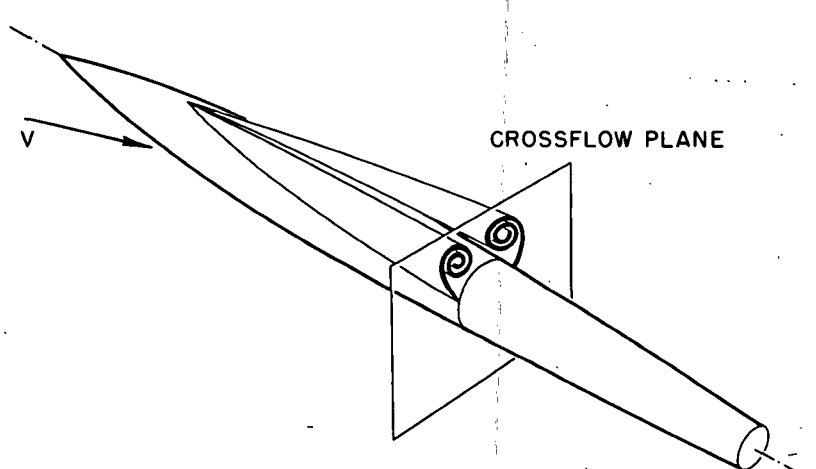

Figure 7

COMPARISON OF CROSSFLOW THEORY AND EXPERIMENT FOR LIFT OF BODY OF REVOLUTION

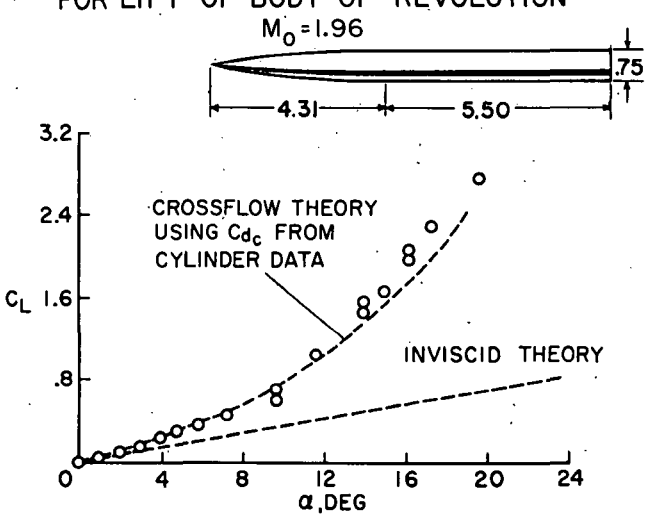

Figure 8

COMPARISON OF LINEAR THEORY AND EXPERIMENT FOR LOADING ON DELTA WING

α=3°; 5% THICK; 50% BLUNT

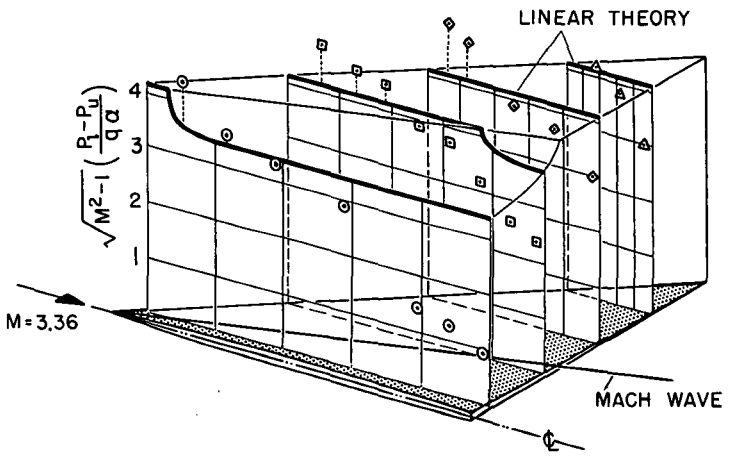

Figure 9

17. TRANSONIC AERODYNAMICS OF WINGS

By Edward C. Polhamus
Langley Aeronautical Laboratory

INTRODUCTION

The purpose of this paper is to summarize briefly some of the experimentally determined aerodynamic characteristics of wings at transonic speeds. For the most part, the aerodynamic characteristics are plotted against Mach number in the range from about 0.6 to 1.2, and the effects of such parameters as thickness, aspect ratio, and sweep angle are shown. The experimental results are generally compared with subsonic and supersonic theory, and pressure distributions and flow pictures are used to explain some of the phenomena.

TWO-DIMENSIONAL FLOW

Before discussing the transonic characteristics of three-dimensional wings, it might be well to look briefly at some two-dimensional characteristics, inasmuch as these characteristics are also evident, to some extent at least, in three-dimensional flow. In two-dimensional flow, the airfoil thickness is generally the most important geometric parameter. Therefore, the effect of thickness on aerodynamic characteristics as obtained in the Langley 4- by 19-inch semiopen tunnel is illustrated in figures 1 and 2. Figure 1 presents the force data for NACA 64A006 and NACA 64A009 airfoil sections in the Mach number range from about 0.6 to 1.0. Figure 2 presents schlieren photographs for the two airfoils at an angle of attack of 4° and at Mach numbers of 0.94 and 1.00. Also shown on the pictures are the experimental chordwise pressure distributions, with the solid line representing the upper-surface pressures, the dashed line those of the lower surface, and the airfoil chord line identifying the zero pressure-coefficient axis with suction pressures plotted above.

It will be noted from the force data (fig. 1) that there is little difference in the characteristics of the 6-percent and 9-percent airfoils, up to a Mach number of about 0.8. Above this Mach number, however, there are rather large differences in the characteristics of the two airfoils. These differences are very pronounced at a Mach number of about 0.93, with the 9-percent airfoil having a considerably lower lift curve slope, higher zero lift drag, and an aerodynamic center that is located approximately 28 percent ahead of that for the 6-percent airfoil. The characteristics of the 9-percent airfoil are also considerably nonlinear at this Mach number, as illustrated by the plot of lift coefficient against angle of attack. The higher zero lift drag for the 9-percent airfoil is, of course, due to the more severe shock and separation effects.

The large effect of thickness on the lift and aerodynamic center in this Mach number range can be explained by the upper two schlieren pictures and pressure diagrams of figure 2. For the 6-percent airfoil, the angle of attack caused a reduction in velocity on the lower surface, so that no strong shocks or large negative pressures occur on the lower surface and positive lift is maintained over the entire chord. For the 9-percent airfoil, however, the velocities are considerably higher, the angle of attack was unable to reduce the lower-surface velocities sufficiently, and a rather strong shock is present on the lower surface aft of the upper-surface shock. The supersonic flow on the lower surface results in large negative pressures that reduce the lift; and, in addition, because of the rearward position of the shock, a reversal of load occurs over the aft 40 percent of the chord. This, of course, accounts for the low lift curve slope and the forward location of the aerodynamic center for this airfoil. The nonlinearities are explained by the fact that, as the angle of attack is increased, the lower-surface velocities are reduced and the negative lift loop gradually decreases. As the Mach number is increased to 1.0 the shocks on both surfaces of both airfoils move to the trailing edge, the flow reattaches, and there is little difference in the pressure distribution of lift and aerodynamic center for the two airfoils. The flow over the airfoil is predominantly supersonic, and further increases in Mach number would have little effect on the flow characteristics. Once the shocks have moved to the trailing edge, the nonlinearities are considerably reduced.

THREE-DIMENSIONAL FLOW

Effect of Aspect Ratio

The preceding figures show that thickness is an extremely important parameter with regard to the transonic aerodynamic characteristics of two-dimensional airfoils. While thickness also plays an important part with regard to the transonic characteristics of finite span wings, its effect is modified somewhat by the three-dimensional nature of the flow. For example, a low-aspect-ratio wing is less sensitive to thickness effects, because a large percentage of the wing can benefit from the leaking off of pressure associated with the tip relief. This favorable effect of tip relief is illustrated in figure 3. In this figure, schlieren photographs obtained in the Langley 4- by 19-inch semi-open tunnel (ref. 1) are presented for infinite-aspect-ratio and aspect-ratio-2 wings having NACA 0012 airfoil sections. The Mach number is 0.83, and pictures for zero lift and a lift coefficient of 0.15 are presented for both aspect ratios. The favorable effect of aspect ratio in reducing shock and separation losses is clearly evident in the pictures. For this thick wing (12 percent) at this particular Mach number, the drag at zero lift for the aspect-ratio-2 wing is only about 30 percent of that for the infinite-aspect-ratio wing.

Transonic flow changes do not, of course, occur simultaneously at all spanwise stations on finite span wings. This is especially true for the lifting case, as illustrated in figure 4, which shows the results of ink-flow studies made in the Langley 16-foot transonic tunnel. The wing, which was mounted on a body of revolution, had an aspect ratio of 4 and an NACA 64A004 airfoil section. The angle of attack was 5°, and results for Mach numbers of 0.85, 0.90, and 1.00 are presented. For these studies, ink was emitted from several orifices along the span near the leading edge. At a Mach number of 0.85, shock-induced separation is indicated by the ink aft of about the 40-percent-chord line. It will be noted, however, that this separation does not extend over the entire span, because of the tip relief and mainly because the lift coefficient is not constant along the span as a result of induced effects. As the Mach number is increased to 0.90 the shock moves rearward to about the 75-percent-chord line, and at a Mach number of 1.00 it moves to the trailing edge and the flow reattaches. (The ink follows the grooves along the leading- and trailing-edge flaps, and this should not be confused with separation.)

In order to illustrate the effects of aspect ratio on the over-all lift forces experienced in the transonic range, figure 5 has been prepared. In this figure the lift-curve slope is plotted against Mach number for unswept wings of several aspect ratios. The wings were all 4-percent thick, and the aspect ratios investigated were infinity (unpublished), 4, and 2 (refs. 2 and 3). The experimental results are plotted as solid lines, and the theoretical results as dashed lines. At subsonic speeds the Weissinger modified lifting line method (refs. 4 and 5) was used in conjunction with the three-dimensional Prandtl-Glauert transformation (ref. 6). At supersonic speeds, the linearized theory of Lomax and Sluder (ref. 7) was used. The experimental results are in fairly good agreement with theory for Mach numbers below the force break, a decrease in aspect ratio being accompanied by a reduction in lift and less rapid rise with Mach number due to the increased effect of the induced angle. At higher Mach numbers, the theory overestimates the lift-curve slope. The results also indicate that the large loss of lift in the transonic range associated with the infinite aspect ratio is considerably reduced as the aspect ratio decreases. In addition to the three-dimensional effects discussed in the preceding figures, this improvement is due to the fact that a loss of lift is accompanied by a reduction in induced angle, thereby relieving an additional amount of the geometric angle to produce lift.

Aspect ratio also has a rather pronounced effect on the aerodynamic-center location, as illustrated in figure 6. Here, the aerodynamic-center location aft of the leading edge is plotted against Mach number for two 4-percent-thick wings, one having an aspect ratio of infinity (unpublished) and the other an aspect ratio of 2 (ref. 3). The results of first-order theories are presented as dashed lines. The theory for

the infinite aspect ratio indicates the aerodynamic center to be located at the quarter-chord up to a Mach number of 1.0 above which it is located at the half-chord. The theory for the aspect-ratio-2 wing (ref. 7) indicates the aerodynamic center to be considerably ahead of that for the infinite aspect ratio. This forward shift, which is due to the induced camber associated with the chordwise variation of induced downwash, increases with Mach number until, at a Mach number of 1.0, the aerodynamic center is located at the leading edge. As the Mach number increases in the supersonic range the aerodynamic center moves rearward, approaching the two-dimensional location as the Mach lines intersect less of the wing, thereby reducing the three-dimensional effects. The experimental results substantiate the trends but are in relatively poor agreement with regard to magnitude. The disagreement at high subsonic speeds is not surprising, since the mixed subsonic and supersonic flow associated with the finite thickness has a critical effect on the chordwise loading. At supersonic speeds better agreement might have been obtained for the aspect-ratio-2 wing if second-order solutions were available, since two-dimensional second-order theories indicate the aerodynamic center to be ahead of the half-chord (see ref. 8).

Effect of Sweep

So far, it has been shown that both thickness and aspect ratio are important with regard to transonic aerodynamics and that the undesirable characteristics in this range are associated with shock and separation losses that usually occur once speeds somewhat in excess of the speed of sound are reached at some point on the wing. Another geometric parameter that is of considerable importance with regard to transonic aerodynamics is wing sweep. On a swept wing, even the attainment of speeds in excess of the speed of sound locally does not necessarily denote any occurrence of shocks and corresponding flow changes. The reason for this is, of course, explained by the well-known simple sweep theory (see ref. 9, e.g.), which is illustrated in figure 7. For an untapered wing, the isobars (constant-pressure lines) are generally parallel to the leading edge; and, since only the component of velocity normal to the isobars affects the pressures, shocks will not occur until the flow normal to the leading edge exceeds the speed of sound at some point on the wing. (See refs. 10 and 11 for experimental verification of simple sweep theory.) This, of course, would delay the undesirable transonic characteristics to considerably higher Mach numbers than for unswept wings. However, the simple sweep theory actually applies only to portions of the wing that are sufficiently removed from the root and tip. It has been shown theoretically (refs. 12 and 13) and substantiated experimentally (ref. 14) that in these root and tip regions the isobars are curves as shown in the sketch. The rearward displacement of pressures at the root results in pressure drag in that

region, while the forward displacement at the tip results in thrust, with the over-all pressure drag in incompressible flow remaining zero. At higher speeds, however, the fact that the isobars have relatively little sweep in the region of the root results in localized shocks occurring at Mach numbers considerably lower than in the regions where the isobars are parallel to the wing. The formation of shocks in the tip region is delayed by the aforementioned favorable tip relief. The zero-lift transonic drag rise, therefore, occurs first at the root of swept wings and at Mach numbers considerably lower than indicated by simple sweep theory.

The effect of sweep on the over-all drag in the transonic range is shown in figure 8. In this figure, the zero-lift drag coefficient is plotted as a function of Mach number for A = 4 wings having NACA 65A006 airfoil sections streamwise and sweep angles of 0°, 45°, and 60° as obtained from tests in the Langley high-speed 7- by 10-foot tunnel by the transonic-bump method (refs. 2, 15, and 16). Since theoretical results are not available for the airfoils used, linear theory results for wings having 6-percent-thick biconvex sections (ref. 17) with an increment of 0.005 added to approximately account for profile drag are shown. The results indicate the favorable effect of sweep in delaying and reducing the transonic drag rise. It will be noted, however, that, while the simple sweep theory (based on thickness normal to sweep line) would indicate the drag rise of the 45° wing to be delayed to a Mach number of about 1.2, the experimental and linearized theory results show the drag rise occurring at considerably lower speeds. This illustrates the important roll the adverse effects at the root play with regard to the over-all drag of sweptback wings.

The effect of sweep angle on the variation of the lift-curve slope with Mach number is shown in figure 9 for the same series of wings. In addition to the experimental results, the theoretical variations (refs. 5, 7, 18, and 19) are presented as dashed lines. The results indicate good agreement with theory at subsonic speeds, with sweep decreasing both the lift-curve slope and its variation with Mach number. At transonic speeds, however, the theory overestimates the lift-curve slope, especially for the unswept and 45°-swept wings. The agreement for the 60° wing, however, is rather good. It will be noted that, as was the case for the drag data, the force break occurs considerably earlier than would be predicted by simple sweep theory because of the supercritical conditions occurring at the root. In connection with the condition existing at the root, it should be pointed out that, although the theory and experiment are for an isolated wing, similar conditions would be expected to exist at the intersection of a wing and fuselage, inasmuch as the fuselage acts somewhat as a reflection plane. The conditions, however, would be modified somewhat because of fuselage-induced velocities and the three-dimensional type of flow about the fuselage.

The discussion of swept wings so far has been limited to relatively low angles of attack. Figure 10 illustrates some of the types of flow encountered on swept wings at moderate and high angles of attack. In the upper left corner, the subsonic type of flow on a sweptback wing is illustrated by an ink-flow picture, which shows the characteristic spanwise flow of the boundary layer toward the tip. This spanwise flow, in conjunction with the relatively high tip loadings of a sweptback wing, results in separation at the tip. An additional phenomenon that occurs on thin sweptback wings is illustrated in the lower sketch. For thin wings with relatively sharp leading edges, a laminar separation bubble occurs at the leading edge and produces a free vortex that lies along the upper surface as illustrated. This vortex moves inboard with increasing angle of attack and modifies the local stalling characteristics, as discussed later. In the upper right corner of the figure the transonic flow is illustrated by ink flow, and the shock and separation are evident. A sketch of the shock and separation pattern is shown in the lower sketch. The regions of separated flow are very similar in both subsonic and transonic flow.

3556

Since the wing pitching moments are most sensitive to these types of flow, the variation of pitching moment with lift coefficient is illustrated in figure 11. The wing had 45° sweepback, an aspect ratio of 4, a taper ratio of 0.6, and NACA 65A006 airfoil sections parallel to the plane of symmetry. The experimental results (ref. 20) are shown for a subsonic Mach number of 0.6 and a transonic Mach number of 0.97. The similarity in pitching-moment characteristics above a lift coefficient of about 0.5, where an undesirable pitch-up tendency occurs, is evident and reflects the similarity in the tip stalling for both subsonic and transonic types of flow that was illustrated in figure 10. However, in the lower lift range, the characteristics for the two Mach numbers are somewhat different. The increase in stability at low lifts as the Mach number is increased is due mainly to the effect of compressibility on the chordwise loading. It will be noted, however, that at a lift coefficient of about 0.3 there is a stable break in the $M = 0.6$ curve. This variation is associated with the vortex type of flow common to swept wings with relatively sharp leading edges, which was illustrated in figure 10. In this lift range, the vortex has a beneficial effect on the lift of the outboard stations, thereby causing an increase in stability. As the lift increases, however, the vortex moves inboard, leaving the outboard stations in a stalled flow and thereby resulting in the pitch-up characteristics.

It has been shown that thin wings are desirable with respect to zero-lift drag. However, with regard to drag due to lift, the separation at the leading edge associated with the small leading-edge radius of a thin wing results in a loss of suction that causes an increase in drag due to lift. This is shown in figure 12 for an unswept and a 45°-sweptback wing. Both wings had aspect ratios of 4, taper ratios of

0.6, and NACA 65A006 airfoil sections parallel to the plane of symmetry. The experimental data were obtained from tests in the Langley high-speed 7- by 10-foot tunnel by the transonic-bump technique (refs. 2 and 15) and are presented in terms of the drag-rise factor $\Delta C_D/C_L^2$ as a function of Mach number. In addition to the experimental results, several theoretical curves are presented. The lower (dashed) curves represent the potential-flow theoretical results (refs. 5, 18, and 21), which at subsonic speeds are relatively independent of sweep angle and Mach number, depending almost entirely on the aspect ratio. At supersonic speeds, however, the potential-flow theory results depend on Mach number and sweep in addition to aspect ratio. Also shown are the theoretical curves for the condition of zero leading-edge suction. For this condition, the resultant force, is, of course, normal to the chord plane, and the drag-rise factor is given by the reciprocal of the lift-curve slope. The drag due to lift for this case is dependent to a large extent on Mach number and sweep through their effects on the lift-curve slope. For the unswept wing the two theories are coincident above a Mach number of about 1.03. This is due to the fact that for an unswept wing at supersonic speeds no upwash can be transmitted ahead and the stagnation point therefore is at the leading edge rather than on the lower surface and no suction is developed even in the potential-flow case. For the swept wing, however, suction can be developed at supersonic speeds, providing the leading edge is swept behind the Mach cone. For this condition, inboard stations can produce upwash ahead of outboard stations, causing a subsonic type of flow resulting in suction that increases toward the tip and decreases with Mach number, reaching a value of zero when the Mach cone is coincident with the leading edge. The experimental results for both wings indicate drag-due-to-lift values considerably higher than the potential-flow theory. At low speeds, it appears that, because of leading-edge separation on these thin wings, only about 50 percent of the leading-edge suction is developed. As the Mach number is increased, the drag due to lift increases and for the unswept wing even exceeds the zero suction theory results. This is due in part to the fact that the lift-curve slope is considerably lower than theory in the transonic range and in part to the variation of the shock and separation characteristics with lift coefficient. It should be pointed out that, at the lower subsonic speeds, increases in Reynolds number would have some beneficial effect on the drag due to lift. However, at transonic speeds where compressibility effects play an important roll, little benefit would be expected from an increase in Reynolds number.

AIRCRAFT CONFIGURATIONS

Although the transonic flow about the various components of an aircraft configuration is fairly well understood, it is usually necessary

to test a model of the configuration in a wind tunnel in order to determine accurately the manner in which the various flow fields combine. A flow study of such a configuration is illustrated in figure 13 by schlieren pictures obtained in the Langley 4- by 19-inch semiopen tunnel. The model consisted of a 45°-sweptback wing having a biconvex air-flow section mounted on a fuselage and a 45°-sweptback horizontal tail mounted slightly above the fuselage on a sweptback vertical tail. Such phenomena as the rearward movements of the shocks, the complicated nature of the flow field in the vicinity of the tail, and the premature wing bow wave caused by the supersonic flow induced by the fuselage are evident in the pictures.

CONCLUDING REMARKS

In summary, it can be said that, while thickness ratio is probably the primary factor with regard to transonic aerodynamics, low aspect ratios and wing sweep also play an important role in minimizing some of the undesirable characteristics. It has also been shown, however, that the use of thin swept wings, while minimizing some of the transonic problems, leads to new problems such as high drag due to lift and undesirable longitudinal stability characteristics.

With regard to subsonic and supersonic theory it was indicated that, while the trends with Mach number at subsonic and supersonic speeds can be estimated, there is considerable discrepancy with regard to magnitude in the transonic range.

REFERENCES

1. Lindsey, W. F., and Humphreys, Milton D.: Effects of Aspect Ratio on Air Flow at High Subsonic Mach Numbers. NACA TN 2720, 1952. (Supersedes NACA RM L8G23.)

2. Goodson, Kenneth W., and Morrison, William D., Jr.: Aerodynamic Characteristics of a Wing with Unswept Quarter-Chord Line, Aspect Ratio 4, Taper Ratio 0.6, and NACA 65A006 Airfoil Section. Transonic Bump Method. NACA RM L9H22, 1949.

3. Polhamus, Edward C., and Campbell, George S.: Aerodynamic Characteristics of a Wing with Unswept Quarter-Chord Lines, Aspect Ratio 2, Taper Ratio 0.78, and NACA 65A004 Airfoil Section. Transonic Bump Method. NACA RM L50A18, 1950.

4. Weissinger, J.: The Lift Distribution of Swept-Back Wings. NACA TM 1120, 1947.

5. DeYoung, John, and Harper, Charles W.: Theoretical Symmetric Span Loading at Subsonic Speeds for Wings Having Arbitrary Plan Form. NACA Rep. 921, 1948. (Supersedes NACA TN's 1476, 1491, and 1772.)

6. Gothert, B.: Plane and Three-Dimensional Flow at High Subsonic Speeds. NACA TM 1105, 1946.

7. Lomax, Harvard, and Sluder, Loma: Chordwise and Compressiblity Corrections to Slender-Wing Theory. NACA TN 2295, 1951.

8. Ames Research Staff: Equations, Tables, and Charts for Compressible Flow. NACA Rep. 1135, 1953. (Supersedes NACA TN 1428.)

9. Jones, Robert T.: Wing Plan Forms for High-Speed Flight. NACA Rep. 863, 1947. (Supersedes NACA TN 1033.)

10. Dannenberg, Robert E.: Measurements of Section Characteristics of a 45° Swept Wing Spanning a Rectangular Low-Speed Wind Tunnel as Affected by the Tunnel Walls. NACA TN 2160, 1950.

11. Lippisch, A., and Beuschausen, W.: Pressure Distribution Measurements at High Speed and Oblique Incidence of Flow. NACA TM 1115, 1947.

12. Jones, Robert T.: Subsonic Flow over Thin Oblique Airfoils at Zero Lift. NACA Rep. 902, 1948. (Supersedes NACA TN 1340.)

13. Neumark, S.: Critical Mach Numbers for Thin Untapered Swept Wings at Zero Incidence. Rep. No. Aero 2355, British R.A.E., Nov. 1949.

14. Edwards, George G., and Boltz, Frederick W.: An Analysis of the Forces and Pressure Distribution on a Wing with the Leading Edge Swept Back 37.25°. NACA RM A9K01, 1950.

15. Weil, Joseph, and Goodson, Kenneth W.: Aerodynamic Characteristics of a Wing with Quarter-Chord Line Swept Back 45°, Aspect Ratio 4, Taper Ratio 0.6, and NACA 65A006 Airfoil Section. Transonic Bump Method. NACA RM L9A21, 1949.

16. King, Thomas J., Jr., and Myers, Boyd C., II: Aerodynamic Characteristics of a Wing with Quarter-Chord Line Swept Back 60°, Aspect Ratio 4, Taper Ratio 0.6, and NACA 65A006 Airfoil Section. Transonic Bump Method. NACA RM L9G27, 1949.

17. Lawrence, T.: Charts of the Wave Drag of Wings at Zero Lift. Tech. Note Aero. 2139, British R.A.E., Nov. 1952.

18. Cohen, Doris: Formulas and Charts for the Supersonic Lift and Drag of Flat Swept-Back Wings with Interacting Leading and Trailing Edges. NACA TN 2093, 1950.

19. Dickson, R.: The Relationship Between the Compressible Flow Round a Swept-Back Aerofoil and the Incompressible Flow Round Equivalent Aerofoils. Rep. No. Aero. 2146, British R.A.E., 1946.

20. Turner, Thomas R.: Effects of Sweep on the Maximum-Lift Characteristics of Four Aspect-Ratio-4 Wings at Transonic Speeds. NACA RM L50H11, 1950.

21. Jones, Robert T.: Estimated Lift-Drag Ratios at Supersonic Speed. NACA TN 1350, 1947.

3556

EFFECT OF THICKNESS ON AIRFOIL CHARACTERISTICS

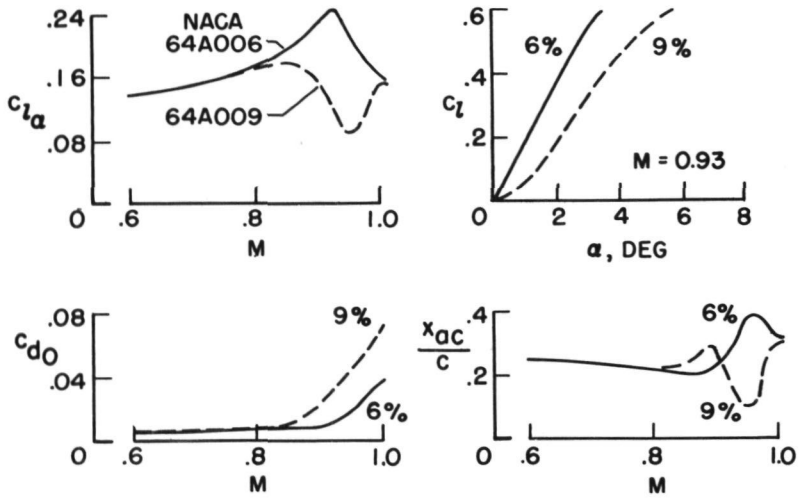

Figure 1

EFFECT OF AIRFOIL THICKNESS ON TRANSONIC FLOW

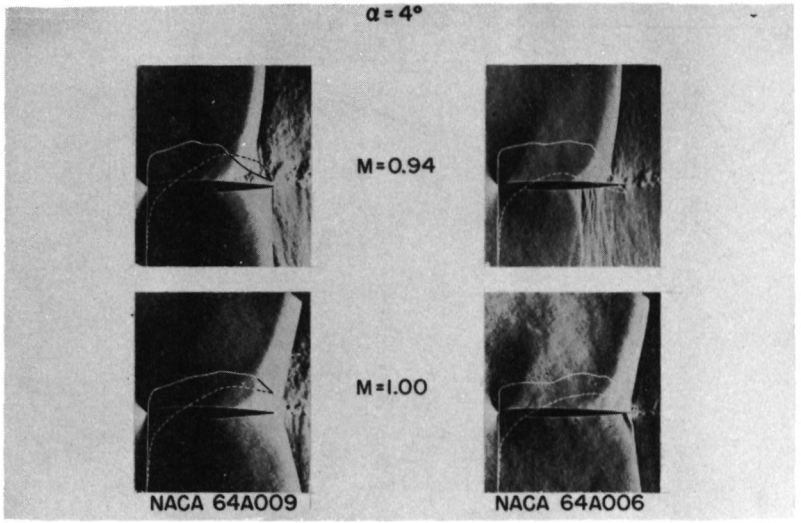

Figure 2

EFFECT OF ASPECT RATIO ON FLOW
M=0.83; NACA 0012

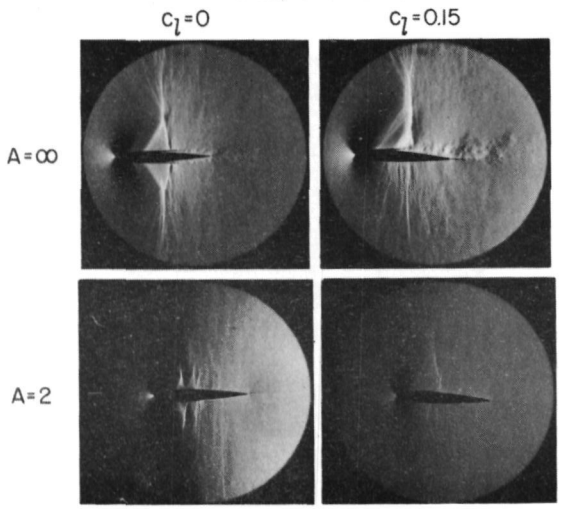

Figure 3

INK-FLOW STUDIES ON FINITE-SPAN WING
A=4; NACA 64A004; α=5°

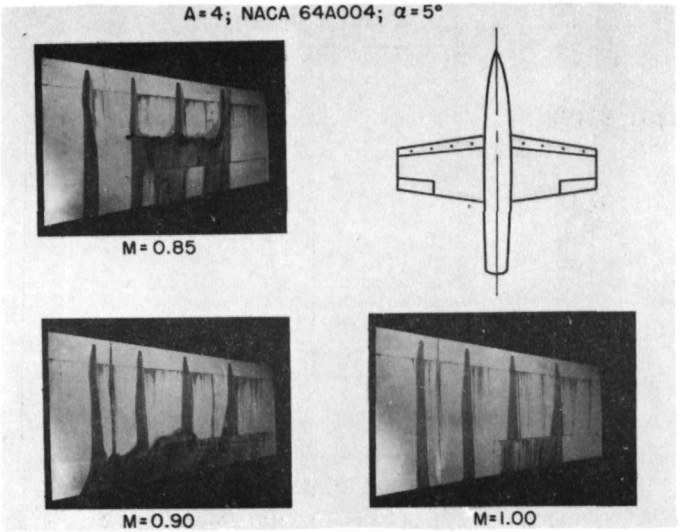

Figure 4

EFFECT OF ASPECT RATIO ON
LIFT-CURVE SLOPE
Λ=0°; NACA 65A004

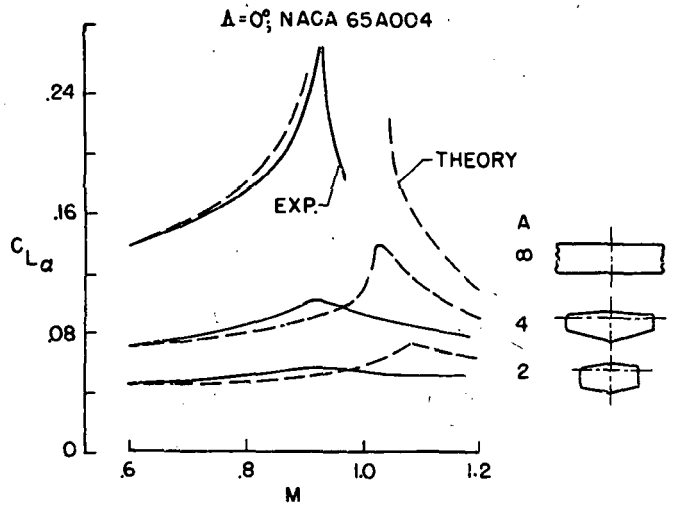

Figure 5

EFFECT OF ASPECT RATIO ON
AERODYNAMIC-CENTER LOCATION
Λ=0°; NACA 65A004

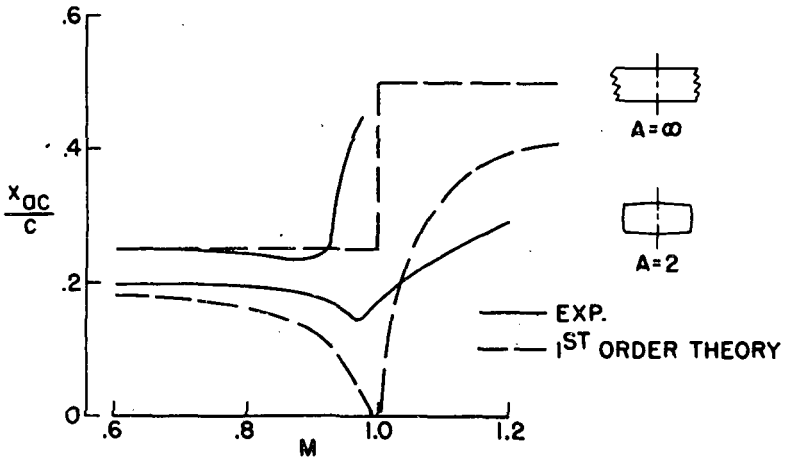

Figure 6

EFFECT OF WING SWEEP ANGLE ON PRESSURE-DRAG
DISTRIBUTION

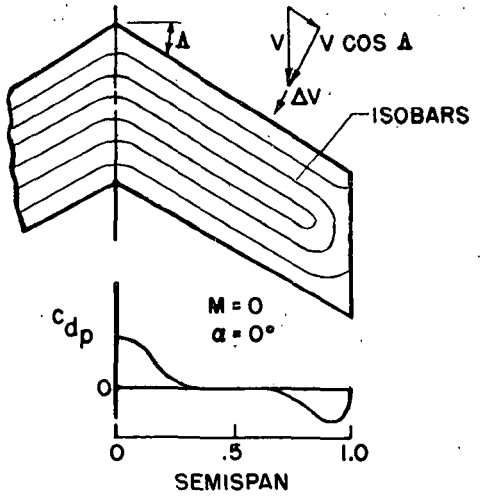

Figure 7

EFFECT OF SWEEP ANGLE ON DRAG AT ZERO LIFT
A=4; λ=0.6; NACA 65A006

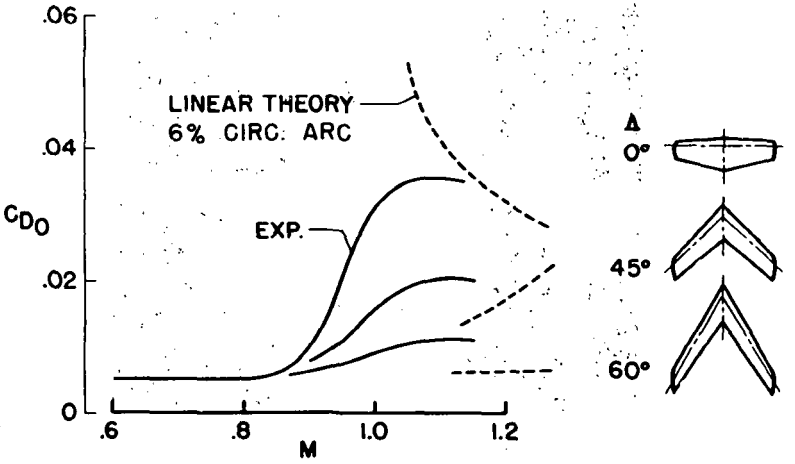

Figure 8

EFFECT OF SWEEP ANGLE ON
LIFT-CURVE SLOPE
A=4; λ = 0.6; NACA 65A006

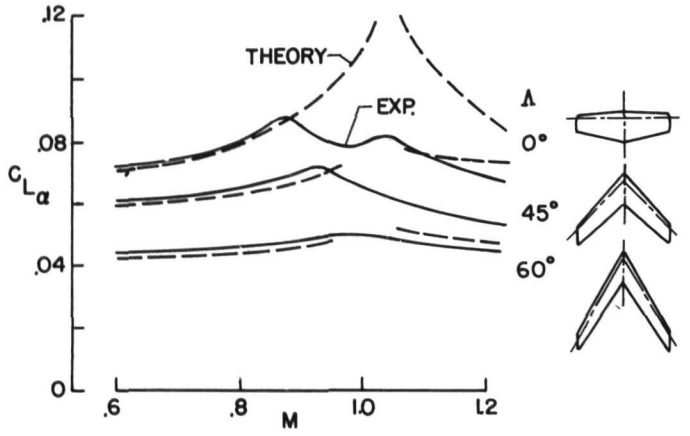

Figure 9

FLOW CHARACTERISTICS ON LIFTING SWEPT WINGS

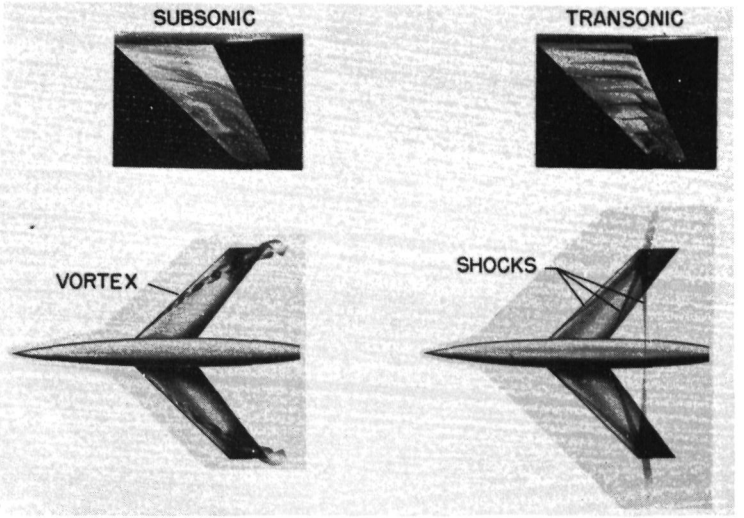

Figure 10

EFFECT OF MACH NUMBER ON PITCHING MOMENT
Λ = 45°; A = 4; λ = 0.6; NACA 65A006

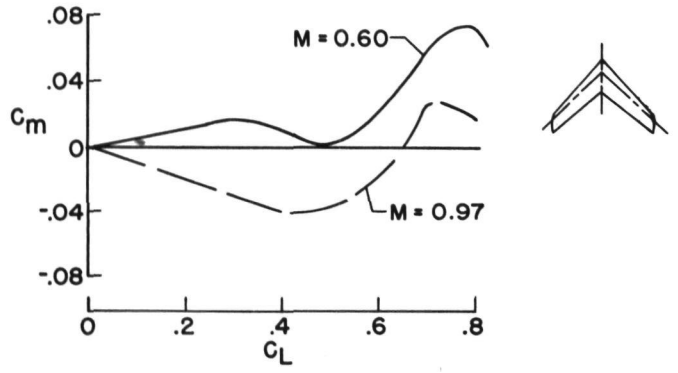

Figure 11

EFFECT OF SWEEP ON
DRAG DUE TO LIFT
A = 4°, λ = 0.6; NACA 65A006

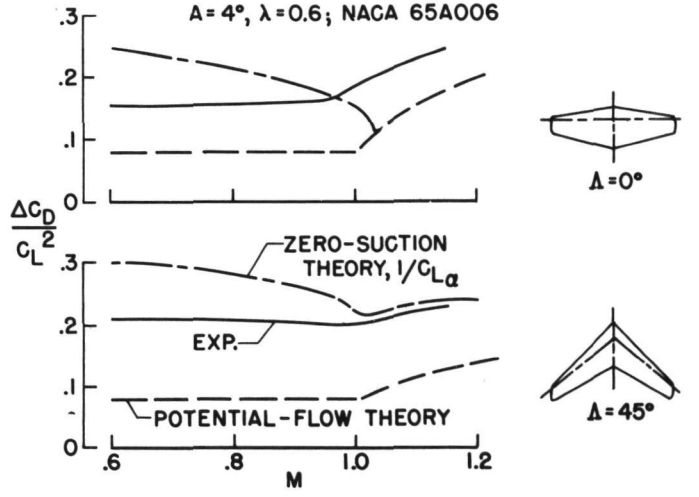

Figure 12

TRANSONIC FLOW OF AIRCRAFT CONFIGURATION

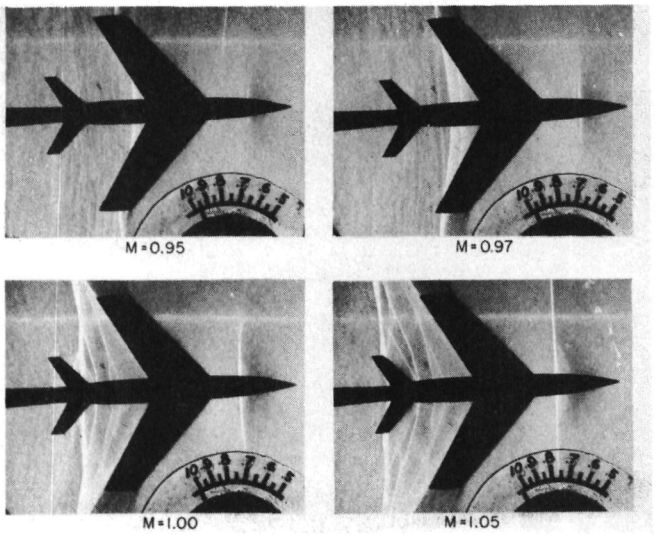

Figure 13

18. THEORETICAL AND EXPERIMENTAL ANALYSIS OF TRANSONIC FLOW FIELDS

By John R. Spreiter
Ames Aeronautical Laboratory

Progress in the theory of transonic flows has been slow compared with that for both the subsonic and supersonic speed ranges. In a sense, it can be said that the difficulties stem from the fact that subsonic and supersonic flows are so different. At Mach numbers less than a certain critical value, the velocities are subsonic everywhere in the flow field, the influence of the body extends infintely far in all directions, and the streamlines curve smoothly as illustrated in the sketch on the left in figure 1. At Mach numbers greater than a second critical value, the velocities are supersonic everywhere in the flow field, the influence of the body is confined to limited regions, and the streamlines often bend abruptly on passing through shock waves as shown in the sketch on the right in figure 1. The transonic range lies between these two Mach numbers and can be subdivided according to whether the free-stream Mach number is less than or greater than unity. The distinctive features of transonic flow are the presence of both subsonic and supersonic velocities in a single flow field and the occurrence of normal, as well as oblique, shock waves.

It is shown in the preceeding papers that linearized compressible flow theory is generally successful in dealing with many problems involving purely subsonic or purely supersonic flow, but that it often fails in the transonic range. Consequently, a different small disturbance theory has emerged for the study of transonic flow about thin wings and slender bodies. This theory, originating in the work of Oswatitsch and Wieghardt, Busemann and Guderley, von Kármán, and others (refs. 1 to 6), is now supplying a growing fund of knowledge regarding transonic flow about both two- and three-dimensional aerodynamic shapes. The basic equations of this theory have been written in many slightly different forms (see ref. 7). One form, which appears to have considerable merit, is outlined in figure 2. Regardless of their origin, all transonic flow solutions to be presented in the following discussion have been converted so as to be consistent with the present formulation of the theory.

Let the free-stream velocity be U_o, the perturbation velocity potential be ϕ, and the perturbation velocity components in Cartesian coordinates be ϕ_x, ϕ_y, ϕ_z, as indicated. For thin wings, the boundary condition is approximated to first order by equation (1), where Z represents the ordinates of the airfoil surface. The pressure coefficient is likewise approximated to first order by equation (2). These relations are all familar from linear theory, but apply equally for transonic theory. The differential equations for the potential ϕ are not the

same, however, but are as given in equations (3) and (4). In transonic and supersonic flow, it is also necessary to provide for the discontinuous changes in velocity that occur, at the shock surfaces. The equations for the shock relations, which are also different in linear theory and in transonic theory, are given in equations (5) and (6). It can be seen that only one additional term is added to the differential equation and to the shock relation. Certain elementary aspects of compressible flow and the type of improvement brought about by the use of transonic theory follow.

Figure 3 shows the variation of the critical pressure coefficient with Mach number M_o. The curve in figure 3(a) is exact for isentropic flow. If C_p lies above the curve, the flow is locally supersonic, as indicated, and conversely. It is essential that a theory for transonic flow provide a good approximation to this curve.

In the theoretical study of compressible flow, the differential equation for ϕ is of elliptic type wherever the velocity is subsonic, and of hyperbolic type wherever the velocity is supersonic. In the case of linear theory, the differential equation is of either elliptic or hyperbolic type, depending on whether the free-stream Mach number is less than or greater than unity, and the flow is always approximated as though it were either entirely subsonic or entirely supersonic, as indicated in figure 3(b). The inclusion of the additional term in the differential equation of transonic flow theory alters this situation, however, as the equation is of mixed elliptic-hyperbolic type. That transonic theory provides a good approximation is apparent from the comparison shown in figure 3(c).

Figure 4 shows how the shock polar is approximated by linear theory and by transonic theory. The exact form of the shock polar for a Mach number of 1.2 is shown in figure 4(a). The exact shock polar is repeated by the dotted line in figure 4(b), and the approximation furnished by linear theory is indicated by the solid line. It can be seen that shock polar is approximated by a straight-line tangent. As a result, all shock waves are treated as though they were weak oblique waves, or Mach waves. The corresponding approximation furnished by transonic flow theory is shown by the solid line in figure 4(c). The approximate relation provides not only the correct tangent at the weak shock end of the polar, but also the correct jump in velocity through a normal shock. Similar comparisons can be made with other elementary aspects of compressible flows, but the foregoing should define the pattern and indicate that the small disturbance theory of transonic flow is a reasonably accurate model. The foregoing comparisons are discussed in greater detail in reference 7.

One of the most striking features of transonic flow is that the local Mach number distribution on an airfoil section becomes independent of the free-stream Mach number as the latter approaches unity (see refs. 8 to 10). This is illustrated in figure 5 by a series of local Mach number distributions measured on a single-wedge section at several free-stream Mach numbers. The local Mach numbers remain virtually unchanged, or frozen, as the free-stream Mach number varies from 0.85 to 1.24. Although the theoretical solutions for two-dimensional transonic flows display the same result, research has not yet established the full range of configurations for which this phenomenon occurs.

Figure 6 shows the pressure drag of single-wedge sections. Part (a) shows a conventional plot of $_{o}C_{d_p}$ against M_o for three wedges having semiapex angles of $4\frac{1}{2}^{o}$, $7\frac{1}{2}^{o}$, and 10^{o}. The experimental data are from references 8 and 9, and the theoretical results are from references 11 to 13. The latter are readjusted to be consistent with the formulation of transonic theory given in figure 2. The experimental data points for each section fall very close to the corresponding theoretical curves given by transonic theory. The same results are replotted in part (b) in a manner indicated by the transonic similarity rules. Here the coordinates are not simply C_{d_p} and M_o, but their reduced counterparts $\overline{C_{d_p}}$ and ξ_o defined as indicated on the graph. The virtue of this method of plotting is that the data for all three wedges are collapsed onto a single line.

This figure can serve as an introduction to two ways in which transonic theory can be useful to the engineer. If the theoretical solution is known, the aerodynamic characteristics can, of course, be computed outright. If the theoretical solution is not known, transonic theory is still of value, since it provides similarity rules which help organize the aerodynamic properties of entire families of wings.

The single-wedge section is good for illustrating the foregoing points because of the completeness of both the theoretical and experimental results, and because severe viscous phenomena (i.e., separation, etc.) are avoided. The variation of drag with Mach number, however, is different from that of actual airfoils, which close at the rear.

Figure 7 shows a more typical result, that for the pressure drag of a symmetrical double-wedge profile. Again the experimental data (refs. 14 and 15) show general agreement with the computed results of transonic flow theory (refs. 12, 13, and 16). Perhaps the principal feature of note is the zero slope of $\overline{C_{d_p}}$ with ξ_o at $\xi_o = 0$, or $M_o = 1$. This is associated with the Mach number freeze discussed previously. At Mach numbers considerably removed from unity, the predictions

of transonic theory become substantially the same as those of linear theory.

The lifting characteristics of single- and double-wedge sections are reviewed in figure 8 (see refs. 14 and 17 to 19). In this case, knowledge is incomplete, since the transonic solution for Mach numbers less than unity is still unknown. Examination of the theoretical curves discloses that the phenomenon of the Mach number freeze results in a zero slope to the curve $\overline{C_l/\alpha}$ against ξ_0 at $\xi_0 = 0$. Perhaps the most striking feature of the results is the symmetry about the vertical axis - that is, about $M_0 = 1$. Although the results are symmetric, the causes are not. The peak at subsonic speeds is associated primarily with the pressures on the rear half of the airfoil; whereas, the peak at supersonic speeds is associated primarily with the pressures on the front half of the airfoil. Viscous effects on lift are often large in the transonic range, and the shapes of these peaks can alter markedly with changes in the thickness or angle of attack.

All the theoretical results for wedge sections were obtained with the hodograph transformation. This procedure has the advantage that the differential equation for two-dimensional flow is linearized without approximation, but the disadvantage that the boundary conditions are difficult to specify, except for wedge or flat-sided sections in flows having M_0 equal to or greater than unity. There also exists a large body of literature in which solutions of the complete equations for compressible flow are sought by iteration. This method, as applied to the equations of three-dimensional transonic flow theory, is sketched briefly in figure 9. Equation (7) is the transonic equation for ϕ_x or u. The solution of this equation can be represented by suitable distributions of sources and doublets. More formally, this method proceeds through the application of Green's theorem to the contours shown in the sketch in a manner exactly analogous to that employed in reference 20 in the solution of the equations of linear theory (see ref. 21). This results in equation (8), an integral equation that can be interpreted as stating that the transonic solution u is equal to the linear theory solution u_L (for a wing having the same planform, thickness distribution, and load distribution as the given wing), plus a correction term given by the integral. The latter can be thought of as the u velocity field of a distribution of sources scattered throughout space proportional to the magnitude of the nonlinear term of equation (7). The classical iteration method for solving equation (8) consists of equating u to u_L as a first approximation, then substituting u_L for u in the integral and integrating for the second approximation, and so on. This method produces a power series expansion for u in terms of thickness. As an example, the first two terms for u at the midpoint of a biconvex profile are shown in equation (9). Second-order pressure distributions on a 4-percent-thick biconex section are shown

for several Mach numbers in the small graph. These results represent the transonic approximation to the complete second-order results of references 22 and 23 and are typical, inasmuch as the method always leads to shock-free, dragless flows for all Mach numbers up to unity. It is now generally believed, however, that this method breaks down with the occurrence of mixed flow. (See refs. 24 and 25 for a résumé.)

The method just outlined must be modified if it is to be applied to transonic flows. First of all, the contour for Green's theorem must be changed so as to exclude any shocks, as shown in the sketch of figure 10. This change results in an additional term as indicated in equation (10). Second, the integral equation can be put in a better form for attempting an iteration solution for Mach numbers approaching unity by integrating the volume integral twice by parts, thereby producing equation (11). The function f_2 differs from f_1, and has the property that it vanishes for normal shock waves. The exact forms of the functions f_1 and f_2 are too lengthy to be written here, but can be found in reference 21. (These equations had been considered previously, but f_1 and f_2 were either omitted (refs. 26 and 27), or evaluated incorrectly (ref. 28).) The iteration solution is now carried out by inserting an approximate relation for u into the integrals, and solving the resulting quadratic equation for u. That is, the integral equation is rewritten in the form shown in equation (12) and solved for u using the quadratic formula. The plus sign must be used where the flow is locally supersonic, and the minus sign where the flow is locally subsonic. The classical iteration method, in effect, treats the equations as though they were linear, thereby losing the quadratic feature of the solution.

This method, with the aid of some simplifying assumptions, has been applied in reference 21 to determine approximate solutions for transonic flows about biconvex airfoils for all Mach numbers up to unity. A résumé of the results, as applied to a 4-percent-thick profile, is shown in figure 11. Part (a) shows that the pressure distributions for subcritical Mach numbers are symmetrical and shock-free, just as the second-order solutions shown in figure 9. The maximum negative pressure coefficients increase slowly with increasing Mach number, more or less as indicated by the Prandtl-Glauert rule or the Kármán-Tsien rule. Part (b) shows that shock waves make their appearance as the Mach number exceeds the critical, move rapidly rearward with increasing Mach number, and reach the trailing edge at a Mach number of 0.92. Part (c) shows the results for Mach numbers between 0.92 and 1.00. The asymmetric nature of the pressure distributions shown in parts (b) and (c) results in drag at all Mach numbers greater than the critical.

Numerous studies (e.g., refs. 29 and 30) have shown that boundary-layer shock-wave interaction can have a profound influence on a transonic

flow field. In order to better illustrate the nature of these effects, two interferograms from reference 31 of the flow about 12-percent-thick biconvex airfoils are shown in figure 12. The conditions for the two flows differ only in that the boundary layer is laminar in part (a) and turbulent in part (b). The interferogram for the laminar case shows that the shock waves are of the λ type and that the flow separates near the midchord station. When the boundary layer is turbulent, however, it may be seen that the shock wave is of the single-wave type, and that separation is delayed until about 70-percent chord. Comparison of the theoretical and measured pressure distributions corresponding to these two flows indicates substantial agreement over the portion of the air foil forward of the separation point, but quite different behavior over the remainder of the profile. This points to the fact that methods must be developed not only for determining the inviscid flow, but also for dealing with boundary-layer shock-wave interaction phenomena. Flight tests (ref. 32) indicate that this problem might be somewhat less difficult at larger Reynolds numbers, inasmuch as the shock wave appears to be of the single-wave type for laminar, as well as turbulent, boundary layers.

Although many features of transonic flow are revealed by considering two-dimensional flows, the effects of finite span are not small and must also be determined. Some idea of the magnitudes involved may be had by examining the experimental data from reference 33 shown in figure 13, wherein the variations of drag and lift with Mach number are displayed in the usual coefficient form. It can be seen that the curves for aspect ratio 6 are much the same as for the two-dimensional cases discussed previously. The variation with Mach number diminishes steadily as the aspect ratio is reduced, however, until finally almost no effect of Mach number is apparent for wings of aspect ratio 1. Another point to observe involves the slope of the drag curves at $M_o = 1$. The curves for larger aspect ratios have a slight negative slope in accordance with the phenomenon of the freeze. For smaller aspect ratio wings, however, C_D increases with M_o at $M_o = 1$. This is contrary to the prediction, and it would appear that the freeze is no longer occurring.

Certain features of transonic flow are brought into sharper focus by replotting the data in the manner indicated by the similarity rules. Greatest simplicity is achieved by considering the situation at $M_o = 1$, since, as illustrated in figure 14, the data for entire families of affinely related wings will form single curves (see ref. 7). In the present case, pressure drag and lift results are presented by plotting $C_{D_p}/(t/c)^{5/3}$ and $(t/c)^{1/3} C_{L_\alpha}$ against $A(t/c)^{1/3}$. The curves representing the zero-lift pressure drag (part (a)) and the lift (part (b)) both have the same general form. Moreover, the curves appear to display one trend for low-aspect-ratio wings and another for high-aspect-ratio wings.

They approach straight lines through the origin for low-aspect-ratio wings and horizontal lines for high-aspect-ratio wings. The results for the wings of larger aspect ratio are not too different from the theoretical values for double-wedge profiles. For $A(t/c)^{1/3}$ less than about 1, the experimental values for the lift practically coincide with the predictions given by linear theory (e.g., refs. 7 and 34). Linear theory does not provide a good approximation to the pressure distribution, or the drag, however, since it would predict infinite values. It is apparent that a transonic theory for wings of small aspect ratio is needed. A start towards such a theory is contained in the transonic equivalence rule stated by Oswatitsch at the Eighth International Congress of Theoretical and Applied Mechanics in Istanbul (ref. 35). An abstract of this paper has only recently become available.

The NACA has preferred to place less emphasis on the equivalence aspect of the rule and more on the nature of the solution and its relation to the now well-established slender-body theory of linearized subsonic and supersonic theory. Thus, consider the problem of compressible flow about the slender wing shown in figure 15. The general procedure is to consider first the complete three-dimensional problem, and then to introduce simplifying assumptions consistent with the restriction of slender planforms. The resulting solution for the potential can be expressed as the sum of four parts. Here ϕ_I, ϕ_{II}, ϕ_{III} are solutions of the two-dimensional Laplace equation as indicated. Thus, ϕ_I corresponds to the two-dimensional incompressible-flow solution for translation of the cross section, and ϕ_{II} to that for the growth of the cross section. These two terms satisfy the boundary conditions at the body, but do not furnish a satisfactory approximation, because they fail to provide the correct behavior at infinity. The error can be removed to a sufficient degree, however, by adding a negative axisymmetric solution ϕ_{III}, as calculated with the two-dimensional equation (thereby cancelling ϕ_{II} at infinity), and replacing it with the corresponding positive solution ϕ_{IV} calculated with the three-dimensional theory. If ϕ_{IV} is determined using the differential equation of linear theory, the usual formulas of subsonic and supersonic slender-body theory result (see refs. 36 to 39). These formulas are often written in a slightly different form by evaluating the sum of ϕ_{III} and ϕ_{IV} near the wing, thereby forming a function of x alone. Although the linear theory approximation is unsatisfactory at $M_o = 1$, the pattern for obtaining the corresponding result for transonic flow theory is intuitively established. The desired expressions will be had if ϕ_{IV} is determined using the transonic equation.

Since the determination of transonic solutions is very difficult and the determination of ϕ_I, ϕ_{II}, ϕ_{III} is very simple, it is evident

that the power of this theory is that it enables one to build many transonic solutions from a small number of axisymmetric transonic solutions. It appears very worthwhile to develop general methods for solving such problems. Meanwhile, the general idea can still be used by determining ϕ_{IV} from experimental data.

At the present time, one of the few axisymmetric transonic solutions is that of reference 40 for the circular cone-cylinder. As illustrated in figure 16, this solution can be used to determine the pressure on a thin elliptic cone at a Mach number of 1. The pressure distribution at zero angle of attack is shown in part (a) and the load distribution due to angle of attack is shown in part (b). Although the pressure distribution at zero angle of attack is not the same as given by linear theory, the load distribution on the lifting wing is contributed solely by ϕ_I, and is therefore the same as given by simple slender-wing theory. Consequently, lift of a slender wing at $M_0 = 1$ is the same as given by linear theory, and all the reciprocal and reverse-flow relations of linear theory for lifting surfaces hold equally for slender wings in transonic flow. It should be remarked in closing that transonic slender theory does not require the aspect ratio to be as low as does subsonic or supersonic slender-wing theory. In a more formal derivation of the relations of figure 15, it is only necessary to assume that the longitudinal perturbation velocities and their gradients be of the same order as the lateral velocities and their gradients, rather than of smaller order. This is in accordance with the fact that the trends displayed by low-aspect-ratio rectangular wings in figure 14 persist until the product of the aspect ratio and cube root of the thickness ratio is about 1, which corresponds to an aspect ratio of 3 for a wing having profiles 4 percent thick.

REFERENCES

1. Oswatitsch, K., and Wieghardt, K.: Theoretische Untersuchungen über stationäre Potentialströmungen und Grenzschichten bei hohen Geschwindigkeiten. Lilienthal-Gesellschaft für Luftfahrtforschung, Ber. 13/1, 1942, pp. 7-24. (Also available as NACA TM 1189.)

2. Busemann, A., and Guderley, K. Gottfried: The Problem of Drag at High Subsonic Speeds. Rep. and Trans. No. 184, British M.A.P., Mar. 1947.

3. Guderley, K. Gottfried: Considerations of the Structure of Mixed Subsonic - Supersonic Flow Patterns. Tech Rep. F-TR-2168-ND, AAF, Air Material Command, Wright Field, Oct. 1947.

4. Guderley, K. Gottfried: On the Transition from a Transonic Potential Flow to a Flow with Shocks. Tech. Rep. F-TR-2160-ND, AAF, Air Materiel Command, Wright Field, Aug. 1947.

5. von Kármán, Theodore: Supersonic Aerodynamics - Principles and Applications. Jour. Aero. Sci., vol. 14, no. 7, July 1947, pp. 373-402; discussion, pp. 403-409.

6. von Kármán, Theodore: The Similarity Law of Transonic Flow. Jour. Math. Phys., vol. XXVI, no. 3, Oct. 1947, pp. 182-190.

7. Spreiter, John R.: On the Application of Transonic Similarity Rules to Wings of Finite Span. NACA Rep. 1153, 1953. (Supersedes NACA TN 2726.)

8. Liepmann, H. W., and Bryson, A. E., Jr.: Transonic Flow Past Wedge Sections. Jour. Aero. Sci., vol. 17, no. 12, Dec. 1950, pp. 745-755.

9. Bryson, Arthur Earl, Jr.: An Experimental Investigation of Transonic Flow Past Two-Dimensional Wedge and Circular-Arc Sections Using a Mach-Zehnder Interferometer. NACA Rep. 1094, 1952. (Supersedes NACA TN 2560.)

10. Guderley, K. Gottfried: Two-Dimensional Flow Patterns with a Free-Stream Mach Number Close to One. AF Tech. Rep. No. 6343, U. S. Air Force, May 1951.

11. Cole, Julian D.: Drag of Finite Wedge at High Subsonic Speeds. Jour. Math. Phys., vol. 30, no. 2, July 1951, pp. 79-93.

12. Guderley, Gottfried, and Yoshihara, Hideo: The Flow over a Wedge Profile at Mach Number 1. Jour. Aero. Sci., vol. 17, no. 11, Nov. 1950, pp. 723-735.

13. Vincenti, Walter G., and Wagoner, Cleo B.: Transonic Flow Past a Wedge Profile with Detached Bow Wave. NACA Rep. 1095, 1952. (Supersedes NACA TN's 2339 and 2588.)

14. Vincenti, Walter G., Dugan, Duane W., and Phelps, E. Ray: An Experimental Study of the Lift and Pressure Distribution on a Double-Wedge Profile at Mach Numbers Near Shock Attachment. NACA TN 3225, 1954.

15. Humphreys, Milton D.: Transonic Investigation of a 10 Percent-Thick Symmetrical Double-Wedge Airfoil at Lifting Conditions. (Proposed NACA TN.)

16. Trilling, Leon: Transonic Flow Past a Wedge at Zero Angle of Attack. Z.a.M.P., vol. IV, Fasc. S, Sept. 1953.

17. Gunderley, Gottfried, and Yoshihara, Hideo: Two-Dimensional Unsymmetric Flow Patterns at Mach Number 1. Jour. Aero. Sci., vol. 20, no. 11, Nov. 1953, pp. 757-768.

18. Vincenti, Walter G., and Wagoner, Cleo B.: Theoretical Study of the Transonic Lift of a Double-Wedge Profile with Detached Bow Wave. NACA TN 2832, 1952.

19. Willmarth, William W.: The Lift of Thin Airfoils at High Subsonic Speeds. Ph. D. Thesis, C.I.T., 1953.

20. Heaslet, Max A., and Lomax, Harvard: The Use of Source-Sink and Doublet Distributions Extended to the Solution of Arbitrary Boundary Value Problems in Supersonic Flow. NACA Rep. 900, 1948. (Supersedes NACA TN 1515.)

21. Spreiter, John R., and Alkene, Alberta: Theoretical Prediction of Pressure Distributions on Nonlifting Airfoils at High Subsonic Speeds. NACA TN 3096, 1954.

22. Hantzsche, W., und Wendt, H.: Der Kompressibilitätseinfluss für dünne wenig gekrümpte Profile bei Unterschallgeschwindigkeit. Z.a.M.M., Bd. 22, Nr. 2, Apr. 1942.

23. Van Dyke, Milton D.: Second-Order Subsonic Airfoil Theory. (Proposed NACA TN.)

24. Gunderley, Gottfried: On the Presence of Shocks in Mixed Subsonic-Supersonic Flow Patterns. Advances in Appl. Mech., vol. III, 1953, pp. 145-184.

25. Bers, Lipman: Results and Conjectures in the Mathematical Theory of Subsonic and Transonic Gas Flows. Communications on Pure and Appl. Math., vol. VII, no. 1, Feb. 1954.

26. Oswatitsch, K.: Die Geschwindigkeitsverteilung bei lokalen Überschallgebieten an flachen Profilen. Z.f.a.M.M., Bd. 30, Nr. 1/2, Jan./Feb. 1950, pp. 17-24.

27. Oswatitsch, K.: Die Geschwindigkeitsverteilung an symmetrischen Profilen beim Auftreten lokaler Überschallgebiete. Acta Phys. Austriaca, Bd. 4, Nr. 2-3, Dec. 1950, pp. 228-271.

28. Gullstrand, Tore R.: The Flow over Symmetrical Aerofoils Without Incidence in the Lower Transonic Range. KTH Aero TN 20, Roy. Inst. Tech., Stockholm, Sweden, 1951.

29. Liepmann, H. W.: The Interaction Between Boundary Layer and Shock Waves in Transonic Flow. Jour. Aero. Sci., vol. 13, no. 12, Dec. 1946, pp. 623-637.

30. Ackeret, J., Feldmann, F., and Rott, N.: Untersuchungen au Verdichtungsstössen und Grenzschichten in schnell bewegten Gasen. Mitteilungen aus dem Institut für Aerodynamik, Nr. 10, Zurich 1946. (Also available as NACA TM 1113.)

31. Wood, George P., and Gooderum, Paul B.: Investigation with an Interferometer of the Flow Around a Circular-Arc Airfoil at Mach Numbers Between 0.6 and 0.9. NACA TN 2801, 1952.

32. Harrin, Eziaslav N.: A Flight Investigation of the Effect of Shape and Thickness of the Boundary Layer on the Pressure Distribution in the Presence of Shock. NACA TN 2765, 1952.

33. Nelson, Warren H., and McDevitt, John B.: The Transonic Characteristics of 17 Rectangular, Symmetrical Wing Models of Varying Aspect Ratio and Thickness. NACA RM A51A12, 1951.

34. Heaslet, Max A., Lomax, Harvard, and Spreiter, John R.: Linearized Compressible-Flow Theory for Sonic Flight Speeds. NACA Rep. 956, 1950. (Supersedes NACA TN 1824.)

35. Oswatitsch, K.: Die Theoretischen Arbeiten Über Schallnahe Stromunger am Flugtechnischen Instut der Kungl. Tekniska Hökskolan, Stockholm. Proc. of Eighth Int. Cong. on Theoretical and Appl Mech., 1953. (See also Hayes, W.D.: Pseudo-Transonic Similitude and First Order Wave Structure. Inst. Aero. Sci., Preprint, 1954.)

36. Ward, G. N.: Supersonic Flow Past Slender Pointed Bodies. Quart. Jour. Mech. and Appl. Math., vol. II, no. 1, Mar. 1949, pp. 75-97.

37. Heaslet, Max A., and Lomax, Harvard: The Calculation of Pressure on Slender Airplanes in Subsonic and Supersonic Flow. NACA TN 2900, 1953.

38. Adams, Mac C., and Sears, W. R.: Slender-Body Theory - Review and Extension. Jour. Aero. Sci., vol. 20, no. 2, Feb. 1953, pp. 85-98.

39. Keune, Friedrich, and Oswatitsch, Klaus: Nicht Angestellte Körper-kleiner Spannweite in Unter-und Überschallstroming. Zs. f. Flugwissenschaften, Jahrg. 1, Heft 6, Nov. 1953, pp. 137-145.

40. Yoshihara, Hideo: On the Flow over a Cone-Cylinder Body at Mach Number One. WADC Tech. Rep. 52-295, 1952.

FLOW REGIMES

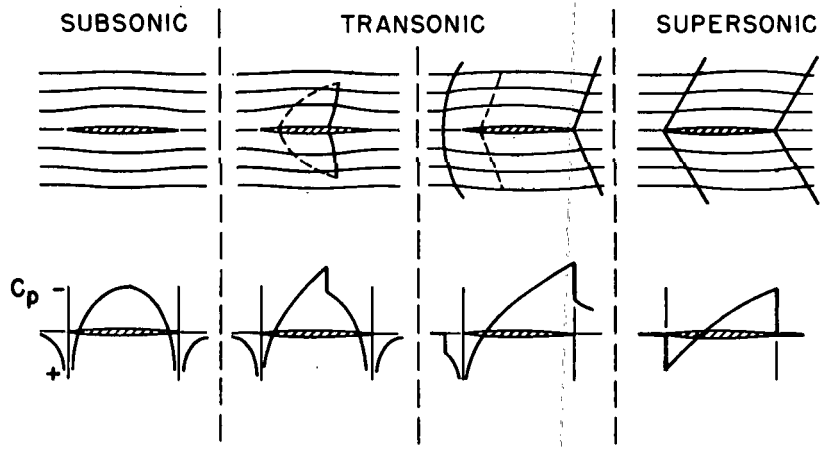

Figure 1

EQUATIONS OF WING THEORY

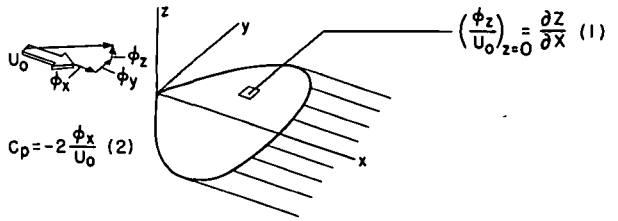

DIFFERENTIAL EQUATION

$$(1-M_0^2)\phi_{xx}+\phi_{yy}+\phi_{zz} = \begin{cases} 0 & \text{LINEAR (3)} \\ M_0^2\frac{\gamma+1}{U_0}\phi_x\phi_{xx} & \text{TRANSONIC (4)} \end{cases}$$

SHOCK RELATION

$$(1-M_0^2)(u_1-u_2)^2+(v_1-v_2)^2+(w_1-w_2)^2 = \begin{cases} 0 & \text{LINEAR (5)} \\ M_0^2\frac{\gamma+1}{U_0}\left(\frac{u_1+u_2}{2}\right)(u_1-u_2)^2 & \text{TRANSONIC (6)} \end{cases}$$

Figure 2

CRITICAL PRESSURE COEFFICIENT

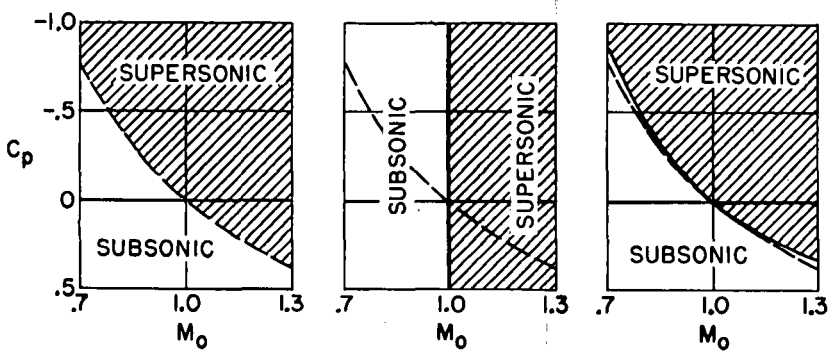

Figure 3

SHOCK RELATIONS

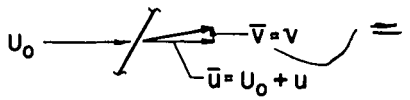

SHOCK POLARS FOR $M_0 = 1.2$

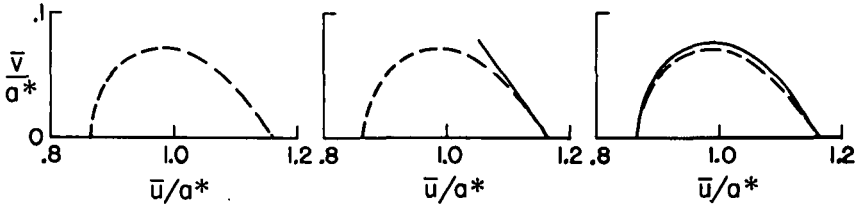

Figure 4

EXAMPLE OF MACH NUMBER FREEZE

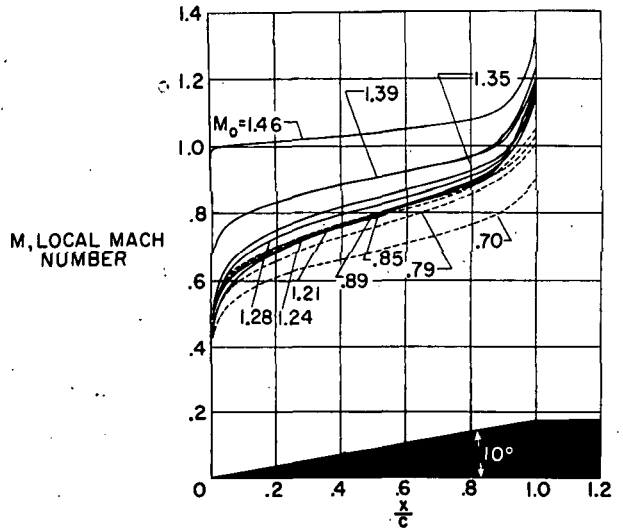

Figure 5

PRESSURE DRAG OF SINGLE-WEDGE SECTIONS

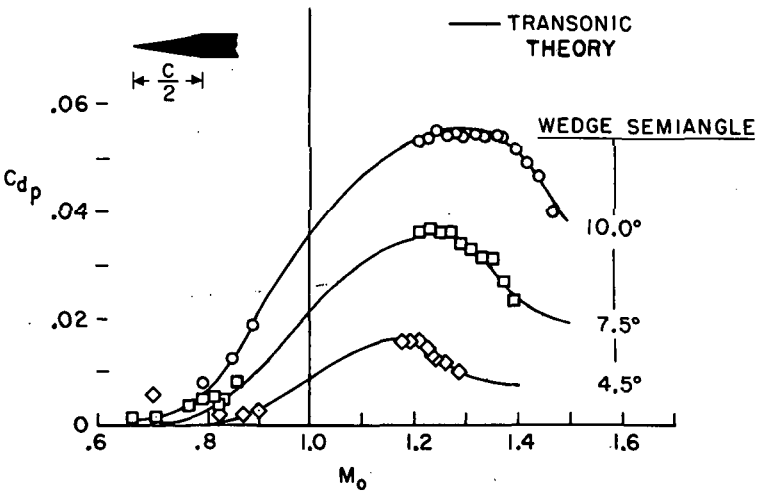

Figure 6a

PRESSURE DRAG OF SINGLE-WEDGE SECTIONS

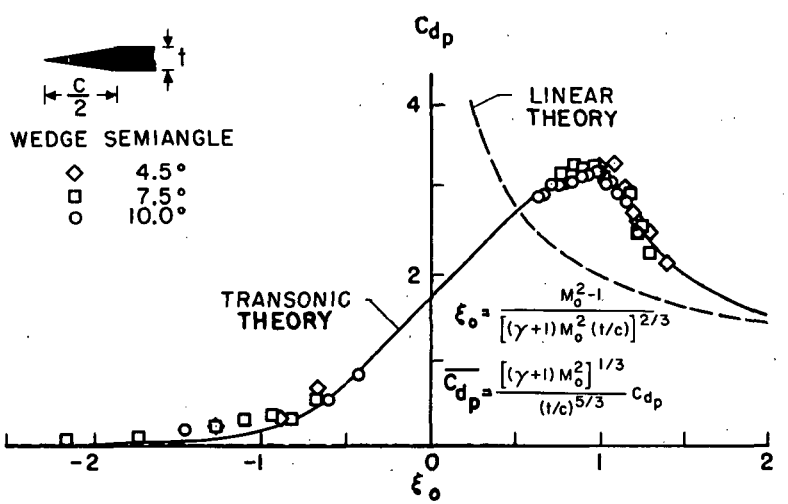

Figure 6b

PRESSURE DRAG OF DOUBLE-WEDGE SECTION

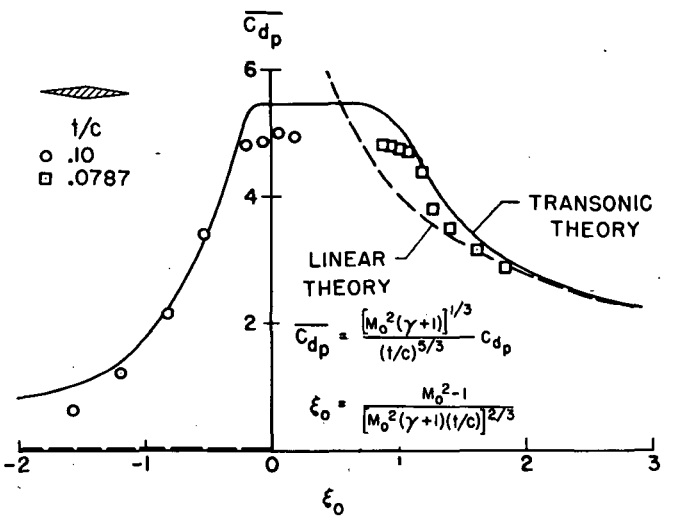

Figure 7

LIFT OF DOUBLE-WEDGE SECTION

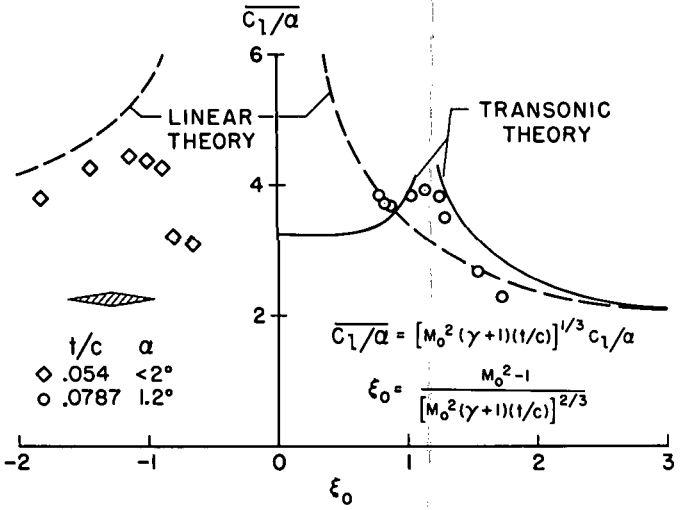

Figure 8

SUBSONIC ITERATION METHOD

DIFFERENTIAL EQUATION

$$\beta^2 u_{xx} + u_{yy} + u_{zz} = K \frac{\partial^2}{\partial x^2}\left(\frac{u^2}{2}\right) \qquad (7)$$

$\beta^2 = 1 - M_o^2$ $\qquad$ $K = M_o^2 \frac{\gamma+1}{u_o}$

GREEN'S THEOREM

INTEGRAL EQUATION

$$u = u_L - \frac{1}{4\pi}\iiint_R \{\text{SOURCE}\} K \frac{\partial^2}{\partial \xi^2}\left(\frac{u^2}{2}\right) dR \qquad (8)$$

$$\text{SOURCE} = \frac{1}{r} = \frac{1}{\sqrt{(x-\xi)^2 - \beta^2[(y-\eta)^2 + (z-\zeta)^2]}}$$

APPLICATION TO BICONVEX SECTION

$$\left(\frac{Ku}{\beta^2}\right)_{MAX.} = \frac{4}{\pi}\bar{\tau} + \left(\frac{5}{\pi^2} - \frac{1}{4}\right)\bar{\tau}^2 + \ldots. \qquad (9)$$

$$\bar{\tau} = \frac{Ku_o}{\beta^3}\frac{t}{c}$$

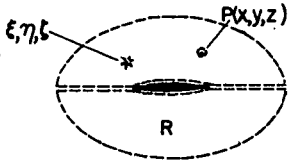

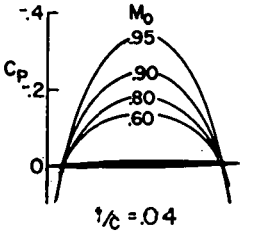

Figure 9

TRANSONIC ITERATION METHOD

$$u = u_L - \frac{K}{4\pi}\iiint \frac{1}{r}\frac{\partial^2}{\partial \xi^2}\left(\frac{u^2}{2}\right) dR + \iint_S f_1\, dS \qquad (10)$$

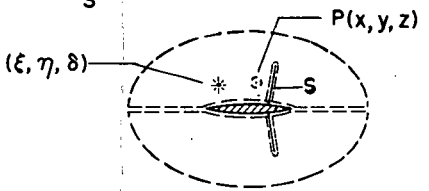

$$u = u_L + \frac{K}{\beta^2}\frac{u^2}{2} - \underbrace{\frac{K}{4\pi}\iiint \frac{u^2}{2}\frac{\partial^2}{\partial \xi^2}\left(\frac{1}{r}\right) dR + \iint_S f_2\, dS}_{I} \qquad (11)$$

$$u = u_L + \frac{K}{\beta^2}\frac{u^2}{2} - \frac{I}{2} \qquad (12)$$

$$\frac{K}{\beta^2}u = 1 \pm \sqrt{\frac{K}{\beta^2}I - \left(\frac{2K}{\beta^2}u_L - 1\right)} \qquad (13)$$

Figure 10

PRESSURE DISTRIBUTION
BICONVEX PROFILE, t/c =.04

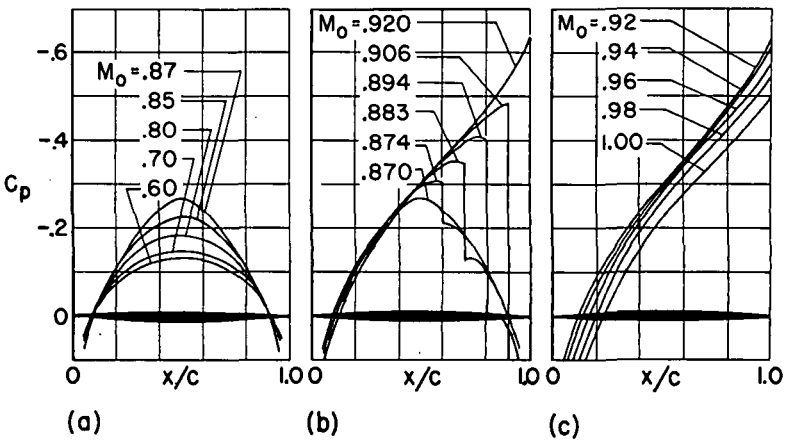

Figure 11

EFFECT OF THE BOUNDARY LAYER

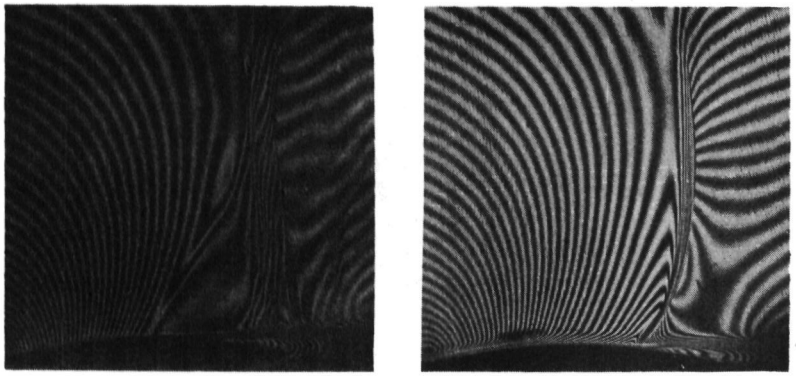

(a) LAMINAR (b) TURBULENT

$t/c = .12$, $M_0 = .88$, $R_e = 600{,}000$

Figure 12

EFFECT OF FINITE SPAN

RECTANGULAR WINGS - NACA 65A006 PROFILES

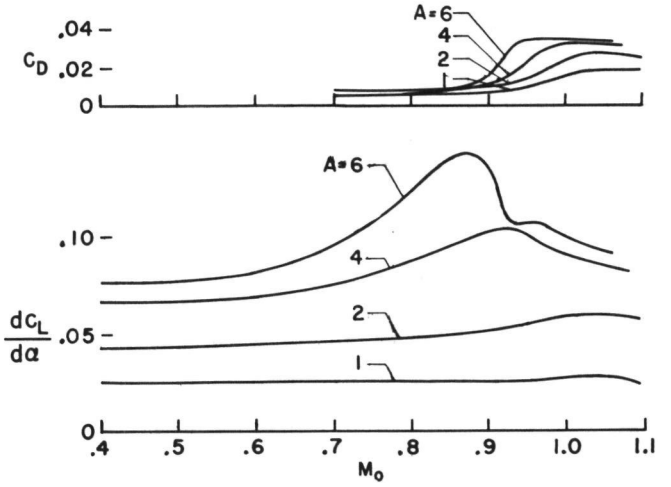

Figure 13

DRAG AND LIFT AT $M_0 = 1$

RECTANGULAR WINGS - NACA 65AOXX PROFILES

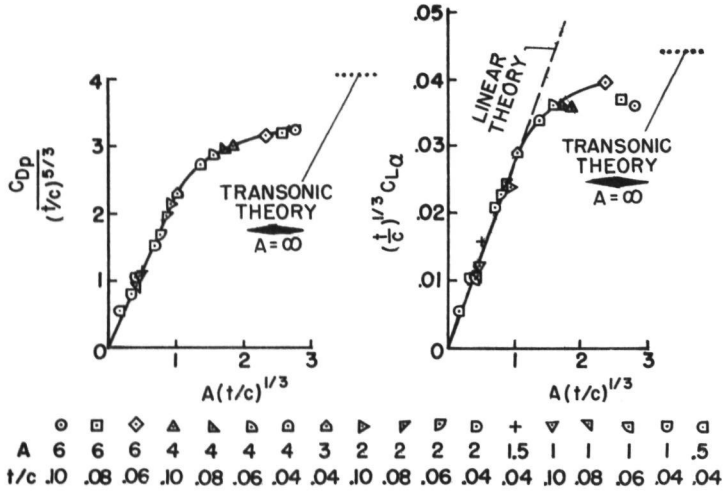
$\frac{C_{Dp}}{(t/c)^{5/3}}$
TRANSONIC THEORY
A = ∞
$A(t/c)^{1/3}$
$(\frac{t}{c})^{1/3} C_{L\alpha}$
LINEAR THEORY
TRANSONIC THEORY
A = ∞
$A(t/c)^{1/3}$
A 6 6 6 4 4 4 4 3 2 2 2 2 1.5 1 1 1 1 .5
t/c .10 .08 .06 .10 .08 .06 .04 .04 .10 .08 .06 .04 .04 .10 .08 .06 .04 .04

Figure 14

SLENDER WING THEORY

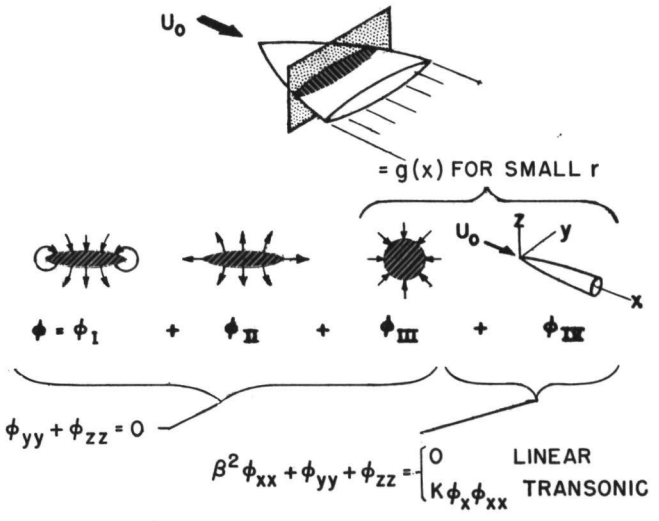
U_0
= g(x) FOR SMALL r
z
y
x
$\phi = \phi_I + \phi_{II} + \phi_{III} + \phi_{IV}$
$\phi_{yy} + \phi_{zz} = 0$
$\beta^2 \phi_{xx} + \phi_{yy} + \phi_{zz} = \begin{cases} 0 & \text{LINEAR} \\ K\phi_x \phi_{xx} & \text{TRANSONIC} \end{cases}$

Figure 15

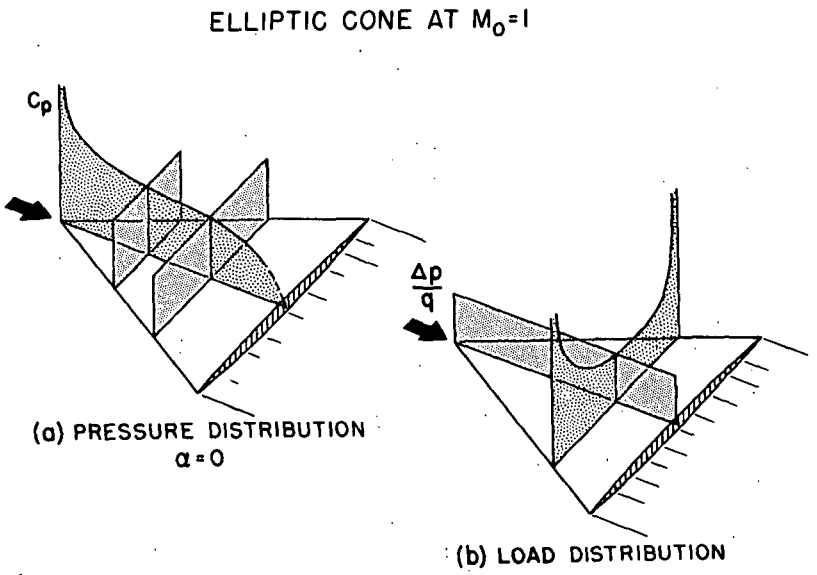
ELLIPTIC CONE AT $M_0=1$
C_p
$\frac{\Delta p}{q}$
(a) PRESSURE DISTRIBUTION
$\alpha = 0$
(b) LOAD DISTRIBUTION

Figure 16

19. THEORETICAL AND EXPERIMENTAL ANALYSIS OF HYPERSONIC FLOW FIELDS

By A. J. Eggers, Jr., and Clarence A. Syvertson
Ames Aeronautical Laboratory

Some features of hypersonic flows as predicted theoretically and observed experimentally are considered. This paper is concerned primarily with the essentially inviscid phenomena occurring outside the boundary layer.

It is well known that flows at hypersonic speeds differ from those at lower supersonic speeds in many important respects. One of the foremost of these differences is that hypersonic flows are not usually isentropic. This point is illustrated in figure 1, where supersonic and hypersonic flow about a slender airfoil are shown schematically for a Mach number of about 1.5 and a Mach number of about 5. At supersonic speeds, pressure disturbances created by the airfoil can be considered to propagate along simple sound or Mach waves. These waves can be considered straight, and the disturbed flow can, accordingly, be considered isentropic. At hypersonic speeds, however, even a slender airfoil produces strong shock waves at its leading and trailing edges. There is a substantial change in entropy across these shock waves. In addition, the interaction with other pressure disturbances created by the airfoil curves these waves. As a result of this curvature, the flow downstream of the shock waves cannot be considered isentropic and, consequently, cannot be treated with a potential theory.

On the basis of these observations, it is not surprising that new methods have been necessary for treating hypersonic flows. Three of these methods or theories that have proven especially useful are considered. The first theory is the classical impact theory proposed by Newton some 250 years ago (ref. 1). Newton realized that this theory would apply when inertia forces were very large compared with elastic forces in a fluid. In present-day aerodynamics, hypersonic flows tend to satisfy this condition. Impact theory is very simple in form, specifying that the pressures acting on a surface are proportional to the component of free-stream momentum normal to the surface. Because of its simplicity, Newton's theory has proved quite useful in the determination of "optimum" shapes. As an example, a number of minimum-pressure-drag bodies of revolution have been derived using this theory in combination with the variational calculus. Several of these bodies are shown in figure 2. They have minimum drag for the conditions of given length and volume, given diameter and volume, given length and diameter, and given surface area and diameter. The effect of the given conditions on shape is apparent. It may be noted especially that those bodies for which the length is limited have blunt noses with a small flat face. Conversely, those for which the length is not limited have pointed noses. Evidently then, if the length is fixed, the total pressure drag is reduced by

accepting high local drag on a blunt nose in return for low local drag on the slightly inclined surface aft of the nose where the projected frontal area is larger.

An experimental check on the validity of this prediction, and more generally, on the accuracy with which impact theory predicts minimum-drag bodies is shown in figure 3. All experimental data presented in figure 3, and subsequently in this paper, were obtained in the NACA Ames 10- by 14-inch wind tunnel. The bodies for which data were obtained all have the same length and diameter, and the family is defined by the equation $(y/r) = (x/l)^n$. The body given by $n = 3/4$ is a close approximation to the minimum-drag shape for the conditions of given length and diameter. For $n = 1$, the body is, of course, a cone. The experimentally determined ratios of body foredrag to cone foredrag at a Mach number of 5, and those predicted by Newtonian theory are shown as a function of the exponent n. The prediction using impact theory that the drag is a minimum for a blunt-nosed body characterized by $n = 3/4$ is verified by the experimental results.

The relative drag of bodies in hypersonic flow is, then, rather accurately predicted by Newtonian theory. The same cannot be said for the absolute drag. This shortcoming of Newtonian theory is not surprising, inasmuch as the theory is strictly applicable only in the limit as the Mach number approaches infinity, and then only for slightly curved bodies. These restrictions, coupled with further limitations on the behavior of the fluid (see ref. 2), make impact theory inadequate for predicting hypersonic flows about particular shapes. Accordingly, much effort has been directed in recent years to finding improved methods of treating hypersonic flow fields. This effort produced an important new theoretical tool, termed the hypersonic similarity law, which has proven useful in correlating our knowledge of hypersonic flows.

The law as it applies to airfoils and noninclined bodies of revolution was first discovered by Tsien (ref. 3). It was later generalized (refs. 4 and 5) to treat both steady and nonsteady three-dimensional flows. The law evolves from the equations of motion for hypersonic flow about slender shapes. Briefly stated, it specifies that the flow fields about affinely related shapes are similar, provided the free-stream Mach numbers are inversely proportional to surface inclinations. When this condition is satisfied, it is predicted that quantities like the ratio of local to free-stream static pressure will be the same at corresponding points on related shapes. This aspect of the law has been checked extensively for noninclined cones and ogives (refs. 6 and 7) using Taylor-Macoll theory and characteristics theory. The results of this investigation are summarized in figure 4, which shows the area of applicability of the law in terms of Mach number and body fineness ratio. For related bodies of revolution, the law requires that the similarity parameter M_0/f, the ratio of free-stream Mach number to fineness ratio, must be the

same if the pressure ratios are to be the same. The dashed lines correspond to constant values of M_o/f. The law is applicable over a wide range of Mach number and fineness ratio.

The applicability of the hypersonic similarity law to inclined bodies has been studied less extensively. Of the results obtained to date, however, those shown in figure 5 are more or less typical. According to the law for inclined bodies (see ref. 5), not only M_o/f but also $M_o\alpha$, the product of free-stream Mach number and angle of attack, must be the same if the pressure ratios are to be the same. These requirements were satisfied in the tests of the two ogives shown here. The fineness-ratio-3 ogive was tested at a Mach number of 3 and 10° angle of attack. The fineness-ratio-5 ogive was tested at a Mach number of 5 and 6° angle of attack. In both cases, then, M_o/f was 1 and $M_o\alpha$ was 30°. The measured pressures are shown for 3 meridian planes on both bodies corresponding to the bottom, the side, and the top. The pressures correlate reasonably well, the differences being within the accuracy of the law.

The hypersonic similarity law can also be used to relate aerodynamic coefficients. For example, if all the pertinent similarity parameters are the same, lift and moment coefficients are inversely proportional to the free-stream Mach numbers, and drag coefficients are inversely proportional to the square of the Mach numbers (for coefficients based on cross-sectional area). Similarity laws have their limitations, however; for while they relate similar flow fields, they do not provide solutions to new and more complex problems. As a final point in this paper, then, a recently developed method of analysis is discussed that has been used with success in obtaining such solutions.

This method is termed the generalized shock-expansion method (ref. 8). While it derives from the classical shock-expansion method for two-dimensional supersonic flow, it has the virtue of being applicable to both two- and three-dimensional hypersonic flows.

The generalized method hinges on two important properties of hypersonic flow. First, if a flow is two-dimensional, then Mach waves are largely absorbed in shock waves propagating in the same direction. Second, although a flow is three-dimensional in the broad view, it often appears locally two-dimensional. The first property has been well established by theoretical research on airfoils (see refs. 9 to 11). It is an essential property, because the generalized method assumes that weak disturbances are, in fact, entirely absorbed in shock waves with which they interact (refs. 8 and 9). The second property is crucial in that it determines when and how the method can be applied to three-dimensional hypersonic flows. Figure 6 will help to demonstrate this point. (See ref. 8 for a complete treatment of the subject.) A three-dimensional hypersonic flow can be treated with the generalized method when disturbances associated with the divergence θ of streamlines in

planes tangent to the surface of a body are of secondary importance compared with those associated with the deflection δ of streamlines in planes normal to the surface. The remaining question to be answered, then, is how the generalized shock-expansion method can be employed. Part of this answer is self-evident; namely, the flow in planes normal to the surface and tangent to the surface streamlines may be treated as two-dimensional, and Mach waves are considered to be entirely absorbed in a shock wave. The real problem is to locate the surface streamlines. These streamlines are fixed by the condition on when the method can be applied. According to this condition, the disturbed air is subjected only to forces acting in the normal planes, and hence the surface streamlines may be approximated by geodesics.

Geodesics are, of course, functions of the geometry of the surface, and are perhaps most often identified as lines of shortest distance between two points. However, for the present problem the important property of geodesics is that they are uniquely defined if their directions are known at a point. This is a useful property in many cases, because streamline directions can often be determined at the leading edges, or edge, of an object in hypersonic flow, independent of the complexity of its general shape (see ref. 8 for further discussion).

The generalized shock-expansion method will now be applied to the calculation of three-dimensional flow about a particular shape. Consider the body of revolution at small angle of attack.[1] An analysis (ref. 13) has indicated that the method is applicable to bodies of revolution when the parameter M_o/f is greater than about 1. The next problem is to determine the geodesics that may be taken as surface streamlines. These streamlines originate at the vertex. The only pertinent geodesics passing through the vertex are the meridian lines; hence, the meridian lines are, to the accuracy of the method, the surface streamlines. The calculation of the flow about a body proceeds as follows: Flow at the vertex is assumed conical and known from either theory or experiment. Flow downstream of the vertex along surface streamlines is determined with the Prandtl-Meyer expansion equations. The flow field away from the surface in each meridian plane is constructed on the assumptions that the pressure changes only slightly along each Mach line emanating from the surface and that flow along each streamline is given by the Prandtl-Meyer equations, except at a shock wave where the Rankine-Hugoniot equations apply. This gives, then, the theory of when and how the generalized shock expansion can be applied to inclined bodies of revolution.

In order to discover whether the method really works, consider first the pressure distributions on two ogives at a Mach number of 5.05 and an angle of attack of 10^o. As shown in figure 7, one ogive has a fineness

[1]For a more complete treatment of the application of the generalized shock-expansion method to inclined bodies of revolution, see ref. 12.

ratio of 5, corresponding to $M_o/f = 1.01$, and the other has a fineness ratio of 3, corresponding to $M_o/f = 1.68$. The predictions of the generalized method, based on theoretical conical flow results at the nose (ref. 12), and the experimental pressure distributions are compared for three meridian planes corresponding to the bottom, the side, and the top of each body. In general, theory and experiment are in good agreement, except on the top or extreme leeward sides of the bodies where viscous crossflow effects (ref. 14) might first be expected to appear.

Surface pressures provide, of course, only a partial check of the generalized shock-expansion method - a check, so to speak, only at the inner boundary of the disturbed flow field. It is of interest, then, to check the method at the outer boundary of the disturbed flow, that is, at the bow shock wave. For this purpose, the predictions of the generalized shock-expansion method and experimentally determined shock-wave shapes are compared for the plane of symmetry in figure 8. Again, the Mach number is 5.05 and the angle of attack is 10^o. The experimental data were obtained from schlieren photographs. The conical shock waves created by cones having the same vertex angles as the ogives are shown for contrast. Theory and experiment are observed to be in quite good agreement.

As an over-all check on the generalized shock-expansion method, the normal-force coefficients for the two ogives were obtained by integration of theoretical and experimental pressure distributions. The results are shown in figure 9. The agreement between theory and experiment is somewhat better for the larger value of M_o/f, indicating, as might be expected, that the accuracy of the theory improves with increasing M_o/f. Axial forces have also been obtained, and the method was found to apply with essentially the same accuracy.

Now it is well to mention some of the other applications of the method. For example, it was early recognized that if the shock-expansion method applied to two-dimensional airfoils, then it should also apply to wings of finite span in hypersonic flow, inasmuch as the regions influenced by tip effects are usually quite small. This point was first verified experimentally in tests conducted in the Langley 11-inch hypersonic wind tunnel (ref. 15). The method also appears to be useful in predicting the flow about controls and about wing-body combinations at hypersonic speeds. In many respects, then, the generalized shock-expansion method is proving as useful in the treatment of hypersonic flows as linearized theory has been in the treatment of supersonic flows.

In conclusion, it is appropriate to review briefly the major points of this paper. First, it was pointed out that a major difference between supersonic and hypersonic flows is that hypersonic flows are generally not isentropic. Consequently, the potential theories of supersonic flow have been replaced by other methods of analysis in studying hypersonic

flows. Three of these methods were described. First, the classical impact theory of Newton was cited as being useful in determining optimum body shapes. Second, the hypersonic similarity law was discussed for its value in correlating our knowledge of hypersonic flows. Finally, the generalized shock-expansion method was presented as a simple yet powerful tool for accurately treating both two- and three-dimensional hypersonic flows. The utility of each of the three methods was demonstrated by comparison of theory with experiment.

REFERENCES

1. Newton, Isaac: Principia - Motte's Translation Revised. Univ. of Calif. Press, 1946, pp. 333; 657-661.

2. Busemann, A.: Flussigkeits-und Gasbewung. Handworterbuch der Naturwissenschaften, Zweite Auflage, Gustov Fischer, Jena, 1933, pp. 266-279.

3. Tsien, Hsue-Shen: Similarity Laws of Hypersonic Flows. Jour. Math. and Phys., vol. 25, no. 3, Oct. 1946, pp. 247-251.

4. Hayes, Wallace D.: On Hypersonic Similitude. Quart. Appl. Math., vol. V, no. 1, Apr. 1947, pp. 105-106.

5. Hamaker, Frank M., Neice, Stanford E., and Wong, Thomas J.: The Similarity Law for Hypersonic Flow and Requirements for Dynamic Similarity of Related Bodies in Free Flight. NACA Rep. 1147, 1953. (Supersedes NACA TN's 2443 and 2631.)

6. Ehret, Dorris M., Rossow, Vernon J., and Stevens, Victor I.: An Analysis of the Applicability of the Hypersonic Similarity Law to the Study of Flow about Bodies of Revolution at Zero Angle of Attack. NACA TN 2250, 1950.

7. Rossow, Vernon J.: Applicability of the Hypersonic Similarity Rule to Pressure Distributions Which Include the Effects of Rotation for Bodies of Revolution at Zero Angle of Attack. NACA TN 2399, 1951.

8. Eggers, A. J., Jr.: On the Calculation of Flow about Objects Traveling at High Supersonic Speeds. NACA TN 2811, 1952.

9. Eggers, A. J., Jr., Syvertson, Clarence A., and Kraus, Samuel: A Study of Inviscid Flow about Airfoils at High Supersonic Speeds. NACA Rep. 1123, 1953. (Supersedes NACA TN's 2646 and 2729.)

10. Crocco, Luigi: Singolorità della Corrente Gassosa Iperacustica Nell' Intorne di Una Prora a Diedro. L'Aerotecnica, vol. 17, no. 6, June 1937, pp. 519-534.

11. Munk, M. M., and Prim, R. C.: Surface-Pressure Gradient and Shock-Front Curvature at the Edge of a Plane Ogive with Attached Shock Front. Jour. Aero. Sci., vol. 15, no. 11, Nov. 1948, pp. 691-695.

12. Savin, Raymond C.: Application of the Generalized Shock-Expansion Method to Inclined Bodies of Revolution Traveling at High Supersonic Airspeeds. (Proposed NACA TN.)

13. Eggers, A. J., Jr., and Savin, Raymond C.: Approximate Methods for Calculating the Flow about Nonlifting Bodies of Revolution at High Supersonic Airspeeds. NACA TN 2579, 1951.

14. Allen, H. Julian, and Perkins, Edward W.: A Study of Effects of Viscosity on Flow over Slender Inclined Bodies of Revolution. NACA Rep. 1048, 1951. (Supersedes NACA TN 2044.)

15. McLellan, Charles H.: Exploratory Wind-Tunnel Investigation of Wings and Bodies at M = 6.9. Jour. Aero. Sci., vol. 18, no. 10, Oct. 1951, pp. 641-648.

BIBLIOGRAPHY

1. Grimminger, G., Williams, E. P., and Young, G. B. W.: Lift on Inclined Bodies of Revolution in Hypersonic Flow. Jour. Aero. Sci., vol. 17, no. 11, Nov. 1950, pp. 675-690.

2. Ivey, H. Reese, Klunker, E. Bernard, and Bowen, Edward N.: A Method for Determining the Aerodynamic Characteristics of Two- and Three-Dimensional Shapes at Hypersonic Speeds. NACA TN 1613, 1948.

3. Sanger, Eugene: Raketen-flugtecknik. R. Oldenburg (Berlin), 1933, pp. 120-121.

4. Epstein, Paul S.: On the Air Resistance of Projectiles. Proc. Nat. Acad. Sci., vol. 17, 1931, pp. 532-547.

5. Oswatitsch, Klaus: Similarity Laws for Hypersonic Flow. KTH Aero. TN 16, Royal Inst. of Tech. Div. of Aero., (Stockholm, Sweden), 1950.

6. Dorrance, William H.: Three-Dimensional Hypersonic Flow Similarity Parameters. Consolidated Vultee Rep. ZA-7-001, Proj. Atlas, Sept. 1951.

7. Van Dyke, Milton D.: The Combined Supersonic-Hypersonic Similarity Rule. Jour. Aero. Sci., vol. 18, no. 7, July 1951, pp. 499-500.

8. Linnell, Richard D.: Two-Dimensional Airfoils in Hypersonic Flows. Jour. Aero. Sci., vol. 16, no. 1, Jan. 1949, pp. 22-30.

9. Goldsworthy, F. A.: Two-Dimensional Rotational Flow at High Mach Number Past Thin Airfoils. Quart. Jour. Mech. and Appl. Math., vol. V, pt. 1, Nov., 1952, pp. 54-63.

10. Dorrance, William H.: Two-Dimensional Airfoils at Moderate Hypersonic Velocities. Jour. Aero. Sci., vol. 19, no. 9, Sept. 1952, pp. 593-600.

11. Van Dyke, Milton D.: A Study of Hypersonic Small-Disturbance Theory. NACA TN 3173, 1954.

12. Eggers, A. J., Jr.: One-Dimensional Flows of an Imperfect Diatomic Gas. NACA Rep. 959, 1950. (Supersedes NACA TN 1861.)

13. Ivey, H. Reese, and Cline, Charles W.: Effect of Heat-Capacity Lag on the Flow Through Oblique Shock Waves. NACA TN 2196, 1950.

14. Meyer, Th.: The Two-Dimensional Phenomena of Motion in a Gas Flowing at Supersonic Velocity. Cornell Research Foundation, Inc., (Buffalo, New York), Aug. 1945. (Trans. from: Mitteilungen über Forschungsorbeiten Auf dena Gebiete des Ingenieunwesens, Heft 62, 1908, pp. 31-67.)

15. Eggers, A. J., Jr., and Kraus, Samuel: Approximate Calculation of Axisymmetric Flow Near the Vertex of a Body Traveling at High Supersonic Speeds. Jour. Aero. Sci., vol. 20, no. 3, Mar. 1953, pp. 215-217.

COMPARISON OF SUPERSONIC AND HYPERSONIC FLOWS

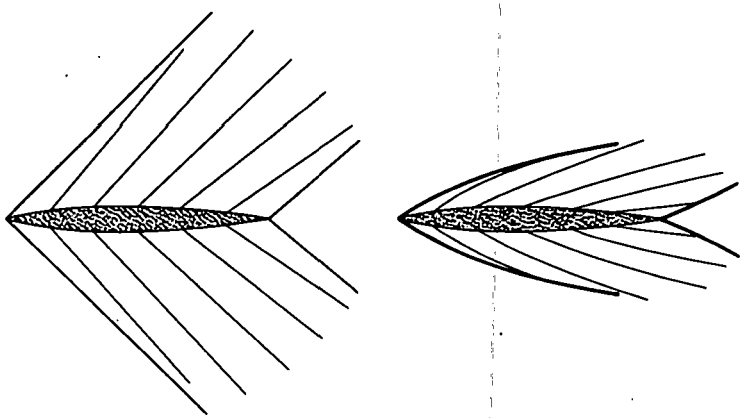

Figure 1

MINIMUM-DRAG BODIES BY NEWTONIAN THEORY

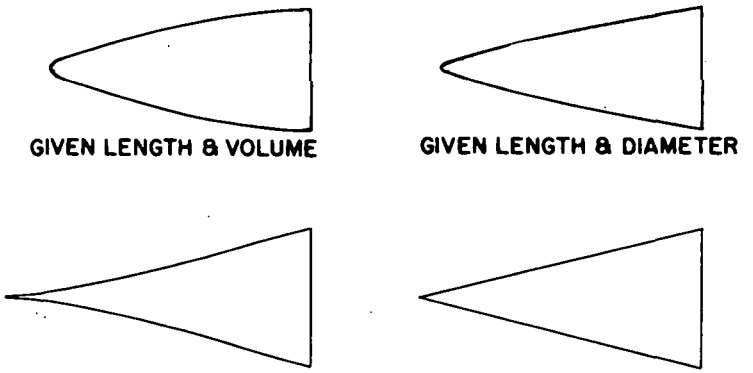

Figure 2

RELATIVE DRAG OF BODIES HAVING SAME LENGTH AND DIAMETER

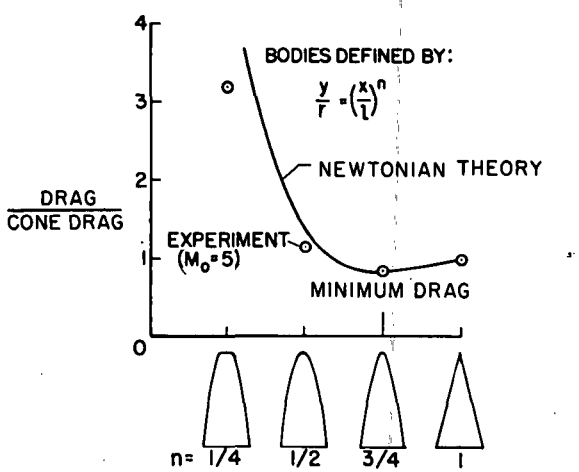

Figure 3

APPLICABILITY OF HYPERSONIC SIMILARITY LAW TO NONINCLINED BODIES

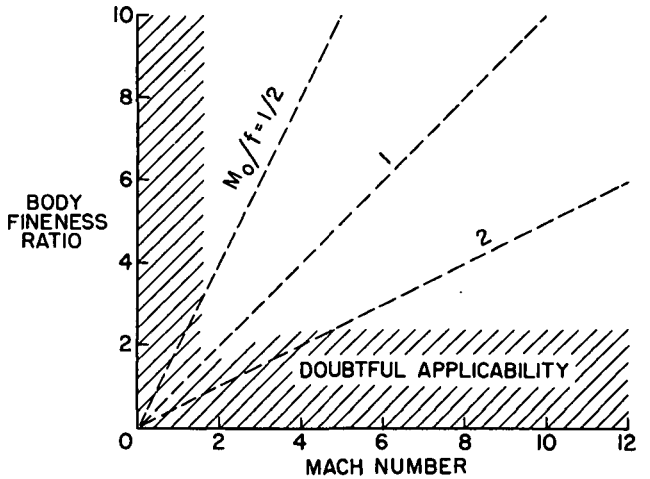

Figure 4

APPLICABILITY OF HYPERSONIC SIMILARITY LAW TO INCLINED OGIVES

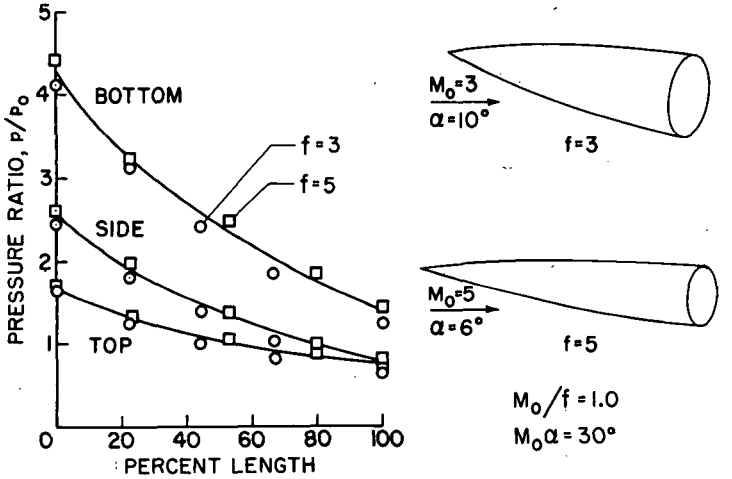

Figure 5

GENERALIZED SHOCK-EXPANSION METHOD

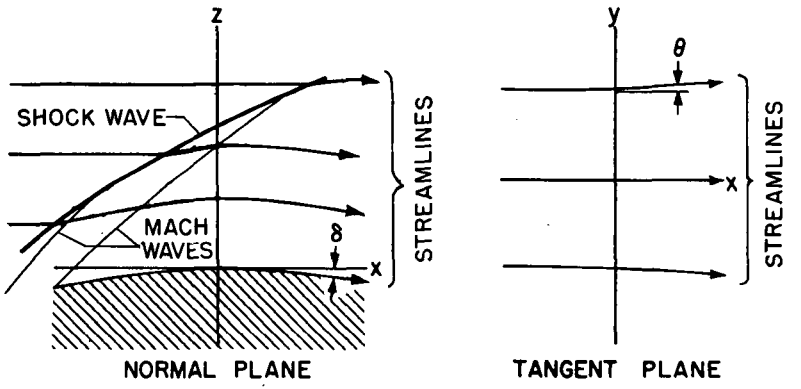

Figure 6

PRESSURES ACTING ON OGIVES AT M_0=5.05 AND α=10°

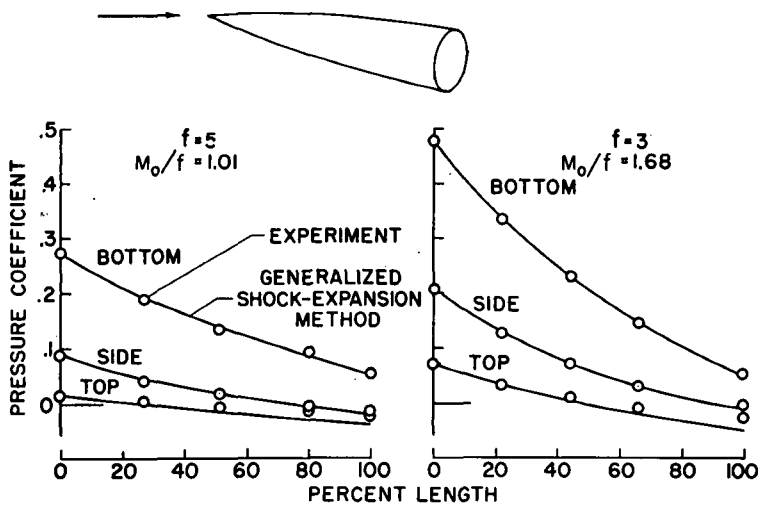

Figure 7

SHOCK WAVES FOR OGIVES AT M_0=5.05 AND α=10°

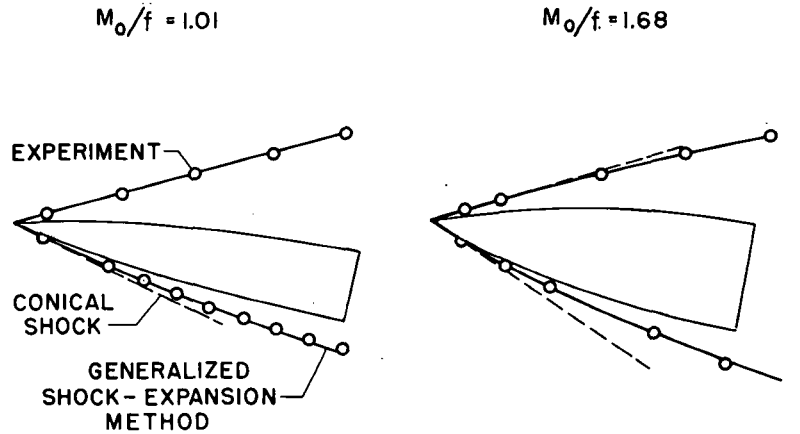

Figure 8

NORMAL FORCES ACTING ON OGIVES AT M_0=5.05

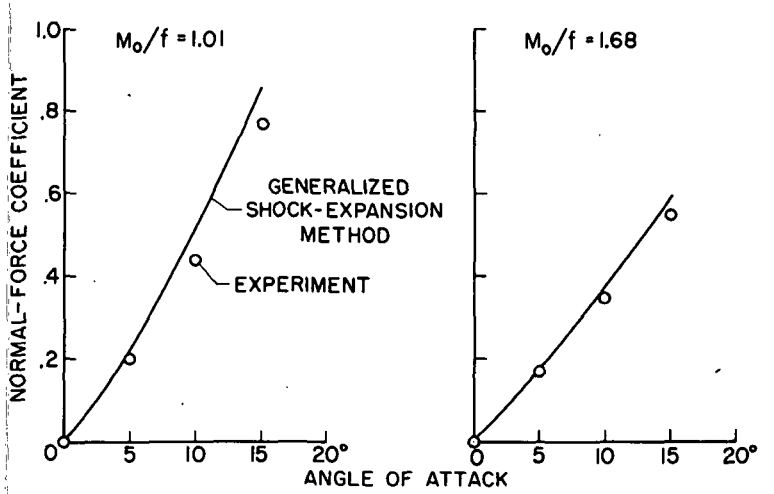

Figure 9

20. TRANSONIC TEST SECTIONS

By William J. Nelson and Ray H. Wright
Langley Aeronautical Laboratory

INTRODUCTION

The increasing speed of aircraft demands a corresponding increase in speed of model testing facilities to explore the many new problems encountered. Hindering such an increase into the transonic range were wall interference and choking in closed wind tunnels and jet boundary interference, flow pulsations, and large power requirements for open wind tunnels.

The fact that the wall interference effects in open tunnels are opposite in sign to those in closed tunnels led to the hypothesis that, with a proper combination of open and closed sections in the boundary, interference due to solid blockage might be eliminated. Analytical work by Wright was based on the use of discrete longitudinal slots and, in 1948, this analysis, together with an experimental verification, was reported in reference 1. Those experiments also established that such a tunnel could be operated at low supersonic Mach numbers without modification of the wall contour. It was this work which led the NACA to the development of the slotted transonic test section. A typical installation, shown schematically in figure 1, consists of the slotted test section enclosed in a relatively large chamber with the air approaching the test section accelerated through an entrance bell of conventional design and compressed downstream through a low-angle diffuser.

In the subsequent development of transonic facilities, many have participated in both the analytical and experimental phases of the problem. It is the purpose of the present paper to review some of the highlights in the development of the transonic tunnel as a research tool and to discuss briefly some of the characteristics of such a facility.

TRANSONIC TUNNEL DESIGN

Flow Generation

In the design of a transonic tunnel, one of the first problems to be solved is that of obtaining uniform flow through the test section. At subsonic speeds, this proved to be relatively easy, for the Mach number at the end of the nozzle was continued through the slotted section. To attain supersonic Mach numbers in this type of tunnel, the flow, accelerated to $M = 1$ in the nozzle, is further expanded by

diverting part of the air into the chamber. Preliminary tests (ref. 2) established that with slots of rectangular plan form the initial expansion to supersonic velocities followed closely that calculated for Prandtl-Meyer flow about a sharp corner as in the open jet, but that the extent of the initial expansion was a function of both slot area and profile. The effects of slot spacing and wall divergence were also investigated, and satisfactory transonic flows were obtained in several tunnels of different cross section. The Mach number distributions of figure 2 are typical of those obtained in large-scale transonic facilities. The maximum Mach number variations along the test section are on the order of ± 0.005 and occur at the higher speeds.

An alternative method of generating supersonic flow utilizes a conventional supersonic nozzle ahead of the slotted test section. This method, described in some detail in reference 3, also results in very uniform velocity distributions.

The NACA was also active in the use of porous and perforated media for wind-tunnel walls and, in 1950, published a simplified analysis of the supersonic flow generation problem which, based upon the concept of a material whose flow characteristics were independent of velocity components parallel to the surface, resulted in only general agreement with the experimental distributions (ref. 4). Subsequent research on perforated plates (ref. 5) showed that the flow coefficient of such materials was strongly influenced by lateral velocity components. With a complete flow calibration in the presence of flow parallel to the surface, it should be possible to carry out point-by-point calculations of the supersonic flow pattern and to develop uniform flows over a substantial Mach number range. The calibration of slots in the presence of axial flow is somewhat more complicated because of the end effects, that part of the slot closest to the nozzle having somewhat different flow coefficient from sections farther downstream where substantial axial velocities are encountered in the slot proper. Although the theory does not permit accurate calculation of Mach number distributions in slotted tunnels, it has been very useful in developing final slot shapes.

Subsonic Blocking

The initial attack on the subsonic blockage problem was analytical; in fact, Wieselsberger (ref. 6) showed in 1942 that, in a rectangular tunnel with two open sides and two closed sides, the blockage interference at the center was theoretically reduced to zero if the width of the closed sides was 1.17 times that of the open sides. In the analytical work reported in reference 1, the case of a doublet located at the center of a circular test section with equally spaced longitudinal slots was selected (fig. 3). In the resulting symmetry of flow, it was necessary to treat only one sector, from the center of a closed segment to the

center of an adjacent slot. Along the boundary, the conditions expressed in terms of the doublet potential φ and an additional potential φ^* signified uniform pressure across the slot and zero radial velocity along the solid wall. The additional potential φ^*, like the doublet potential φ, must satisfy Laplace's equation

$$\varphi + \left(\frac{d}{\pi} \log_e \csc \frac{\pi}{2} \frac{a}{d}\right) \frac{\partial \varphi}{\partial n} = 0$$

which, solved in terms of a Fourier series and integral, leads to an expression of the axial interference velocity as the function of slot width and spacing. For circular tunnels with two slots and with ten slots, the interference velocity function R^3u^*/m varies with open area ratio as shown in figure 4, where R is the tunnel radius, m the doublet strength, and u^* the interference velocity. The closed-tunnel interference is shown at abscissa zero and the open jet interference at an open area ratio of 1.0. From these calculations, it was estimated that, to obtain zero blockage interference in a 10-slotted circular tunnel, approximately one-eighth of the total periphery should be open. For ratios of open-to-total periphery somewhat greater than that required for zero interference, the blockage is seen to be rather insensitive to open ratio, so that great accuracy of estimation is not required. The portion of open area required for zero interference increases as the number of slots decreases.

These calculations were verified, at least qualitatively, in tests of a prolate spheroid in a circular tunnel whose boundaries in successive tests were closed, open, and slotted (fig. 5). The slotted wall configuration used was that estimated to give zero interference velocity at the model. The model used was much larger than would normally be considered, in order that the interference effects might be magnified. The Mach number increment ΔM plotted here as the ordinate is the difference between the indicated stream Mach number and the effective Mach number. The experimental data indicate that the interference at the center of this model was practically eliminated. However, with this large model, a small pressure gradient was introduced into the effective test stream.

The boundary conditions assumed in this derivation are, of course, not exact. The strong mixing at the slots produces a thick mixing region, so that the boundary conditions assumed are at best only a reasonable approximation to the average conditions. Any error involved is minimized by providing few rather than very many slots, since the boundary layer then becomes of relatively less importance.

Another type of departure from the assumed boundary conditions occurs when the slots are deep in a direction perpendicular to the tunnel axis. In this case, the potential in the slot at the tunnel radius is different from the assumed zero value by the amount of the line integral

of the velocity along the radius from the actual stream boundary to the tunnel radius. Since this difference varies with distance along the tunnel axis and with model and flow conditions, depending on the depth to which the tunnel flow fills the slots, it is not conveniently taken into account. The validity of the theory, therefore, requires that the slot edges be made thin and that the space just outside these edges be rapidly enlarged, so that the constant-pressure boundary condition is established very close to the assumed position. Increasing the depth of a slot has somewhat the same effect as making it narrower. Another type of departure from the assumed conditions occurs if the downstream end of the contraction or the upstream end of the diffuser entrance is too close to the model. From theory developed for lifting wings in closed tunnels (ref. 7), it is inferred that the effect of the finite jet length is negligible, provided the model is located at least half a tunnel height from the entrance and exit regions.

3556

The effect of compressibility on the interference is also derived in reference 7, and it is shown that, in the slotted as in the closed tunnel, the axial interference velocities are increased by compressibility in the ratio $1/(1 - M^2)^{3/2}$. Within the applicability of the linearized theory, a slotted tunnel with zero blockage at low speeds should have zero blockage at all subsonic Mach numbers. Once the region of supersonic velocities reaches the tunnel wall, the theory ceases to be valid. This attainment of supersonic velocities at the wall corresponds to choking in the closed tunnel; but, in the zero-blockage slotted tunnel where choking cannot occur, it seems reasonable to suppose that, with further increase of speed up to Mach number 1.0, the interference may still be small.

The interference at Mach numbers up to 1.12 was investigated by comparing pressure distributions on a $1\frac{1}{3}$-inch-diameter body in a 12-inch octagonal tunnel with those obtained from tests of the same body in an 8-foot circular closed tunnel (ref. 1). The outline of the model and tunnels is shown in figure 6. Because the cross-sectional area of the 8-foot tunnel was some 5000 times that of the model, it may be considered interference-free. Typical surface pressure distributions from those tests are presented in figure 7. At subsonic speeds, the interference is approximately zero, as previously surmised. At $M = 1.12$, the bow shock was reflected from the walls of the slotted tunnel to increase the pressures locally on the forebody. The length of this model was on the order of 2/3 the tunnel diameter.

The same effects are shown for a complete model in figure 8, where the drag coefficient obtained in Langley 8-foot transonic tunnel tests of a complete model whose length was approximately 1/3 of the tunnel diameter is presented as a function of Mach number (ref. 8). The solid

curve, used as a reference for evaluating the effects of wall interference, was obtained from flight tests of a similar model. The subsonic interference is negligible, and even the supersonic interference is small up to a Mach number of 1.04. With further increases in Mach number, the drag is first too great and then too small, corresponding to the progression of the deflected bow wave from nose to tail over the model.

The only type of subsonic interference so far discussed is that due to solid blockage, but it is obvious that the effects of wake blockage must also be zero. It is reasonable to suppose that the pressure gradient due to wake blockage would be reduced by slotting the tunnel boundary and with a proper slot configuration might reasonably be expected to go to zero.

Lift Interference

The lift interference problem at transonic speeds is not critical as is the blockage, because, with constant lift coefficient, this type of interference is insensitive to change of Mach number. The advantage of a partially open test section for the reduction of lift interference has long been known and has been treated by many authors. The theory applicable to the treatment of lift interference due to the trailing vortex system in a many-slotted circular test section is given in reference 9 and has been applied and extended to the case of rectangular test sections in reference 10. It is found that, for most practical configurations, the slot width suitable for the elimination of solid blockage is too great to eliminate the lift interference, so that a residual lift interference of the kind experienced in open tunnels still exists.

Preliminary tests with lifting airfoils in the Langley 7- by 10-foot high-speed tunnel and in a $4\frac{1}{2}$- by $6\frac{1}{4}$-inch rectangular tunnel whose upper and lower walls in successive tests were closed, open, and slotted are presented in reference 11. Figure 9 shows the relative size of the tunnels with the semispan model mounted from the side wall. The same model and balance were used in all tests, and all were made at the same Reynolds number. Typical results presented in figure 10 show that the lift-curve slope at $C_L = 0$ from the slotted-tunnel tests followed closely that obtained in the interference-free tests from the 7- by 10-foot tunnel, while the closed-tunnel data indicated substantially higher slopes, and the open tunnel much lower slopes. With a model of this size, conventional closed tunnels would be choked at $M = 0.85$. The experiments are again in qualitative agreement with theory.

Simplified Boundary Condition

The boundary conditions are greatly simplified in reference 12 by substituting for a system of discrete slots an equivalent average boundary condition, as shown schematically in the flow cross section of figure 11. The slotted boundary is indicated along the bottom of the figure; below the wall, the velocity in the chamber is zero; above it, streamlines in the crossflow become nearly vertical. At some small distance $-n_1$ above the wall, where the flow is nearly uniform, an average boundary condition may be substituted for the real flow; here it is only necessary that the force on the flow between the model and $-n_1$ be the same. For a representative sector, the potential φ required by the average boundary condition is shown in the figure, where a is the slot width, d the slot spacing, and n the distance from the wall. By use of the simplified boundary condition, the lift and blockage interference have been treated in the circular tunnel, in the rectangular tunnel with top and bottom walls slotted, and in the two-dimensional tunnel with slotted walls. In addition, the lift interference in a rectangular tunnel with all walls slotted has been considered. Comparison with more exact calculations by the method of reference 10 shows good accuracy even for as few as four slots in one case; and it is believed that the method is generally reliable so long as the spacing between slots is not too great.

Shock Reflection

Supersonic interference, the effects of which have been previously observed in the experiments, is now considered. This problem is illustrated in figure 12, where the characteristic net for the flow about a representative body is shown. In a conventional tunnel, where the bow shock is reflected from the solid boundary, only the flow upstream from the reflected shock is free from interference. Behind the reflected shock, the flow remains supersonic and disturbances that originated on the body are reflected in like sign. Moving the wall closer to the model results in a forward movement of the reflected shock and a decrease in the length of the interference-free flow over the model. The problem, then, is to replace this wall with one having such characteristics that the flow field between the wall and the model will remain unchanged; this requires not only that the reflection of incident disturbance be prevented but that the effect of disturbances coming in from the outside field be simulated. These disturbances constitute an effect of the flow over the model forebody on that over the rear. For the design of a wall to accomplish this purpose, a prior knowledge of the required flow field near the wall seems necessary. A wall that will completely eliminate the supersonic interference, therefore, appears impractical, even from theoretical considerations.

If a wall is placed far enough from the model to render negligible the error due to cutting off the disturbances coming in from the outside field, the interference might still be significantly reduced by merely preventing the reflections. However, caution must be exercised in judging whether the cut-off part of the upstream influence is actually negligible, lest a cumulative error over the rear of the model lead to falsification of the test results (drag, in particular). The possibility of eliminating wall reflection seems plausible, because, again, the open-tunnel interference is of opposite kind to that in a closed tunnel. A shock wave, for instance, is reflected from an open boundary as an expansion; whereas, from a closed boundary, it is reflected as another shock wave. The use of slots as a means of reducing supersonic interference was investigated by Wood, who showed, by means of interferograms, that substantial amelioration of the reflected shock waves could be effected. The reflected disturbance, however, consisted of a shock wave reflected from the bars with an expansion from the slot, which, being propagated at a smaller angle, failed to cancel the shock.

Other experiments directed toward evaluation of the shock cancellation potential of materials of more uniform porosity are reported in references 13 and 14. The problem of shock reflection from porous surfaces is illustrated in the schlieren photograph of figure 13. A 4° wedge was mounted in a tunnel, two walls of which were constructed of porous sintered bronze; the wedge was mounted off-axis to increase the effective height of the tunnel. This picture was taken at a stream Mach number of approximately 1.17; the stream deviation through the incident shock wave was approximately 2°. From the slope of the Mach lines, it is clear that the reflected disturbance consists of an expansion followed by a compression; since the latter are propagated along steeper lines, they merge, and, at large distances from the wall, substantial softening might be expected. The difference in slope of the Mach lines ahead of the reflected disturbance from those well downstream indicates that the stream deviation across this reflected disturbance was on the order of 0.7°, a substantial reduction from the 2° change across the incident wave.

Theory indicates that complete elimination of shock reflections can be expected from a given porous wall for a shock of only one deviation at any given Mach number. The problem of shock reflection is further complicated by the presence of a boundary layer along the walls which, acting under the influence of the incident disturbance, undergoes rapid changes in thickness, thus introducing additional disturbances into the flow. Because of these and many other factors, many problems associated with the wall reflection of disturbances at supersonic Mach numbers remain unsolved. It is apparent, however, that disturbances reflected from either slotted or porous walls will be weaker than corresponding reflections from solid walls or from an open boundary. Testing at low supersonic Mach numbers is possible and, by the use of relatively short models, the Mach number range over which significant interferences occur becomes negligible.

Power

The power requirements of slotted tunnels are substantially higher than those of closed tunnels of equal size; but, because the closed tunnel required to test a given model is much larger than the corresponding slotted tunnel, the latter maintains a substantial advantage over the tunnel of conventional design. Progress is being made in an effort to reduce the power required by the slotted tunnel by divergence of the walls to reduce the amount of air drawn from the circuit, by the use of auxiliary suction to avoid re-entry of the retarded air of the chamber in the diffuser, and by improvement in diffuser design.

CONCLUSIONS

From the results obtained to date, it is clear that:

1. Slotted or porous walled tunnels may be operated through the transonic range without choking.

2. Subsonic wall interference effects have been reduced to the point where for most practical purposes they may be neglected.

3. Wall interference associated with the reflection of shock waves at supersonic Mach numbers, although not eliminated, has been somewhat reduced. By the use of relatively short models, the Mach number range of significant interference becomes negligible.

REFERENCES

1. Wright, Ray H., and Ward, Vernon G.: NACA Transonic Wind-Tunnel Test Sections. NACA RM L8J06, 1948.

2. Nelson, William J., and Bloetscher, Frederick: Preliminary Investigation of a Variable Mach Number Two-Dimensional Supersonic Tunnel of Fixed Geometry. NACA RM L9D29a, 1949.

3. Allen, H. Julian, and Spiegel, Joseph: Transonic Wind Tunnel Development at the NACA Aeronautical Laboratory. Inst. Aero. Sci. meeting June 21-24, 1954.

4. Nelson, William J., and Klevatt, Paul L.: Preliminary Investigation of Constant-Geometry, Variable Mach Number, Supersonic Tunnel with Porous Walls. NACA RM L50B01, 1950.

5. Stokes, George M., Davis, Don D., Jr., and Sellers, Thomas B.: An Experimental Study of Porosity Characteristics of Perforated Materials in Normal and Parallel Flow. NACA TN 3085, 1954.

6. Wieselsberger, Carl: Uber den Einfluss der Windkanalbegrenzung auf den Widerstand insbesondere im Berliche der kompressiblen Stromung. Luftfahrtforschung, Bd. 19, Lfg. 4, May 6, 1942, pp. 124-128.

7. Katzoff, S., Gardner, Clifford S., Diesendruck, Leo, and Eisenstadt, Bertram J.: Linear Theory of Boundary Effects in Open Wind Tunnels with Finite Jet Length. NACA Rep. 976, 1950. (Supersedes NACA TN 1826.)

8. Stack, John, and Mattson, Axel: Transonic Test Sections. Inst. Aero. Sci. meeting June 21-24, 1954.

9. Pistolesi, E.: On the Interference of a Wind Tunnel with Mixed Boundary. Cornell Aero. Lab., Inc., Dec. 1949.

10. Matthews, Clarence W.: Theoretical Study of the Tunnel-Boundary Lift Interference Due to Slotted Walls in the Presence of the Trailing-Vortex System of a Lifting Model. NACA RM L53A26, 1953.

11. Sleeman, William C., Jr., Klevatt, Paul L., and Linsley, Edward L.: Comparison of Transonic Characteristics of Lifting Wing from Experiments in a Small Slotted Tunnel and the Langley High-Speed 7- and 10-Foot Tunnel. NACA RM L51F14, 1952.

12. Davis, Don D., Jr., and Moore, Dewey: Analytical Study of Blockage- and Lift-Interference Corrections for Slotted Tunnels Obtained by the Substitution of and Equivalent Homogeneous Boundary for the Discrete Slots. NACA RM L53E07b, 1953.

13. Nelson, William J., and Bloetscher, Frederick: Preliminary Investigation of Porous Walls as a Means of Reducing Tunnel Boundary Effects at Low-Supersonic Mach Numbers. NACA RM L50D27, 1950.

14. Davis, Don D., Jr., and Wood, George P.: Preliminary Investigation of Reflections of Oblique Waves from a Porous Wall. NACA RM L50G19a, 1950.

TYPICAL SLOTTED-TUNNEL ARRANGEMENT

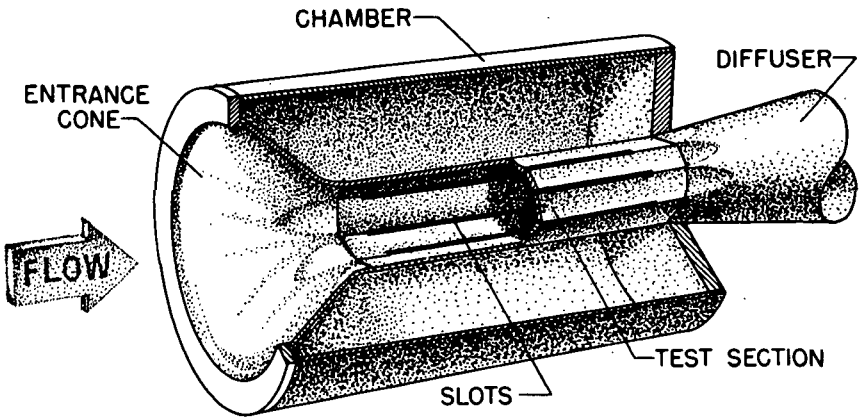

Figure 1

MACH NUMBER DISTRIBUTION
SLOTTED TUNNEL

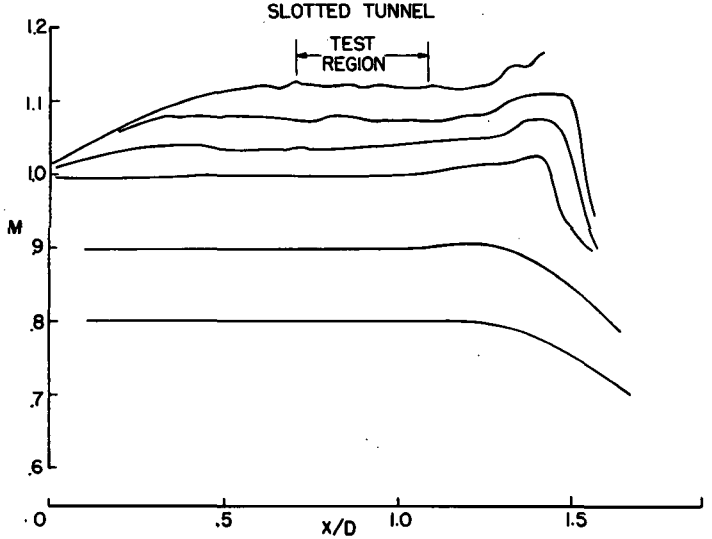

Figure 2

SLOTTED-TUNNEL CROSS SECTION

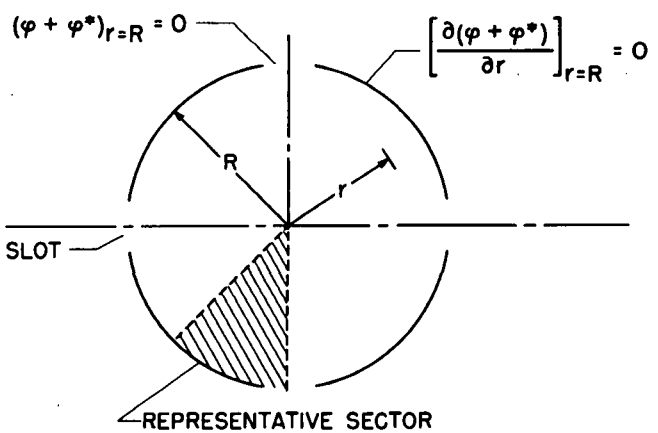

$$\frac{\partial^2\varphi^*}{\partial r^2} + \frac{1}{r}\frac{\partial\varphi^*}{\partial r} + \frac{1}{r^2}\cdot\frac{\partial^2\varphi^*}{\partial\theta^2} + \frac{\partial^2\varphi^*}{\partial x^2} = 0$$

Figure 3

AXIAL-INTERFERENCE VELOCITY FUNCTION
CIRCULAR TUNNEL

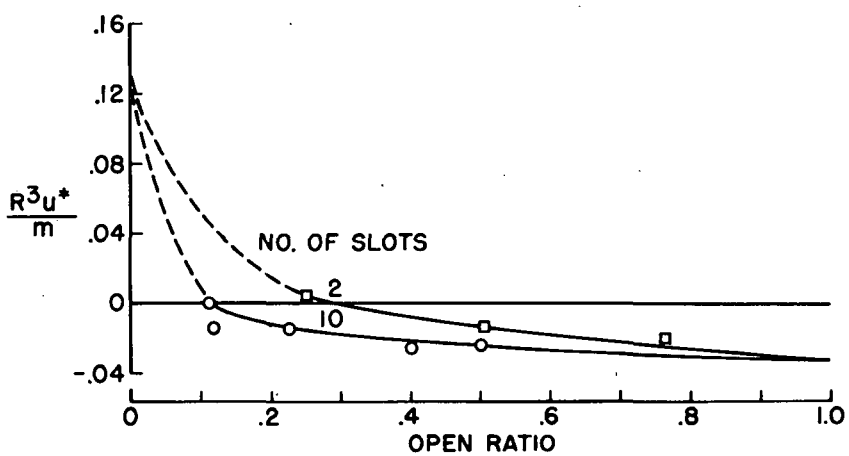

Figure 4

INTERFERENCE AT CENTER OF PROLATE SPHEROID

FINENESS RATIO = 6

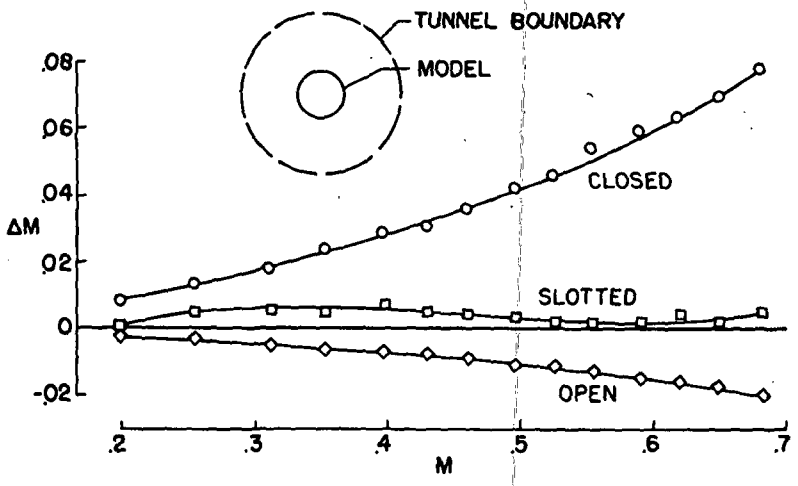

Figure 5

WIND-TUNNEL SETUP FOR BLOCKAGE TESTS

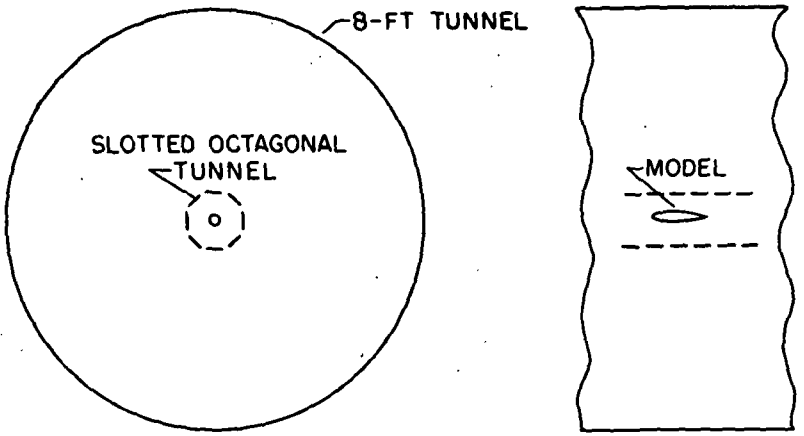

Figure 6

SURFACE-PRESSURE DISTRIBUTION

PROLATE SPHEROID

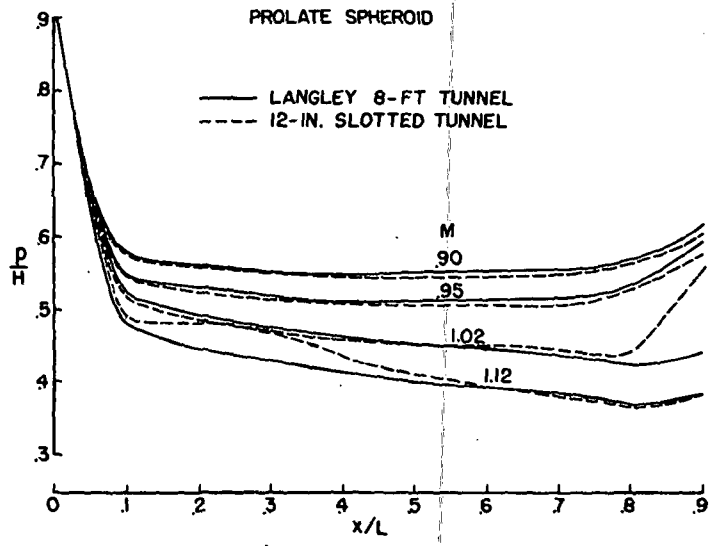

Figure 7

EFFECTS OF BOUNDARY INTERFERENCE

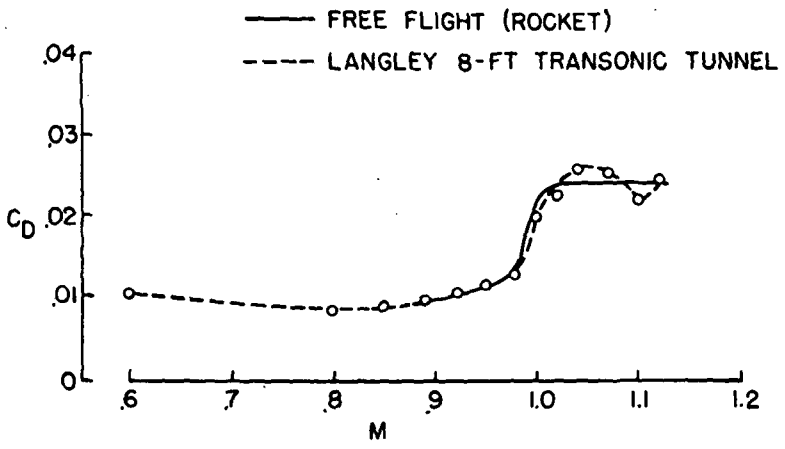

Figure 8

WIND-TUNNEL SETUP FOR LIFTING-WING TESTS

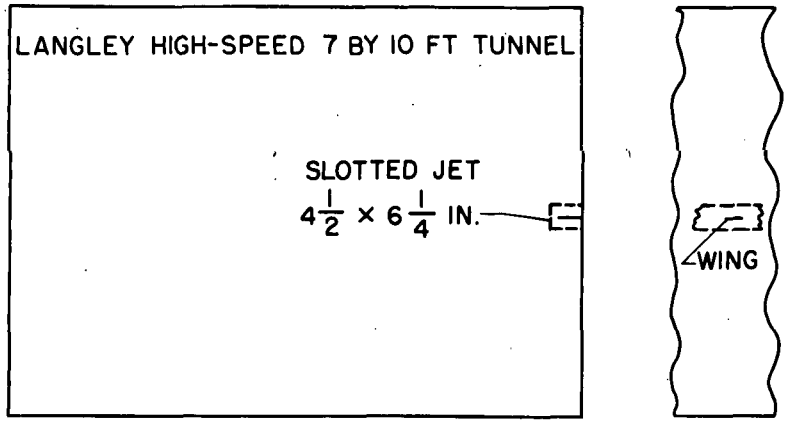

Figure 9

LIFT INTERFERENCE AT $C_L = 0$

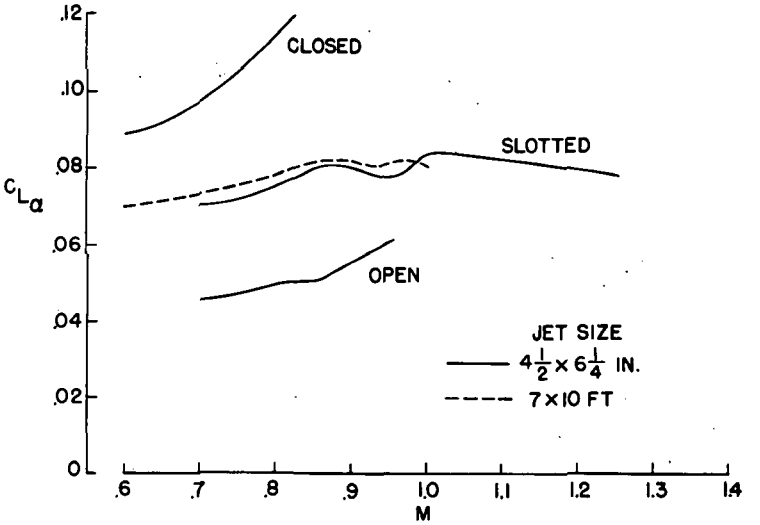

Figure 10

APPROXIMATE BOUNDARY CONDITION

$$\varphi + \left(\frac{d}{\pi} \log_e \csc \frac{\pi}{2} \frac{a}{d}\right) \frac{\partial \varphi}{\partial n} = 0$$

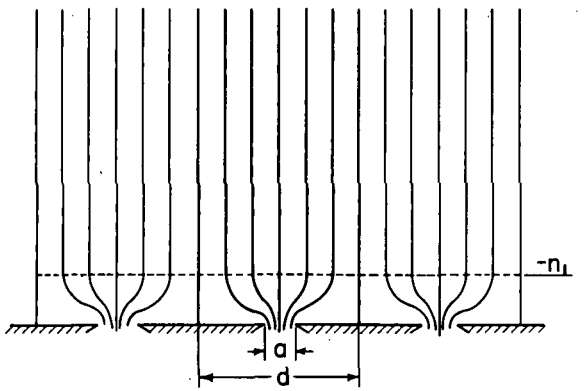

Figure 11

SUPERSONIC INTERFERENCE

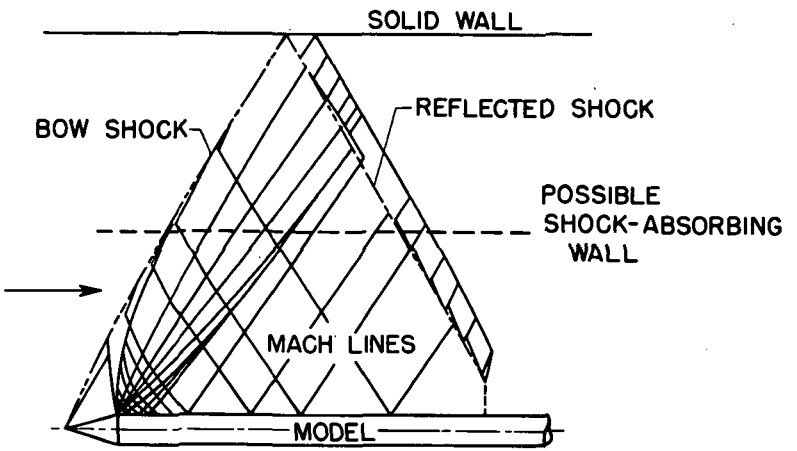

Figure 12

SHOCK REFLECTION FROM POROUS WALL

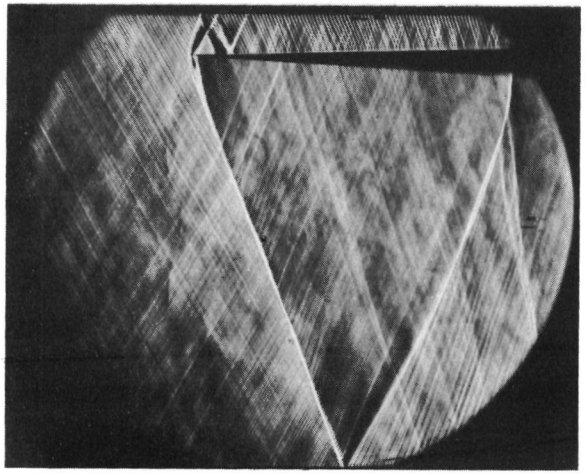

Figure 13